UNIVERSIDAD AUTÓNOMA DE SAN LUÍS POTOSÍ

Doctorado Institucional en Ingeniería y Ciencia de Materiales

Mechanisms of Advanced Chemical Oxidation in Refractory Gold Ore Pretreatment and Cyanide-Free Leaching

TESIS

QUE PARA OBTENER EL GRADO DE

DOCTOR EN INGENIERÍA Y CIENCIA DE MATERIALES

QUE PRESENTA

Lei Hou

DIRECTORES

Dr. Alejandro López Valdivieso (†)

Dra. Aurora Robledo Cabrera

PATROCINADO POR SECIHTI Beca número 848160

San Luis Potosí, S.L.P., junio de 2026

UNIVERSIDAD AUTÓNOMA DE SAN LUÍS POTOSÍ

Doctorado Institucional en Ingeniería y Ciencia de Materiales

Mechanisms of Advanced Chemical Oxidation in Refractory Gold Ore Pretreatment and Cyanide-Free Leaching

TESIS

QUE PARA OBTENER EL GRADO DE

DOCTOR EN INGENIERÍA Y CIENCIA DE MATERIALES

PRESENTA

Lei Hou

DIRECTORS

Dr. Alejandro López Valdivieso (†)

Dra. Aurora Robledo Cabrera

Comité tutorial:

Dra. Aurora Robledo Cabrera_____

Dra. Jessica Viridiana García Meza_____

Dra. Mildred Quintana Ruiz_____

Dra. María Selene Berber Mendoza_____

Dr. Mario Alberto Corona Arroyo_____

San Luis Potosí, S.L.P., junio de 2026

Acknowledgement

This work was supported by the Secretaría de Ciencia, Humanidades, Tecnología e Innovación (SECIHTI), Mexico, through a PhD scholarship (Grant No. 848160). I also sincerely acknowledge the financial support from the National Key Research and Development Program of China (2023YFE0104200).

I would like to first express my sincere gratitude to Dr. Shaoxian Song and Dra. Feifei Jia. Dr. Song, thank you for providing LaMCC, an excellent laboratory. It gave me a very good place to learn, grow, and do my research. This lab has been like a big family to me, and I have always felt supported here. Dr. Jia, your careful guidance and strong support made this thesis possible. I am also deeply grateful for your advice in life and for your encouragement whenever I felt lost or uncertain. Because of your support, I had the chance to see a bigger world and gain many valuable experiences.

My deepest gratitude goes to Dr. Alejandro López Valdivieso and Dra. Aurora Robledo Cabrera from Laboratorio Química de Superficies. Dr. Valdivieso had profound knowledge and a rigorous academic attitude. He guided me with great patience. Every time we talked, he filled the whole blackboard to make sure that I understood every detail clearly. He was also a warm and kind person. I will always remember his guidance, kindness, and encouragement. May he rest in peace. I am also very grateful to Dra. Aurora. After Dr. Valdivieso passed away, she continued to guide my thesis and gave me support. Without her help, I could not have completed this thesis.

I am sincerely grateful to my committee members, Dra. Jessica Viridiana García Meza, Dra. Mildred Quintana Ruiz, Dra. María Selene Berber Mendoza and Dr. Mario Alberto Corona Arroyo. Thank you all for your efforts over the past four years on this project. I am grateful for every seminar, every discussion, and all the valuable comments you gave on my thesis. Your advice helped me improve my work and think more carefully about my research. I would especially like to thank Dr. Viridianna for your care and kindness. With your support, we never felt alone.

I need to thank all the staff at the Instituto de Metalurgia for their support during my thesis work. I especially thank Q. Izanami López Acosta for her help with chemical analyses, M.M.I.M. Rosa Lina Tovar Tovar for her help with X-ray diffraction analysis, and Dra. Elvia Francisca Alfaro Saldaña for her assistance with electrochemical measurements. I would also like to thank the staff of the Doctorado Institucional en Ingeniería y Ciencia de Materiales, especially Eva, Maricela, and Ubaldo. Their patience and kindness made my study much easier. I am very grateful for their help.

Finally, I would also like to thank my family, Dr. Yanmei Li, Ms. Rong An, and all my friends from the Instituto de Metalurgia and Wuhan University of Technology. Thank you all for your company, support, and friendship during this journey.

Abstract

In gold hydrometallurgical leaching, oxidation plays a decisive role in pretreating refractory ores and cyanide-free leaching. For refractory sulfide ores, the liberation of encapsulated gold from the sulfide matrix under strong oxidative conditions is essential prior to leaching. Likewise, gold leaching by cyanide-free systems requires sufficient oxidizing environments for driving gold dissolution. Accordingly, this study focuses on the development of highly efficient advanced chemical oxidation processes, mainly based on free radical chemistry and coordination chemistry, to enhance gold liberation from refractory pyrite ore (*Chapter III*), and to achieve efficient and stable gold leaching by eco-friendly thiourea (*Chapter IV*), thiosulfate (*Chapters V and VI*), and iodide (*Chapter VII*).

In this thesis, *Chapter I* briefly introduced the justification and objectives of this research. *Chapter II* comprehensively reviewed the previous research state of pretreating refractory sulfide ores and gold leaching in cyanide-free systems, namely, the antecedents. *Chapter III* develops a stepwise chemical oxidation process for pretreating a refractory pyrite concentrate by employing persulfate-activated hydroxyl radical (•OH), in which heat-activation at 55 °C initiated pyrite Step I oxidation (14.20%), and the pyrite dissolved Fe ions activation sustained pyrite Step II oxidation to 40.13%, thereby greatly increased Au and Ag liberation (Au 92.2% and Ag 88.6% by thiosulfate leaching). *Chapter IV* demonstrates that free radicals, generated from the *Fenton* reaction (Fe^{2+}/H_2O_2), enable fast gold dissolution in acidic thiourea media, achieving complete gold leaching from a roasted concentrate within only 30 min. Moreover, using nitrilotriacetic acid (NTA) to complex Fe^{2+}/Fe^{3+} ions can regulate the moderate superoxide radical anion ($\bullet O_2^-$) as the reactive oxidizing species, which effectively suppresses harmful thiourea degradation. *Chapter V* focuses on using electrochemical methods to investigate the dissolution behavior of gold in the thiosulfate system by employing copper(II)-glycine complexes as the oxidant. The results show that $Cu(C_2H_4NO_2)_3^-$ in strongly alkaline media promotes gold dissolution more effectively than $Cu(C_2H_4NO_2)_2^0$ under near-neutral conditions, as evidenced by faster interfacial electron-transfer kinetics and reduced interface passivation. *Chapter VI* uses pentetic acid (DTPA) to stabilize copper(II) as the oxidant in thiosulfate gold leaching. Ammonia (NH_3), released in-situ from $(NH_4)_2S_2O_3$, can couple with $Cu(DTPA)^{3-}$ to form a more reactive $[Cu(DTPA)(NH_3)]^{3-}$ complex, which achieved

gold leaching from a roasted concentrate as high as 97.8%, while thiosulfate consumption remained as low as 8.7 kg/t. *Chapter VII* presents a novel copper (III)/potassium iodide system for gold leaching under near-neutral conditions (pH 5.5), which achieves 94.1% from a gold ore within 60 min and 96.6% from e-waste within 20 min. In this system, copper(III) periodate acts as a catalyst to in-situ generate triiodide (I_3^-) from iodide (I^-), which serves as the reactive oxidizing species driving gold dissolution.

Keywords: Refractory sulfide gold ores, cyanide-free lixiviants, gold leaching, oxidation, free radicals, copper complexes.

Extended Abstract

Gold (Au) is an indispensable precious metal with extensive applications in jewelry and electronics. Hydrometallurgical leaching remains the dominant route for gold industrial extraction, yet two major challenges are increasingly constraining its sustainable development: (i) currently exploited gold resources are becoming progressively more refractory, especially when gold is encapsulated in sulfide minerals; (ii) growing environmental pressure on cyanidation is driving the development of cleaner cyanide-free gold leaching technologies. To address these challenges, this thesis develops a series of advanced chemical oxidation processes based primarily on free-radical chemistry and coordination chemistry, which enable the decomposition of sulfide host minerals to liberate gold in refractory ores, while also providing controllable oxidizing environments for cyanide-free gold leaching. The main findings are summarized as follows:

A stepwise chemical oxidation process was developed for the pretreatment of a refractory pyrite concentrate. In this design, pyrite oxidation is initiated by thermally activated persulfate (55 °C), in which hydroxyl radicals (•OH) promote the rapid oxidation of pyrite into soluble iron species. These dissolved iron species subsequently act as in-situ activators of persulfate, sustaining further •OH generation and enabling continuous pyrite oxidation at room temperature. Mineralogical and microstructural characterization confirms that this oxidation treatment can significantly reduce pyrite particle size, generate pores, and increase specific surface area, thereby exposing previously encapsulated Au and Ag. As a result, downstream thiosulfate leaching was markedly improved, achieving Au and Ag extractions of 92.2% and 88.6%, respectively.

A *Fenton* oxidation-assisted thiourea system was first established for cyanide-free gold leaching, in which free radicals generated from the Fenton reaction (Fe^{2+}/H_2O_2) served as the reactive oxidizing species. This system enabled ultrafast leaching kinetics, achieving 100% gold extraction from a roasted gold concentrate within 30 min. To address the high thiourea consumption, nitrilotriacetic acid (NTA) was further introduced as an additive, which provided two major benefits. First, its efficient coordination with iron species suppressed side reactions between iron and thiourea. Second, it reduced the reactivity of the Fe^{2+}/Fe^{3+} redox couple toward H_2O_2, thereby regulating the generation of the mild superoxide radical anion ($•O_2^-$) dominant. As a result, thiourea consumption was markedly reduced from 45.6% to 11.84% while

maintaining high gold extraction (100% within 60 min).

In thiosulfate leaching, the dissolution behavior of gold in the presence of copper (II)-glycine complexes as oxidants was systematically investigated by electrochemical methods. Electrochemical quartz crystal microbalance (EQCM) measurements revealed that gold anodic dissolution is strongly dependent on the form of the copper (II)-glycine complex. Under strongly alkaline conditions (pH 10.5), the $Cu(C_2H_4NO_2)^{3-}$ complex exhibited better catalytic performance for gold anodic oxidation than the $Cu(C_2H_4NO_2)_2^0$ complex present under near-neutral conditions (pH 8). This superior performance of $Cu(C_2H_4NO_2)^{3-}$ is mainly associated with faster interfacial electron-transfer kinetics and reduced interface passivation. Besides, gold dissolution mainly proceeds through a ligand-exchange pathway from $Au(C_2H_4NO_2)_2^-$ to $Au(S_2O_3)_2^{3-}$, which is beneficial for alleviating harmful surface passivation from sulfur-containing products of thiosulfate decomposition.

To further stabilize the copper(II) oxidant in thiosulfate leaching, pentetic acid (DTPA) was used to construct a novel copper(II)-DTPA oxidation system. The chelated $CuDTPA^{3-}$ complex provides high stability to suppress thiosulfate consumption, while ammonia (NH_3) plays a crucial role in enhancing gold dissolution. Comparative leaching experiments using $(NH_4)_2S_2O_3$ and $Na_2S_2O_3$ indicate that NH_3 promotes the formation of a mixed $[Cu(DTPA)(NH_3)]^{3-}$ complex with higher redox reactivity than $CuDTPA^{3-}$ alone. Under optimized conditions, gold leaching from a pretreated concentrate reached 97.8%, with a low thiosulfate consumption of 8.7 kg/t. In particular, this system shows great operational flexibility, because the benefits of $(NH_4)_2S_2O_3$ can also be provided by low-cost $Na_2S_2O_3$ together with a variety of ammonium salts, like NH_4OH, $(NH_4)_2SO_4$, CH_3COONH_4, and NH_4Cl.

An aqueous copper(III)/potassium iodide system was established that operates efficiently over wide pH ranges from acidic to alkaline media and, notably, enables rapid gold leaching under near-neutral conditions. At pH 5.5, the system achieved 94.1% gold leaching in 60 min from a roasted concentrate and 96.6% in 20 min from waste mobile phone printed circuit boards. Mechanistic investigation revealed pronounced pH-dependent bifunctionality of copper(III) periodate: under alkaline conditions, copper(III) acts as the reactive oxidant that directly drives gold dissolution, whereas at lower pH it increasingly behaves as a catalyst that promotes the in-situ generation of triiodide (I_3^-), which is an effective oxidizing species in iodide leaching.

Overall, in this thesis, radical chemistry and coordination chemistry-based oxidation processes have found promise in the pretreatment of refractory gold ores and cyanide-free gold leaching. These findings could provide new mechanistic insights and practical guidance for the advancement of greener, faster, and more sustainable gold hydrometallurgical processes.

Keywords: Refractory sulfide ores, oxidation, gold leaching, thiosulfate, thiourea, iodide, persulfate, Fenton reaction, copper(II) complexes, copper(III) periodate.

Contents

Index of Figures

Index of Tables

Chapter I. Introduction

1.1 Justification

Gold has fascinating symbolic significance in jewelry, currency, financial assets, and even culture throughout human history, while its uniquely physical properties (electroconductivity, durability, malleability, and corrosion resistance) make it also valuable in various modern industries such as electronics, medicine, and aerospace [1]. Although over 212k tons of gold exist above ground, it is estimated from the World Gold Council that only about 64,000 tons of gold reserves remain to be mined [2]. What's more, the gold resource progressively shifts toward lower grades and greater mineralogical complexity, that is, refractory gold ores becoming dominant, which increases extraction difficulty in the existing hydrometallurgical process [3]. In parallel, an equally important challenge is that growing environmental concerns are driving the gold industry to move away from cyanidation, the most established gold extraction method for a century, toward cleaner hydrometallurgical routes with lower toxicity [4]. Together, these trends highlight an urgent scientific and engineering need to redesign gold-processing flowsheets that can maintain high efficiency for mineralogically refractory ores while meeting increasingly stringent environmental requirements through the use of more eco-friendly gold extraction systems.

For refractory gold ores, the biggest obstacle to extraction is that gold commonly occurs as ultra-fine inclusions, is physically encapsulated, or becomes lattice-bound within pyrite and related sulfides [5]. In such sulfide-hosted gold ores, conventional crushing and grinding cannot effectively liberate the encapsulated or invisible gold from the sulfide matrix and therefore fail to provide sufficient access for leaching reagents to attack gold during cyanidation, resulting in very low extraction efficiency (typically below 80% or less) [6]. For this reason, pretreatment, aiming to open the sulfide matrix to improve gold liberation, is indispensable before leaching. Due to sulfide minerals containing reduced sulfur, under sufficient oxidizing conditions, they can be gradually broken down. So, oxidation can be an ideal pretreatment approach to damage the sulfide matrix, expose the trapped gold, and make the ore much easier to leach. While the established oxidation routes, e.g., roasting oxidation (high temperature) [7], biooxidation (microorganism or bacteria) [8], and pressure oxidation (high temperature and high pressure) [9], can be effective, they often involve unacceptable drawbacks from the factory side, including equipment investment, gas handling, long residence times, sensitivity to ore variability, and rigorous operational control.

Consequently, this thesis is justified by the need for more controllable pretreatment strategies to liberate gold from refractory sulfide gold ores, particularly focused on wet chemical oxidation routes by only employing oxidizing agents under atmospheric conditions, which are technically, economically, or environmentally attractive.

On the other end of the spectrum, cyanide-free gold leaching, for example, using eco-friendly reagents like thiosulfate, thiourea, thiocyanate, or halide as a replacement for toxic cyanide, can significantly lower environmental risks and have a broad base of support [10]. However, compared with conventional cyanidation, gold leaching by these greener alternatives is more difficult. Basically, gold leaching is based on the complexing reaction between gold (I, III) and the leaching reagent, while an oxidizing reaction is also required to convert the metallic gold to an ionized status simultaneously. Thermodynamically, gold dissolution in cyanide solution is spontaneous only with oxygen because cyanide greatly lowers the potential for gold oxidation by strongly complexing gold(I) ($\log\beta = 38.3$), so oxygen is good enough to meet the potential and the role of oxidants [11]. However, those greener alternatives cannot complex with gold as stably as cyanide, so gold dissolution can only occur at a higher potential, that is, they need the leaching system to have stronger oxidizing ability. To achieve this, adding oxidizing agents is a straightforward way to improve the solution potential and thus oxidize gold, and theoretically, the stronger the oxidants, the faster the gold leaching kinetics. But in practice, this does not happen because a stable and cost-efficient oxidation system is hardly achieved, where the oxidizing ability of oxidants is always poorly matched to the leaching reagent [12]. To be specific, the mild oxidants can not offer quick gold dissolution, while inducing severe side reactions and non-selective oxidation, for example, more side reactions and unavoidable oxidation of the leaching reagent [13]. Thus, this thesis is justified by the need to design more efficient and controlled oxidation processes that should provide a balance between gold leaching efficiency and the system's stability, especially minimizing non-productive reagent loss.

Overall, these two directions highlight wet-chemical oxidation as a central strategy in both refractory ore pretreatment and cyanide-free gold leaching. For refractory sulfide gold ores, oxidative decomposition of the sulfide host matrix using appropriate oxidants is both technically feasible and highly desirable because of its potential economic and environmental advantages. More importantly, in cyanide-free hydrometallurgical systems, oxidation governs not only the kinetics of gold dissolution but also the stability and consumption behavior of the lixiviant. Therefore, the oxidizing environment of the system must be carefully regulated to achieve an effective balance

between rapid gold dissolution and minimal reagent degradation. Achieving both objectives requires the development of more efficient and better-controlled oxidation processes.

1.2 Objective

1.2.1 General objective

To develop advanced chemical oxidation systems based on radical and coordination chemistry for enhancing gold extraction from refractory sulfide ores and enabling efficient cyanide-free leaching, while elucidating the underlying mechanisms governing gold liberation and dissolution.

1.2.2 Specific objectives

(1) To develop a persulfate-based radical oxidation system for the pretreatment of refractory sulfide gold ores, and to investigate the structural evolution of pyrite and its effect on the liberation of encapsulated gold.

(2) To establish a Fenton-assisted thiourea system for cyanide-free gold leaching, and to elucidate the role of reactive oxygen species in controlling gold dissolution kinetics and thiourea stability.

(3) To elucidate the mechanistic role of Cu(II)-glycine complexes in thiosulfate leaching using electrochemical techniques, with emphasis on the influence of pH-dependent speciation on gold dissolution and thiosulfate decomposition.

(4) To develop a Cu(II)-DTPA-based oxidation system for thiosulfate leaching, and to evaluate the role of complexation and ammonia in enhancing gold recovery and reducing reagent consumption.

(5) To design a Cu(III)-based catalytic oxidation system in iodide leaching, and to elucidate the reactive oxidative species and mechanisms governing gold dissolution under varying pH conditions.

1.3 References

[1] D.R. McKay, D.A. Peters, The Midas Touch: Gold and Its Role in the Global Economy, Plastic Surgery 25 (2017) 61-63.

[2] S. Liu, Y. Geng, Z. Gao, J. Li, S. Xiao, Uncovering the key features of gold flows and stocks in China, Resources Policy 82 (2023) 103584.

[3] J.P. Vaughan, The process mineralogy of gold: The classification of ore types, JOM

56 (2004) 46-48.
[4] G. Hilson, A.J. Monhemius, Alternatives to cyanide in the gold mining industry: what prospects for the future?, Journal of Cleaner Production 14 (2006) 1158-1167.
[5] M. Merkulova, O. Mathon, P. Glatzel, M. Rovezzi, V. Batanova, P. Marion, M.-C. Boiron, A. Manceau, Revealing the Chemical Form of "Invisible" Gold in Natural Arsenian Pyrite and Arsenopyrite with High Energy-Resolution X-ray Absorption Spectroscopy, ACS Earth and Space Chemistry 3 (2019) 1905-1914.
[6] J. Li, H. Yang, R. Zhao, L. Tong, Q. Chen, Mineralogical characteristics and recovery process optimization analysis of a refractory gold ore with gold particles mainly encapsulated in pyrite and Arsenopyrite, Geochemistry 83 (2023) 125941.
[7] H. Qin, X. Guo, Q. Tian, D. Yu, L. Zhang, Recovery of gold from sulfide refractory gold ore: Oxidation roasting pretreatment and gold extraction, Minerals Engineering 164 (2021) 106822.
[8] A.H. Kaksonen, F. Perrot, C. Morris, S. Rea, B. Benvie, P. Austin, R. Hackl, Evaluation of submerged bio-oxidation concept for refractory gold ores, Hydrometallurgy 141 (2014) 117-125.
[9] F.P. Gudyanga, T. Mahlangu, R.J. Roman, J. Mungoshi, K. Mbeve, An acidic pressure oxidation pre-treatment of refractory gold concentrates from the KweKwe roasting plant, Zimbabwe, Minerals Engineering 12 (1999) 863-875.
[10] Y. Zhang, M. Cui, J. Wang, X. Liu, X. Lyu, A review of gold extraction using alternatives to cyanide: Focus on current status and future prospects of the novel eco-friendly synthetic gold lixiviants, Minerals Engineering 176 (2022) 107336.
[11] P.L. Breuer, X. Dai, M.I. Jeffrey, Leaching of gold and copper minerals in cyanide deficient copper solutions, Hydrometallurgy 78 (2005) 156-165.
[12] Y. Yang, W. Gao, B. Xu, Q. Li, T. Jiang, Study on oxygen pressure thiosulfate leaching of gold without the catalysis of copper and ammonia, Hydrometallurgy 187 (2019) 71-80.
[13] Z. Liu, X. Guo, Q. Tian, L. Zhang, A systematic review of gold extraction: Fundamentals, advancements, and challenges toward alternative lixiviants, Journal of Hazardous Materials 440 (2022) 129778.

Chapter II. Antecedents

2.1 Introduction

Gold (Au) has been used to make ornamental objects and jewelry for thousands of years and has held a prominent place in the development and stabilization of the global economy and world currency markets. Nowadays, its unique physical properties also make it an important raw material in various high-tech industries such as electronics, medicine, and aerospace [1-3]. This leads to high global gold demand; in 2023 alone, gold consumption exceeded 4000 tons, resulting in extensive mining [4]. Over the past decade, more than 38,000 tons of gold, worth over 3 trillion US dollars, have been extracted. The excess mining made the extractable gold resource gradually shift toward lower grades and higher mineralogical complexity, that is, refractory gold ores becoming dominant, which makes efficient extraction by hydrometallurgy more challenging. At the same time, the growing environmental concerns have put pressure on the global gold industry to move away from toxic cyanidation, the most mature gold extraction method, toward cleaner and more sustainable cyanide-free routes [5]. Two trends define current gold-processing research and highlight an urgent scientific and engineering need to redesign gold-processing flowsheets that can maintain high efficiency for mineralogically refractory ores while meeting increasingly stringent environmental requirements through the use of more eco-friendly gold extraction systems.

For refractory gold ores, the biggest obstacle to extraction is that gold commonly occurs as ultra-fine inclusions, is physically encapsulated, or becomes lattice-bound within pyrite and related sulfides. In such sulfide-hosted gold ores, conventional crushing and grinding cannot effectively liberate the encapsulated or invisible gold from the sulfide matrix and therefore fail to provide sufficient access for leaching reagents to attack gold during cyanidation, resulting in very low extraction efficiency (typically below 80% or less) [6]. Based on this reason, pretreatment, aimed at opening the sulfide matrix to improve gold liberation, is indispensable before leaching. Due to sulfide minerals containing reduced sulfur, under sufficient oxidizing conditions, they can be gradually broken down [7]. So, oxidation can be an ideal pretreatment approach to damage the sulfide matrix, expose the trapped gold, and make the ore much easier to leach [8]. On the other end of the spectrum, cyanide-free gold leaching, for example, using eco-friendly reagents like thiosulfate, thiourea, thiocyanate, or halide as a replacement for toxic cyanide, can significantly lower environmental risks and have a

broad base of support. However, compared with conventional cyanidation, gold leaching by these greener alternatives is more difficult. Basically, gold leaching is based on the complexing reaction between gold(I or III) and the leaching reagent, while an oxidizing reaction is also required to convert the metallic gold to an ionized status simultaneously [9]. Thermodynamically, gold dissolution in cyanide solution is spontaneous only with oxygen because cyanide greatly lowers the potential for gold oxidation by strongly complexing gold(I), so oxygen is good enough to meet the potential and the role of oxidants. However, those greener alternatives cannot coordinate with gold as stably as cyanide, so gold dissolution can only occur at a higher potential; that is, they need the leaching system to have a stronger oxidizing ability. To achieve this, adding oxidizing agents is a straightforward way to improve the solution potential and thus oxidize gold, and theoretically, the stronger the oxidants, the faster gold leaching kinetics [10].

Overall, these two directions highlight that oxidation plays a critical role in both refractory ore pretreatment and cyanide-free gold leaching. For refractory sulfide gold ores, oxidative decomposition of the sulfide host matrix is technically feasible to liberate the encapsulated gold. More importantly, in cyanide-free hydrometallurgical systems, oxidation governs the kinetics of gold dissolution. Achieving both objectives requires the development of more efficient and better-controlled oxidation processes. In this review chapter, we critically compare the main oxidative routes (i.e., roasting oxidation, bio-oxidation, pressure oxidation, and chemical oxidation) for the pretreatment of refractory sulfide gold ores. We then synthesize progress in cyanide-free gold leaching from an oxidation-centered perspective, emphasizing how oxidants and coordination environments govern dissolution, stability, and reagent efficiency. Finally, we emphasize the application potential of advanced chemical oxidation, focusing on (i) radical-based oxidation (Fenton/persulfate chemistry) and (ii) transition metal copper-based catalytic oxidation, as two useful oxidation processes more effective and controllable in gold hydrometallurgy.

2.2 Research status on oxidative pretreatment of sulfide refractory gold ore

2.2.1 Natural gold-bearing minerals

Gold occurs naturally as the metal and as various alloys, especially with silver, and as intermetallic compounds (Table 2.1). Native gold and electrum are very common; the gold-tellurides (e.g., Calaverite, Kr ennerite, Sylvanite, Montbrayite, Petzite, Nagyagite, and Kostovite) are uncommon, while the others (e.g., Aurostibnite and

Maldonite) are very rare.

Table 2.1 Naturally occurring gold minerals and compounds [11]

Mineral	Formula	Au content	Color
Native gold	Au	＞75%	Orange yellow
Electrum	(Au, Ag)	45-75%	Pale yellow to white
Calaverite	$AuTe_2$	39.2-42.8%	White or creamy yellow
Krennerite	$(Au, Ag)Te_2$	39.7-43.9%	Silver white
Sylvanite	$(Au, Ag)_2Te_4$	24.2-29.9%	Grey, white, pale yellow silver white
Montbrayite	$(Au,Sb)_2Te_3$	38.6-44.3%	Creamy white
Petzite	Ag_3AuTe_2	19.0-25.2%	Lead-gray to black
Nagyagite	$[Pb_3(Pb,Sb)_3S_6](Au,Te)_3$	7.4-10.2%	Black grey
Kostovite	$CuAuTe_4$	~25.2%	Grayish white
Aurostibnite	$AuSb_2$	43.5-50.9%	White but tarnishes pink
Maldonite	Au_2Bi	64.5-65.1%	Silver white with pink tint

Gold occurs primarily in the form of native gold or as an alloy with Ag (electrum), which represents the most common and economically important forms of gold in many ores. Because Au and Ag form a continuous substitutional solid-solution series, there is no sharp mineralogical boundary between native gold and electrum; instead, compositions grade smoothly from Au-rich to Ag-rich alloys. Native gold is typically high-fineness Au with minor Ag (less than 15 wt%), showing a metallic luster and a characteristic deep yellow color that becomes lighter as Ag increases. Electrum refers to the Ag-rich part of this Au-Ag series, commonly defined as higher than 20 wt% Ag, and its appearance is correspondingly paler, ranging from yellowish to nearly white in high-Ag compositions [12]. Some 70 to 75% of the gold in the deposit occurs as native gold, but a further 20% occurs as tellurides. The remaining 5 to 10% is in the form of invisible gold that has substituted into the crystal structures of various minerals or occurs as minute particles.

Gold-bearing minerals that contain tellurium are called “gold tellurides”, which were first identified in the Golden Mile deposits in May 1896 [13]. The simplest and most common association of tellurium with gold is as the mineral calaverite $AuTe_2$, but other metal associations also occur. Silver associations give rise to the minerals petzite, sylvanite, and krennerite. A gold-telluride association with antimony also occurs with the mineral montbrayite, while kostovite has a copper-gold-tellurium association [14]. Gold tellurides represent a major and, in some districts, economically dominant form of gold occurrence. A classic example is the Golden Mile camp at Kalgoorlie (Western Australia), which has been mined for more than a century and is widely

regarded as a significant Au-(Ag) telluride system; its endowment is on the order of ~1450 t Au, with roughly ~20% of the gold hosted by telluride minerals [15]. Several other well-known deposits also contain a substantial telluride-bound gold component, including Cripple Creek (Colorado; ~875 t Au), Emperor (Fiji; ~360 t Au, with ~10–50% of Au reported as tellurides), and Săcărîmb (Romania) [16]. More recently, the Sandaowanzi deposit (NE China, on the northeastern margin of the Great Xing'an Range) has been reported to contain >25 t Au at an average grade of ~15 g/t [17]. Notably, this deposit has been described as an exceptional case in which precious-metal tellurides constitute the principal gold-bearing ore phase, with >95% of the recovered gold occurring in telluride.

2.2.2 Refractory sulfide gold ore

In mineral processing, gold ores are commonly classified as free-milling, mildly refractory, moderately refractory and highly refractory (Table 2.2), where the free-milling ore type has high gold recovery (>90%) by standard cyanidation, while the refractory one has a recovery of lower than 90% [18].

Table 2.2 Classification of gold ore based on refractoriness

Gold Recovery	Degree of Refractoriness
< 50%	Highly Refractory
50 - 80%	Moderately Refractory
80 - 90%	Mildly Refractory
> 90%	Free Milling

Gold ore refractoriness arises from several factors, including physical encapsulation of native gold and electrum within host minerals, chemical binding of gold as alloys with other metals (e.g., gold tellurides), the presence of submicroscopic invisible gold within sulfide lattices, reactive gangue minerals that drive high cyanide consumption, as well as preg-robbing carbonaceous matter that adsorbs dissolved gold species [19]. As seen in Figure 2.1, free milling ores are typically gold liberation, placers, quartz vein-lode ores, and oxidized ores, which generally show good leachability when ground to 80% passing less than 75 μm [20]. With the evolving landscape of gold mineral resource development and utilization, free milling ores are continuously decreasing, while refractory ores are becoming important. Refractory ores commonly include Fe/As-sulfide ores, Sb/Bi-bearing sulfide ores, telluride ores, and carbonaceous sulfide ores, often showing poor leachability even after grinding. Refractoriness typically results from gold being encapsulated in pyrite/pyrrhotite,

present as solid solution or ultrafine inclusions in arsenopyrite and other As sulfides, tied to Sb/Bi phases that impede cyanidation or host gold in complex inclusions/alloys, bound in Au-Te minerals (e.g., calaverite, sylvanite, petzite), or preg-robbed by carbonaceous matter.

Figure 2.1 Gold ore types based on mineralogical characteristics

Sulfide refractory gold ores are the most common type of refractory gold ore and are typically dominated by pyrite or arsenopyrite hosts. As illustrated in Figure 2.2, gold in sulfide ores can occur across a spectrum of textural associations, ranging from readily liberated particles (Type 1) to progressively more refractory forms, including gold along grain boundaries (Type 2), fully enclosed grains within pyrite/other sulfides (Type 3), gold trapped at intergranular sulfide boundaries (Type 4), gold concentrated in fractures/crystal defects within pyrite (Type 5), and colloidal particles or invisible-gold present as solid solution/chemically bound Au in sulfide lattices (Type 6). In sulfide refractory gold ores, gold deportment is commonly dominated by Types 3 to 6, so grinding alone may not generate sufficient free gold surface area for efficient cyanidation, because the sulfide host remains intact and/or gold occurs at submicron to lattice-bound scales [21]. Microscopic gold inclusions in sulfide minerals cannot typically be extracted by conventional cyanidation nor by many alternative lixiviants (e.g., thiourea, thiosulfate, thiocyanate, halides, and so on). The gold ore must be pretreated to oxidize sulfide minerals associated with gold and to remove other minerals and chemical compounds that interfere with the cyanidation leaching process [22]. Consequently, oxidative pretreatment (e.g., roasting oxidation, pressure oxidation, bio-oxidation, and chemical oxidation) is typically required to decompose sulfide minerals (e.g., pyrite and arsenopyrite), create porosity, and convert locked or invisible gold into a leachable form, thereby improving subsequent gold recovery.

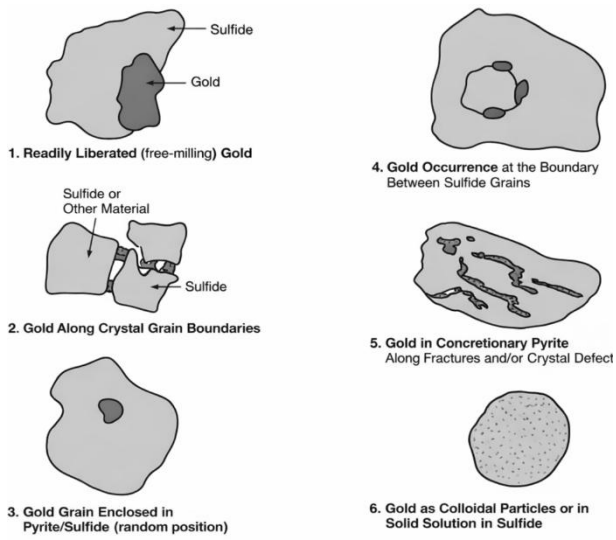

Figure 2.2 Schematic representation of gold associations with sulfide minerals [11]

2.2.3 Roasting oxidation

Roasting oxidation is the earliest pretreatment route for sulfide refractory gold ore. When gold is only locked within pyrite (FeS_2), upon roasting at high temperature (600 ^oC), the pyrite concentrate is converted into an iron-oxide-rich calcine (Fe_2O_3) with a more open, porous texture and higher surface area, which promotes the exposure of ultrafine gold for subsequent leaching (Eq. 2-1) [23]. In the meantime, sulfur is oxidized mainly to SO_2, which is typically captured to produce sulfuric acid rather than atmospheric release [24].

$$4FeS_2 + 11O_2 \rightarrow 2Fe_2O_3 + 8SO_2 \quad (2\text{-}1)$$

When arsenopyrite is dominant, it is first oxidized to magnetite (Fe_3O_4), which is further oxidized to hematite (Fe_2O_3), breaking down the encapsulation of gold (Eqs. 2-2 and 2-3). However, direct roasting can cause Fe_2O_3 to undergo side reactions with As_2O_3 at high temperature, forming a dense secondary encapsulation ($FeAsO_4$) around gold and thereby hindering subsequent gold leaching, as seen in Eq. (2-4) and Eq. (2-5) [25]. Therefore, when the arsenic content is high, a two-stage roasting process is adopted. The first stage is carried out under a mild temperature (400 to 500 ^oC) to remove arsenic, and the second stage is performed under a strongly oxidizing atmosphere (600 to 700 ^oC) for deep desulfurization [26]. Qin et al. [27] investigated a refractory gold ore ($<$ 50% gold cyanidation) with arsenopyrite by a "two-stage roasting" process, the first stage was conducted at 500 °C for 45 min with an air flow rate of 10 mL/min, followed by a second stage at 650 °C for 60 min with an air flow rate of 100 mL/min. The results showed that two-stage roasting successfully removed

arsenic (96.98%) and sulfur (97.19%), increasing the gold exposure to 84.11%. Moreover, combining thiourea leaching enabled a total gold recovery of up to 98.06%.

$$12FeAsS + 29O_2 \rightarrow 6As_2O_3 + 4Fe_3O_4 + 12SO_2 \quad (2\text{-}2)$$

$$4Fe_3O_4 + O_2 \rightarrow 6Fe_2O_3 \quad (2\text{-}3)$$

$$4Fe_2O_3 + As_2O_3 + O_2 \rightarrow 2FeAsO_4 \quad (2\text{-}4)$$

$$Fe_2O_3 + As_2O_5 \rightarrow 2FeAsO_4 \quad (2\text{-}5)$$

Roasting oxidation has undergone rapid innovation in both technologies and equipment. Before the 1940s, rotary kilns and multi-hearth roasters were mainly used to conduct roasting. After 1940, with industrial development, fluidized-bed roasters and circulating fluidized-bed (CFB) roasters were introduced. After the 1980s, oxygen-enriched fluidized-bed roasters emerged [28]. A summary of the first industrial applications of various roasting technologies is provided in Table 2.3. Two-stage roasting, CFB roasting, oxygen-enriched air roasting, and stabilization roasting are all industrial processes all over the world. In recent years, pellet-coating roasting, flash roasting, and microwave-assisted roasting have remained at the laboratory stage, with no reported industrial applications [29].

Table 2.3 The industrial application of roasting technologies in history [28]

Name of Mine	Country	Year	Roasting Technique	Throughput
Goldfields	South Africa	1969	Single-stage roasting	250 t/d
Freepotr McMoRan	United States	1990	Two-stages roasting	3200 t/d
North Kalgoorlie	Australia	1989	Circulating fluidized bed (CFB) roasting	575 t/d
Sprott Mining	United States	1989	Oxygen-enriched air roasting	3600 t/d
Newmont	United States	1996	Stabilization roasting	2160 t/d

2.2.4 Biooxidation

Biooxidation achieves effective pretreatment of sulfide refractory gold ore by employing specific groups of microorganisms, including bacteria, archaea, fungi, eukaryotes, and so on. These microorganisms do not leach the gold itself; instead, they facilitate the liberation of gold by decomposing the surrounding mineral structure into

soluble or less refractory forms. The mechanism of bio-oxidation always involves complicated biochemical or chemical reactions and generally works in two routes: direct microbial oxidation and indirect bio-catalytic oxidation.

Direct microbial oxidation: fungi such as *Phanerochaete chrysosporium* adhere to the surface of the sulfide minerals and initiate oxidation in the presence of dissolved oxygen. Through enzymatic activity, the sulfur component in the sulfide matrix is directly oxidized to sulfate ions (SO_4^{2-}), while iron is released as ferrous ions ($FeSO_4$) [30]. This reaction occurs without the accumulation of intermediate sulfur species, such as elemental sulfur or thiosulfate, which is a distinctive feature of microbial catalysis under these conditions [31].

$$2FeS_2 + 7O_2 + 2H_2O \rightarrow 2FeSO_4 + 2H_2SO_4 \quad (2\text{-}6)$$

$$2FeAsS_2 + 13O_2 + 6H_2O \rightarrow 4FeSO_4 + 4H_3AsO_4 \quad (2\text{-}7)$$

Indirect bio-catalytic oxidation: ferrous iron (Fe^{2+}) is oxidized by microorganisms to ferric iron (Fe^{3+}), which acts as a powerful chemical oxidant to attack the arsenopyrite or other sulfide-containing flotation concentrate, causing sulfide dissolution and regeneration of Fe^{2+} [32]. This cycle continues with the microbial reoxidation of Fe^{2+} to Fe^{3+}, sustaining the oxidative environment. This indirect mechanism significantly enhances the decomposition of sulfide matrices, and this bio-catalytic regeneration of Fe^{3+} is essential in maintaining the oxidative power of the system over time. Microorganisms such as *Acidithiobacillus ferrooxidans* and *At. thiooxidans* play distinct roles in this cycle: the former catalyzes iron oxidation, while the latter contributes to sulfur oxidation, ultimately forming sulfuric acid [33].

$$4FeSO_4 + O_2 + 2H_2SO_4 \rightarrow 2Fe_2(SO_4)_3 + 2H_2O \quad (2\text{-}8)$$

$$2FeAsS_2 + 13Fe_2(SO_4)_3 + 16H_2O \rightarrow 28FeSO_4 + 2H_3AsO_4 + 13H_2SO_4 \quad (2\text{-}9)$$

The world's first gold plant using bio-oxidation pretreatment was commissioned in 1986 at Fairview (South Africa), and the technology was subsequently adopted in the United States, Australia, Ghana, China, and elsewhere. In practice, bio-oxidation of sulfide refractory ore is usually operated under strongly acidic conditions (pH less than 1.5), enabling stable industrial application in China (e.g., 50 t/d at Liaoning Tianli Gold Industry Co., Ltd., and 180 t/d at Shandong Humon Smelting Co., Ltd.) [34]. To reduce acid consumption and broaden operating conditions, recent studies have shifted attention toward near-neutral bio-oxidation. Guillermo et al. [35] reported that *P. chrysosporium* showed higher sulfide-oxidation efficiency at pH 5.8, increasing gold

recovery by 2.4 %. However, studies also indicate that changes in the solution chemistry and mineral matrix can hinder bio-oxidation; for instance, Li et al. [36] showed that dissolution of common gangue minerals (feldspar > mica > quartz) can inhibit pyrite bio-oxidation by releasing interfering ions, forming passivation products (e.g., $FeSO_4 \cdot H_2O$ and $Fe(OH)SO_4$), and reshaping microbial communities.

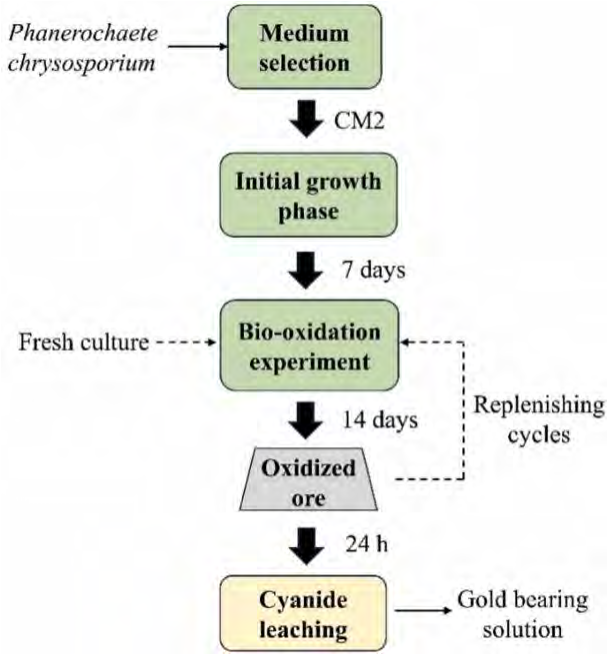

Figure 2.3 General scheme of biooxidation for sulfides using *P. chrysosporium* [35]

2.2.5 Pressure oxidation

Pressure oxidation is a hydrometallurgical process to liberate encapsulated gold in which gold-bearing sulfides are oxidatively decomposed in an acidic or alkaline medium under elevated temperature, high pressure, and an oxygenated atmosphere [37]. The choice between acidic and alkaline is primarily governed by the abundance of gangue minerals. When the gangue is dominated by alkaline-consuming components such as quartz and silicates, an acidic condition is generally preferred; conversely, an alkaline system is adopted when the ore contains gangue that is more problematic under acidic conditions [38].

For acidic oxidation, H_2SO_4 is commonly used as the reaction medium, with typical operating conditions of 180-225 °C, total pressure 2.0-3.5 MPa, oxygen partial pressure 0.35-0.7 MPa, and a residence time of 0.5-2.0 h [39]. During pyrite oxidation, iron is ultimately converted into stable iron oxides (Fe_2O_3), whereas arsenopyrite undergoes a sequence of oxidation reactions in which arsenic is immobilized in the

residue as environmentally benign ferric arsenate phases ($FeAsO_4$) [40]. However, iron oxidation can also generate secondary precipitates; basic ferric sulfate (typically favored at 160-200 °C and H_2SO_4 higher than 20 g L^{-1}) and potassium jarosite (typically favored at 140-200 °C and H_2SO_4 higher than 20 g L^{-1}) may form and re-encapsulate liberated gold, reducing accessibility [41]. Therefore, acidic oxidation flowsheets often include additional steps for phase transformation of basic ferric sulfate and decomposition of jarosite to prevent secondary passivation and maximize gold exposure [42].

Alkaline pressure oxidation is particularly suitable for refractory gold ores whose gangue minerals are alkaline or weakly acidic [43]. Under alkaline conditions, sulfur and iron in sulfide minerals such as pyrite and arsenopyrite are oxidatively decomposed to form iron oxides and sulfates, while arsenic is converted into arsenate species (Eq. (2-10) and Eq. (2-11)) [44]. Historically, alkaline pressure oxidation was first applied in the alumina industry for extracting Al_2O_3 from bauxite [45]; in 1988, Barrick Gold commissioned the world's first alkaline pressure oxidation plant.

$$4FeS_2 + 16NaOH + 15O_2 \rightarrow 2Fe_2O_3 + 8Na_2SO_4 + 8H_2O \quad (2\text{-}10)$$

$$2FeAsS + 10NaOH + 7O_2 \rightarrow Fe_2O_3 + 2Na_2SO_4 + 2Na_3AsO_4 + 5H_2O \quad (2\text{-}11)$$

Pressure oxidation is environmentally attractive because it produces no harmful off-gases and immobilizes arsenic as stable arsenate phases; however, it must be performed in high-temperature, high-pressure autoclaves that require strong resistance to acidic or alkaline media, which increases capital investment, maintenance costs, and the demand for precise process control [46]. Moreover, for highly carbonaceous ores, pressure oxidation is often less competitive than roasting, so synergistic pretreatment strategies are frequently adopted to improve overall performance and economics. For example, Lee et al. [47] studied alkaline pressure oxidation followed by mechanical activation for the carbon- and sulfur-bearing refractory Goldstrike ore (United States) and found that hematite formed during alkaline pressure oxidation could cause secondary encapsulation of liberated gold, limiting gold extraction to 59.5%; in contrast, subsequent mechanical activation (ball-to-ore ratio 5:1, pulp density 50 wt%, 60 mins) reduced the particle size P80 from 56.5 micrometers to 8.54 micrometers and increased gold extraction to 72.1% by thiosulfate leaching (0.2 mol/L $Na_2S_2O_4$ with 50 mg/L Cu^{2+} for 24 h), although further recovery was still constrained because residual gold occurred as ultrafine grains (less than 2 um) locked in sulfides. Similarly, Boduen et al. [48] evaluated combined bio-oxidation and pressure oxidation for a high-sulfur refractory gold concentrate from the Bestobe deposit (Kazakhstan) and observed that direct

cyanidation recovered only 58% gold, bio-oxidation alone (6 days) improved gold recovery to 87% with 78.7% sulfur oxidation; importantly, the combined bio-oxidation and pressure oxidation route delivered about 98% sulfur oxidation and about 97% gold recovery. In this hybrid route, bio-oxidation partially removes sulfur prior to pressure oxidation, allowing operation at higher slurry density and potentially lowering cyanide consumption and overall processing costs.

2.2.6 Chemical oxidation

Chemical oxidation refers to the use of chemical oxidants to oxidatively break down the sulfide host phases that encapsulate gold, thereby increasing gold exposure and improving subsequent gold leaching. Early process reviews of refractory-gold treatment explicitly recognize "chemical pretreatments" as a distinct family alongside roasting, pressure oxidation, and biological oxidation. Chemical oxidants used mainly include nitric acid (HNO_3), ozone (O_3), alkali (NaOH), and persulfate ($S_2O_8^{2-}$).

2.2.6.1 Nitric acid oxidation

Nitric acid (HNO_3) has a strong oxidation potential relative to refractory sulphide ores, and several processes have been reported in the literature for nitric or nitrous acid leaching of complex sulphide ores. Nitric oxide gas produced is further oxidized. The NO produced from this process is used to prepare nitric acid, and a little of the NO is oxidized to NO_2 [49].

$$2FeS_2 + 10HNO_3 \rightarrow H_2SO_4 + Fe_2(SO_4)_3 + 10NO + 4H_2O \quad (2\text{-}12)$$

$$2FeAsS + 8HNO_3 + H_2SO_4 \rightarrow Fe_2(SO_4)_3 + 2H_3AsO_4 + 8NO + 2H_2O \quad (2\text{-}13)$$

$$2NO + O_2 \rightarrow 2NO_2 \quad (2\text{-}14)$$

The Nitrox process, which treats the ore for 1 to 2 h in nitric acid in the presence of air at atmospheric pressure to oxidize pyrite and arsenopyrite before cyanidation, claims to increase gold recoveries from 30% to 90% [50]. Gao et al. [51] studied the oxidation pretreatment of high-arsenic refractory gold concentrate by dilute HNO_3 under mild conditions, including particle size (50-335 μm), reaction temperature (25-85 °C), initial acid concentration (10-30 wt.%), and stirring speed (400-800 rpm). It is obvious that the iron leaching rate increases with the rise of initial HNO_3 concentration, reaction time, and stirring speed, but decreases with the increase of particle size. Oxidation kinetics indicate that the rate of reaction is diffusion-controlled. The activation energies were determined to be 10.70 kJ/mol in the 10% HNO_3 and

12.25 kJ/mol in the 25% HNO_3.

2.2.6.2 Alkali oxidation

Alkali oxidation is a chemical pretreatment in which a strong alkali (most commonly NaOH or CaO) is added to the ore slurry while an oxidizing gas (air or O_2) is introduced, so that sulfide-hosted gold can be oxidatively decomposed and the encapsulation of gold is opened. This approach is particularly effective for refractory ores containing arsenic, sulfur, and even antimony, because oxidation in a highly alkaline medium can transform these phases into more stable and leachable products. Representative reactions involved in the alkaline oxidative breakdown of major sulfide minerals include the following [52]:

$$2FeS_2 + 4NaOH + 3O_2 \rightarrow 2Fe(OH)_2 + 2Na_2S_2O_3 \quad (2\text{-}15)$$

$$FeAsS + 3O_2 + 2NaOH \rightarrow FeAsO_3 + Na_2SO_4 + H_2O \quad (2\text{-}16)$$

In practice, the pretreatment efficiency is strongly governed by alkali concentration, temperature, and particle size: increasing alkali dosage and temperature, and reducing particle size, generally accelerate the oxidation of sulfides and sulfosalts and thus enhance gold exposure. Snyder and co-workers [53] reported that gold recovery increased systematically with higher pretreatment temperature and higher NaOH concentration. Alp and co-workers [54] summarized alkaline pretreatment for a refractory antimony-gold ore and showed that higher temperature and finer grinding all improved gold and silver extraction; alkaline pretreatment decomposed antimony sulfide minerals, achieving up to 98% antimony removal, while increasing gold extraction from below 49% to 83% and silver extraction from below 18% to 90%. Mesa Espitia and co-workers [55] also demonstrated that NaOH pretreatment of an arsenopyrite-rich refractory ore could raise gold extraction to 81%, whereas direct cyanidation and thiosulfate leaching without pretreatment yielded only 23% and 29%, respectively. Alp et al. [56] further reported that potassium hydroxide effectively disrupted gold encapsulation by antimony-bearing phases, and higher KOH concentration and temperature, together with finer particle size, increased gold and silver extraction to 87.6% and 94.5%, respectively, with 85.5% antimony removal.

From a mineralogical perspective, Bidari and co-workers [57] used scanning electron microscopy coupled with energy-dispersive X-ray spectroscopy and electron probe microanalysis to characterize pyrite in an Iranian Carlin-type refractory ore and found that gold tended to occur near the edges of cubic pyrite grains rather than at their

centers; after alkaline oxidative pretreatment, gold extraction increased markedly, consistent with enhanced access to edge-hosted and micro-inclusion gold once the sulfide matrix was oxidatively weakened.

2.2.6.3 Ozone oxidation

Ozone oxidation is a chemical pretreatment in which ozone (O_3) is introduced into an ore slurry (typically by bubbling) to create a highly oxidizing environment that partially oxidizes sulfide minerals. Ozone is a strong oxidant in both acidic and alkaline media, with redox potentials of 2.07 V and 1.24 V, respectively [58]. This strong oxidizing ability allows it to oxidize pyrite-hosted gold and even arsenopyrite-hosted gold under relatively mild temperature and pressure. In practice, ozone can be delivered as ozone bubbles, ozone-saturated water, or even ozone ice, and its effectiveness is strongly governed by gas-liquid mass transfer and solution chemistry. Increasing the ozone fraction in the carrying gas always increases the driving force for ozone transfer into the aqueous phase and generally accelerates sulfide oxidation, promoting gold liberation [59]. A key advantage is that ozonation can often be performed at near-ambient conditions with comparatively simple equipment; however, large-scale deployment has historically been limited by the capital and operating costs of ozone generation, although improved generators and contactor designs have renewed interest.

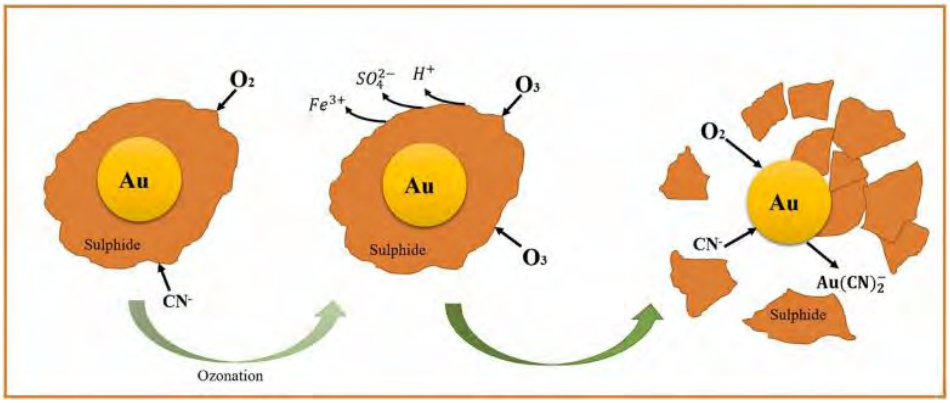

Figure 2.4 A schematic diagram for ozone oxidation of sulfide-hosted gold ore [59]

Published studies consistently show that ozonation can substantially enhance gold recovery from refractory materials. For example, Nava-Alonso and co-workers compared indirect ozonation (repeated washing with ozone-saturated water) and direct ozonation (bubbling ozone into the slurry) for two refractory Mexican ores. The indirect method increased gold recovery for one sample from 53% to 88% and silver recovery from 26% to 78%, while direct ozonation reduced the time required to reach maximum

recovery (for silver) from 40 h to 24 h, indicating that ozonation can both improve recovery and shorten leaching time depending on mineralogy and contact mode [60]. In a South African study on a double refractory ore, Bazhko and Yahorava reported that direct cyanidation recovered only ~10% Au (increasing to 23% when resin was added, evidencing preg-robbing). After acidifying the slurry to pH 1-2 and applying ozonation, sulphide oxidation and partial deactivation of the preg-robbing component markedly improved subsequent cyanidation performance, boosting Au recovery from ~10% to ~70% under the optimized acidic ozonation conditions [61].

2.2.6.4 Persulfate oxidation

Persulfate oxidation is a chemical pretreatment method in which peroxydisulfate ($S_2O_8^{2-}$), typically added as sodium persulfate, potassium persulfate, and ammonium persulfate, is used to oxidize sulfide minerals that encapsulate gold. The key feature of this method is that persulfate can be activated (for example, by heat, ultraviolet irradiation, ultrasound, or catalytic metal ions) to generate highly reactive oxidizing species, especially the sulfate radical ($SO_4^{\bullet-}$) and, through secondary reactions, the hydroxyl radical (•OH), both of which can aggressively attack sulfide lattices. Sulfate radicals are widely recognized for their strong oxidation capability and relatively longer lifetime compared with hydroxyl radicals, which helps sustain oxidation in heterogeneous slurry systems [62].

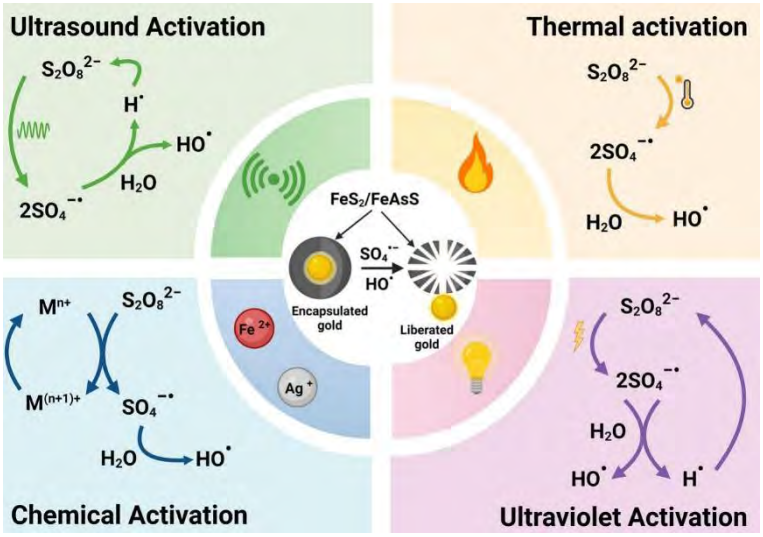

Figure 2.5 Schematic diagram of persulfate oxidation of refractory sulfide gold ore [63]

Recent hydrometallurgical studies have directly demonstrated the value of persulfate oxidation for refractory gold materials. Barbouchi and co-workers developed

a persulfate-based radical pretreatment for a refractory gold concentrate and showed that direct cyanidation recovered only 62.6% gold, whereas persulfate activation substantially improved extraction; among the activation modes evaluated, ultraviolet and ultrasound were the most effective, giving 86.4% (ultrasound) and 88.1% (ultraviolet) gold extraction after pretreatment, and probe tests indicated that sulfate and hydroxyl radicals were the dominant oxidizing species responsible for pyrite/arsenopyrite oxidation [63]. In a related study, Gui et al. reported that ultrasound-activated persulfate efficiently disrupted pyrite structure and achieved a maximum gold leaching efficiency of 86.9% after 3 h of pretreatment, with oxidation efficiency notably higher than conventional thermal activation [64].

From a mineral chemistry perspective, persulfate oxidation can also strongly modify arsenopyrite surfaces. For instance, sodium persulfate treatment was found to oxidize arsenopyrite more strongly than some other sulfides (in flotation-separation contexts) by promoting the formation of hydrophilic oxide species on the arsenopyrite surface, evidence consistent with its ability to oxidatively "open" sulfide-hosted gold textures in pretreatment applications [65]. Key controlling factors for persulfate oxidation in gold pretreatment include oxidant dosage, activation mode, slurry pH/ORP, particle size, and management of secondary products that may passivate surfaces. For example, pyrite oxidation tests comparing strong oxidants found $S_2O_8^{2-}$ to be particularly effective, with an optimum pH window reported around pH 6 for persulfate in that study and oxidation efficiency reaching 76.51% after 6 h, attributed to sulfate-radical formation via Fe^{2+} activation [66].

Overall, persulfate oxidation is attractive because it can provide high oxidative power under comparatively mild conditions and can be intensified through physical activation (e.g., ultraviolet or ultrasound). Its main challenges are oxidant utilization efficiency in slurries, potential radical scavenging by dissolved species, and sulfate-bearing effluents that may require downstream water management.

2.3 Research status of gold oxidizing leaching in cyanide-free systems

2.3.1 General mechanism of gold oxidizing leaching

Due to its noble nature, gold exhibits remarkable resistance to oxidation and corrosion in moisture, air, and most acidic or alkaline environments, dissolving only in aqua regia, a 1:3 mixture of nitric acid and hydrochloric acid [67]. The extraction of gold from its minerals is achieved through hydrometallurgical processes and must rely

on the principles of coordination, wherein gold is transformed into a soluble ionic complex through interaction with suitable ligands. The ligands that can coordinate with gold are very limited, just cyanide (CN^-), thiosulfate ($S_2O_3^{2-}$), thiourea ($CS(NH_2)_2$), thiocyanate (SCN^-), halides (Cl^-, I^-, Br^-), hydrogen sulfide (HS^-), glycine (NH_2CH_2COOH), ammonia (NH_3), and sulfites (SO_3^{2-}) are reported can stable complex with gold in works of literature (Table 2.4). Among them, cyanide has been the dominant lixiviant in the gold mining industry for over a century; in contrast, cyanide-free lixiviants such as thiosulfate, thiourea, thiocyanate, and halide systems remain largely in the experimental or pilot-scale stage, while others are rarely reported.

Table 2.4 Stability constants for gold complexes [68]

Ligand	Au(I) or Au(III) complex	$\log\beta_2$ or β_4
CN^-	$Au(CN)_2^-$	38.3
$S_2O_3^{2-}$	$Au(S_2O_3)_2^{3-}$	28.7
$CS(NH_2)_2$	$Au(NH_2CSNH_2)_2$	23.3
Cl^-	$AuCl_2^-$	9.1
	$AuCl_4^-$	25.3
Br^-	$AuBr_2^-$	12
	$AuBr_4^-$	32.8
I^-	AuI_2^-	18.6
	AuI_4^-	47.7
HS^-	$Au(HS)_2^-$	29.9
NH_3	$Au(NH_3)_2^+$	26.5
Glycine	$Au(NH_2CH_2COO)_2^-$	18
SCN^-	$Au(SCN)_2^-$	17.1
	$Au(SCN)_4^-$	43.9
SO_3^{2-}	$Au(SO_3)_2^{3-}$	15.4

Before the coordination with ligands, gold dissolution proceeds through an initial oxidation step driven by multiple oxidants, wherein gold is transformed from Au(0) to Au(I) or Au(III). This process can release electrons into the surrounding environment to maintain electrochemical neutrality and prevent the buildup of excess electrons, known as electrode polarization. A corresponding electron-accepting process (i.e., reduction of an oxidant) must occur simultaneously [69]. This redox balance underpins an electrochemical model that effectively describes the dissolution behavior of gold, as illustrated in Figure 2.6a. According to this model, oxidation and coordination are coupled to an anode, while the cathode primarily facilitates the electron-accepting reduction of the oxidant [70].

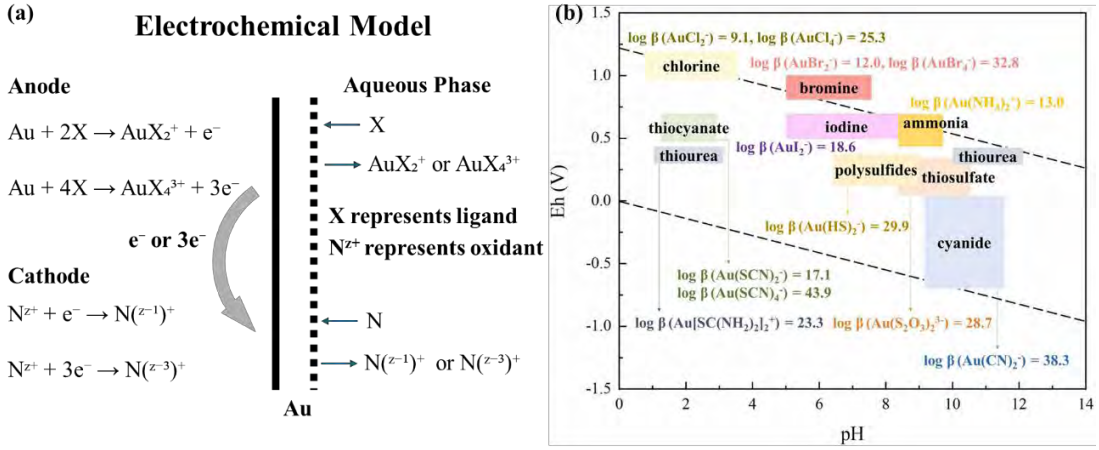

Figure 2.6 (a) Electrochemical model of gold dissolution. (b) Operating Eh-pH regions for different gold lixiviants [71]

Building on this electrochemical framework, the Eh-pH diagram (Figure 2.6b) highlights the central importance of the oxidant: gold can only be activated for dissolution when the solution maintains an Eh high enough to oxidize Au(0) into Au(I)/Au(III) within the relevant pH window. In conventional cyanidation, the exceptionally stable $Au(CN)_2^-$ ($log\beta_2$ 38.3) facilitates dissolution at a comparatively lower oxidative driving force, so dissolved O_2 supplied by air/oxygen is commonly sufficient to serve as the cathodic electron acceptor [72]. In contrast, many non-cyanide lixiviant systems require a more demanding redox environment and are more sensitive to Eh decay; for example, thiosulfate leaching typically relies on Cu(II) (often with NH_3) to mediate gold oxidation, while thiourea leaching commonly needs relatively strong oxidants (Fe(III)) yet also benefits from careful potential control to suppress parasitic oxidation of the lixiviant. Accordingly, research on non-cyanide gold leaching is largely centered on oxidant selection and oxidation-process control to achieve fast, stable, and reagent-efficient dissolution [73].

2.3.2 Thiosulfate leaching with Cu(II) as oxidant

Thiosulfate leaching is a non-cyanide route in which the active lixiviant is the thiosulfate anion ($S_2O_3^{2-}$). Once gold is oxidized to Au(I), it is rapidly stabilized in solution as the highly soluble bis-thiosulfate complex $Au(S_2O_3)_2^{3-}$, which drives continued dissolution by removing Au(I) from the metal surface and shifting the equilibrium forward. As schematically shown in Figure 2.7a, the practical system relies on the Cu(II)-NH_3 complex to initiate and sustain gold oxidation. In anodic micro-regions on the gold surface, cupric ammine $Cu(NH_3)_4^{2+}$ oxidizes Au(0) to Au(I); Au(I) can be transiently stabilized by $Au(NH_3)_2^+$ and is then rapidly converted via ligand

exchange to the more stable $Au(S_2O_3)_2^{3-}$. In cathodic regions, Cu(II) is reduced to Cu(I) (often present as thiosulfate complexes), and dissolved O_2 in air re-oxidizes Cu(I) back to Cu(II), closing the redox-catalytic cycle. Overall, NH_3 is essential because it keeps Cu(II) soluble in alkaline media and accelerates effective Au(I) capture by thiosulfate [74]. Nevertheless, a major drawback highlighted in Figure 2.7b is the parasitic oxidation/decomposition of thiosulfate that leads to excessive reagent consumption: $S_2O_3^{2-}$ can be oxidized by $Cu(NH_3)_4^{2+}$ to tetrathionate ($S_4O_6^{2-}$) and other polythionates, which may further transform along sulfur-oxyanion pathways toward $SO_3^{2-}$and SO_4^{2-}; mechanistically, thiosulfate can enter the Cu(II) coordination sphere at an axial site to form a mixed-ligand intermediate (often described as $Cu(NH_3)_4S_2O_3$, enabling inner-sphere electron transfer where Cu(II) is reduced while thiosulfate is oxidized and thiosulfate may also self-decompose or be converted to S^0, S^{2-}, and SO_3^{2-}.

$$Au + 5S_2O_3^{2-} + Cu(NH_3)_4^{2+} \rightarrow Au(S_2O_3)_2^{3-} + 4NH_3 + Cu(S_2O_3)_3^{5-} \qquad (2\text{-}17)$$

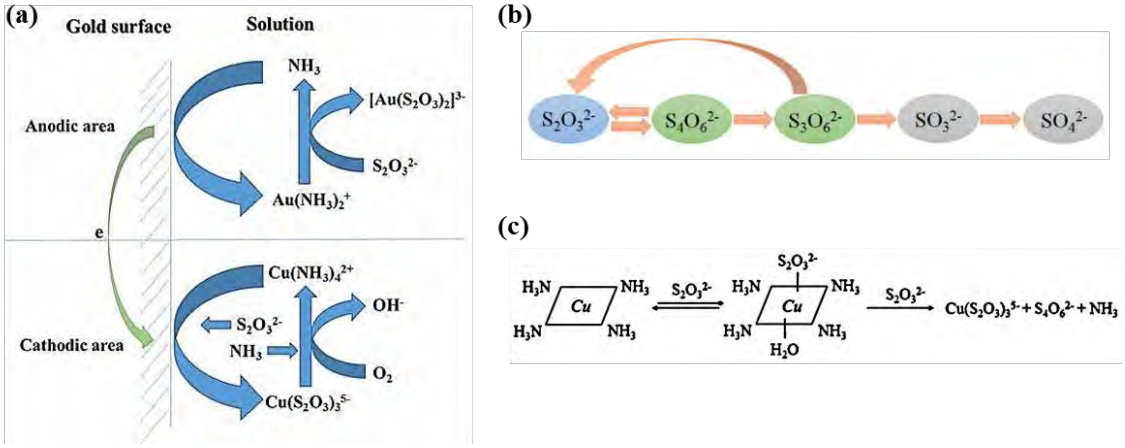

Figure 2.7 (a) Electrochemical model of gold dissolution by thiosulfate. (b) Oxidation of thiosulfate. (c) Thiosulfate react with $Cu(NH_3)_4^{2+}$ [74]

A widely adopted approach to curb the excessive thiosulfate consumption in the Cu(II)-NH_3 system is the use of additives (Table 2.5), such as triethanolamine (TEA), EDTA, amino acids (L-histidine), humic acid (HA), carboxymethyl cellulose (CMC), thiourea, thiocyanate, and so on. These additives mainly work via two complementary routes: (i) tuning copper redox chemistry and (ii) modulating interfacial reactions to mitigate passivation**.** Chelating agents (TEA, EDTA, amino acids) partially "bind and shield" Cu(II)/Cu(I), reducing the activity of free Cu(II) that catalyzes thiosulfate oxidation, while adjusting the mixed potential to a window that still supports Au oxidation but suppresses thiosulfate decomposition [75-77]. In parallel, macromolecular organics (CMC, HA) improve surface conditions by adsorption-

induced charge regulation and enhanced dispersion/hydrophilicity, thereby limiting the deposition of hydrophobic decomposition products and inhibiting the formation of passivating layers on gold and ore surfaces [78, 79]. Sulfur-containing additives provide an additional benefit: thiourea can facilitate rapid removal of Au(I) via cooperative Au(I)-thiourea complexation, whereas SCN^- tends to suppress thiosulfate breakdown and the generation of passivating species such as S^0 and Cu_2S [80, 81].

Table 2.5 Additives for thiosulfate leaching in Cu(II)-NH_3 system

Additives	Ore types	Leaching efficiency	Thiosulfate consumption	Ref.
TEA	Low sulfur gold concentrate	73.4%	32% decreased	[75]
EDTA	Sulphide gold ore	~100%	3.85 kg/t	[76]
L-histidine	Pyrite concentrate	~65%	4.5 kg/t	[77]
CMC	Sulphide gold ore	~100%	/	[78]
HA	Refractory gold concentrate calcine	81.4%	13.2%	[79]
Thiocyanate	Gold concentrate calcine	88.45%	79.37 kg/t	[80]
Thiourea	Gold concentrate calcine	91.7%	/	[81]

A second strategy, closely aligned with the above, is to replace ammonia with ammonia-free ligands that can deliver the same enabling functions (i.e., Cu(II) stabilization and redox mediation) while avoiding NH_3-related environmental and handling concerns. In the Cu-thiosulfate system, excessive thiosulfate loss is largely triggered by free Cu(II) that catalyzes $S_2O_3^{2-}$ oxidation to tetrathionate/polythionates and promotes passivating deposits (S^0, Cu_xS). Accordingly, NH_3 substitutes, typically organic ligands bearing amine and carboxylate groups**,** are designed to strongly chelate Cu(II) and reshape its coordination sphere. As summarized in Table 2.6, ligands such as ethylenediamine (en) [82], citrate (Cit) [83], EDDHA [84], malic acid (Mal) [85], tartrate (Tart) [86], and glycine [87] form Cu(II)-ligand chelates with high stability, which reduces the availability of free Cu(II) and thereby suppresses Cu(II)-driven thiosulfate decomposition and reagent loss. At the same time, these chelating environments often buffer the mixed potential (Eh) to a lower, more stable window**,** decreasing the propensity for thiosulfate oxidation and limiting the formation of passivating sulfur/copper sulfide species, while still maintaining sufficient oxidative capacity for Au dissolution. In this sense, ammonia replacement functions as a “built-in” chemical control lever, simultaneously managing copper speciation and redox conditions, to improve thiosulfate utilization efficiency and leaching stability in NH_3-

free systems.

Table 2.6 Current investigations on alternative ligands for thiosulfate leaching

Ligand	Ore types	Leaching efficiency	Thiosulfate consumption	Ref.
Ethanediamine	Gold ore	80.3%	4.14 kg/t	[82]
citrate	Free milling ore	~84.5%	~7.5 kg/t	[83]
EDDHA	Rosted gold concentrate	82.84 %	10.54 kg/t	[84]
Malic Acid	Refractory gold concentrate	65.45%	15.2 kg/t	[85]
Tartrate	Carbonaceous gold concentrate	73.69%	~0	[86]
Glycine	Rosted gold concentrate	75.1%	13.6%	[87]

The thiosulfate leaching of precious metal was initially proposed in the 1900s, known as the Von Patera Process [88]. In the late 1970's, the ammonia thiosulfate was applied to recover the precious metals from the flotation concentrate of copper-bearing sulfide by pressure leaching [89]. In the following years, more work has been done on the atmospheric thiosulfate-ammonium-cupric ion system. The commercialization of a thiosulfate gold leaching has become a reality in 2014 at the Barrick Goldstrike mine in Nevada [90]. Nevertheless, despite its advantages in environmental and human-health terms, thiosulfate has not replaced cyanidation at an industry-wide scale, largely because persistent challenges, especially high reagent consumption and process-control complexities, still limit broad deployment beyond selected ore types and operations.

2.3.3 Thiourea leaching with Fe(III) as oxidant

Thiourea (TU), $(NH_2)_2CS$, is a soft S-donor ligand with a resonance-stabilized C=S group, and it binds Au(I) predominantly through sulfur to form the stable linear complex $Au(TU)_2^+$ [91]. Acidic media are most widely used because thiourea is comparatively more stable in strong acid but decomposes much more readily as acidity decreases, which reduces the effective ligand concentration available for gold complexation. Consistent with this rationale, Table 2.7 shows that acidic systems (near pH 1.0) achieve strong gold leaching, especially from electronic wastes. In such acidic conditions, the Fe(III) is widely considered an appropriate oxidant pair because it can efficiently oxidize Au^0 to $Au(TU)_2^+$ while being reduced to Fe(II), and both iron species generally remain highly soluble [92].

$$Au + 2SC(NH_2)_2 + Fe^{3+} \rightarrow Au(SC(NH_2)_2)_2^+ + Fe^{2+} \qquad (2\text{-}17)$$

Table 2.7 Optimal parameters for acidic thiourea leaching from e-wastes

[TU]	[Fe^{3+}]	Acidity	Temperature	Leaching time	Gold recovery	Ref.
70 g/L	13 g/L	1.8 M H_2SO_4	Ambient	7 h	100%	[93]
24 g/L	6 g/L	pH 1.0	25 °C	2 h	90%	[94]
38.06 g/L	0.5 g/L	0.05 M H_2SO_4	45 °C	2 h	90%	[95]
20 g/L	6 g/L	pH 1.4	Ambient	3.5 h	82%	[96]
24 g/L	6 g/L	pH 1.0	25 °C	39 h	50%	[97]

Controlling ferric iron concentration is critical in acidic thiourea leaching because Fe(III) largely governs the solution redox potential (Eh), thereby dictating the extent of thiourea oxidation and reagent loss. Under moderately oxidizing conditions, thiourea is reversibly converted to formamidine disulfide (FDS) via the TU/FDS redox couple ($E^\circ \approx 0.42$ V in acidic media, Eq. (2-18)), and FDS can participate in (and even catalyze) the anodic dissolution of gold [98]. However, when the potential becomes overly oxidizing, FDS is driven toward irreversible degradation pathways that generate more oxidized sulfur species (e.g., elemental sulfur/colloids and ultimately sulfate) together with nitrogen-containing byproducts (e.g., cyanamide and its hydrolysis products), leading to accelerated thiourea consumption and deteriorated process economics [99]. Consequently, practical operation requires maintaining an appropriate oxidant level (and Eh window) that sustains productive Au dissolution while suppressing over-oxidation of thiourea; notably, the TU/FDS ratio has been reported to strongly affect stability, with an excess of thiourea (TU/FDS 10:1) minimizing thiourea decomposition while maintaining a high dissolution rate [100].

$$2SC(NH_2)_2 \rightarrow (SC(NH)NH_2)_2 + 2H^+ + 2e^- \qquad (2\text{-}18)$$

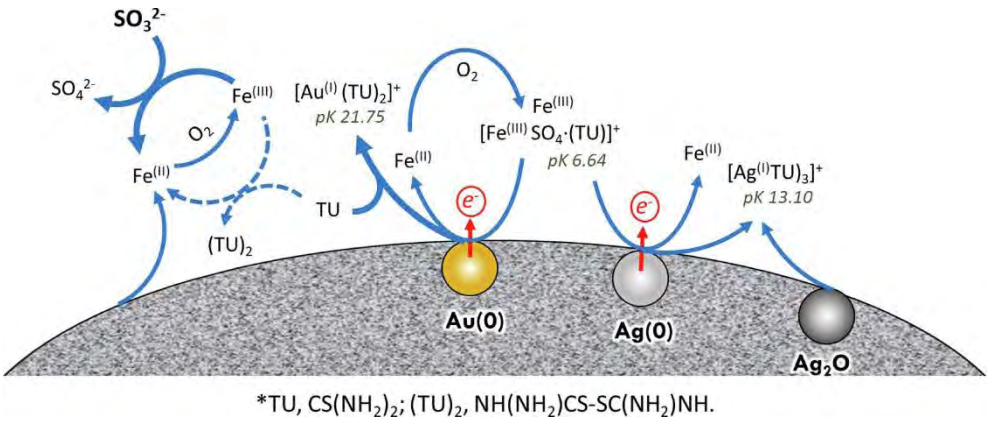

Figure 2.8 Schematic illustration of thiourea (TU) leaching of Au and Ag [101]

Compared with acidic thiourea media, where protonated thiourea is more reactive but corrosion and non-selective dissolution of base metals are serious, alkaline

conditions can improve selectivity toward Au by suppressing the dissolution of many associated metals, yet they introduce a fundamental stability problem: thiourea becomes chemically unstable as pH increases (often cited as unstable above pH 4.3) and is prone to decomposition, producing intermediate sulfur species and eventually elemental sulfur that passivates the gold surface and arrests dissolution [102]. Because Fe^{3+} is not stable at high pH (rapid hydrolysis/precipitation), alkaline thiourea systems typically rely on milder oxidizing environments, most commonly dissolved oxygen, so that the solution potential is sufficient to sustain Au oxidation while minimizing over-oxidation of thiourea; the cathodic half-reaction can be expressed as:

$$O_2 + 2H_2O + 4e^- \rightarrow 4\ OH^- \qquad (2\text{-}19)$$

Accordingly, alkaline thiourea leaching is usually “additive-driven”, where stabilizers (and sometimes auxiliary oxidants) are introduced to simultaneously (i) suppress thiourea’s irreversible degradation and sulfur passivation, and (ii) maintain a redox window favorable for $Au(Tu)_2^+$ persistence and Au dissolution [103]. Sodium sulfite (Na_2SO_3) is the most widely reported stabilizer [104]: electrochemical studies show it markedly increases the anodic dissolution current of Au in alkaline thiourea, lowers the polarization/dissolution potential, improves selectivity, and can reduce the apparent activation energy, yet it may be consumed significantly because sulfite itself is oxidizable in the relevant potential range [105, 106]. Mechanistically, sulfite also helps stabilize Au(I)-thiourea chemistry at alkaline pH, where $Au(Tu)_2^+$ otherwise tends to undergo irreversible decomposition/deprotonation and form a solid phase. Beyond sulfite, sodium silicate (Na_2SiO_3) and sodium selenite (Na_2SeO_3) have been evaluated as alternative stabilizers; comparative work indicates Na_2SiO_3 can provide stronger stabilization than Na_2SO_3 (e.g., substantially lowering thiourea decomposition and producing higher Au dissolution currents at comparable potentials), making it a promising “efficient stable reagent” for alkaline thiourea systems [107, 108].

Thiourea leaching of gold was first reported in 1941 and has since undergone several waves of renewed academic interest, particularly after mechanistic and electrochemical studies clarified the key role of controlled redox conditions and Au–thiourea complex formation [109]. Nevertheless, unlike cyanidation, thiourea has never been firmly established as a mainstream industrial technology; only a limited number of industrial applications were reported during the period 1984 to 1992 [110], and most subsequent efforts remained at laboratory or pilot scale [111]. This gap between research and commercialization is largely attributed to intrinsic process drawbacks,

especially thiourea's oxidative instability and associated high reagent consumption (often accompanied by sulfur-containing byproducts and surface passivation), together with the need for tight potential control and downstream solution management. Looking forward, thiourea is more likely to expand in niche scenarios rather than fully replace cyanide: for example, in jurisdictions where cyanide use is restricted, in certain selective flowsheets, and in circular-economy applications such as e-waste/urban mining, where pilot-scale demonstrations have been reported. Its broader industrial prospects will depend on whether advances in stabilizers/oxidants management and closed-loop reagent/recovery strategies can simultaneously deliver acceptable economics, robustness, and environmental compliance.

2.3.4 Thiocyanate leaching with Fe(III) as oxidant

Thiocyanate leaching, in which thiocyanate anions (SCN^-) coordinate dissolved gold, was first reported by White in 1905 [112] and later revisited for acidic, ferric-based systems by Fleming and others [113]. Structurally, thiocyanate is an ambidentate ligand (able to bind through N or S), and its bonding mode depends strongly on the hardness of the metal center; soft metal ions tend to prefer sulfur coordination. In acidic media, metallic gold is oxidized to Au(I) and stabilized by thiocyanate to the linear dithiocyanatoaurate (I) species, $Au(SCN)^{2-}$, consistent with crystallographic observations that gold (I) in thiocyanatoaurate environments is frequently two-coordinate and sulfur-bonded. Under more strongly oxidizing conditions, higher-coordination Au (III)-thiocyanate complexes (i.e., $Au(SCN)_4^-$) can form, but maintaining an appropriate redox potential is generally critical to favor fast dissolution while limiting reagent loss [114].

In practice, thiocyanate leaching is usually operated in a highly acidic solution. The Fe(III)/Fe(II) couple is widely used to supply the oxidizing power, where Fe(III) remains soluble at low pH and can be reduced to Fe(II) while gold is oxidized and complexed, as seen in Eq. (2-20) [115]. A representative case is an oxide gold ore optimized by response surface methodology, where 96% gold extraction was achieved at room temperature using a 500 mM thiocyanate solution together with 100 mM Fe(III) at acidic pH 2 and high 50% pulp density, illustrating that thiocyanate can be a viable cyanide-free lixiviant when the redox and ligand levels are properly controlled [116]. The most influential gold leaching parameters appear to be initial thiocyanate and oxidant concentrations, especially the Fe(III)/SCN^- ratio. On the one hand, the process of thiocyanate leaching is closely linked to redox balance: accumulation of Fe(II)

depresses the solution redox potential and can slow gold oxidation unless Fe(II) is re-oxidized (for example, by aeration/oxygen or other regeneration strategies), so controlling the Fe(III) to Fe(II) ratio is a key operational lever. On the other hand, Fe(III) forms thiocyanate complexes (e.g., $Fe(SCN)_4^-$ and $Fe(SCN)_2^+$), which can "tie up" both oxidant and ligand, lowering the effective activities of free Fe(III) and free thiocyanate available for gold dissolution, and thereby shifting kinetics and reagent demand.

$$Au + 2\ SCN^- + Fe^{3+} \rightarrow Au(SCN)^{2-} + Fe^{2+} \qquad (2\text{-}20)$$

Thiocyanate itself participates in several competing reactions that define both performance and cost. A central drawback is that thiocyanate can be oxidized in Fe (III)-containing acidic solutions through an autoreduction pathway (Fe^{3+} is spontaneously reduced while thiocyanate is oxidized), generating reactive intermediates such as thiocyanogen ($(SCN)_2$) and trithiocyanate ($(SCN)_3^-$) that can transiently act as oxidants/complexants but decompose rapidly by hydrolysis into more stable products, which ultimately manifests as thiocyanate consumption. Thiocyanate can also contribute to surface phenomena: depending on solution chemistry and potential, passive layers (for example, Au(I) thiocyanate-type surface species) have been reported that can retard dissolution, so maintaining suitable acidity, ligand level, and redox potential is important to avoid passivation. Finally, thiocyanate is prone to nonproductive complexation with impurity metals (notably copper), which can further increase reagent consumption and complicate solution management in real ores and concentrates.

Additives are therefore mainly introduced to (i) suppress thiocyanate oxidation, (ii) keep Fe^{3+} available as an oxidant without excessively sequestering thiocyanate, and (iii) mitigate impurity-metal side reactions. Glycine has been reported to reduce thiocyanate consumption by forming comparatively stable Fe(III)-glycine complexes, which can lessen thiocyanate oxidation in acidic media while maintaining gold extraction performance [117]. Mixed-ligand strategies can also be beneficial: adding small amounts of thiourea to Fe(III)-thiocyanate solutions can create a synergistic enhancement in gold dissolution rate and, notably, thiocyanate becomes "considerably more stable towards oxidation" in the presence of thiourea in such mixed systems [118]. In parallel, iodide/iodine additions have been reported to improve dissolution in Fe(III)-thiocyanate media by stabilizing reactive iodine-thiocyanate intermediates (i.e., I_2SCN^- and $I(SCN)_2^-$) and counteracting rapid hydrolytic loss of thiocyanate-derived oxidizing species, thereby boosting kinetics at comparable conditions [119].

2.3.5 Iodide leaching with iodine as oxidant

Iodide leaching is a cyanide-free process in which iodide (I^-) complexes the dissolved gold ions, while iodine (I_2) provides oxidizing power through the formation of triiodide (I_3^-). In aqueous solution, I_2 rapidly associates with I^- to generate I_3^-, as seen in Eq. (2-21), and thermodynamic analysis indicates that I_3^- is the predominant oxidizing species in iodide-iodine systems [120]; thus, the leaching chemistry is often described as a synergy where I^- acts as the complexant and I_3^- acts as the oxidant [121]. A commonly accepted pathway is oxidation of Au^0 to Au(I) followed by stabilization as the soluble diiodoaurate(I) complex (i.e., AuI_2^-), with possible formation of tetraiodoaurate(III) (i.e., AuI_4^-) under stronger oxidizing conditions, as seen in Eqs. (2-22) and (2-23) [122].

$$I^- + I_2 \rightarrow I_3^- \qquad (2\text{-}21)$$

$$2Au + I_3^- + I^- \rightarrow 2AuI_2^- \qquad (2\text{-}22)$$

$$2Au + 3I_3^- \rightarrow 2AuI_4^- + I^- \qquad (2\text{-}23)$$

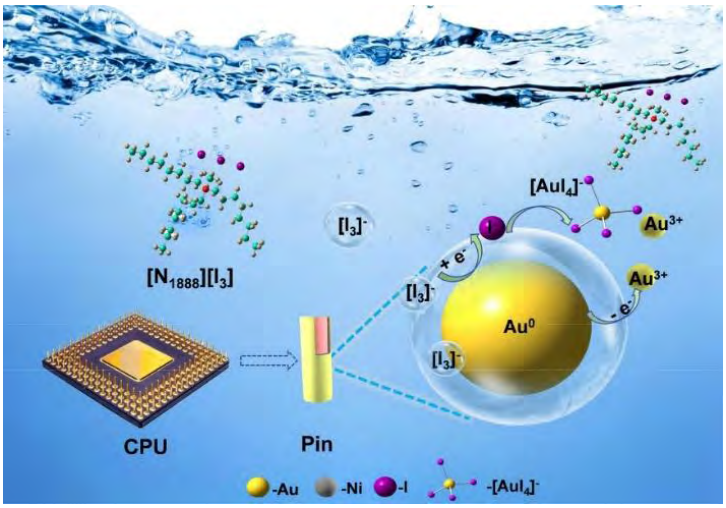

Figure 2.9 Schematic diagram of gold iodide leaching [123]

From an application standpoint, iodine-iodide leaching can achieve high extraction from suitable feeds but is sensitive to ore chemistry and solution management. For instance, for an oxide gold ore, leaching with 20 g/L iodide and 4 g/L iodine reached 77% gold extraction in 6 h and 89% in 24 h, whereas a carbonaceous ore showed only ~20% extraction even at higher iodine, attributed to adsorption of gold-iodide complexes by organic matter; the same work also notes that sulfide/ferrous minerals consume iodine over time [124]. Batnasan et al. demonstrated an iodine-iodide leaching process to recover valuable metals from waste printed circuit boards. The results

indicated that more than 99% of gold was dissolved, while less than 1% of silver and palladium were dissolved under the conditions: iodine/iodide mass ratio of 1/6, pulp density of 10%, agitation speed of 500 rpm, 24 h, and 40 °C [125]. For refractory feeds after oxidation pretreatment, iodide-iodine leaching has also been tested: a roasted auriferous pyrite–arsenopyrite concentrate showed a reported maximum gold recovery of ~60% at 2.6 g/L I_2 and 5.1 g/L I^-, and surface passivation by AuI has been discussed under certain high-oxidant/pH windows. Beyond primary ores, iodide-iodine systems have been actively explored for urban mining, such as integrating pretreatment (for example, supercritical water oxidation) with iodine-iodide leaching to recover precious metals from waste mobile-phone printed circuit boards [126].

A major bottleneck for industrial implementation is not only the cost and consumption of iodine, but also the treatment of pregnant solutions and reagent recycling. Recent studies explicitly point out that iodination leaching is attractive yet challenged by high reagent cost and difficult solution treatment, motivating paired recovery-regeneration strategies [127]. For gold recovery from iodide liquors, strong-base anion-exchange resins can load gold iodide complexes effectively, but triiodide loads extremely strongly and can dissociate/deposit iodine on the resin, fouling the surface and complicating operation [128]. Electrochemical routes are therefore receiving attention because they can couple gold recovery with iodine regeneration (reducing net iodine consumption), and electrodeposition-based schemes have been proposed as a more “closed-loop” approach for iodide systems [129].

2.3.6 Chloride leaching with chlorine as oxidant

Chloride leaching with chlorine is a halide-based route in which chlorine provides the oxidizing power and chloride stabilizes dissolved gold as chloro-complexes. Chlorine is typically introduced by bubbling Cl_2 gas, in situ generation (for example, from hypochlorite and hydrochloric acid), or electro-generation of aqueous chlorine in brines, all of which supply reactive “active chlorine” species in solution [130]. In chloride-rich media, gold dissolution is driven by oxidation of Au(0) to Au(I) or Au(III) and complexation to soluble species, most commonly dichloroaurate (I), $AuCl_2^-$, and tetrachloroaurate (III), $AuCl_4^-$ [37]; for instance, Au (III) formation can be represented by Eq. (2-24). The strong oxidizing nature of chlorine-based oxidants is reflected by their high standard potentials (e.g., $E^0_{(Cl_2/Cl^-)} \approx 1.359$ V and $E^0_{(HClO/Cl^-)} \approx 1.495$ V), which enables rapid oxidation of gold when sufficient chloride is present to stabilize the product complexes [37].

$$2Au + 3Cl_2 + 2Cl^- \rightarrow 2AuCl_4^- \qquad (2\text{-}24)$$

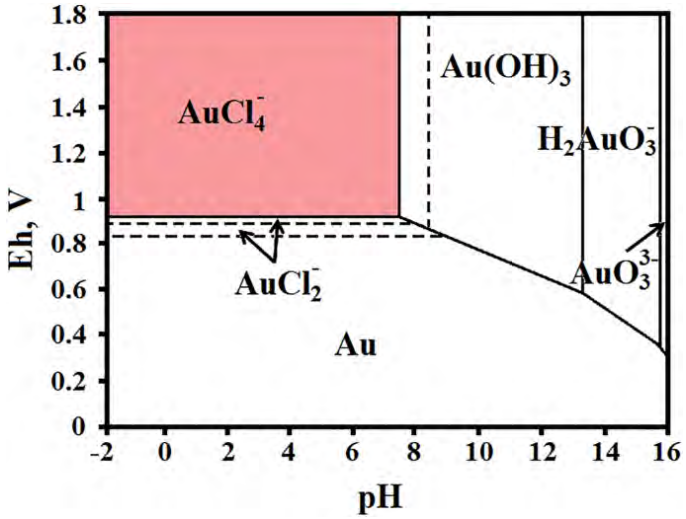

Figure 2.10 Eh–pH diagram of the Au-Cl-H_2O system [131]

Recent studies illustrate how chloride-Cl_2 systems can be engineered for different complex feeds. For metallurgical residues, wet chlorination has been applied after oxidative pretreatment to improve selectivity and oxidant utilization; Olteanu and co-workers reported that the highest gold extraction (98%) from copper-gold slags was obtained using chlorine in the presence of hydrochloric acid, where chlorine was generated in situ by reacting hypochlorite with hydrochloric acid, and the required solution potential for fast leaching (and avoiding gold reduction) was around 950 mV vs. Ag/AgCl [130]. For refractory concentrates, Pak et al. proposed a flowsheet combining pressure oxidation and chlorination leaching, achieving 96.54% gold leaching at pH 4, redox potential above 1.0 V, 75 g/L sodium chloride, 40 °C, and 2 h leaching time [37]. For urban mining, Ilyas et al. demonstrated electro-Cl_2 leaching of printed circuit board waste in brine, reporting >99% gold leaching in 2.0 mol/L sodium chloride at pH 1.0, 50 °C, and 75 min, highlighting the effectiveness of in situ chlorine generation for impurity-rich secondary streams [132].

Despite strong kinetics, industrial implementation of Cl_2-based chloride leaching is mainly limited by chlorine handling/safety, corrosion demands (acidic, chloride-rich, and oxidizing), and the need to capture and recycle unreacted chlorine to reduce emissions and reagent costs [133]. In this context, closed-loop concepts such as electrogenerated chlorine with “innocuous treatment” (electrochemical reduction of unconsumed chlorine back to chloride for reuse) have been proposed to improve process safety and sustainability, demonstrating that chlorine losses can be minimized when leaching and recycling are integrated in a single system [134]. Finally, it is worth

noting that chlorination has historical precedent, used extensively before cyanidation and revisited for certain refractory feeds, yet modern development focuses on safer, more controllable chlorine delivery (electro-generation or in situ formation) and improved downstream solution management to make chloride leaching more practically competitive [133].

2.3.7 Bromide leaching with bromine as oxidant

The main dissolved gold species of bromide leaching are typically aurous $AuBr_2^-$ and, under bromine (Br_2) as oxidant, auric $AuBr_4^-$, consistent with halide complexation behavior of Au(I)/Au(III) and with measured Au(III) halide complex speciation in actual systems (Eq. 2-25). Operationally, bromide systems are often reported to deliver fast gold dissolution kinetics, but they require careful control of Br_2 demand and side reactions. An electrochemical study summarized "typical" bromide leaching conditions on the order of 2-5 g/L bromine, 0-10 g/L sodium bromide, pH 5-6, and a redox potential around ~612 mV versus saturated calomel electrode (SCE), illustrating that effective leaching can be achieved under mildly acidic to near-neutral conditions, unlike many chloride, thiourea and thiocyanate systems that rely on very low pH [135]. At the same time, the broader review literature emphasizes that gold dissolution depends on the bromine-bromide ratio and on the associated minerals in the ore because some dissolved metal species, such as Fe(II), can consume bromine, which directly affects reagent consumption and achievable extraction [133].

$$2Au + 3Br_2 + 2Br^- \rightarrow 2AuBr_4^- \qquad (2\text{-}25)$$

Practical bromide leaching prefers to generate liquid bromine (Br_2) in situ to avoid handling toxic elemental Br_2. Sousa and co-workers evaluated in situ produced bromine for a Portuguese auriferous ore using $NaBr_2$, NaOCl, and HCl (reagents that are easier to handle than elemental bromine), and reported up to ~89% gold dissolution after roasting pretreatment (and ~80% with combined oxidant additions) under elevated-temperature, short-time leaching conditions [136]. This work also explicitly notes that elemental bromine is hazardous and difficult to store/transport, which is a central reason why modern bromide leaching research frequently focuses on bromine generation inside the reactor rather than bulk bromine handling. More interestingly, bromine-based chemistry has also been extended to complex secondary feeds by using "bromine donors" that generate active bromine in situ. For example, studies using N-bromosuccinimide-based systems report that released bromine/active bromine species can rapidly oxidize metallic gold to form soluble $AuBr_4^-$, enabling efficient gold

extraction and supporting the feasibility of bromine-mediated leaching routes for impurity-rich materials when oxidant delivery is engineered [137].

Finally, downstream gold recovery from bromide liquors has been investigated using anion-exchange resins, where gold bromo-complexes can show high resin loading capacity, suggesting potential process advantages if bromine recycle and solution management are integrated effectively [138]. In summary, this bromide route is kinetically strong yet engineering-limited. It can leach gold rapidly, but practical adoption depends on controlling bromine hazards, favoring in situ bromide generation, minimizing bromine consumption, and closing the loop on gold recovery and reagent recycle [136].

2.4 Prospects for the application of advanced chemical oxidation in gold hydrometallurgy

2.4.1 Free radical-based oxidation reaction

Free radical-based oxidation processes refer to highly reactive oxygen species (ROS), most notably hydroxyl radicals (•OH) and sulfate radicals ($\bullet SO_4^-$) generated from the activation of oxidant precursors (e.g., ozone, hydrogen peroxide, persulfate, peroxymonosulfate, etc.), which can drive a variety of electron transfer-based oxidation reactions [139]. For example, in the classic Fenton reaction, Fe^{2+} as an activator can cleave the peroxide bond of H_2O_2 to produce •OH, which is a strong oxidizing species with a standard redox potential of 1.9-2.7 V vs. normal hydrogen electrode [140]. Similarly, persulfate ($S_2O_8^{2-}$) and peroxymonosulfate (HSO_5^-) can be activated by heat, ultraviolet, ultrasound, electrochemistry, or catalysis to form sulfate radicals ($\bullet SO_4^-$), with a standard redox potential of 2.6-3.1 V, which can further yield •OH and other reactive oxygen species through secondary pathways, such as superoxide radicals ($\bullet O_2^-$) and singlet oxygen ($^1O_2$), with standard redox potential of 0.89~1.7 V and 2.2 V, respectively [141].

Although free radical-based oxidation reactions were previously developed for degrading organic pollutants, recent studies show a clear expansion into the area of hydrometallurgical resource recovery. Specifically, free-radical chemistry is used to accelerate oxidative leaching of valuable metals from ores or secondary resources. For example, $\bullet SO_4^-$ and •OH have been used in lithium battery recycling to selectively recover Li by a clean hydrometallurgical leaching route [142]. Ultrasound-persulfate coupling has been reported as an eco-friendly decopperization route for copper anode

slime (a typical metallurgical residue), and $\bullet SO_4^-$ efficiently achieved leaching ~98% copper into soluble sulfate [143]. More broadly, free-radical oxidation has also been applied to phase activation to improve conventional acid leaching, e.g., $\bullet SO_4^-$-driven oxidation of Cu_2O surfaces has been used to boost the efficiency of copper extraction by enhancing interfacial electron transfer and creating more leachable surface chemistry [144]. Moreover, a particularly relevant signal for precious-metal hydrometallurgy is that persulfate has been demonstrated for the selective recovery of Pd and Au from spent catalysts, indicating that free-radical strategies can be designed not only for base-metal but also for targeted noble-metal when coupled with an appropriate reaction [145].

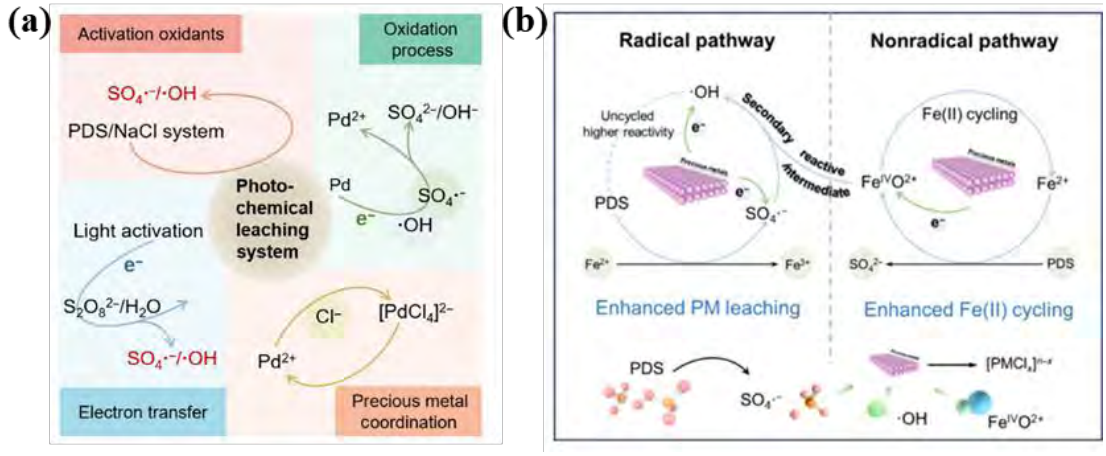

Figure 2.11 Dissolution mechanism of precious metals in the (a) peroxydisulfate/NaCl and (b) peroxydisulfate/$FeCl_2$ solution [145]

Free radical-based oxidation reactions are also attractive in the research area of gold hydrometallurgy, especially for both pretreating sulfide refractory gold ores and building cyanide-free leaching systems. The exceptionally strong oxidative power of free radicals (e.g., $\bullet SO_4^-$ and $\bullet OH$) is sufficient not only to dissolve pyrite but also to oxidize metallic gold. Besides, the generation of free radicals can be implemented as a whole chemical activation route, relying on easy-to-handle oxidant precursors (e.g., H_2O_2 and persulfate) without necessarily introducing extra high temperature and pressure, which is advantageous for simple, scalable operation [146]. More importantly, free radicals generally proceed more efficiently in acidic media, which aligns well with the chemical oxidation of sulfide minerals and with many acidic cyanide-free leaching systems (e.g., thiourea, thiocyanate, and chloride). Last but not least, free radical-based oxidation processes are often viewed as relatively green and environmentally friendly because the oxidant precursors ultimately yield benign end products (e.g., sulfate and

water) and can avoid toxic gas, supporting safer and cleaner gold extraction flowsheets.

2.4.2 Transition metal complex-catalyzed oxidation reaction

Transition metal ions, with variable valence, are widely used in the field of hydrometallurgy as oxidants to catalytically dissolve metals via redox electron-transfer reaction [147]. Typically, the dissolution of valuable metals from minerals by transition metal ions is a galvanic reaction. The high-valence species (e.g., Fe(III) and Cu(II)) can accept electrons from the mineral interface, which is an anodic oxidation reaction converting the target metal into soluble ionic products. At the same time, the metal ions are being reduced at the cathode (e.g., Fe(III) to Fe(II) and Cu(II) to Cu(I)). Because the reduced metal ions can be continuously regenerated to their higher-valence state by dissolved oxygen, the redox couple (e.g., Fe(III)/Fe(II) and Cu(II)/Cu(I)) can sustain a catalytic oxidation process for metal leaching [148].

This catalytic oxidation mechanism is well documented in the hydrometallurgical leaching of base-metal sulfides. In acidic sulfate media, Fe(III) serves as a representative oxidizing agent and has been widely applied to the oxidative dissolution of sulfide minerals such as chalcopyrite [149], sphalerite [150], and pyrite [151]. In these systems, the sulfide phase is converted into soluble metal species or oxidized sulfur-containing products. A similar catalytic role is observed for Cu(II) in chloride media, where cupric chloride has been extensively used for the leaching of copper sulfides, including chalcopyrite [152] and djurleite [153], and has also been reported for nickel-bearing sulfides such as millerite and Ni-Cu sulfide concentrates [154].

As mentioned previously (section 2.3), this catalytic oxidation strategy based on transition metal ions has already been widely adopted in cyanide-free gold leaching, for example, Cu(II) in the thiosulfate leaching system, and Fe(III) in both thiourea and thiocyanate systems. However, a major drawback is that these metal ions can strongly coordinate with the sulfur-containing leaching reagents (e.g., thiosulfate, thiourea, or thiocyanate) [155]. In addition, beyond oxidizing gold, these metal ions are usually highly reactive to oxidize the leaching reagents (e.g., thiosulfate, thiourea, and thiocyanate). Thus, these side reactions significantly increase reagent consumption and make the system more difficult to control. Fortunately, coordination chemistry can tune metal ions and largely mitigate these problems. Using suitable ligands to complex metal ions can greatly lower the fraction of highly reactive free metal ions. For example, in thiosulfate systems, Cu(II) can form $Cu(NH_3)_4^{2+}$, which reduces its direct interaction with leaching reagents. Besides, the formed $Cu(NH_3)_4^{2+}$/$Cu(S_2O_3)_3^{5-}$ have a relatively

low redox potential (E^0=0.22 V), thus the side-reaction of lixiviant oxidation can be effectively suppressed.

In short, when transition metal ions serve as oxidants in cyanide-free gold leaching systems, coordination chemistry acts as a critical structure-function lever for enhancing the system's stability. More generally, by tuning the coordination environment (e.g., the ligand type, metal ion/ligand ratio, and solution pH), the redox potential of the metal redox couple can be controlled within an appropriate window. This helps suppress both non-productive lixiviant oxidation and undesired coordination side reactions, while preserving sufficiently gold dissolution kinetics.

2.5 Conclusions

As gold resources trend toward lower grades and greater mineralogical complexity, sulfide-hosted refractory ores are becoming more dominant, while environmental and regulatory pressures are pushing the search for cyanide-free leaching routes. These two directions are linked by one controlling factor: oxidation. Specifically, oxidation determines (i) whether sulfide matrices can be sufficiently oxidized to liberate gold and (ii) whether the oxidation systems can maintain stable gold leaching by eco-friendly cyanide-free leaching lixiviants.

For refractory sulfide gold ores, gold is commonly locked as fine inclusions, intergranular particles, or "invisible" lattice-bound gold phases in sulfides (e.g., pyrite and arsenopyrite), so grinding alone cannot deliver adequate liberation. Consequently, high gold recovery generally requires oxidative destruction of sulfide hosts to create transport pathways and increase gold exposure. Conventional pretreatments are effective but constrained by distinct bottlenecks, for example, emissions control (roasting oxidation), slow kinetics (biooxidation), and large equipment investment (pressure oxidation). which motivates interest in chemical oxidation options, which provide a more efficient and better-controlled oxidation process.

For cyanide-free gold leaching, such as thiosulfate, thiourea, thiocyanate, iodide, chloride, and bromide, gold dissolution requires anodic oxidation of Au(0), which is coupled with the cathodic reduction of an oxidant as the electron acceptor, while the ligands stabilize Au(I) or Au(III) species to drive the dissolution process forward. However, oxidants govern not only the kinetics of gold dissolution but also the stability of the lixiviant. Therefore, the oxidizing strength of the system must be carefully regulated to achieve an effective balance between rapid gold oxidation and minimal

reagent degradation (e.g., Cu(II) and Fe(III) as oxidants in thiosulfate, thiourea, thiocyanate systems). Besides, some oxidants are also expensive and toxic, such as I_2, Cl_2, and Br_2, as oxidants in iodide, chloride, and bromide leaching systems. Therefore, the industrial barrier is less about "finding a new gold lixiviant" and more about achieving stable, controllable, and cost-effective oxidant management.

In this context, the application of advanced chemical oxidation can be viewed as an enabling oxidation module for gold hydrometallurgy. On the one hand, free radical-based oxidation (e.g., •OH and $•SO_4^-$) offers strong, on-demand oxidizing power from manageable precursors (e.g., H_2O_2 and persulfate), which is sufficient not only to liberate gold by disrupting refractory sulfide matrices but also to oxidize metallic gold to soluble ions. On the other hand, catalytic oxidation based on transition metal complex ions (e.g., Fe(III) and Cu(II) complexes) is promising for suppressing both non-productive oxidation and complexation of the lixiviant in cyanide-free leaching systems. Together, these oxidation strategies can help move gold production toward greener, more efficient, and lower-cost process routes.

2.6 References

[1] M. Peydayesh, E. Boschi, F. Donat, R. Mezzenga, Gold recovery from E-waste by food-waste amyloid aerogels, Adv. Mater. 36 (2024) 2310642.

[2] H. Knosp, R.J. Holliday, C.W. Corti, Gold in dentistry: Alloys, uses and performance, Gold Bulletin 36 (2003) 93-102.

[3] A.S. Alshammari, Heterogeneous Gold Catalysis: From Discovery to Applications, Catalysts 9 (2019) 402.

[4] S. Abubakar, A. Jrad, G. Das, T. Prakasam, S. Aouad, M.A. Olson, A. Trabolsi, From Waste to Wealth: Covalent Organic Frameworks for Gold Detection and Recovery from Secondary Sources, ACS Appl. Mater. Interfaces 17 (2025) 53040-53055.

[5] S. Cherevko, A.A. Topalov, A.R. Zeradjanin, I. Katsounaros, K.J. Mayrhofer, Gold dissolution: towards understanding of noble metal corrosion, RSC Adv. 3 (2013) 16516-16527.

[6] Y. Ou, Y. Yang, L. Wang, K. Li, W. Gao, Y. Zhang, Q. Li, T. Jiang, A clean and efficient innovative technology for refractory sulfide gold ore: In situ gold extraction via self-generated thiosulfate, J. Cleaner Prod. 419 (2023) 138280.

[7] B. Surimbayev, A. Akcil, L. Bolotova, S. Shalgymbayev, A. Baikonurova, Processing of Refractory Gold-Bearing Sulfide Concentrates: A Review, Miner. Process. Extr. Metall. Rev. 45 (2024) 573-591.

[8] P. Altinkaya, Z. Wang, I. Korolev, J. Hamuyuni, M. Haapalainen, E. Kolehmainen, K. Yliniemi, M. Lundström, Leaching and recovery of gold from ore in cyanide-

free glycine media, Miner. Eng. 158 (2020) 106610.
[9] W. Li, S. Liu, Y. Song, J. Wen, G. Zhou, Y. Chen, Comprehensive recovery of gold and base-metal sulfide minerals from a low-grade refractory ore, Int. J. Miner. Metall. Mater. 23 (2016) 1377-1386.
[10] S. Teimouri, J.H. Potgieter, G.S. Simate, L. van Dyk, M. Dworzanowski, Oxidative leaching of refractory sulphidic gold tailings with an ionic liquid, Miner. Eng. 156 (2020) 106484.
[11] J. Marsden, I. House, The chemistry of gold extraction, Society for Mining, Metallurgy, and Exploration, Inc., Littleton, Colorado, U.S.A. 2006.
[12] G.C. Allan, J.T. Woodcock, A review of the flotation of native gold and electrum, Miner. Eng. 14 (2001) 931-962.
[13] P.C. Santos-Munguía, F. Nava-Alonso, V.M. Rodríguez-Chávez, O. Alonso-González, Hidden gold in fire assay of gold telluride ores, Miner. Eng. 141 (2019) 105844.
[14] S. Ellis, Treatment of gold-telluride ores, in: M.D. Adams, B.A. Wills (Eds.) Developments in Mineral Processing, Elsevier2005, pp. 973-984.
[15] J.M. Shackleton, P.G. Spry, R. Bateman, Telluride mineralogy of the golden mile deposit, Kalgoorlie, Western Australia, Can. Mineral. 41 (2003) 1503-1524.
[16] J. Zhao, A. Pring, Mineral Transformations in Gold–(Silver) Tellurides in the Presence of Fluids: Nature and Experiment, Minerals 9 (2019) 167.
[17] J. Liu, S. Zhao, N.J. Cook, X. Bai, Z. Zhang, Z. Zhao, H. Zhao, J. Lu, Bonanza-grade accumulations of gold tellurides in the Early Cretaceous Sandaowanzi deposit, northeast China, Ore Geology Reviews 54 (2013) 110-126.
[18] R. Asamoah, R. Amankwah, J. Addai-Mensah, Cyanidation of refractory gold ores: A review, 3rd UMaT Biennial International Mining and Mineral Conference, 2014, pp. 204-212.
[19] M.K. Guner, G. Bulut, A. Hassanzadeh, S. Lode, K. Aasly, Automated Mineralogy and Diagnostic Leaching Studies on Bulk Sulfide Flotation Concentrate of a Refractory Gold Ore, Minerals 13 (2023) 1243.
[20] I. Alp, O. Celep, H. Deveci, A. Vicil, Recovery of gold from a free-milling ore by centrifugal gravity separator, Iran. J. Sci. Technol. Trans. B: Eng. 32 (2008) 67-71.
[21] N. Iglesias, F. Carranza, Refractory gold-bearing ores: a review of treatment methods and recent advances in biotechnological techniques, Hydrometallurgy 34 (1994) 383-395.
[22] R.R. Fernández, H.Y. Sohn, K.M. LeVier, Process for treating refractory gold ores by roasting under oxidizing conditions, Min. Metall. Explor. 17 (2000) 1-6.
[23] X. Nan, X. Cai, J. Kong, Pretreatment process on refractory gold ores with As, ISIJ international 54 (2014) 543-547.
[24] L. Zang, X. Guo, Q. Tian, S. Zhong, D. Li, H. Qin, Research progress and industrial application of pretreatment methods for refractory gold ores, GOLD 6 (2021) 60-

68. (In Chinese)
[25] S. Zhang, Y. Zheng, P. Cao, C. Li, S. Lai, X. Wang, Process mineralogy characteristics of acid leaching residue produced in low-temperature roasting-acid leaching pretreatment process of refractory gold concentrates, Int. J. Miner. Metall. Mater. 25 (2018) 1132-1139.
[26] R.G. Robins, L.D. Jayaweera, Arsenic in Gold Processing, Miner. Process. Extr. Metall. Rev. 9 (1992) 255-271.
[27] H. Qin, X. Guo, Q. Tian, D. Yu, L. Zhang, Recovery of gold from sulfide refractory gold ore: Oxidation roasting pretreatment and gold extraction, Miner. Eng. 164 (2021) 106822.
[28] X. Zhu, Z. Dong, G. Li, J. Wu, X. Yang, T. Jiang, B. Xu, Research Progress and Industrial Application Status of Pretreatment Technologies for Refractory Gold Ores, Nonferrous Metals (Extractive Metallurgy) 12 (2025) 123-136. (In Chinese)
[29] A. Hapid, S. Zullaikah, Mahfud, A. Kawigraha, Y. Sudiyanto, R. Benita Nareswari, A.T. Quitain, Oxidation of sulfide mineral and metal extraction analysis in the microwave-assisted roasting pretreatment of refractory gold ore, Arabian J. Chem. 17 (2024) 105447.
[30] G. Ofori-Sarpong, K. Osseo-Asare, M. Tien, Fungal pretreatment of sulfides in refractory gold ores, Miner. Eng. 24 (2011) 499-504.
[31] H. Yang, Q. Liu, G. Chen, L. Tong, A. Ali, Bio-dissolution of pyrite by Phanerochaete chrysosporium, Trans. Nonferrous Met. Soc. China 28 (2018) 766-774.
[32] A.E. Jiménez-Paredes, E.F. Alfaro-Saldaña, A. Hernández-Sánchez, J.V. García-Meza, An Autochthonous Acidithiobacillus ferrooxidans Metapopulation Exploited for Two-Step Pyrite Biooxidation Improves Au/Ag Particle Release from Mining Waste, Mining 1 (2021) 335-350.
[33] A.G. Bulaev, T.A. Pivovarova, V.S. Melamud, B.K. Bumazhkin, E.O. Patutina, T.V. Kolganova, B.B. Kuznetsov, T.F. Kondrat'eva, Species composition of the association of acidophilic chemolithotrophic microorganisms participating in the oxidation of gold-arsenic ore concentrate, Microbiology 80 (2011) 842-849.
[34] F.M. Haoran Liu, Siying Xie, Lijia Deng, Research Progress on Pretreatment Technology and Flotation Technology of Refractory Gold Ore in China, Modern Mining 5 (2025) 6-11.
[35] G. Hein, H. Mahandra, A. Ghahreman, Application of Phanerochaete chrysosporium for enhancing gold recovery via bio-oxidation of refractory sulfidic ores in a circumneutral environment, Process Saf. Environ. Prot. 178 (2023) 135-146.
[36] J. Li, H. Yang, L. Tong, Microbial solubilization of gangue minerals and their influence on pyrite bio-oxidation, Geochemistry 81 (2021) 125790.
[37] K. Pak, T. Zhang, C. Kim, G. Kim, Research on chlorination leaching of pressure-

oxidized refractory gold concentrate, Hydrometallurgy 194 (2020) 105325.
[38] V.G. Papangelakis, G.P. Demopoulos, Acid Pressure Oxidation of Arsenopyrite: Part II, Reaction Kinetics, Can. Metall. Q. 29 (1990) 13-20.
[39] R.G. McDonald, D.M. Muir, Pressure oxidation leaching of chalcopyrite: Part II: Comparison of medium temperature kinetics and products and effect of chloride ion, Hydrometallurgy 86 (2007) 206-220.
[40] R.G. McDonald, D.M. Muir, Pressure oxidation leaching of chalcopyrite. Part I. Comparison of high and low temperature reaction kinetics and products, Hydrometallurgy 86 (2007) 191-205.
[41] V.G. Papangelakis, G.P. Demopoulos, Acid Pressure Oxidation of Arsenopyrite: Part I, Reaction Chemistry, Can. Metall. Q. 29 (1990) 1-12.
[42] L. Zhang, X.-y. Guo, Q.-h. Tian, S.-p. Zhong, H. Qin, Extraction of gold from typical Carlin gold concentrate by pressure oxidation pretreatment - Sodium jarosite decomposition and polysulfide leaching, Hydrometallurgy 208 (2022) 105743.
[43] C.A. Fleming, Basic iron sulfate-a potential killer in the processing of refractory gold concentrates by pressure oxidation, Min. Metall. Explor. 27 (2010) 81-88.
[44] J. Wu, J. Ahn, J. Lee, Gold deportment and leaching study from a pressure oxidation residue of chalcopyrite concentrate, Hydrometallurgy 201 (2021) 105583.
[45] J.B. Hiskey, V.M. Sanchez, Alkaline Pressure Oxidation of a Gold-Bearing Arsenopyrite Concentrate, Miner. Process. Extr. Metall. Rev. 15 (1995) 61-74.
[46] J.C. Soto-Uribe, J.L. Valenzuela-Garcia, M.M. Salazar-Campoy, J.R. Parga-Torres, G. Tiburcio-Munive, M.A. Encinas-Romero, V.M. Vazquez-Vazquez, Gold Extraction from a Refractory Sulfide Concentrate by Simultaneous Pressure Leaching/Oxidation, Minerals 13 (2023) 116.
[47] S. Lee, F. Sadri, A. Ghahreman, Enhanced Gold Recovery from Alkaline Pressure Oxidized Refractory Gold Ore After its Mechanical Activation Followed by Thiosulfate Leaching, J. Sustain. Metall. 8 (2022) 186-196.
[48] A. Boduen, M. Zalesov, V. Melamud, V. Grigorieva, A. Bulaev, Combined Bacterial and Pressure Oxidation for Processing High-Sulfur Refractory Gold Concentrate, Processes 11 (2023) 3062.
[49] D. Li, Developments on the Pretreatment of Refractory Gold Minerals by Nitric Acid, World Gold Conference, The Southern African Institute of Mining and Metallurgy, Southern African, 2009.
[50] M.S. Prasad, R. Mensah-Biney, R.S. Pizarro, Modern trends in gold processing — overview, Miner. Eng. 4 (1991) 1257-1277.
[51] G. Gao, D. Li, Y. Zhou, X. Sun, W. Sun, Kinetics of high-sulphur and high-arsenic refractory gold concentrate oxidation by dilute nitric acid under mild conditions, Miner. Eng. 22 (2009) 111-115.

[52] C.L. Caldeira, V.S.T. Ciminelli, A. Dias, K. Osseo-Asare, Pyrite oxidation in alkaline solutions: nature of the product layer, Int. J. Miner. Process. 72 (2003) 373-386.

[53] C.A. Snyders, G. Akdogan, S.M. Bradshaw, J.H. van Vreden, R. Smith, The development of a caustic pre-leaching step for the recovery of Au from a refractory ore tailings heap, Miner. Eng. 121 (2018) 23-30.

[54] İ. Alp, O. Celep, H. Deveci, Alkaline sulfide pretreatment of an antimonial refractory Au-Ag ore for improved cyanidation, JOM 62 (2010) 41-44.

[55] S.L. Mesa Espitia, G.T. Lapidus, Pretreatment of a refractory arsenopyritic gold ore using hydroxyl ion, Hydrometallurgy 153 (2015) 106-113.

[56] İ. Alp, O. Celep, D. Paktunç, Y. Thibault, Influence of potassium hydroxide pretreatment on the extraction of gold and silver from a refractory ore, Hydrometallurgy 146 (2014) 64-71.

[57] E. Bidari, V. Aghazadeh, Pyrite from Zarshuran Carlin-type gold deposit: Characterization, alkaline oxidation pretreatment, and cyanidation, Hydrometallurgy 179 (2018) 222-231.

[58] D. Alejo-Guerra, A. López-Valdivieso, A. Robledo-Cabrera, Selective removal of Mn^{2+} ions from solutions containing Mn^{2+}, Co^{2+}, and Zn^{2+} ions using ozone, MRS Adv. 10 (2025) 841-845.

[59] Z. Piervandi, Pretreatment of refractory gold minerals by ozonation before the cyanidation process: A review, J. Environ. Chem. Eng. 11 (2023) 109013.

[60] F. Nava-Alonso, E. Elorza-Rodríguez, A. Uribe-Salas, R. Pérez-Garibay, Pretreatment with Ozone for Gold and Silver Recovery from Refractory Ores, Ozone: Sci. Eng. 29 (2007) 101-105.

[61] V. Bazhko, V. Yahorava, Evaluation of ozonation technology for gold recovery and cyanide management during processing of a double refractory gold ore, J. South. Afr. Inst. Min. Metall. 117 (2017) 749-756.

[62] U. Ushani, X. Lu, J. Wang, Z. Zhang, J. Dai, Y. Tan, S. Wang, W. Li, C. Niu, T. Cai, N. Wang, G. Zhen, Sulfate radicals-based advanced oxidation technology in various environmental remediation: A state-of-the–art review, Chem. Eng. J. 402 (2020) 126232.

[63] A. Barbouchi, S. Ayadi, R. Idouhli, M. Khadiri, A. Abouelfida, L. Barfoud, H. Faqir, I. Benzakour, J. Benzakour, Highly efficient pretreatment for refractory gold ores using persulfate, catalyst and free radical based advanced oxidation processes to improve cyanidation, Hydrometallurgy 235 (2025) 106488.

[64] Q. Gui, L. Fu, Y. Hu, H. Di, M. Liang, S. Wang, L. Zhang, E. Dong, Oxidative pretreatment of refractory gold ore using persulfate under ultrasound for efficient leaching of gold by a novel eco-friendly lixiviant: Demonstration of the effect of particle size and economic benefits, Hydrometallurgy 221 (2023) 106110.

[65] K. Feng, D. Wu, J. Cao, J. Li, S. Bai, Surface oxidation modification mechanism

of sodium persulfate on arsenopyrite and its impact on the flotation separation of bornite and arsenopyrite, J. Hazard. Mater. 492 (2025) 138243.

[66] A. Barbouchi, I. Er-Raqi, R. Idouhli, M.-E. KHADIRI, A. Abouelfida, M. Louarrat, M. Mikali, M.A. El Alaoui-Chrifi, H. Faqir, I. Benzakour, Chemical Oxidation of Pyrite by Strong Oxidizing Agents: For Pretreatment of Refractory Pyritic Gold Ores, Acta Montan. Slovaca 29 (2024) 773-786.

[67] S. Cherevko, A.R. Zeradjanin, A.A. Topalov, G.P. Keeley, K.J. Mayrhofer, Effect of temperature on gold dissolution in acidic media, J. Electrochem. Soc. 161 (2014) H501.

[68] M.G. Aylmore, Chapter 27 - Alternative Lixiviants to Cyanide for Leaching Gold Ores, Gold Ore Processing (Second Edition), Elsevier 2016, pp. 447-484.

[69] S.S. Konyratbekova, A. Baikonurova, A. Akcil, Non-cyanide Leaching Processes in Gold Hydrometallurgy and Iodine-Iodide Applications: A Review, Miner. Process. Extr. Metall. Rev. 36 (2015) 198-212.

[70] J. Hiskey, V. Atluri, Dissolution Chemistry of Gold and Silver in Different Lixiviants, Miner. Process. Extr. Metall. Rev. 4 (1988) 95-134.

[71] Z. Liu, X. Guo, Q. Tian, L. Zhang, A systematic review of gold extraction: Fundamentals, advancements, and challenges toward alternative lixiviants, J. Hazard. Mater. 440 (2022) 129778.

[72] G. Senanayake, Kinetics and reaction mechanism of gold cyanidation: Surface reaction model via Au(I)-OH-CN complexes, Hydrometallurgy 80 (2005) 1-12.

[73] P.L. Breuer, M.I. Jeffrey, An electrochemical study of gold leaching in thiosulfate solutions containing copper and ammonia, Hydrometallurgy 65 (2002) 145-157.

[74] B. Xu, W. Kong, Q. Li, Y. Yang, T. Jiang, X. Liu, A Review of Thiosulfate Leaching of Gold: Focus on Thiosulfate Consumption and Gold Recovery from Pregnant Solution, Metals 7 (2017) 222.

[75] H.F. Zhao, H.Y. Yang, X. Chen, G.B. Chen, L.L. Tong, Z.N. Jin, Effect of Triethanolamine as a New and Efficient Additive on Thiosulfate-Copper-Ammonia System Leaching of Gold, JOM 72 (2020) 946-952.

[76] D. Feng, J.S.J. van Deventer, Thiosulphate leaching of gold in the presence of ethylenediaminetetraacetic acid (EDTA), Miner. Eng. 23 (2010) 143-150.

[77] D. Feng, J.S.J. van Deventer, The role of amino acids in the thiosulphate leaching of gold, Miner. Eng. 24 (2011) 1022-1024.

[78] D. Feng, J.S.J. van Deventer, Thiosulphate leaching of gold in the presence of carboxymethyl cellulose (CMC), Miner. Eng. 24 (2011) 115-121.

[79] B. Xu, Y. Yang, T. Jiang, Q. Li, X. Zhang, D. Wang, Improved thiosulfate leaching of a refractory gold concentrate calcine with additives, Hydrometallurgy 152 (2015) 214-222.

[80] Y. Lin, X. Hu, F. Zi, Thiocyanate facilitating thiosulfate extraction of gold via inhibiting formation of passive layer, Sustainable Mater. Technol. 40 (2024)

e00878.
[81] Y. Lin, X. Hu, F. Zi, Y. Chen, S. Chen, X. Li, L. Zhao, Y. Li, Synergistical thiourea and thiosulfate leaching gold from a gold concentrate calcine with copper-ammonia catalysis, Sep. Purif. Technol. 327 (2023) 124928.
[82] Q. Wang, X. Hu, F. Zi, P. Yang, Y. Chen, S. Chen, Environmentally friendly extraction of gold from refractory concentrate using a copper – ethylenediamine – thiosulfate solution, J. Cleaner Prod. 214 (2019) 860-872.
[83] J. Wang, F. Xie, W. Wang, Y. Bai, Y. Fu, Y. Chang, Leaching of gold from a free milling gold ore in copper-citrate-thiosulfate solutions at elevated temperatures, Miner. Eng. 155 (2020) 106476.
[84] G. Zhang, L. Hou, P. Chen, Q. Zhang, Y. Chen, N.Z. Zainiddinovich, C. Wu, L.V. Alejandro, F. Jia, Efficient and stable leaching of gold in a novel ethydiaminedhephen acetic-thiosulfate system, Miner. Eng. 209 (2024) 108639.
[85] J. Chen, F. Xie, H. Zhang, W. Wang, Research on Gold Leaching from a Refractory Gold Concentrate in Copper-Malic Acid-Thiosulfate Solutions, Min. Metall. Explor. 40 (2023) 1501-1512.
[86] J. Chen, F. Xie, W. Wang, Y. Fu, J. Wang, Leaching of a carbonaceous gold concentrate in copper-tartrate-thiosulfate solutions, Miner. Eng. 183 (2022) 107605.
[87] L. Hou, A. López Valdivieso, P. Chen, G. Zhang, Q. Zhang, Y. Chen, S. Song, F. Jia, An electrochemical study of the dissolution behavior of gold in a novel glycine-thiosulfate system, Miner. Eng. 202 (2023) 108273.
[88] M.G. Aylmore, D.M. Muir, Thiosulfate leaching of gold - A review, Miner. Eng. 14 (2001) 135-174.
[89] C. Han, G. Wang, C. Cheng, C. Shi, Y. Yang, M. Zou, A kinetic and mechanism study of silver-thiosulfate complex photolysis by UV-C irradiation, Hydrometallurgy 191 (2020) 105212.
[90] J. McNeice, H. Mahandra, A. Ghahreman, Biogenic Production of Thiosulfate from Organic and Inorganic Sulfur Substrates for Application to Gold Leaching, Sustainability 14 (2022) 16666.
[91] O.E. Piro, E.E. Castellano, R.C. Piatti, A.A. Bolzán, A.J. Arvia, Two thiourea-containing gold(I) complexes, Acta Crystallogr C 58 (2002) M252-255.
[92] M. Terzi, Gold Extraction from an Oxide Ore by Thiourea Leaching with Hydrogen Peroxide as an Oxidant, Russ. J. Non-Ferr. Met. 62 (2021) 514-521.
[93] C. Lee, L. Tang, S.R. Popuri, A study on the recycling of scrap integrated circuits by leaching, Waste Manage. Res. 29 (2011) 677-685.
[94] J. Li, X. Xu, W. Liu, Thiourea leaching gold and silver from the printed circuit boards of waste mobile phones, Waste Manag. 32 (2012) 1209-1212.
[95] M. Gurung, B.B. Adhikari, H. Kawakita, K. Ohto, K. Inoue, S. Alam, Recovery of gold and silver from spent mobile phones by means of acidothiourea leaching

followed by adsorption using biosorbent prepared from persimmon tannin, Hydrometallurgy 133 (2013) 84-93.

[96] I. Birloaga, I. De Michelis, F. Ferella, M. Buzatu, F. Vegliò, Study on the influence of various factors in the hydrometallurgical processing of waste printed circuit boards for copper and gold recovery, Waste Manag. 33 (2013) 935-941.

[97] S. Camelino, J. Rao, R.L. Padilla, R. Lucci, Initial Studies about Gold Leaching from Printed Circuit Boards (PCB's) of Waste Cell Phones, Procedia Mater. Sci. 9 (2015) 105-112.

[98] L. Zhang, X. Guo, Q. Tian, D. Li, S. Zhong, H. Qin, Improved thiourea leaching of gold with additives from calcine by mechanical activation and its mechanism, Miner. Eng. 178 (2022) 107403.

[99] D. Calla-Choque, F. Nava-Alonso, Thiourea determination for the precious metals leaching process by iodate titration, Rev. Mex. Ing. Quim. 19 (2020) 275-284.

[100] X. Yang, M.S. Moats, J.D. Miller, The interaction of thiourea and formamidine disulfide in the dissolution of gold in sulfuric acid solutions, Miner. Eng. 23 (2010) 698-704.

[101] K. Sasaki, I. Suyama, Y. Aoki, K.T. Konadu, Cindy, C. Chuaicham, H. Miki, T. Hirajima, Significance of Fe contents on the surface of the gold ores in gold leaching by thiourea and ethylene thiourea, Miner. Eng. 191 (2023) 107957.

[102] S. Zheng, Y. Wang, L. Chai, Research status and prospect of gold leaching in alkaline thiourea solution, Miner. Eng. 19 (2006) 1301-1306.

[103] I.V. Mironov, D.B. Kal'nyi, V.V. Kokovkin, On Gold(I) Complexes and Anodic Gold Dissolution in Sulfite-Thiourea Solutions, J. Solution Chem. 46 (2017) 989-1003.

[104] C. Zhang, L. Chai, H. Zhong, M. Okido, R. Ichino, Selective dissolution of gold in an alkaline thiourea solution by electrolysis, J. Cent. South Univ. Technol. (Engl. Ed.) 4 (1997) 73-78.

[105] C. Vargas, P. Navarro, D. Espinoza, J. Manríquez, E. Mejía, Dissolution behavior of gold in alkaline media using thiourea, Int. J. Nonferrous Metall. 8 (2018) 1-8.

[106] L. Chai, Y. Wang, Mechanism of gold dissolving in alkaline thiourea solution, J. Cent. South Univ. Technol. (Engl. Ed.) 14 (2007) 485-489.

[107] L. Chai, M. Okido, W. Wei, Effect of Na_2SO_3 on electrochemical aspects of gold dissolution in alkaline thiourea solution, Hydrometallurgy 53 (1999) 255-266.

[108] Y. Wang, L. Chai, X. Min, D. He, B. Peng, Optimization of efficient stable reagent of alkaline thiourea solution for gold leaching, J. Cent. South Univ. Technol. (Engl. Ed.) 10 (2003) 292-296.

[109] I. Plaskin, M. Kozhukhova, The solubility of gold and silver in thiourea, Dokl. Akad. Nauk SSSR 31 (1941) 671-674.

[110] J. Li, J. Miller, A review of gold leaching in acid thiourea solutions, Miner. Process. Extr. Metall. Rev. 27 (2006) 177-214.

[111] I. Birloaga, N.M. Ippolito, F. Vegliò, A Mobile Pilot Plant for the Recovery of Precious and Critical Raw Materials, in: P. Rosa, S. Terzi (Eds.) New Business Models for the Reuse of Secondary Resources from WEEEs: The FENIX Project, Springer International Publishing, Cham, 2021, pp. 49-63.
[112] H. White, The solubility of gold in thiosulphates and thiocyanates, S. Afr. J. Sci. 1 (1905) 211-215.
[113] O. Barbosa-Filho, A. Monhemius, Leaching of gold in thiocyanate solutions: Part 1: chemistry and thermodynamics, Trans. Inst. Min. Metall. Sect. C, Miner. Process. Extr. Metall. 103 (1994) C105.
[114] J.L. Broadhurst, J.G.H. du Perez, A thermodynamic study of the dissolution of gold in an acidic aqueous thiocyanate medium using iron (III) sulphate as an oxidant, Hydrometallurgy 32 (1993) 317-344.
[115] J. Li, M.S. Safarzadeh, M.S. Moats, J.D. Miller, K.M. LeVier, M. Dietrich, R.Y. Wan, Thiocyanate hydrometallurgy for the recovery of goldPart III: Thiocyanate stability, Hydrometallurgy 113-114 (2012) 19-24.
[116] A. Azizitorghabeh, H. Mahandra, J. Ramsay, A. Ghahreman, Gold leaching from an oxide ore using thiocyanate as a lixiviant: process optimization and kinetics, ACS Omega 6 (2021) 17183-17193.
[117] H. Wu, Y. Feng, W. Huang, H. Li, S. Liao, The role of glycine in the ammonium thiocyanate leaching of gold, Hydrometallurgy 185 (2019) 111-116.
[118] X. Yang, M.S. Moats, J.D. Miller, X. Wang, X. Shi, H. Xu, Thiourea–thiocyanate leaching system for gold, Hydrometallurgy 106 (2011) 58-63.
[119] O. Barbosa-Filho, A.J. Monhemius, Iodide-thiocyanate leaching system for gold, Hydrometallurgy ’94, Springer Netherlands, Dordrecht, 1994, pp. 425-440.
[120] S.Y. Khaing, Y. Sugai, K. Sasaki, Gold Dissolution from Ore with Iodide-Oxidising Bacteria, Scientific Reports 9 (2019) 4178.
[121] A. Davis, T. Tran, D.R. Young, Solution chemistry of iodide leaching of gold, Hydrometallurgy 32 (1993) 143-159.
[122] S. Anusaraporn, R. Dolphen, P. Thiravetyan, Importance of laccase enzyme and triiodide for gold leaching from silicate ore by marine bacterium Acinetobacter sp, Process Saf. Environ. Prot. 161 (2022) 788-800.
[123] X. Yin, R. Liu, Y. Yue, J. Li, Y. Yang, Ultra-fast and selective recycling of gold from electronic waste based on triiodide ionic liquids, AIChE J. 71 (2025) e18773.
[124] M. Baghalha, The leaching kinetics of an oxide gold ore with iodide/iodine solutions, Hydrometallurgy 113-114 (2012) 42-50.
[125] A. Batnasan, K. Haga, A. Shibayama, Recovery of Valuable Metals from Waste Printed Circuit Boards by Using Iodine-Iodide Leaching and Precipitation, Rare Metal Technology, Springer International Publishing, Cham, 2018, pp. 131-142.
[126] F. Xiu, Y. Qi, F. Zhang, Leaching of Au, Ag, and Pd from waste printed circuit boards of mobile phone by iodide lixiviant after supercritical water pre-treatment,

Waste Manag. 41 (2015) 134-141.
[127] Q. Meng, X. Yan, G. Li, Eco-friendly and reagent recyclable gold extraction by iodination leaching-electrodeposition recovery, J. Cleaner Prod. 323 (2021) 129115.
[128] H. Zhang, C.A. Jeffery, M.I. Jeffrey, Ion exchange recovery of gold from iodine–iodide solutions, Hydrometallurgy 125-126 (2012) 69-75.
[129] Z. Liu, J. Kou, C. Sun, Highly efficient electroextraction of gold and simultaneous iodine regeneration using ionic liquid 1-ethyl-3-methylimidazolium dicyanamide, Sep. Purif. Technol. 318 (2023) 123961.
[130] A. Filcenco Olteanu, T. Dobre, E. Panturu, A.D. Radu, A. Akcil, Experimental process analysis and mathematical modeling for selective gold leaching from slag through wet chlorination, Hydrometallurgy 144-145 (2014) 170-185.
[131] M.A. Topçu, A. Rüşen, V. Kalem, Ö. Küçük, Gold Leaching from Copper Anode Slime with 1-Butly-3-Methyl Imidazolium Chloride, JOM 74 (2022) 2120-2128.
[132] S. Ilyas, R.R. Srivastava, H. Kim, Gold recovery from secondary waste of PCBs by electro-Cl_2 leaching in brine solution and solvo-chemical separation with tri-butyl phosphate, J. Cleaner Prod. 295 (2021) 126389.
[133] M.G. Aylmore, Alternative lixiviants to cyanide for leaching gold ores, Dev. Miner. Process., Elsevier2005, pp. 501-539.
[134] M. Kim, S. Park, J. Lee, P.K. Choubey, A novel zero emission concept for electrogenerated chlorine leaching and its application to extraction of platinum group metals from spent automotive catalyst, Hydrometallurgy 159 (2016) 19-27.
[135] M.T. van Meersbergen, L. Lorenzen, J.S.J. van Deventer, The electrochemical dissolution of gold in bromine medium, Miner. Eng. 6 (1993) 1067-1079.
[136] R. Sousa, A. Futuro, A. Fiúza, M.C. Vila, M.L. Dinis, Bromine leaching as an alternative method for gold dissolution, Miner. Eng. 118 (2018) 16-23.
[137] Z. Xiong, Y. Huang, Y. Li, C. Sheng, L. Sun, J. Ma, B. Chi, J. Tan, X. Tang, R. Zha, X. Zhan, Selective recovery of Au from waste printed circuit board by water-soluble organic leaching: The key role of in situ bromine mediation and identificationof pathway, J. Hazard. Mater. 480 (2024) 136255.
[138] R. Mensah-Biney, M.T. Hepworth, K.J. Reid, Loading of gold bromo species onto anion exchange resin, Miner. Eng. 6 (1993) 173-191.
[139] C.P. Huang, C. Dong, Z. Tang, Advanced chemical oxidation: Its present role and potential future in hazardous waste treatment, Waste Manag. 13 (1993) 361-377.
[140] W. Chen, Z. Gu, C. He, Q. Li, Molecular composition of hydroxyl radical-resistant organics in municipal solid waste leachate, Journal of Hazardous Materials 486 (2025) 137014.
[141] L.D. Abo, M. Jayakumar, A.S. Jeyapaul, M. Rangaraju, H.A. Areti, A. Assefa Adugna, Comprehensive review on co-integration of conventional systems and advanced oxidation processes for industrial and agricultural wastewater treatment

applications, Environ. Adv. 20 (2025) 100638.
[142] W. Lv, Z. Wang, X. Zheng, H. Cao, M. He, Y. Zhang, H. Yu, Z. Sun, Selective Recovery of Lithium from Spent Lithium-Ion Batteries by Coupling Advanced Oxidation Processes and Chemical Leaching Processes, ACS Sustainable Chem. Eng. 8 (2020) 5165-5174.
[143] J. Liu, S. Wang, Y. Zhang, L. Zhang, D. Kong, Synergistic mechanism and decopperization kinetics for copper anode slime via an integrated ultrasound-sodium persulfate process, Applied Surface Science 589 (2022) 153032.
[144] Q. Zuo, D. Wu, S. Wen, J. Cao, Z. Wang, H. Chen, Advanced oxidation using sulfate radicals for the surface oxidation of Cu2O and the separation of copper via acid leaching, J. Mol. Liq. 390 (2023) 123195.
[145] A. Ding, M. Li, C. Liu, T. Chee, Q. Yan, L. Lei, C. Xiao, Recovering palladium and gold by peroxydisulfate-based advanced oxidation process, Sci. Adv. 10 (2024) eadm9311.
[146] K. Altendji, S. Hamoudi, Aqueous Atrazine Photocatalytic Degradation over g-C_3N_4/graphene/$NiFe_2O_4$ Nanocomposite in the Presence of Potassium Peroxymonosulfate, Water, Air, Soil Pollut. 236 (2024) 28.
[147] S. Yu, B. Yang, C. Fang, Y. Zhang, S. Liu, Y. Zhang, L. Shen, J. Xie, J. Wang, Dissolution mechanism of the oxidation process of covellite by ferric and ferrous ions, Hydrometallurgy 201 (2021) 105585.
[148] D. Feng, J.S.J. van Deventer, The role of oxygen in thiosulphate leaching of gold, Hydrometallurgy 85 (2007) 193-202.
[149] E.M. Córdoba, J.A. Muñoz, M.L. Blázquez, F. González, A. Ballester, Leaching of chalcopyrite with ferric ion. Part I: General aspects, Hydrometallurgy 93 (2008) 81-87.
[150] J.E. Dutrizac, The dissolution of sphalerite in ferric sulfate media, Metallurgical and Materials Transactions B 37 (2006) 161-171.
[151] S.C. Bouffard, B.F. Rivera-Vasquez, D.G. Dixon, Leaching kinetics and stoichiometry of pyrite oxidation from a pyrite–marcasite concentrate in acid ferric sulfate media, Hydrometallurgy 84 (2006) 225-238.
[152] M. Bonan, J.M. Demarthe, H. Renon, F. Baratin, Chalcopyrite leaching by $CuCl_2$ in strong NaCl solutions, Metallurgical Transactions B 12 (1981) 269-274.
[153] O. Herreros, R. Quiroz, H. Longueira, G. Fuentes, J. Viñals, Leaching of djurleite in Cu^{2+}/Cl^{-} media, Hydrometallurgy 82 (2006) 32-39.
[154] R.C. Hubli, T.K. Mukherjee, S. Venkatachalam, R.G. Bautista, C.K. Gupta, Kinetics of millerite dissolution in cupric chloride solutions, Hydrometallurgy 38 (1995) 149-159.
[155] K. Li, Q. Li, Y. Zhang, X. Liu, Y. Yang, T. Jiang, Improved thiourea leaching of gold from a gold ore using additives, Hydrometallurgy 222 (2023) 106204.

Chapter III. Stepwise oxidation of refractory pyrite using persulfate for efficient leaching of gold and silver by an eco-friendly copper(II)-glycine-thiosulfate system

3.1 Introduction

Gold (Au) and silver (Ag), as representative precious metals, are traditionally known for their use in jewelry and currency [1]. With the development of science and technology, they have been extensively employed as corrosion-resistant electrical connectors and are increasingly applied in the assembly of nanomaterials (e.g., nanoclusters [2], nanosuspensions [3], nanocomposites [4], nanocermet films [5], and nanocoatings [6]). Hydrometallurgical leaching of Au and Ag from ores is essential for meeting the growing demand in these applications. As high-quality gold mines are gradually depleted, refractory ores rich in sulfur, arsenic, and carbon have become the primary resources for gold mining [7, 8]. Pyrite (FeS_2), the most abundant sulfide ore, commonly hosts Au and Ag in microscopic enclosures [9,10]. Although separating Au and Ag from pyrite could significantly enhance its utilization value, hydrometallurgical leaching faces significant challenges with refractory pyrite enclosures, as encapsulated Au and Ag particles struggle to access reagent ions, whether in conventional cyanidation or novel systems like thiourea, thiosulfate, or thiocyanate [11, 12].

Oxidation pretreatment is crucial for enhancing Au and Ag extraction from refractory sulfide ores. Roasting oxidation, with over 70 years of use, is considered the most mature technology for pretreating refractory sulfide ores in gold mining. However, it causes significant tail gas air pollution (SO_2), leading to environmental and public health issues [13]. Additionally, the secondary encapsulation of gold by phase-transformed silicates and iron oxides at high temperatures can significantly affect subsequent leaching performance [14]. Pressure oxidation has become widely used for pretreating refractory gold ores, especially pyrite and arsenopyrite. However, challenges such as high pressure, elevated temperatures, excessive alkalinity, and significant equipment costs persist [15]. Bio-oxidation effectively addresses sulfide ore inhibition during gold leaching and is environmentally friendly, but its slower kinetics and complex bacteria cultivation limit its industrial appeal [16]. Despite these explorations, developing alternative oxidation methods for the efficient utilization of refractory sulfide ores in gold mining remains a key research focus.

The vast majority of literatures indicate that chemical oxidation is a milder, safer, and efficient approach for pretreating refractory sulfide ores [17]. It typically offers faster reaction kinetics than bio-oxidation, leading to shorter operation times and higher throughput. Unlike pressure oxidation, chemical oxidation allows precise control over temperature, pH, and reagent concentration without substantial equipment investment and energy input [18]. Current efforts have focused on the selection of oxidizing reagents to improve the oxidation efficiency of sulfide phases. Several oxidants have been investigated, including hydrogen peroxide (H_2O_2) [19], nitric acid (HNO_3) [20], ozone (O_3) [21], sodium hydroxide (NaOH) [22], and ferric ions (Fe^{3+}) [23]. While the experimental evaluation of these reagents has been conducted previously, they have not achieved large-scale industrialization. Recently, persulfate-based advanced oxidation processes (AOPs) have gained attention for the chemical oxidation of refractory gold ore with pyrite enclosures [24]. As a novel and environmentally friendly oxidizing agent, persulfate offers stronger oxidation potential due to the formation of powerful free radicals (e.g., $\bullet SO_4^-$ and •OH). As described in the mechanism, the proper activation of persulfate, using methods such as photochemical, thermal, radiolytic, or transition metals, is crucial to effectively release free radicals for sulfide oxidation, making it a key area of research for improving gold extraction from refractory ore.

From the perspective of environmental protection, it is imperative to realize Au and Ag production through clean technologies, especially to replace the commanding position of cyanidation [25, 26]. Thiosulfate leaching has been widely verified as an eco-friendly process, which is one of the potential alternatives for cyanidation [27]. In this work, a stepwise oxidation process is proposed to enhance the extraction of encapsulated Au and Ag from a refractory pyrite concentrate, beginning with heating-activated persulfate (Step I) and continuing with pyrite self-dissolved Fe ions activating persulfate (Step II). Furthermore, an eco-friendly copper-glycine-thiosulfate system was adopted to assess the impact of oxidation pretreatment on gold leaching efficiency. After each test, research efforts were directed toward understanding the pyrite oxidation mechanism and the relationship between the evolution of pyrite's mineralogical structure and Ag/Au leaching. This research attempts to broaden the understanding of pyrite oxidation by persulfate and to provide theoretical guidance for the eco-friendly extraction of Au and Ag from refractory ores, as well as the high-value utilization of pyrite resources.

3.2 Materials and methods

3.2.1 Materials and reagents

The Au/Ag-bearing pyrite sample used in this work was obtained from Chihuahua, México, which is a flotation concentrate. The pyrite concentrate is of high purity according to the X-ray diffraction (XRD) spectrum, showing the presence of only quartz as a detectable contaminant (Figure 3.1 a). Scanning electron microscope (SEM) images (Figure 3.1 b) show that Au and Ag are mainly encapsulated in pyrite in the forms of invisible Au-Ag alloy, and Ag-Sb-S or Ag-Pb-S compounds (Figure 3.1c), which is typically a refractory ore.

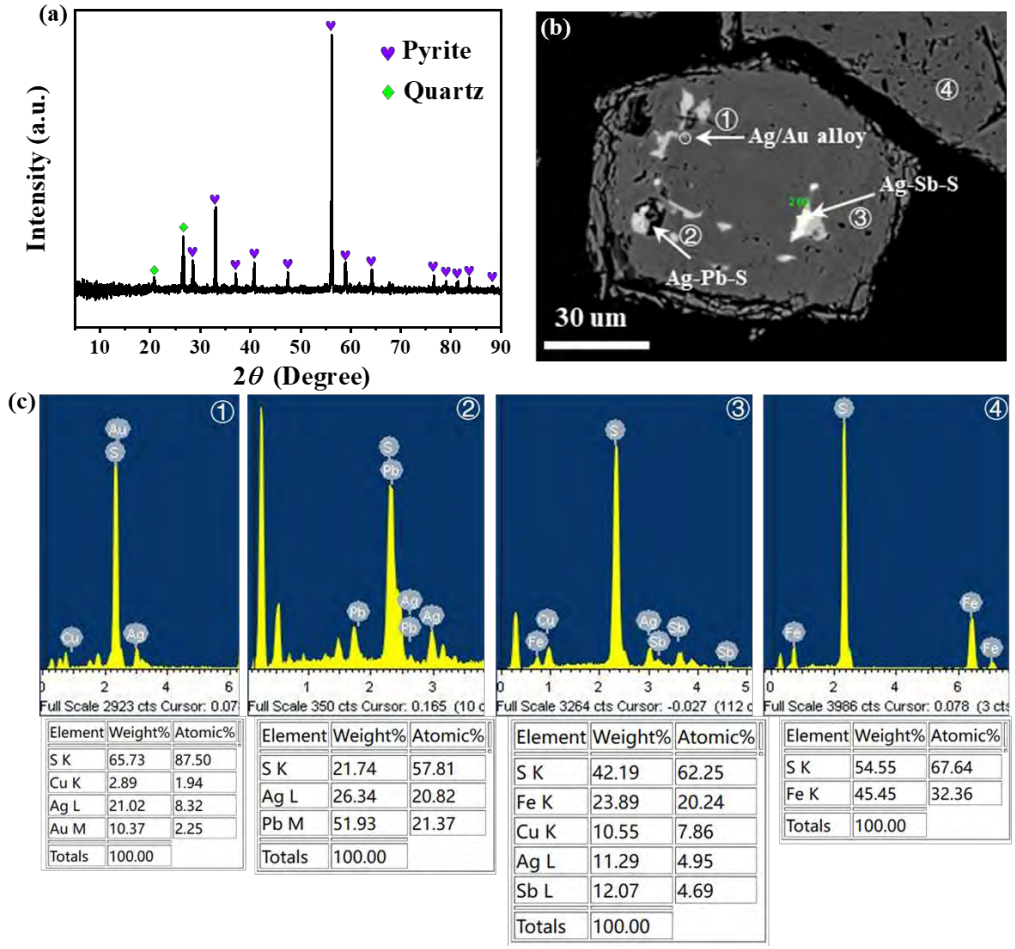

Figure 3.1 Characterization of the pyrite concentrate. (a) XRD pattern. (b) Internal SEM images. (c) EDS spectrum

Chemical element analysis (Table 3.1) shows a high amount of Fe (41.15 wt%) and S (48.00 wt%), along with a small amount of Zn, Pb, Cu, As, Sb, and Cd. The grades of 13.11 g/t Au and 358.34 g/t Ag are of recovery value.

Table 3.1 Chemical composition of pyrite concentrate sample wt %

Element	S	Fe	Zn	Pb	Cu	As	Sb	Cd	Insoluble	Au(g/t)	Ag(g/t)
Amount	48.00	41.15	1.80	1.20	0.14	0.65	0.05	0.01	6.60	13.11	358.34

Ammonium persulfate (PS, $(NH_4)_2S_2O_8$) was used for oxidizing pyrite. An eco-friendly system based on lixiviants of ammonium thiosulfate ($(NH_4)_2S_2O_3$), glycine ($C_2H_5NO_2$), and cupric sulfate ($CuSO_4 \cdot 5H_2O$) was employed for Au/Ag leaching from oxidized pyrite concentrate. All reagents were of analytical grade, and solutions were prepared using ultrapure water.

3.2.2 Oxidative pretreatment procedures

The pyrite concentrate was oxidized through a two-step process using $(NH_4)_2S_2O_8$ (PS) as the oxidant. Experiments were carried out in a 125 mL Erlenmeyer flask with magnetic stirring (500 rpm), containing 100 mL deionized water and 10 g pyrite concentrate. The experimental conditions, detailed in Table 3.2, involved dissolving PS into the pyrite-containing solution at concentrations of 0.1, 0.5, 1.0, and 1.5 mol/L, with Step I conducted at 40°C to 85°C and Step II at room temperature using the same solution. The pH remained unadjusted as the initial acidity sufficed for pyrite dissolution. At fixed leaching times, liquor samples were taken for analysis of Fe by atomic absorption spectrometry (AAS). The pyrite oxidation efficiency (%) was calculated with the following Eq. (3-1).

$$\text{Pyrite oxidation (\%)} = \frac{C_{Fe} \times V}{m \times \omega_{Fe}} \times 100\% \quad (3\text{-}1)$$

where C_{Fe} is the total iron concentration in the solution after treatment due to pyrite oxidation, V is the volume of the solution, m is the mass of refractory pyrite ore, and ω_{Fe} is the total iron content of the pyrite ore.

Table 3.2 Conditions of the stepwise oxidation process assisted by persulfate (PS)

Step I (with heating)		Step II (without heating)	
Temperature	PS (mol/L)	Temperature	PS (mol/L)
40℃	0.1, 0.5, 1.0, 1.5	Ambient (22 ±3℃)	0.1, 0.5, 1.0, 1.5
55℃	0.1, 0.5, 1.0, 1.5		
70℃	0.1, 0.5, 1.0, 1.5		
85℃	0.1, 0.5, 1.0, 1.5		

After oxidation, the oxidized residues were collected for leaching tests of Au and Ag. In the following text, fresh pyrite, oxidation residue from Step I, and oxidation

residue from Step II are referred to as Raw pyrite, Pyrite-step I, and Pyrite-step II, respectively.

3.2.3 Gold and silver leaching procedures

An eco-friendly copper(II)-glycine-thiosulfate system was used for Au and Ag leaching from oxidized residues. Leaching tests were performed in a 100 mL glass conical flask equipped with stirring (500 rpm) at room temperature and normal pressure. The copper(II)-glycine-thiosulfate solution (80 mL) was prepared by mixing 3 mmol/L $CuSO_4 \cdot 5H_2O$ with 0.1 mol/L glycine, adjusting the pH to alkaline with NaOH to form a blue solution, and then adding $(NH_4)_2S_2O_3$ (0.4 mol/L). After preparation, 15 g of oxidized pyrite samples were added to the solution, and the pH was immediately adjusted to 9.0. After 24 hours of leaching, the slurry was filtered with a vacuum pump. The resulting filter cake was washed with ultrapure water and oven-dried at 80°C. The content of Au and Ag in leached residues was then determined, and the corresponding leaching percentage (%) was calculated based on the Au and Ag grades in the oxidized residues and the leached residue, as shown in Eq. (3-2).

$$\text{Au/Ag leaching percentage (\%)} = \frac{m_1 \times a - m_2 \times b}{m_1 \times a} \times 100\% \quad (3\text{-}2)$$

where a is the content of Au or Ag in oxidized pyrite samples (g/t), b is the content of Au or Ag in the leached residue (g/t), m_1 is the mass of the oxidized pyrite samples (g), and m_2 is the mass of the leached residue (g).

3.2.4 Analytical and characterization techniques

The content of Fe and other metal ions in the solution was analyzed using atomic absorption spectrometry (AAS, AA-200, Agilent, USA). Fe^{2+} was quantified through redox titration by potassium dichromate [28], while Fe^{3+} was calculated as the difference between the concentrations of Fe^{2+} and total Fe. SO_4^{2-} was determined by gravimetric analysis using barium chloride [29], while SO_3^{2-} and $S_2O_3^{2-}$ were analyzed by iodometric titration with starch as an indicator [30]. The mineral phases of pyrite samples were identified by X-ray diffraction (XRD, D8 Advance, Bruker, Japan), and the microstructure was examined using a scanning electron microscope (SEM, JSM-6610LV, JEOL, Japan), equipped with an energy dispersive spectroscopy (EDS). The particle size was determined by a Laser particle size analyzer (Mastersizer 2000, Malvern Panalytical, England). Nitrogen adsorption/desorption technique (Autosorb-1, Quantachrome, USA) was used to determine the specific surface and pore size

distribution, calculated using the Brunauer-Emmett-Teller (BET) equation and Barrett-Joyner-Halenda (BJH) method, respectively. The surface oxidation of pyrite was determined by X-ray photoelectron spectroscopy (XPS, K-Alpha, Thermo Fisher, USA) and Raman spectrum at 100~1200 cm^{-1} (Raman, XploRA, HORIBA, France). The free radicals generated by persulfate were determined by electron paramagnetic resonance (EPR, EMXplus-6/1, Bruker, Germany). The solution potential (ORP) and pH during pyrite oxidation were determined by a pH/ion concentration meter (Orion DUAL STAR, Thermo Fisher, USA), equipped with an ORP electrode (vs. SHE) and a pH electrode, respectively. Electrochemical experiments, such as linear sweep voltammetry (LSV), open circuit potential (OCP), and potentiodynamic polarization (PDP), were conducted on an electrochemical workstation (CHI660D, Shanghai Chenhua, China), using a three-electrode system including a pyrite working electrode, a graphite counter electrode, and an Ag/AgCl reference electrode.

3.3 Results and discussion

3.3.1 Performance of stepwise pyrite oxidation and its impact on Au/Ag leaching

3.3.1.1 Initial oxidation of pyrite with heating (Step I)

The usage of persulfate (PS) has been widely considered an advanced oxidation process. Heating is the most common activation method for PS, which requires exposing PS to temperatures of more than 40 °C. Once the heating activation of PS starts running, some strongly oxidizing free radicals, such as $\bullet SO_4^-$ and •OH, are easily generated according to Eqs. (3-3) and (3-4) [31-33]. In this part, batch-oxidation experiments were conducted to investigate the pyrite oxidation rate at different temperatures (40, 55, 70, and 85 °C) and persulfate concentrations (0.1, 0.5, 1.0, and 1.5 mol/L). As shown in Figure 3.2, persulfate concentrations show significant effects on pyrite oxidation, which improved continuously with PS concentrations from 0.1 mol/L to 1.0 mol/L, but no significant change was observed at 1.5 mol/L. Besides, temperatures are a key determinant for the reaction period (the plateau for pyrite oxidation), which decreased from 24 h at 40 °C to 1.5 h at 85 °C (1.0 mol/L PS). This observation could be due to the efficient decomposition of PS at high temperatures, enhancing its oxidizing ability [34]. Notably, the maximum pyrite oxidation reached 14.2% at a moderate temperature of 55 °C in Step I, correlating with a 7 h reaction.

$$S_2O_8^{2-} \xrightarrow{Heat} \bullet SO_4^- \quad (3\text{-}3)$$

$$\bullet SO_4^- + H_2O \rightarrow H^+ + SO_4^{2-} + \bullet OH \quad (3\text{-}4)$$

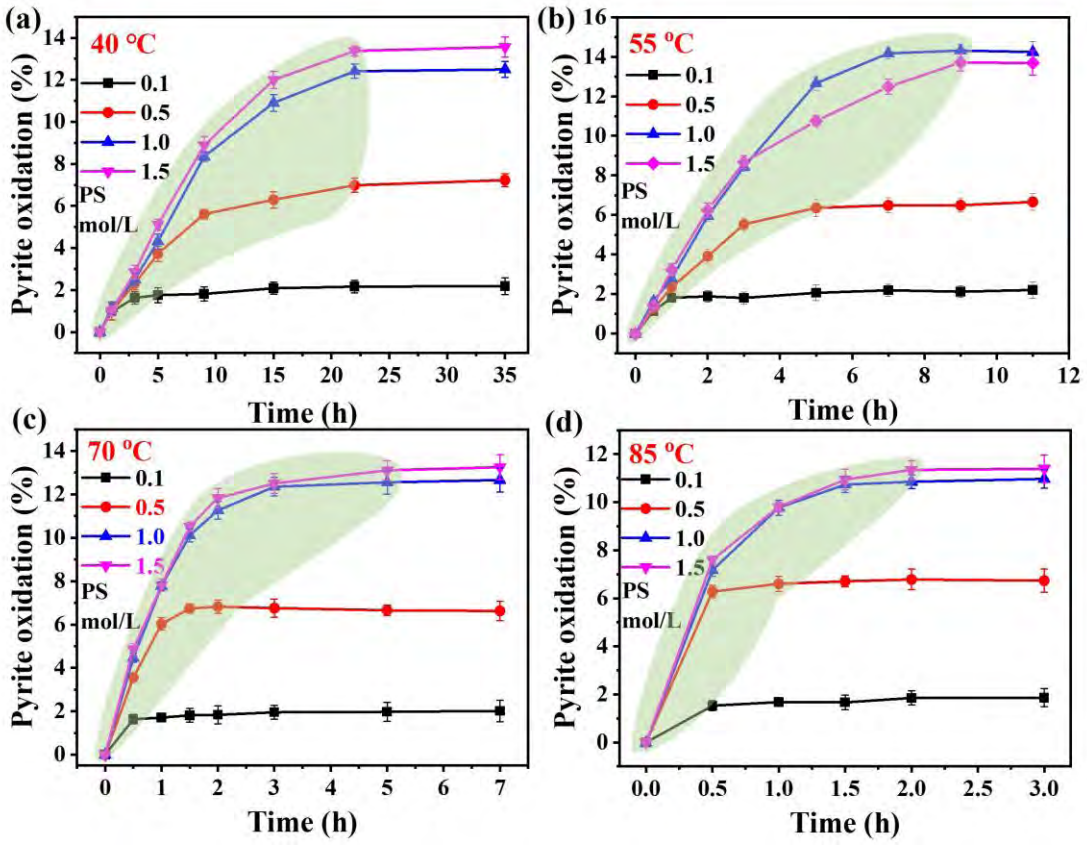

Figure 3.2 Step I pyrite oxidation at (a) 40 °C, (b) 55 °C, (c) 70 °C, and (d) 85 °C with persulfate concentrations ranging from 0.1 to 1.5 mol/L

The performance of oxidizing regents for sulfide ore oxidation is commonly determined by redox potential (ORP) [35, 36]. As depicted in Figure 3.3a, there is a close affinity between ORP and pyrite oxidation, with an increasing trend in pyrite oxidation as ORP rises. When ORP had stalled at a PS concentration of 1.0 mol/L, the oxidation of pyrite almost stopped growing. ORP also correlated with the pyrite oxidation reaction period, with higher temperatures accelerating pyrite oxidation. However, exhaust temperature (85 °C) has led to a very fast decomposition of persulfate, which is why both ORP and pyrite oxidation have been reduced. Additionally, as the reaction progresses, ORP gradually decreases to around 500 mV, where pyrite oxidation reaches a plateau. The decrease in pH with increasing persulfate concentrations suggests the generation of a highly acidic solution (Figure 3.3b), likely due to H^+ production from pyrite oxidation and •OH formation (Eqs. 3-3 and 3-4) [37].

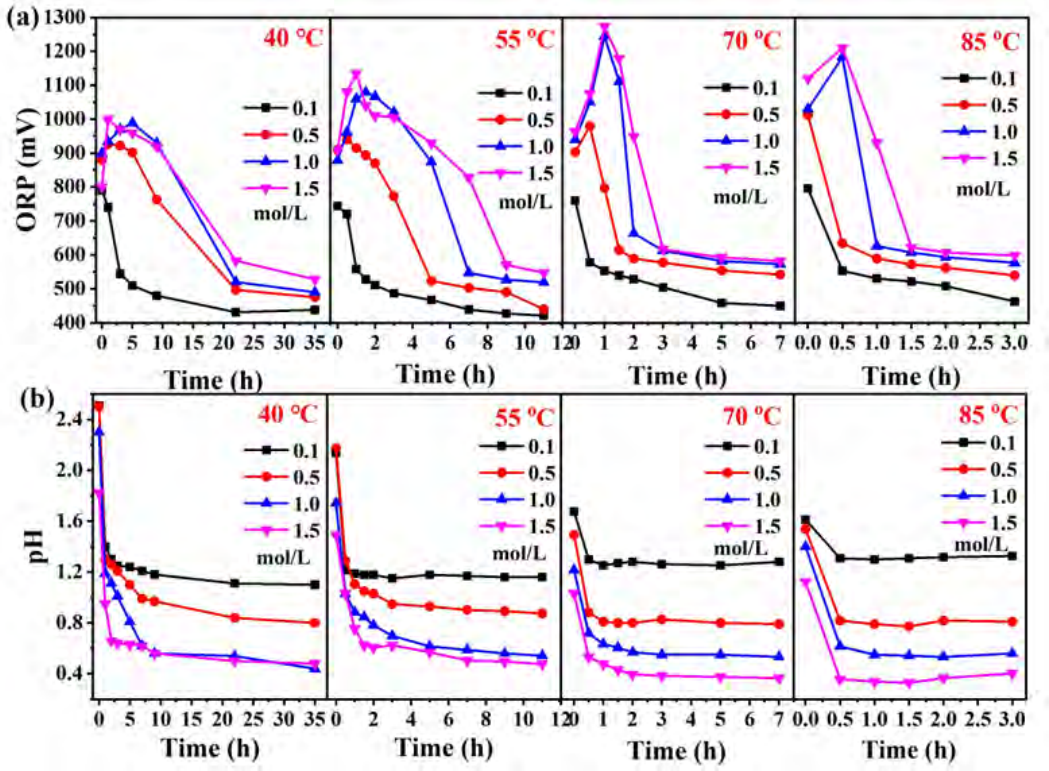

Figure 3.3 Variation of (a) ORP and (b) solution pH during step I pyrite oxidation at various temperatures (40~85 °C)

The chemical oxidation of pyrite, a typical heterogeneous reaction between liquid and solid, follows the shrinking core model and can be controlled by either chemical reaction or diffusion, as described by Eqs. (3-5) and (3-6) [38, 39]. The kinetics of pyrite oxidation at different temperatures were analyzed using the oxidation data presented in Figure 3.2. As shown in Figure 3.4, the R^2 values for the chemical reaction model at 40°C, 55°C, 70°C, and 85°C were 0.922, 0.960, 0.832, and 0.795, respectively, while those for the diffusion model were 0.976, 0.971, 0.945, and 0.952. This indicates that the diffusion model better fits the data, suggesting that the oxidation process (Step I) is primarily controlled by diffusion.

$$1- (1-x)^{1/3} = k_r t \quad (3-5)$$

$$1-3(1-x)^{2/3} + 2(1-x) = k_d t \quad (3-6)$$

where x is the oxidation efficiency of pyrite at any time (t), and k_r and k_d are rate constants for the chemical reaction and diffusion control, respectively.

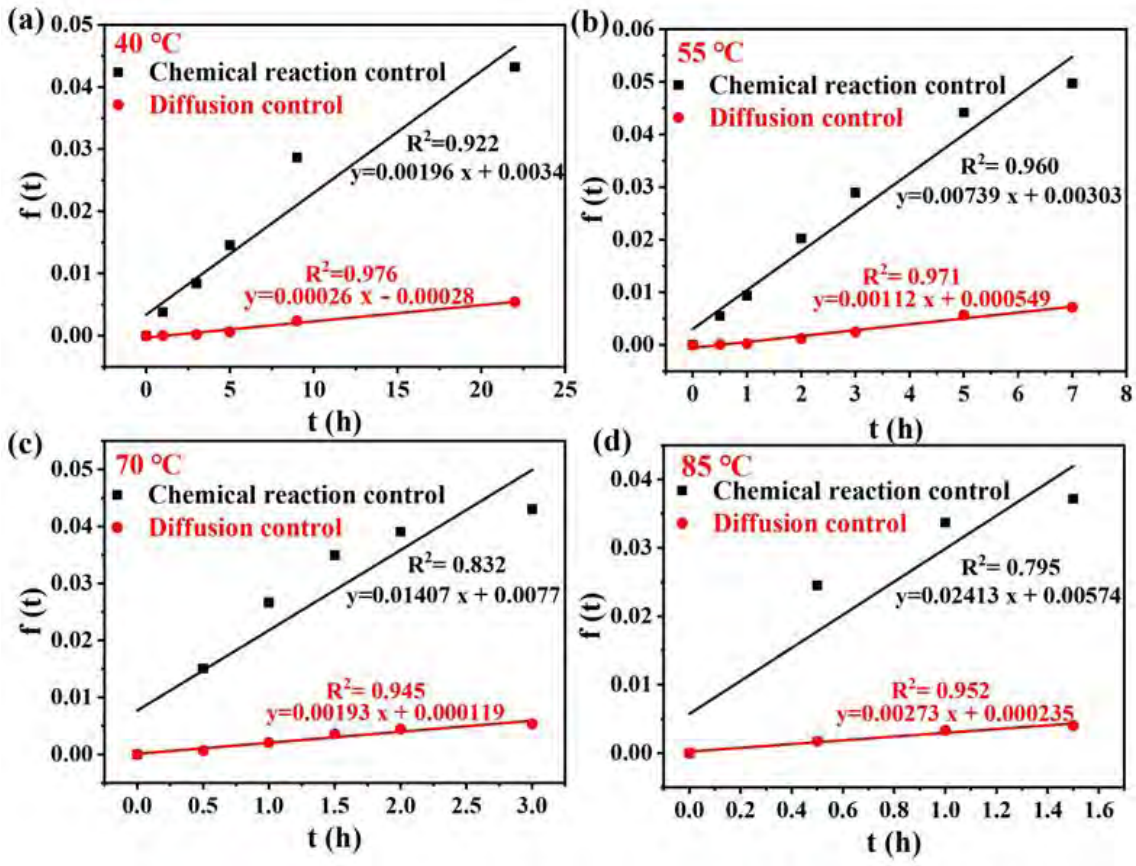

Figure 3.4 Kinetics fitting based on shrinking core models for step I pyrite oxidation at (a) 40 °C, (b) 55 °C, (c) 70 °C, and (d) 85 °C (1.0 mol/L persulfate)

Oxidation pretreatment is crucial in refractory pyrite processing, as it exposes Au and Ag particles to the lixiviant and provides a path for facilitating the penetration of reagent ions into the interior of the pyrite enclosure [40]. Furthermore, an eco-friendly copper(II)-glycine-thiosulfate system was employed to assess the extraction performance of Au and Ag. As shown in Eqs. (3-7) and (3-8), a copper(II)-glycine complex (i.e., $Cu(C_2H_4NO_2)_2$) forms under alkaline conditions, acting as the oxidant, while thiosulfate serves as the gold lixiviant. During the redox process, the copper(II)-glycine complex oxidizes gold and silver (Au^0/Ag^0) to ions (Au^+/Ag^+), and thiosulfate ($S_2O_3^{2-}$) dissolves them into solution as stable complex ions (i.e., $Ag(S_2O_3)_2^{3-}$ and $Au(S_2O_3)_2^{3-}$) [41, 42]. Figure 3.5 showed a distinct refractory feature of the original pyrite concentrate due to low leaching efficiency for Au (25.4%) and Ag (22.9%) [43]. Obviously, a significant improvement in Au and Ag leaching was observed after oxidation pretreatment. As stated above, the oxidation degree of pyrite increased at higher PS concentration (1.0 mol/L), and the best oxidation (14.2%) was achieved at 55 °C. Figure 3.5 also shows that the gold leaching rate increases with the degree of

pyrite oxidation, achieving leaching rates of 64.9% for Au and 56.2% for Ag under the optimized pretreatment condition of 1.0 mol/L PS and 55 ºC.

$$Au + 5S_2O_3^{2-} + Cu(C_2H_4NO_2)_2 \rightarrow Au(S_2O_3)_2^{3-} + 2C_2H_4NO_2^{2-} + Cu(S_2O_3)_3^{5-} \quad (3\text{-}7)$$

$$Ag + 5S_2O_3^{2-} + Cu(C_2H_4NO_2)_2 \rightarrow Ag(S_2O_3)_2^{3-} + 2C_2H_4NO_2^{2-} + Cu(S_2O_3)_3^{5-} \quad (3\text{-}8)$$

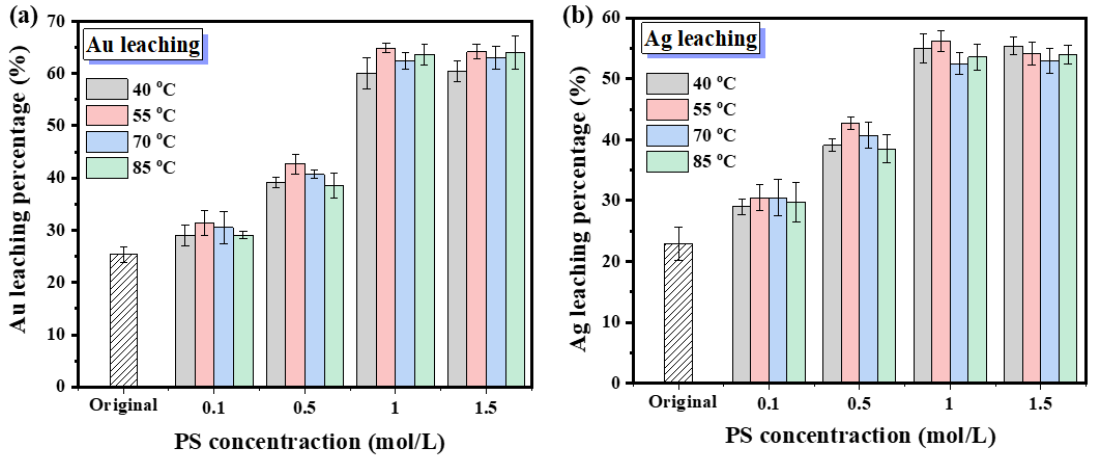

Figure 3.5 Leaching efficiency of (a) Au and (b) Ag from oxidized residues of Step I. (Condition: 3 mmol/L [Cu^{2+}], 0.4 mol/L [$S_2O_3^{2-}$], 0.1 mol/L glycine, pH=9)

3.3.1.2 Sustainable oxidation of pyrite at room temperature (Step II)

Step I oxidation improved Au (64.9%) and Ag (56.2%) leaching efficiencies, but it was still unsatisfactory for extraction. This is likely due to insufficient dissociation of encapsulated Au and Ag at this level of pyrite oxidation. To enhance leaching performance, a sustainable oxidation process (Step II) was developed. Iron (e.g., Fe^0, Fe^{2+}, Fe^{3+}, and Fe-based materials) has been widely used as a moderate activator in the PS oxidation process, achieving free radical ($\bullet SO_4^-$ and •OH) generation similar to the heating process [44]. As a result of Step I oxidation, pyrite produced a large amount of Fe ions, creating an acidic solution. This acid and Fe-rich solution was expected to further activate persulfate. After Step I oxidation, the reaction system was cooled to room temperature, and a desired concentration of PS was added to the solution (Figure 3.6a). The pyrite oxidation rate of 14.2% achieved in Step I (55 °C and 1.0 mol/L PS) was used as a baseline for evaluating the pyrite oxidation rate in Step II.

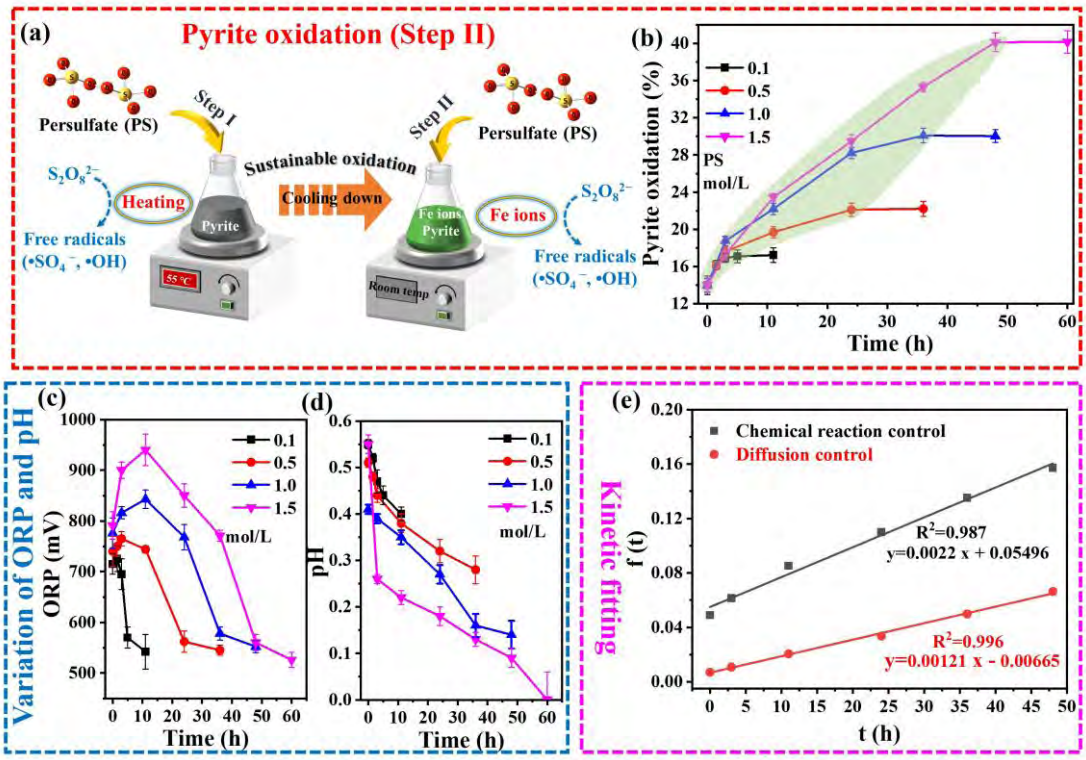

Figure 3.6 Step II pyrite oxidation. (a) Schematic diagram. (b) Pyrite oxidation efficiency. (c) Variations of ORP. (d) Variations of pH. (e) Kinetics fitting (1.5 mol/L persulfate)

As shown in Figure 3.6b, pyrite oxidation efficiency was substantially increased. Compared to Step I, the slower oxidation kinetics in Step II are likely due to moderate Fe ions causing a gradual conversion of persulfate into free radicals [45]. Particularly noteworthy was the substantial enhancement in the pyrite oxidation rate to 40.13% at a persulfate concentration of 1.5 mol/L, with a reaction time of 48 h. Like Step I oxidation, the oxidation of pyrite in Step II exhibited a close correlation with ORP, but the value of ORP was relatively low (Figure 3.6c). This difference is probably due to the higher reaction activity of heating than that of Fe ions for decomposing persulfate. Additionally, the solution pH continually decreased to approximately 0, creating a distinctly acidic system (Figure 3.6d). Figure 3.6e illustrates the kinetic fitting plots for Step II oxidation based on chemical reaction and diffusion controls. A similar observation indicates that Step II oxidation was also controlled by the diffusion model due to a better linear fitting ($R^2 = 0.996$).

The Au and Ag leaching results of the refractory pyrite concentrate after two oxidation steps are shown in Figure 3.7. Remarkably, the final oxidized residue with

the highest oxidation degree (43%, 1.5 mol/L PS) achieved excellent leaching percentages of 92.2% for Au and 88.6% for Ag. It was concluded that the proposed process is effective for improving gold leaching efficiency, and the higher the degree of pyrite oxidation, the greater the Au/Ag exposure, leading to higher leaching efficiency.

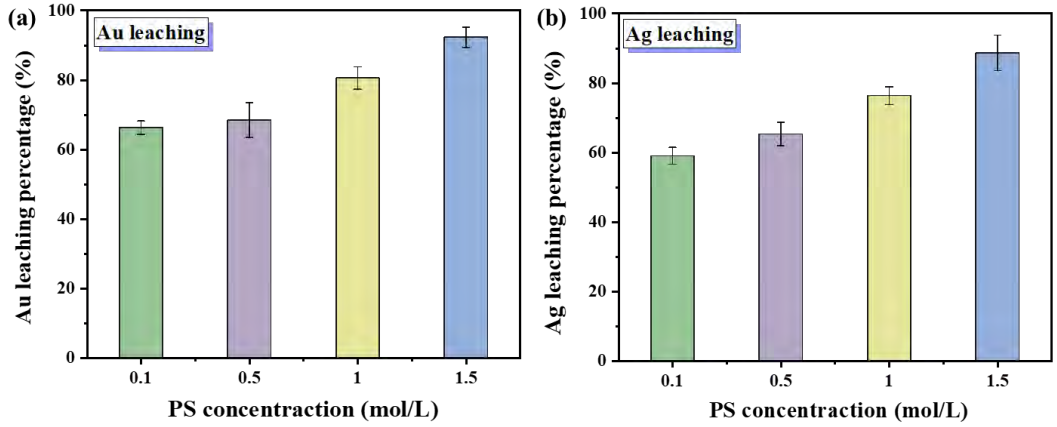

Figure 3.7 Leaching efficiency of (a) Au and (b) Ag from oxidized residues of Step II. (Condition: 3 mmol/L [Cu^{2+}], 0.4 mol/L [$S_2O_3^{2-}$], 0.1 mol/L glycine, pH=9)

3.3.2 Mechanism of pyrite oxidation in the stepwise processes

3.3.2.1 Release of Fe and S

In mineralogy, pyrite is composed of a ferrous cation (Fe^{2+}) and a sulfide anion (S_2^{2-}) with a ratio of 1:2 [46]. Other metals, such as Zn, As, Cu, Pb, Au, and Ag, are commonly found in pyrite mixtures. Reports indicate that the chemical oxidation of pyrite not only significantly releases Fe and S, but also dissolves these metal ions [47]. As illustrated in Figures 3.8a and 3.8b, base metals such as Fe, Zn, As, and Cu were dissolved during the two-step oxidation processes, while Au, Ag, and Pb remained undissolved due to their nobility [48]. Undoubtedly, Fe was the main product due to its ultrahigh concentration, with Step I predominantly yielding ferrous ions (Fe^{2+}) and Step II producing ferric ions (Fe^{3+}) as shown in Figure 3.8c. This result suggests that Fe^{2+} was dominant at the start of Step II oxidation, likely serving as an activator for persulfate. On the other hand, while pyrite oxidation in alkaline solutions often produces thiosulfate ($S_2O_3^{2-}$) and sulfite ions (SO_3^{2-}), this test exclusively detected increasing sulfate ions (SO_4^{2-}) in the acidic solution from Step I to Step II (Figure 3.8d). The source of SO_4^{2-} could be the release of S from pyrite and a decomposition product of persulfate. Therefore, Eqs. (3-9) to (3-12) explicitly expressed the generation of Fe

and S ions from pyrite with persulfate as oxidizing species [49-51].

$$FeS_2(pyrite) + 7S_2O_8^{2-} + 8H_2 \rightarrow Fe^{2+} + 16SO_4^{2-} + 16H^+ \quad (3\text{-}9)$$

$$FeS_2\ (pyrite) + 14\ \bullet SO_4^- + 8H_2O \rightarrow Fe^{2+} + 16SO_4^{2-} + 16H^+ \quad (3\text{-}10)$$

$$FeS_2\ (pyrite) \quad + 14 \bullet HO \rightarrow Fe^{2+} + 2SO_4^{2-} + 2H^+ + 6H_2O \quad (3\text{-}11)$$

$$S_2O_8^{2-} + Fe^{2+} \rightarrow \bullet SO_4^- + SO_4^{2-} + Fe^{3+} \quad (3\text{-}12)$$

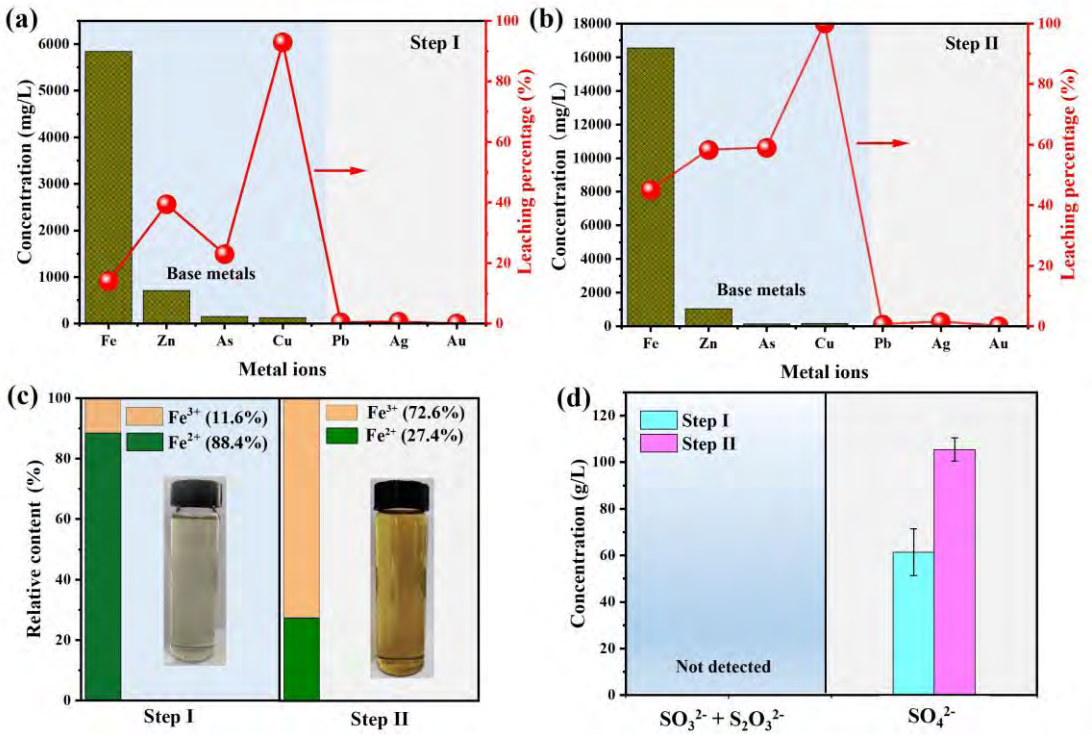

Figure 3.8 Products characterization of pyrite dissolution. Dissolved metal ions during (a) Step I and (b) Step II. (c) Relative content of Fe^{2+} and Fe^{3+} in solution. (d) Dissolved S species in solution

3.3.2.2 Formation of free radicals

When using persulfate as an oxidant, the effective oxidizing substances present in the system are free radicals [52]. Typically, when the system contains Fe ions as an activator or under heating, persulfate can easily decompose into $\bullet SO_4^-$ and then some of them react with H_2O to generate •HO [53]. To accurately detect the reactive radicals produced in the stepwise oxidation process, electron spin resonance (EPR) tests were performed at the actual oxidation conditions of Step I and Step II, using 5,5 dimethyl-L-pyrroline-N-oxide (DMPO) as a spin-trapping reagent. Based on the hyperfine splitting constants in previous studies, the characteristic peaks of a 1:1:1:1:1:1 sextet

and a 1:2:2:1 quartet were supposed to be the DMPO-•SO_4^- and DMPO-•OH adducts, respectively [54]. Therefore, Figure 3.9a confirmed that •OH was mainly produced in these systems, while the generation of •SO_4^- was insufficient evidence. This also provides strong evidence for our conjecture about the activation of persulfate by Fe ions, since •OH can be generated in step II even in the oxidation system without heating.

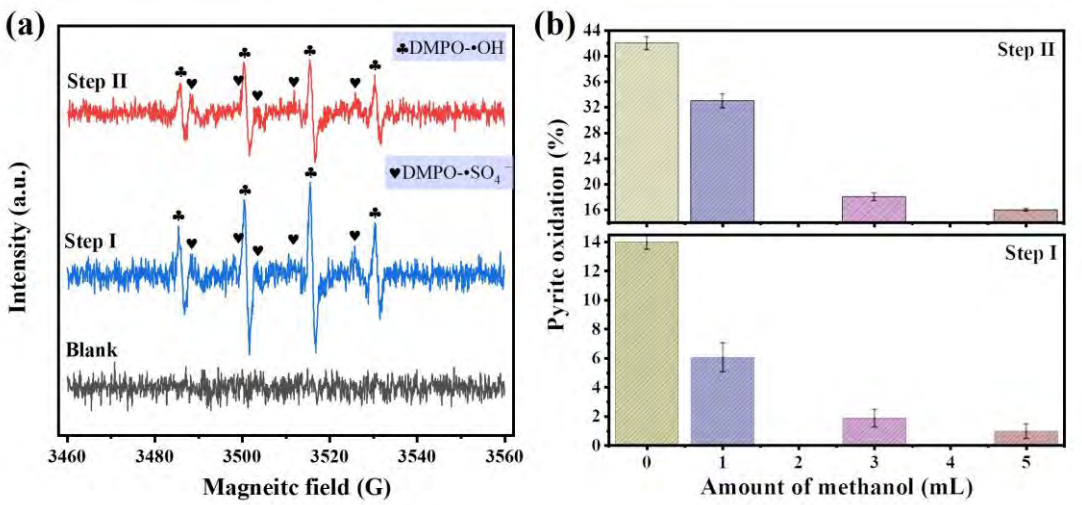

Figure 3.9 Characterization of reactive oxidizing species. (a) EPR spectra for the DMPO-•OH and DMPO-•SO_4^{2-} adducts. (b) Effect of methanol as a scavenger for •OH on the stepwise pyrite oxidation

To investigate the contribution of free radicals to pyrite oxidation, scavenging experiments were further conducted. As is well known, methanol was widely used as a scavenging reagent for •OH [55]. As shown in Figure 3.9b, without the addition of methanol, the oxidation of pyrite was 14.2% in Step I, and that in Step II was 40.13%, which could be attributed to the presence of •OH as the actual oxidizing species. Surprisingly, the oxidation rate of pyrite in both Step I and Step II oxidation was significantly reduced when methanol was added to the actual reaction, which suggested that pyrite oxidation during both steps was significantly inhibited by methanol. This could be a result of •OH playing a remarkable role in oxidizing pyrite.

3.3.2.3 Electrochemical analysis

Electrochemical measurements are powerful tools for analyzing the oxidation behavior of pyrite [56]. A pyrite block, from the same mine as the pyrite concentrate, was cut into a 1×1 cm^2 piece for use as a working electrode (Figure 3.10a), and its surface was carefully polished before each test. The Step I oxidation was tested at 55°C using a persulfate solution as an electrolyte, while the Step II oxidation was tested at

room temperature, employing the actual leach solution of Step I as an electrolyte (with persulfate). Figure 3.10a shows the cyclic voltammetry (CV) curves under Step I and Step II conditions (scan speed: 5 mV/s), with the results further divided into anodic and cathodic reactions in Figure 3.10b. In the anodic reaction, the current density increases from a voltage range of 0.6 V to 1.0 V, indicating significant pyrite oxidation without passivation [57], while the cathodic reaction in Step II shows a reduction peak at 0.2 V, due to Fe^{3+} reducing to Fe^{2+} in the Fe-rich leach liquor [58].

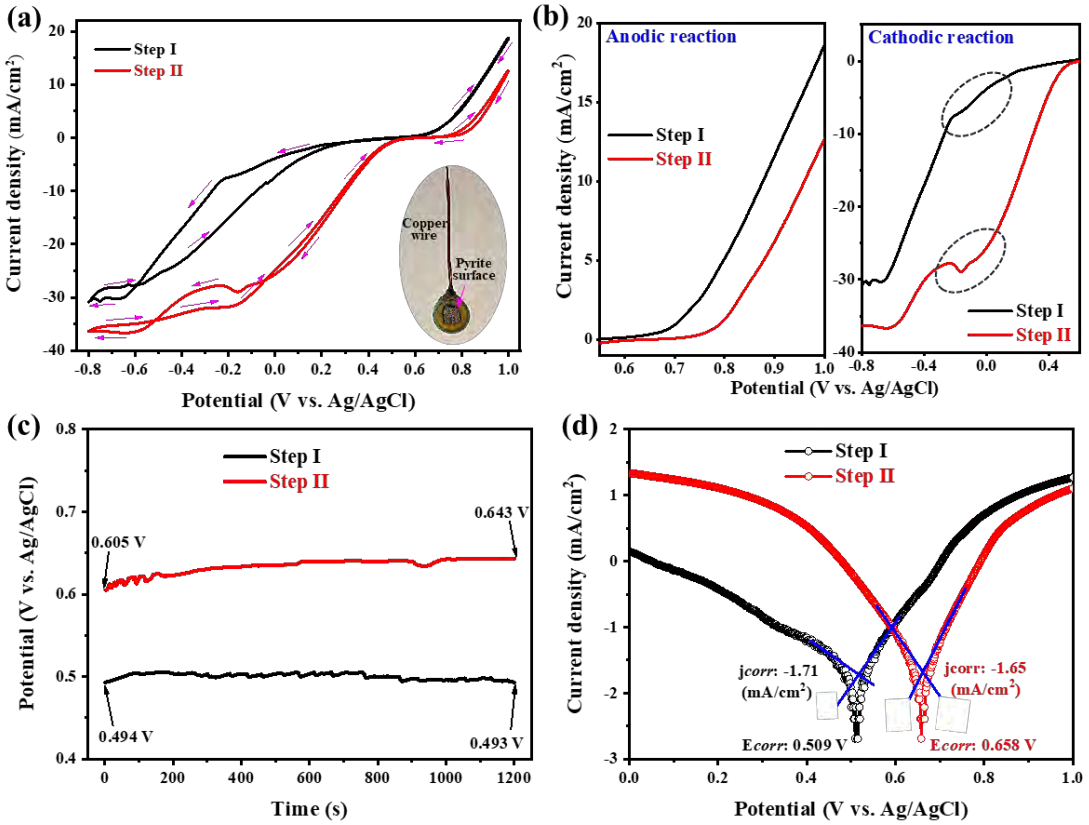

Figure 3.10 Electrochemical analysis of pyrite oxidation. (a, b) Cyclic voltammetry (CV), (c) open circuit potential (OCP), and (d) potentiodynamic polarization (PDP) curves for the pyrite electrode under stepwise oxidation

As depicted in Figure 3.10c, open circuit potential (OCP) increased from 0.605 V to 0.643 V during Step I but remained stable in Step II, fluctuating between 0.494 V and 0.493 V, indicating a stable reaction system [59]. Figure 3.10d shows potentiodynamic polarization (PDP) curves with corrosion potential (E_{corr}) and corrosion current density (j_{corr}), which are calculated based on a Tafel extrapolation method [60]. The lower E_{corr} and j_{corr} during Step I indicated a higher oxidizing capability [61]. In brief, the above results provided strong evidence that the higher oxidative capability of Step I and pyrite self-dissolved Fe ions can activate persulfate

to produce free radicals in Step II. Besides, the higher pyrite oxidation achieved in Step II is likely due to the moderate activation of persulfate by Fe ions, which improved the utilization efficiency of persulfate.

3.3.3 Correlation between mineralogical structure of pyrite and Au/Ag leaching

3.3.3.1 Phase changes and surface transformations

The change of phase and chemical composition of the pyrite surface during two-stage oxidation was analyzed by XRD and Raman. The XRD patterns showed that the crystalline phase of pyrite residue after two-stage oxidation has no obvious changes, mainly containing pyrite and impurities of quartz (Figure 3.11a). The new peaks at 23.1°, 25.6°, and 27.77° (2θ) with increased intensity during the gradual oxidation represented S^0. Raman spectra (Figure 3.11b) also detected element S^0 in the pyrite residue after two stages of oxidation. A slight peak of Fe_2O_3, or $Fe(OH)_3$, was detected in the oxidized pyrite samples, which inferred that elements sulfur (S^0), Fe_2O_3, or $Fe(OH)_3$ were the main solid products of the oxidation process (Eqs. 3-13 and 3-14) [62].

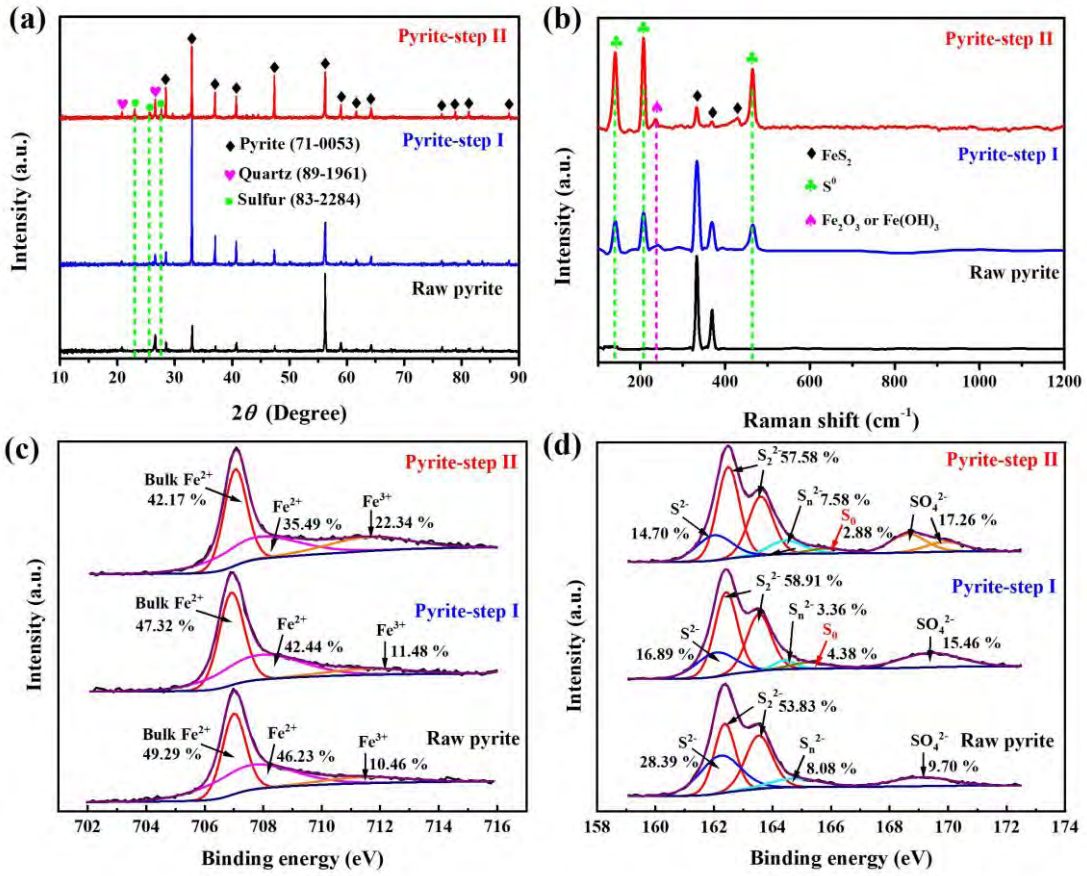

Figure 3.11 Structural evolution of pyrite during stepwise oxidation. (a) XRD patterns, (b) Raman spectra, and high-resolution (c) Fe 2p and (d) S 2p XPS spectra

$$FeS_2 \rightarrow Fe^{2+} + S^0 + S^{2-} \quad (3\text{-}13)$$

$$2Fe^{3+} + 3H_2O \rightarrow Fe(OH)_3 + 3H^+ \quad (3\text{-}14)$$

XPS was employed to compare chemical information on the surface of pyrite before and after oxidation. As depicted in Figure 3.11c, the peaks of 707.6 eV and 708.1 eV (Fe $2p_{3/2}$) correspond to high-spin Fe^{2+} cations bonded to S^{2-} anion in bulk pyrite (FeS_2), while the peak at 711.8 eV is assigned to some oxidized Fe^{3+} species [63]. For the sulfur species (Figure 3.11d), the peak at 162.6 eV was assigned to bulk S_2^{2-} of pyrite, while the peaks at 164.8, 165.4, and 169.2eV suggested the presence of S_n^{2-}, S_0, and SO_4^{2-}, respectively [64]. Before oxidation, the chemical state of iron and sulfur was mainly Fe^{2+} and S^{2-} of pyrite, with only small peaks of Fe^{2+} and SO_4^{2-} species. As oxidation continues, the intensity of the Fe^{2+} peak at 707.6 eV and 708.1 eV decreased, and the Fe^{3+} peak increased (the peak possibly represents hematite and goethite). Similarly, the intensity of the S^{2-} peak at 162.6 eV decreased, and S_0 and SO_4^{2-} increased. This result verified the partial oxidation of the pyrite surface, which was caused by the dissolution of iron and sulfur species.

3.3.3.2 Microstructure variations

SEM image of raw pyrite showed a large size, a smooth surface, and a dense bulk structure (Figures 3.12a and 3.12 b). It is obvious that the size of pyrite residues was reduced after oxidation, and abundant pores were produced on the pyrite surface (Figure 3.12c and 3.12 d). The oxidation residue of Pyrite-step II has an irregular appearance with a higher roughness on the surface (Figure 3.12e and 3.12f). As shown in Figure 3.12g, the particle size decreased progressively in the sequence from Raw pyrite, Pyrite-step I, and Pyrite-step II, which indicated that the oxidation process caused the shrinking of particles due to surface dissolution. For the two-stage oxidation residues, the particle size (D80) was approximately 46.25 μm for Pyrite-step I and 11.17 μm for Pyrite-step II, respectively. As shown in Figures 3.12h to 3.12i, the specific surface area (BET) of the final pyrite residual (Pyrite-step II) was 1.87 m^2/g, which is about 4 times larger than Raw pyrite (0.46 m^2/g). Meanwhile, the pore volume of Pyrite-step II (0.003 m^3/g) also increased by 4 times compared with Raw pyrite (0.012 m^3/g).

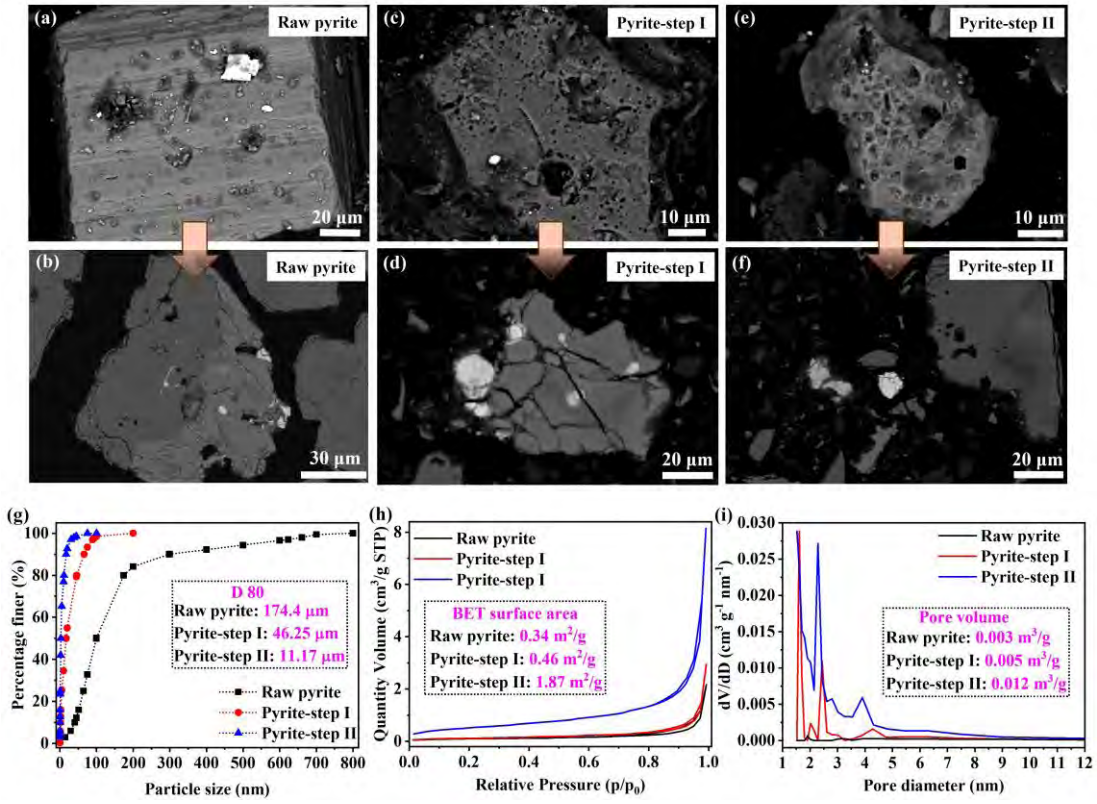

Figure 3.12 Microstructure of raw pyrite and oxidized residues (Pyrite-step I and Pyrite-step II). (a~f) SEM images. (g) Particle size distribution. (h) N_2 adsorption/desorption isotherm curves. (i) Pore size distribution

All the evidence shows that the stepwise pretreatment process successfully oxidized the pyrite enclosure, resulting in abundant pore generation, reduced particle size, and increased specific surface area. Furthermore, a schematic diagram (Figure 3.13) illustrates how these microstructural changes during pyrite oxidation enhance Au/Ag extraction. On one hand, as pyrite particle size decreases, most Au and Ag particles become exposed, making them reachable by the thiosulfate lixiviant [65]. On the other hand, the porous structure and larger specific surface area increase the lixiviant's contact with interior Au and Ag particles, enhancing their extraction potential [66]. For these reasons, pretreatment of refractory pyrite by the stepwise oxidation process using persulfate can be effective in improving the leaching performance of Au and Ag.

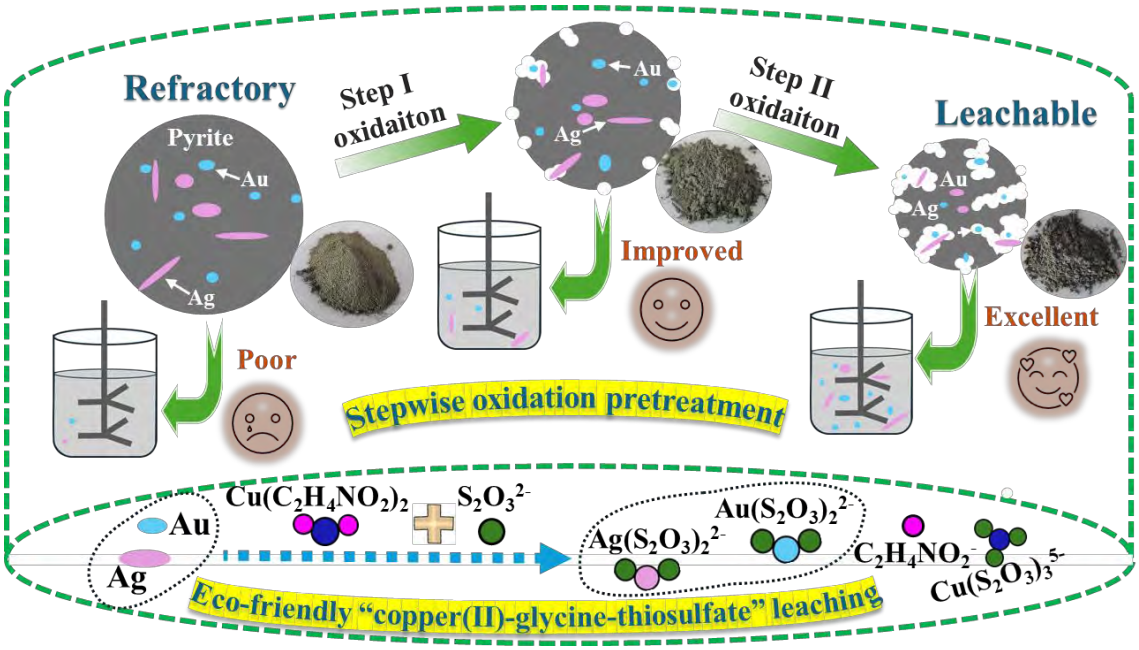

Figure 3.13 Schematic diagram of the contribution of the stepwise oxidation pretreatment for Au/Ag leaching by thiosulfate

3.3.4 Discussion of application prospects

Roasting oxidation pretreatment of refractory gold ore has been widely used for many years in gold mining. However, the increasing complexity of refractory ores has diminished the effectiveness of traditional roasting methods, necessitating supplementary techniques to achieve acceptable Au and Ag recovery (e.g., reduction roasting [67], suspension roasting [68], fluidized roasting [69], microwave-assisted roasting [70], $Na_2SO_4/CaCl_2$-assisted roasting [71, 72], etc.), which complicate operations and raise costs. Thus, it has yet to replace the role of roasting oxidation in industrial production, especially in ores becoming more complex and refractory.

Compared with current oxidation methods (Table 3.3), the proposed stepwise oxidation processes using persulfate can be seen as simple, only adding persulfate as an oxidant, and the activation process is performed at mild and sustainable conditions. The cost may be more economical when refractory ores contain a high amount of sulfide enclosure. Besides, this pretreatment process stands an absolute advantage in improving Au and Ag extraction from an exceedingly refractory ore, i.e., a pyrite concentrate, demonstrating high pretreatment effectiveness. Importantly, from the perspective of environmental protection, the whole process of "persulfate oxidation-thiosulfate leaching" is imperative to realize gold production by eco-friendly technologies, which has a bright prospect in industrial applications for refractory ores treatment, especially the extraction of Au and Ag from sulfide-containing ores.

Table 3.3 Summary of refractory ores pretreatment and Au/Ag leaching

Refractory ores	Pretreatment methods	leaching systems (leaching efficiency)	Ref.
Carbonaceous gold ore	Reduction roasting oxidation (Ar /1100 °C)	Cyanidation (83.25% Au)	[67]
Carbonaceous gold ore	Suspension roasting oxidation (O_2 and N_2 /650 °C)	Cyanidation (84.83% Au)	[68]
Polymetallic sulfide concentrate	Fluidized roasting oxidation (610~620 °C)	Chlorination (93.6% Au; 70.4% Ag)	[69]
Sulfide gold ore	Microwave-assisted roasting oxidation	HCl-$NaClO_3$ solution (92.5% Au)	[70]
Sulfide gold ore	Na_2SO_4-assisted roasting oxidation	Alkaline Na_2S solution (95% Au)	[71]
Sulfide gold ore	$CaCl_2$-assisted two stages roasting oxidation	Thiourea (85.37% Au)	[72]
Pyrite concentrate	Roasting oxidation at 500 °C/6h	Cyanidation (86% Au; 73% Ag)	[73]
Refractory pyrite-bearing gold ore	Pressure oxidation (200 °C /2800 Kpa)	Trichloroisocynauric acid (88.64% Au)	[74]
Low-grade As-bearing sulfide ore	Bio-oxidation (60 days)	Lvjin 83% Au	[75]
Fine-disseminated gold ore	Chemical oxidation by CaO and Na_2CO_3	Lime-Sulfur-Synthetic-Solution (LSSS) (86.55% Au)	[76]
As/Sb-bearing sulfide gold ore	Chemical oxidation by MnO_2 and HCl	Chlorination (97.2 % Au)	[77]
Pyrite concentrate	Stepwise chemical oxidation by persulfate	Copper(II)-glycine-thiosulfate system (92.2% Au; 88.6% Ag)	This work

3.4 Conclusions

Overall, the proposed stepwise oxidation processes for refractory pyrite pretreatment involved the generation of persulfate-based free radicals (mainly of •OH) via a beginning heating-activation (55 °C) and a subsequent pyrite self-dissolved Fe ions activation. Experiments revealed that both oxidation steps were subject to diffusion control and had a close relationship with solution potential (ORP). Although heating activation (Step I) was beneficial for free radicals (•OH) generation, the moderated Fe ions activation (Step II) achieved higher pyrite oxidation. Importantly, the mineralogical structure of pyrite was significantly changed after oxidation, including an oxidized surface, reduced particle size, increased specific surface area, developed porous channels, and exposure of the enclosed Au and Ag particles. As a result, the

leaching efficiency of Au and Ag significantly improved as high as 92.2% and 88.6% by an eco-friendly copper(II)-glycine-thiosulfate system, respectively. This work provides a promising "persulfate oxidation-thiosulfate leaching" process for precious metals (Au/Ag) extraction from refractory pyrite resources.

3.5 References

[1] Z. Jamshidi, N. Asadi-Aghbolaghi, R. Morad, E. Mahmoudi, S. Sen, M. Maaza, L. Visscher, Comparing the nature of quantum plasmonic excitations for closely spaced silver and gold dimers, J. Chem. Phys. 156 (2022) 074102.

[2] A.C. Ferdinand, D. Manikandan, P. Manikandan, G. Kavitha, R. Gaur, M. Maaza, E. Manikandan, Nobel Ag–Cu ion-exchange bimetallic nanoclusters formation over gold ion (Au^{2+}) implanted materials RBS and optical study, Radiat. Eff. Defects Solids 176 (2021) 955-966.

[3] M. Maaza, H. Chambalo, S. Ekambaram, O. Nemraoui, B.D. Ngom, N. Manyala, Pulsed laser liquid-solid interaction synthesis of Pt, Au, Ag and Cu nanosuspensions and their stability, Int. J. Nanopart. 1 (2008) 212-223.

[4] M. Maaza, O. Nemraoui, C. Sella, A.C. Beye, Surface Plasmon Resonance Tunability in Au−VO_2 Thermochromic Nano-composites, Gold Bull. 38 (2005) 100-106.

[5] A. Dakka, J. Lafait, C. Sella, S. Berthier, M. Abd-Lefdil, J.C. Martin, M. Maaza, Optical properties of Ag-TiO_2 nanocermet films prepared by cosputtering and multilayer deposition techniques, Appl. Opt. 39 (2000) 2745-2753.

[6] Z.Y. Nuru, C.J. Arendse, R. Nemutudi, O. Nemraoui, M. Maaza, Pt–Al_2O_3 nanocoatings for high temperature concentrated solar thermal power applications, Physica B: Condensed Matter 407 (2012) 1634-1637.

[7] V. Ibarra-Galvan, A. López-Valdivieso, X. Tong, Y. Cui, Role of oxygen and ammonium ions in silver leaching with thiosulfate–ammonia–cupric ions, Rare Met. 33 (2014) 225-229.

[8] D. Liu, Y. Wang, Y. Xian, S. Wen, Electronic structure and flotability of gold-bearing pyrite: A density functional theory study, J. Cent. South Univ. 24 (2017) 2288-2293.

[9] R.R. Large, L. Danyushevsky, C. Hollit, V. Maslennikov, S. Meffre, S. Gilbert, S. Bull, R. Scott, P. Emsbo, H. Thomas, Gold and trace element zonation in pyrite using a laser imaging technique: Implications for the timing of gold in orogenic and Carlin-style sediment-hosted deposits, Econ. Geol. 104 (2009) 635-668.

[10] P. Gopon, J.O. Douglas, M.A. Auger, L. Hansen, J. Wade, J.S. Cline, L.J. Robb, M.P. Moody, A nanoscale investigation of Carlin-type gold deposits: An atom-scale elemental and isotopic perspective, Econ. Geol. 114 (2019) 1123-1133.

[11] R.K. Asamoah, W. Skinner, J. Addai-Mensah, Leaching behaviour of mechano-

chemically activated bio-oxidised refractory flotation gold concentrates, Powder Technol. 331 (2018) 258-269.
[12] F. Xie, J. Chen, J. Wang, W. Wang, Review of gold leaching in thiosulfate-based solutions, Trans. Nonferrous Met. Soc. China 31 (2021) 3506-3529.
[13] Y. Zhao, H. Zhao, T. Abashina, M. Vainshtein, Review on arsenic removal from sulfide minerals: An emphasis on enargite and arsenopyrite, Miner. Eng. 172 (2021) 107133.
[14] R. Wang, C. Liu, Y. Yang, J. Zhou, Y. Guo, B. Xie, Pretreatment of refractory gold concentrate calcine using ammonium bifluoride and sulfuric acid solution, Miner. Eng. 187 (2022) 107778.
[15] Y. Liu, W.S. Ng, M. Chen, Acid pressure oxidation leaching of arsenopyrite in the presence of pyrite: Oxygen consumption kinetics, Miner. Eng. 195 (2023) 108025.
[16] H. Shang, W. Gao, B. Wu, J. Wen, Bioleaching and dissolution kinetics of pyrite, chalcocite and covellite, J. Cent. South Univ. 28 (2021) 2037-2051.
[17] X. Li, N. Hiroyoshi, C.B. Tabelin, K. Naruwa, C. Harada, M. Ito, Suppressive effects of ferric-catecholate complexes on pyrite oxidation, Chemosphere 214 (2019) 70-78.
[18] Z. Dong, Y. Zhu, Y. Han, X. Gu, K.J.M.E. Jiang, Study of pyrite oxidation with chlorine dioxide under mild conditions, Miner. Eng. 133 (2019) 106-114.
[19] M. Su, H. Liu, C. Zhang, C. Liu, Y. Pei, H_2O_2 mediated oxidation mechanism of pyrite (0 0 1) surface in the presence of oxygen and water, Appl. Surf. Sci. 617 (2023) 156568.
[20] D. Rogozhnikov, K. Karimov, A. Shoppert, O. Dizer, S. Naboichenko, Kinetics and mechanism of arsenopyrite leaching in nitric acid solutions in the presence of pyrite and Fe (III) ions, Hydrometallurgy 199 (2021) 105525.
[21] R. Zhang, H. Wang, E. Hu, Z. Lei, F. Hu, W. Hou, Q. Wang, Oxidation of pyrite using ozone micro-nano bubbles, Mining, Metallurgy & Exploration 39 (2022) 709-719.
[22] M. Chen, Z. Zhang, X. Hu, J. Tian, Z. Lu, J. Wang, R. Wan, X. Zhou, X. Zhou, P. Shen, Oxidation mechanism of arsenopyrite under alkaline conditions: Experimental and theoretical analyses, J. Cleaner Prod. 358 (2022) 131987.
[23] P.R. Holmes, F.K. Crundwell, The kinetics of the oxidation of pyrite by ferric ions and dissolved oxygen: an electrochemical study, Geochim. Cosmochim. Acta 64 (2000) 263-274.
[24] Q. Gui, L. Fu, Y. Hu, H. Di, M. Liang, S. Wang, L. Zhang, E. Dong, Oxidative pretreatment of refractory gold ore using persulfate under ultrasound for efficient leaching of gold by a novel eco-friendly lixiviant: Demonstration of the effect of particle size and economic benefits, Hydrometallurgy 221 (2023) 106110.
[25] B.N. Ezealigo, A.C. Nwanya, A. Simo, R. Bucher, R.U. Osuji, M. Maaza, M.V. Reddy, F.I. Ezema, A study on solution deposited CuSCN thin films: Structural,

electrochemical, optical properties, Arabian J. Chem. 13 (2020) 346-356.
[26] I. De Michelis, A. Olivieri, S. Ubaldini, F. Ferella, F. Beolchini, F. Vegliò, Roasting and chlorine leaching of gold-bearing refractory concentrate: Experimental and process analysis, Int. J. Min. Sci. Technol. 23 (2013) 709-715.
[27] Q. Weng, S. Song, W. Zhan, X. Zhang, Z. Xiang, J. Gao, F. Jia, Novel recovery of a low-concentration gold thiosulfate complex through electroreduction via a walnut shell charcoal electrode, Green and Smart Mining Engineering 1 (2024) 58-66.
[28] M. Ostadrahimi, S. Farrokhpay, K. Karimnejad, A. Rahimian, M. Molavi, G. Shahkarami, A comparison of Fe(III) to Fe(II) reduction methods in iron analysis via titration, Chemical Papers 78 (2024) 5407-5414.
[29] S.J. Kochor, Determination of barium, sulfur, and sulfates, Ind. Eng. Chem. Anal. Ed. 9 (1937) 331-333.
[30] G. Zhang, L. Hou, P. Chen, Q. Zhang, Y. Chen, N.Z. Zainiddinovich, C. Wu, L.V. Alejandro, F. Jia, Efficient and stable leaching of gold in a novel ethydiaminedhephen acetic-thiosulfate system, Minerals Engineering 209 (2024) 108639.
[31] N. Li, S. Wu, H. Dai, Z. Cheng, W. Peng, B. Yan, G. Chen, S. Wang, X. Duan, Thermal activation of persulfates for organic wastewater purification: Heating modes, mechanism and influencing factors, Chem. Eng. J. 450 (2022) 137976.
[32] Y. Guo, H. Liang, L. Bai, K. Huang, B. Xie, D. Xu, J. Wang, G. Li, X. Tang, Application of heat-activated peroxydisulfate pre-oxidation for degrading contaminants and mitigating ultrafiltration membrane fouling in the natural surface water treatment, Water Res. 179 (2020) 115905.
[33] C. Liu, G. Zhang, H. Zhang, J. Zhao, Y. Wang, F. Jia, S. Song, Construction of Ag/MoS_2@Fe-CS aerogel as excellent PMS activator via synergistic photocatalysis and photothermal effects, Chem. Eng. J. 455 (2023) 140814.
[34] X. Duan, S. Indrawirawan, J. Kang, W. Tian, H. Zhang, X. Duan, X. Zhou, H. Sun, S. Wang, Synergy of carbocatalytic and heat activation of persulfate for evolution of reactive radicals toward metal-free oxidation, Catal. Today 355 (2020) 319-324.
[35] T. Liu, Y. Hu, N. Chen, Q. He, C. Feng, High redox potential promotes oxidation of pyrite under neutral conditions: Implications for optimizing pyrite autotrophic denitrification, J. Hazard. Mater. 416 (2021) 125844.
[36] X. Huang, R. Liao, B. Yang, S. Yu, B. Wu, M. Hong, J. Wang, H. Zhao, M. Gan, F. Jiao, W. Qin, G. Qiu, Role and maintenance of redox potential on chalcopyrite biohydrometallurgy: An overview, J. Cent. South Univ. 27 (2020) 1351-1366.
[37] P. Zhang, S. Yuan, P. Liao, Mechanisms of hydroxyl radical production from abiotic oxidation of pyrite under acidic conditions, Geochim. Cosmochim. Acta 172 (2016) 444-457.
[38] S. Zhong, Leaching kinetics of gold bearing pyrite in H_2SO_4–$Fe_2(SO_4)_3$ system,

Trans. Nonferrous Met. Soc. China 25 (2015) 3461-3466.
[39] Y. Lin, X. Hu, F. Zi, Thiocyanate facilitating thiosulfate extraction of gold via inhibiting formation of passive layer, Sustainable Mater. Technol. 40 (2024) e00878.
[40] S. Faraz, D. Hossna, B. Rezgar, Z. Piroz, Improved recovery of a low-grade refractory gold ore using flotation–preoxidation–cyanidation methods, Int. J. Min. Sci. Technol. 24 (2014) 537-542.
[41] L. Hou, A. López Valdivieso, P. Chen, G. Zhang, Q. Zhang, Y. Chen, S. Song, F. Jia, An electrochemical study of the dissolution behavior of gold in a novel glycine-thiosulfate system, Miner. Eng. 202 (2023) 108273.
[42] J. Wang, R. Wang, Y. Pan, F. Liu, Z. Xu, Thermodynamic analysis of gold leaching by copper-glycine-thiosulfate solutions using Eh-pH and species distribution diagrams, Miner. Eng. 179 (2022) 107438.
[43] J. Li, H. Yang, R. Zhao, L. Tong, Q. Chen, Mineralogical characteristics and recovery process optimization analysis of a refractory gold ore with gold particles mainly encapsulated in pyrite and arsenopyrite, Geochemistry 83 (2023) 125941.
[44] S. Xiao, M. Cheng, H. Zhong, Z. Liu, Y. Liu, X. Yang, Q. Liang, Iron-mediated activation of persulfate and peroxymonosulfate in both homogeneous and heterogeneous ways: A review, Chem. Eng. J. 384 (2020) 123265.
[45] Y. Tang, G. Li, Y. Yang, J. Ma, Y. Zhi, Y. Yao, L. Zheng, B. Tuo, Oxidation of Gold-Bearing Pyrite by Ammonium Persulfate, Journal of Sustainable Metallurgy 7 (2021) 1280-1292.
[46] M. Descostes, P. Vitorge, C. Beaucaire, Pyrite dissolution in acidic media, Geochim. Cosmochim. Acta 68 (2004) 4559-4569.
[47] Y. Zhu, F. Di Capua, D. Li, H. Li, Enhancement and mechanisms of micron-pyrite driven autotrophic denitrification with different pretreatments for treating organic-limited waters, Chemosphere 308 (2022) 136306.
[48] W. Zhan, X. Zhang, Y. Yuan, Q. Weng, S. Song, M. Martínez-López, J.L. Arauz-Lara, F. Jia, Regulating Chemisorption and Electrosorption Activity for Efficient Uptake of Rare Earth Elements in Low Concentration on Oxygen-Doped Molybdenum Disulfide, ACS nano 18 (2024) 7298–7310.
[49] Y. Ou, Y. Yang, K. Li, W. Gao, L. Wang, Q. Li, T. Jiang, Eco-friendly and low-energy innovative scheme of self-generated thiosulfate by atmospheric oxidation for green gold extraction, J. Cleaner Prod. 387 (2023) 135818.
[50] Z. Dong, T. Jiang, B. Xu, Y. Yang, Q.o.C.P. Li, An eco-friendly and efficient process of low potential thiosulfate leaching-resin adsorption recovery for extracting gold from a roasted gold concentrate, J. Cleaner Prod. 229 (2019) 387-398.
[51] Y. Ou, Y. Yang, L. Wang, W. Gao, K. Li, Y. Zhang, Q. Li, T. Jiang, Process Mechanism for Production of Green Lixiviant Thiosulfate at Atmospheric

Pressure, ACS Sustainable Chem. Eng. 11 (2023) 10471-10481.
[52] H. Zhang, L. Qiao, J. He, N. Li, D. Zhang, K. Yu, H. You, J. Jiang, Activating peroxymonosulfate by halogenated and methylated quinones: performance and mechanism, RSC Adv. 9 (2019) 27224-27230.
[53] W. Huang, S. Xiao, H. Zhong, M. Yan, X. Yang, Activation of persulfates by carbonaceous materials: A review, Chem. Eng. J. 418 (2021) 129297.
[54] C. Qi, G. Yu, J. Huang, B. Wang, Y. Wang, S. Deng, Activation of persulfate by modified drinking water treatment residuals for sulfamethoxazole degradation, Chem. Eng. J. 353 (2018) 490-498.
[55] Y. Chen, K. Zhu, Y. Huang, J. Zhang, X. Li, Z. Zheng, Z. Jiang, D. Hu, S. Luo, P. Fang, K. Yan, Facile synthesis of fine-grained $CoFe_2O_4$ anchored on porous carbon for simultaneous removal of tetracycline and arsenite via peroxymonosulfate activation, Sep. Purif. Technol. 328 (2024) 125131.
[56] Y. Zhang, C. Cui, S. Lin, H. Li, L. Yang, Y. Xie, H. Hu, L. Zhou, H. Wang, C. Li, In-situ electrochemical study on the effects of Fe(III) on kinetics of pyrite acidic pressure oxidation, Acta Geochimica 43 (2024) 814-825.
[57] D.P. Tao, P.E. Richardson, G.H. Luttrell, R.H. Yoon, Electrochemical studies of pyrite oxidation and reduction using freshly-fractured electrodes and rotating ring-disc electrodes, Electrochim. Acta 48 (2003) 3615-3623.
[58] A. Rafsanjani-Abbasi, A. Davoodi, Electrochemical Characterization of Natural Chalcopyrite Dissolution in Sulfuric Acid Solution in Presence of Peroxydisulfate, Electrochim. Acta 212 (2016) 921-928.
[59] D. Li, C. Liu, Y. Liu, X. Chen, W. Wu, F. Li, J. Tian, Z. Dang, Tannic acid as an eco-friendly natural passivator for the inhibition of pyrite oxidation to prevent acid mine drainage at the source, Appl. Surf. Sci. 591 (2022) 153172.
[60] B. Xu, Y. Nie, X. Feng, Q. Wang, Dissolution patterns of gold on various structural surfaces in thiosulfate solutions: The effect of interface adsorption on thiosulfate oxidation and gold atom dissociation, Electrochimica Acta 497 (2024) 144602.
[61] Y. Zhang, F. Zi, X. Hu, Z. Chen, P. Yang, Y. Chen, X. Qin, S. Chen, P. He, Y. Lin, L. Zhao, Mechanism of pyrite oxidation in copper(II)-ethylenediamine-thiosulphate gold leaching system, Electrochim. Acta 390 (2021) 138752.
[62] A.P. Chandra, A.R. Gerson, The mechanisms of pyrite oxidation and leaching: A fundamental perspective, Surf. Sci. Rep. 65 (2010) 293-315.
[63] M. Descostes, F. Mercier, C. Beaucaire, P. Zuddas, P. Trocellier, Nature and distribution of chemical species on oxidized pyrite surface: Complementarity of XPS and nuclear microprobe analysis, Nucl. Instr. and Meth. B 181 (2001) 603-609.
[64] S. Mattila, J.A. Leiro, M. Heinonen, XPS study of the oxidized pyrite surface, Surf. Sci. 566-568 (2004) 1097-1101.
[65] E. Bidari, V. Aghazadeh, Pyrite oxidation in the presence of calcite and dolomite:

Alkaline leaching, chemical modeling and surface characterization, Trans. Nonferrous Met. Soc. China 28 (2018) 1433-1443.

[66] O. Celep, İ. Alp, H. Devecİ, M. Vicil, Characterization of refractory behaviour of complex gold/silver ore by diagnostic leaching, Trans. Nonferrous Met. Soc. China 19 (2009) 707-713.

[67] X. Zhang, Y. Song, L. Wu, P. Dong, M. Zhou, G. Liu, Improvement of the leach efficiency of carbonaceous gold concentrates using reduction roasting pretreatment technology, Advanced Powder Technology 33 (2022) 103387.

[68] H. Xiao, J. Jin, F. He, Y. Han, Y. Sun, Z. Tang, Z. Dong, Accelerating the decarbonization of carbonaceous gold ore by suspension oxidation roasting towards the improvement of gold leaching efficiency, Adv. Powder Technol. 33 (2022) 103833.

[69] B. Xu, Y. Yang, Q. Li, G. Li, T. Jiang, Fluidized roasting-stage leaching of a silver and gold bearing polymetallic sulfide concentrate, Hydrometallurgy 147-148 (2014) 79-82.

[70] A. Hapid, S. Zullaikah, Mahfud, A. Kawigraha, Y. Sudiyanto, R. Benita Nareswari, A.T. Quitain, Oxidation of sulfide mineral and metal extraction analysis in the microwave-assisted roasting pretreatment of refractory gold ore, Arabian J. Chem. 17 (2024) 105447.

[71] X. Liu, Q. Li, Y. Zhang, T. Jiang, Y. Yang, B. Xu, Y. He, Improving gold recovery from a refractory ore via Na2SO4 assisted roasting and alkaline Na2S leaching, Hydrometallurgy 185 (2019) 133-141.

[72] H. Qin, X. Guo, Q. Tian, D. Yu, L. Zhang, Recovery of gold from sulfide refractory gold ore: Oxidation roasting pretreatment and gold extraction, Miner. Eng. 164 (2021) 106822.

[73] Y. Zhang, K. Yang, Y. Fang, A.R. Cabrera, C. Peng, A. López-Valdivieso, Roasting temperature effect on the recovery of refractory gold and silver in pyrite concentrates, J. Min. Metall., Sect. B 57 (2021) 235-243.

[74] H. Niu, H. Yang, L. Tong, Research on gold leaching of carbonaceous pressure-oxidized gold ore via a highly effective, green and low toxic agent trichloroisocyanuric acid, J. Cleaner Prod. 419 (2023) 138062.

[75] J. Li, L. Tong, H. Zhang, Q. Chen, H. Yang, L. Shen, Y. Zhai, R. Yao, Pool bio-oxidation and fitting analysis of low-grade arsenic-containing refractory gold ore, Green Chem. Eng. 5 (2024) 511-518.

[76] Z. Shen, T. Wu, J. Wang, S. Mao, X. Wang, Mechanism of synergistic pretreatment with eco-friendly CaO and Na_2CO_3 to enhance gold leaching efficiency from fine-disseminated gold ores, J. Cleaner Prod. 442 (2024) 141117.

[77] J. Kang, C. Yu, X. Wang, Z. Liu, Y. Wang, A novel non-cyanide extraction method of gold for high As-Sb-bearing refractory gold ore based on Mn-oxide ore acidic oxidation, Chem. Eng. Res. Des. 189 (2023) 347-357.

Chapter IV. A highly efficient clean hydrometallurgy process for gold leaching in a Fenton oxidation-assisted thiourea system

4.1 Introduction

Cyanidation has been used for centuries as an economical and mature hydrometallurgy process for the extraction of gold from various gold-containing raw materials, such as gold ores, concentrates, as well as electronic wastes [1, 2]. However, the conventional cyanidation remains beset by the greatest chemical toxicity, which can result in substantial environmental impacts and public health risks if released into the environment [3]. Besides chemical toxicity, cyanidation tailings not only release hazardous substances into the surrounding soil and water, but also necessitate land for constructing tailing dams, incurring high maintenance costs [4]. Hence, various global environmental groups have been calling for a ban on cyanidation to eliminate its harmful effects. In response to advancements in environmental protection laws and sustainable technologies, clean hydrometallurgy processes (CHPs), noted for their efficiency, safety, and environmental friendliness, have been gradually evaluated to ensure the sustainable development of gold extraction mining [5, 7].

Currently, the development of CHPs in gold leaching primarily revolves around "oxidant-ligand" systems, which require an oxidant (oxidation catalysts) to oxidize noble gold and a ligand to complex with the oxidative gold ion (Au^{+} or Au^{3+}). These systems are typically implemented using either aqueous or organic solvents, respectively. The aqueous systems are most widely studied in gold leaching over the past several decades, employing a wide variety of nonhazardous ligands as alternative lixiviants, such as thiosulfate ($S_2O_3^{2-}$), thiourea ($CS(NH_2)_2$), halogenation (Cl^{-}, Br^{-}, and I^{-}), thiocyanate (SCN^{-}), and glycine ($NH_2CH_2COO^{-}$) [8]. The solution chemistry of these aqueous systems is very complicated, and using a series of oxidation catalysts (e.g., Cu^{2+}, Fe^{3+}, H_2O_2, I_2, HClO, $KMNO_4$, Na_2O_2, etc.) is crucial for successful dissolution of gold [9]. Topically, oxidants are capable for reducing the activation energy of the reaction between gold and lixiviant, facilitating the breakage of Au-Au bonds to form water-soluble Au-complex ions, such as $Au(S_2O_3)_2^{3-}$, $Au(CS(NH_2)_2)_2^{+}$, $Au(SCN)_2^{-}$, AuI_2^{-}, $AuBr_2^{-}$, $AuCl_2^{-}$, $Au(NH_2CH_2COO)_2^{-}$, and so on [10]. CHPs based on aqueous solvent have attracted extensive attention for gold leaching from low-grade

gold ore, refractory gold ore, gold concentrate calcine, and gold bearing wasters in laboratory scale, exhibiting higher leaching efficiency than the conventional cyanidation process. Besides, these aqueous systems can better meet the fundamental requirements for gold leaching in mining without necessitating changes to the existing cyanidation equipment, while also avoiding the generation of large amounts of harmful waste residue or wastewater [11]. Despite these efforts to develop environmentally friendly aqueous systems for gold leaching, research on benign production scale has yet to make significant progress because of large reagent consumption and relatively low kinetics [12]. Hence, alternative systems have been pursued, particularly the use of organic solvents as replacements, aiming to achieve more sustainable and selective leaching of gold.

Research has demonstrated that the use of "organic aqua regia" composed of thionyl chloride ($SOCl_2$) as solvent and organic reagents (i.e., pyridine, N, N-dimethylformamide, and imidazole) can selectively dissolve gold from mixtures of coexisting precious metals like Pt/Au/Pd and Au/Pd mixtures [13]. Like this, Yue and co-workers reported a gold dissolution strategy based on the combination of N-bromosuccinimide (NBS) as oxidant and pyridine (Py) as ligand, and the final product was $(Py)AuBr_3$, a water-soluble salt [14]. Using acetone as a solvent, Serpe et al. exploited iodine (I_2) to mildly oxidize Au^0 to Au^{3+} complexes in the presence of sulfur-donor ligands such as dithioxamides and tetraalkylthiuram disulfides [15]. Similarly, Repo and co-workers developed the use of pyridine thiols (ligand) and H_2O_2 (oxidant) in ethanol solvent to dissolve gold [16]. Further, this group achieved the dissolution of gold quantitatively in ethanol using 2-mercaptobenzimidazole as a ligand in the presence of the oxidant iodine [17]. Besides, systems employing halogen-halide polar organic solvents [18], dihalogen-sulphur-containing ligand adducts [19], sulphur-containing triiodide ligands [20], and aromatic thiol ligands [21] have been proposed as promising means for dissolving gold, mainly using various tri-halide derivatives as oxidants [22]. In a recent publication, Bian et al. developed a photocatalytic method for the efficient dissolution of chemically inert gold and other precious metals in acetonitrile and dichloromethane as solvents. Utilizing sunlight as energy, the reactive oxygen species (ROS) generated from the TiO_2 photocatalyst acted as the oxidant, facilitating the rapid dissolution of gold within tens of minutes [23, 25]. Broadly speaking, the organic solvent-based CHPs offer the advantages of fast reaction kinetics and higher selectivity than aqueous systems. However, while these processes hold potential for small-scale recycling of secondary resources like gold-bearing waste

circuit boards and waste catalysts, their application in large-scale mining operations is inevitably hindered by high costs. Besides, these processes are associated with severe environmental concerns due to the generation of large quantities of wastewaters and the use of volatile organic solvents. Therefore, a clean hydrometallurgy process that simultaneously avoids toxic reagents and enables gold extraction into a safe solvent has remained out of reach and is urgently needed.

Inspired by the above, this work focused on the efficient, benign, and scalable leaching of gold from a roasted gold concentrate via a clean hydrometallurgy process, based on the Fenton oxidation-assisted thiourea system. The process variables (H_2O_2, Fe^{2+}, and TU concentrations and pH) and the operation parameters (stirring speed and pulp density) were systematically optimized. Besides, more insights were provided by incorporating nitrilotriacetic acid (NTA) as an additive to reduce the thiourea consumption. Importantly, the gold leaching mechanisms, with an emphasis on the contribution of ROS on gold dissolution, were investigated by electron paramagnetic resonance (EPR), chemical scavenging experiments, linear sweep voltammetry (LSV), and frontier orbital theory using the energy level of the highest occupied molecular orbital (E_{HOMO}). This study is expected to develop a clean hydrometallurgy system for replacing the cyanidation process in gold mining.

4.2 Materials and methods

4.2.1 Materials and reagents

The gold ore used in this study is a multi-stage pretreated concentrate prepared by roasting and subsequent sulfuric acid leaching for copper removal, which is provided by Jinyuan Mining Co., Ltd (Henan province, China). As seen in Table 4.1, the semiquantitative chemical analysis of the gold ore predominantly consists of Si, Fe, Al, and Ca. The gold grade of the roasted gold concentrate was determined as 43.9 g/t by fire assay. X-ray diffraction (XRD) pattern shows several gangue minerals of quartz (SiO_2), hematite (Fe_2O_3), lead sulfate ($PbSO_4$), and calcium sulfate ($CaSO_4$) (Figure 4.1a). The particle size distribution is shown in Figure 4.1b, which shows that over 80 wt% of ore particles are smaller than 187.34 μm. It is known from the results of mineral liberation analysis (MLA) that the gold particle is exposed, as displayed in Figure 4.1c. Since near 100% of gold was leached by cyanidation in the factory (66 h), this gold ore was chosen as a representative sample to standardly evaluate the leaching efficiency in the following experiments. Besides, the waste printed circuit boards (WPCBs) used in this study were from spent mobile phone motherboards.

Table 4.1 Chemical composition of the gold ore sample. wt%

Elements	Fe	SiO_2	Al_2O_3	S	Ca	C	K	Pb	As	Au(g/t)
Content	27.27	29.67	6.89	5.33	2.93	1.48	1.23	0.765	0.287	43.9

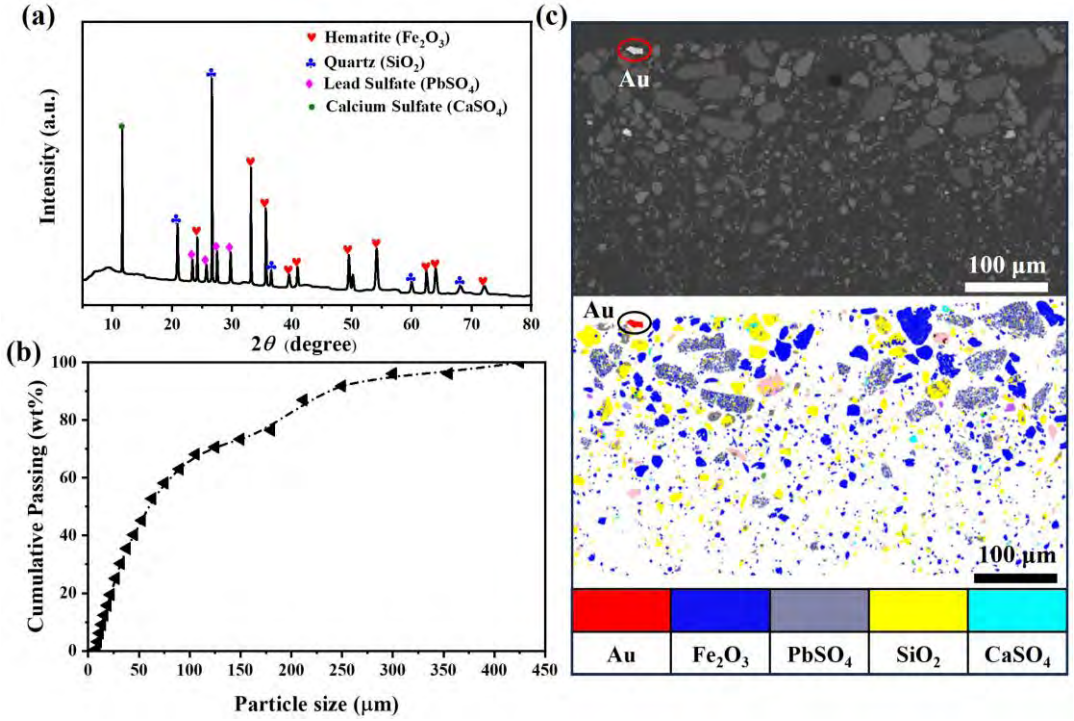

Figure 4.1 Characterization of gold ore sample. (a) XRD spectrogram, (b) Particle size distribution, and (c) Mineral Liberation Analysis (MLA) mapping

The analytical grade reagents, such as hydrogen peroxide (H_2O_2, 30% *w*/*v*), ferrous sulfate ($FeSO_4 \cdot 7H_2O$), thiourea (TU, $CS(NH_2)_2$), and Nitrilotriacetic acid (NTA), utilized in this study were supplied by Sigma-Aldrich. Unless specified otherwise, Fe^{2+} and TU refer to $FeSO_4 \cdot 7H_2O$ and thiourea, respectively. Additionally, all the leaching solutions were prepared using deionized water.

4.2.2 Gold leaching procedures

Gold ore leaching was performed in a 250 mL glass conical flask using a mechanical stirrer under the conditions of ambient temperature and atmospheric pressure. The leaching solution was first prepared by mixing Fe^{2+}, TU, and NTA (if needed) into deionized water, with a certain amount of the gold ore sample. Subsequently, the pH of the leaching solution was adjusted to a certain value via H_2SO_4 (20%). Finally, H_2O_2 is added to the above leaching solution to start the Fenton reaction. At fixed leaching times (t = 5, 10, 20, 30, 40, 50, 60 min), multiple filtered aqueous

samples were diluted to analyze the Au leaching efficiency (η).

$$\eta = \frac{C\ V}{m\ \beta} \times 100\% \quad (4\text{-}1)$$

where η (%) is the leaching efficiency of gold; C (mg/L) is the content of dissolved gold ions in the lixiviants; V (mL) is the volume of lixiviants; m (g) is the mass of feeding ore, and β (g/t) is the gold grade.

The research focus of gold ore leaching is primarily divided into two aspects. On the one hand, the optimization of the Fenton oxidation-assisted thiourea leaching process (noted as Fenton/TU system) was conducted. Correspondingly, the effects of Fenton reagents (H_2O_2/Fe^{2+}), TU concentrations, and initial solution pH were first examined at the stirring speed of 400 rpm and the pulp density of 25% (solids by weight). On the other hand, NTA was chosen to modify the Fenton oxidation process (noted as Fenton/TU/NTA system), and the effect of NTA concentration (10~200 mM), initial pH (1.5~5.5), stirring speed, and pulp density were further investigated under the above optimum conditions.

4.2.3 Analytical and characterization techniques

The amount of dissolved Au in filtrates was determined by atomic adsorption spectroscopy (AAS, 280Z AA, Agilent, USA). The concentration of TU in solution was analyzed by a mercuric nitrate ($Hg(NO_3)_2$) titration with diphenyl carbamide as an indicator. Ultraviolet-visible spectroscopy (UV-vis, GENESYS, Thermo Fisher Scientific, USA) was used to measure the absorbance of the Fe^{3+} complex in solution. Furthermore, the concentration of Fe^{2+} was quantified with UV-vis spectrophotometry at 510 nm using 1,1-o-phenanthroline as the chromogenic agent. The Fe^{3+} concentration was calculated as the difference in concentrations between Fe^{2+} and total iron (total iron was measured through AAS). The software of HSC Chemistry 6.0 and Medusa-Hydra for Windows were used to construct the E_h-pH diagram and the distribution diagram of Fe^{3+} speciation. A scanning electron microscope (SEM, pw-100-017, Phenom, Holland), equipped with an energy dispersive spectroscopy (EDS), was utilized to characterize the surface chemical component of WPCB sheets. Reactive oxygen species (ROS) were detected via an electron paramagnetic resonance (EPR, EMX PLUS, Bruck, GER); spin traps including DMPO and TEMP were utilized to detect •OH, $•O^{2-}$, and $^1O_2$, respectively. Density functional theory (DFT) calculations were employed to provide a more detailed analysis of the highest occupied molecular orbital (HOMO) and the corresponding energy levels (E_{HOMO}) of Fe^{3+} complexes. All calculations were achieved

by using the GAUSSIAN 09 program, based on the B3LYP functional in combination with the def2SVP basis set. Linear sweep voltammetry (LSV) measurements were conducted on an electrochemical workstation (CHI400E, Shanghai Chenhua, China) to analyze the stability of the Fe^{3+} complex, utilizing both Pt and Au electrodes. The solution potential (ORP) of the lixiviants was determined by a pH/ion concentration meter (Orion DUAL STAR, Thermo Fisher Scientific, USA) equipped with an ORP electrode (vs. SHE).

4.3 Results and discussion

4.3.1 Feasibility analysis of Au dissolution in Fenton/TU system

Thiourea ($CS(NH_2)_2$) can solubilize gold via forming a stable Au^+ complex species (Eq. 4-2), with a redox couple of $Au[CS(NH_2)_2]_2^+/Au^0$ (E^0 = ~0.38V) [26, 27]. The Eh-pH diagram indicates the stability of the $Au(TU)_2^+$ complex across a broad pH range, but thiourea instability leads to breakdown into other compounds under alkaline conditions, necessitating gold leaching in acidic conditions (Figure 4.2a). Besides, gold dissolution rate in acidic thiourea solution is very slow, and the oxidation catalysts (oxidants) are necessary for fast dissolution kinetics [28]. Due to the limited versatility of acidic conditions, extensive research has focused solely on the use of Fe^{3+} to drive the oxidation of gold, effectively shortening the gold leaching reaction by several hours. This is attributed to the high redox potential (E^0 = ~0.77 V) and the relative stability under acidic conditions of Fe^{3+} [29]. Compared with the Fe^{3+} oxidant, the acidic Fenton oxidation technology seems to be a more efficient oxidation catalyst. Benefiting from the weaker O-O bands in its structure, hydrogen peroxide (H_2O_2) can react with Fe^{2+} to yield various reactive oxygen species (ROS) in acid solution, such as hydroxyl radicals (•OH), superoxide radicals ($•O_2^-$), hydroperoxyl radicals ($•HO_2$), and singlet oxygen ($^1O_2$) [30]. This process is widely known as the Fenton reaction, and Fe^{2+} and H_2O_2 are called Fenton reagents. Obviously, the redox potential (E^0) of these ROS is higher than that of Fe^{3+} in acidic solution (Table 4.2). So, the Fenton oxidation is capable of enhancing gold dissolution in TU solution [31] (Figure 4.2b). Here, waste printed circuit boards (WPCB) sheets were selected to assess the performance of Au dissolution in the proposed Fenton/TU system. As depicted in Figure 4.2c**,** the surface of the fresh WPCB sheet shows a color of golden yellow, primarily comprising approximately 31.4 wt% Au. Surprisingly, upon immersion of the WPCB sheet into the Fenton/TU solution, rapid dissolution of surface Au occurred within just 2 min (Figure 4.2d), which indicates that the Fenton reaction greatly improves the gold dissolution in TU solution.

$$Au^0 + 2CS(NH_2)_2 \rightarrow Au[CS(NH_2)_2]_2^+ + e^- \qquad (4\text{-}2)$$

Table 4.2 Redox potential (E^0) of oxidative species in Fenton oxidation [32, 33]

Oxidant	H_2O_2	•OH	$•O_2^-$	$^1O_2$	$•HO_2$	Fe^{3+}
E_0 (eV)	1.76 V	2.7 V	0.89~1.7 V	2.2 V	0.79 V	0.77 V

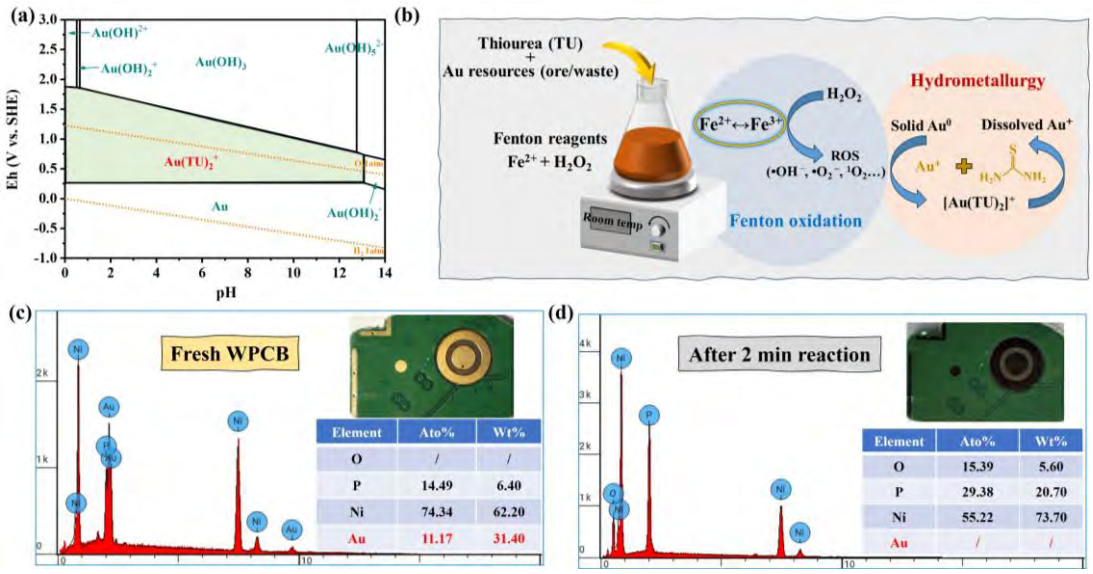

Figure 4.2 (a) Eh-pH diagram for Au-TU-water system (0.0001M Au, 0.2 M TU, 25 °C, 1 atm). (b) The proposed gold dissolution process in the Fenton/TU system. EDS spectra of a WPCB sheet (c) before reaction and (d) after reaction (2 min) in the Fenton/TU system

4.3.2 Gold leaching from a roasted concentrate in Fenton/thiourea system

In this section, a roasted gold concentrate was chosen to further investigate the role of Fenton oxidation for Au leaching in the aqueous TU system. All leaching experiments were performed at 25 % pulp density (solids by weight) and stirring speed of 400 rpm to show the effects of H_2O_2 (5~200 mM), Fe^{2+} ions (10~200 mM), TU (5~30 g/L), and the initial pH (1.0~3.0). Shown in Figures 4.3a and 4.3b, the efficiency of Au leaching significantly enhanced with the addition of Fenton reagents, reaching its maximum efficiency (100% leaching within 30 min) at 100 mM H_2O_2 and 50 mM Fe^{2+}. The beneficial impact of Fenton reagents could be ascribed to the activation of H_2O_2 by Fe^{2+} ions, along with the generation of ROS as an oxidizing agent to oxidize the element Au^0 to Au^+ ions [34]. As a typical ligand for oxidized Au^+, the dosage of TU exerted a significant role on gold extraction [35]. As displayed in Figure 4.3c, Au leaching percentage increased from 27.4% to 100% with the increment of TU concentrations from 5 g/L to 20 g/L. However, further increasing TU concentration to 30 g/L resulted

in a slight decrease in gold extraction efficiency. This negative effect could be attributed to the oxidative decomposition of excess thiourea, which hampers gold dissolution by forming a passive layer on the gold surface [36, 37]. Additionally, the stability of TU and $AuTU^{2+}$ complexes is highly sensitive to solution pH [38]. Figure 4.3d presents a 100% leaching of Au under highly acidic conditions (pH=1.0, 1.5, and 2.0), but Au leaching begins to decrease when the pH exceeds 2.0. The decrease in Au leaching may be attributed not only to the decomposition of TU and $AuTU^{2+}$ complex but also to the unavoidable precipitation of iron ions in the form of ferric oxyhydroxides, which reduced the utilization efficiency of H_2O_2 in generating ROS [39]. Hence, the process variables of gold leaching in the Fenton/TU system can be optimized by 100 mM H_2O_2, 50 mM Fe^{2+}, 20 g/L TU, and initial pH 1.5.

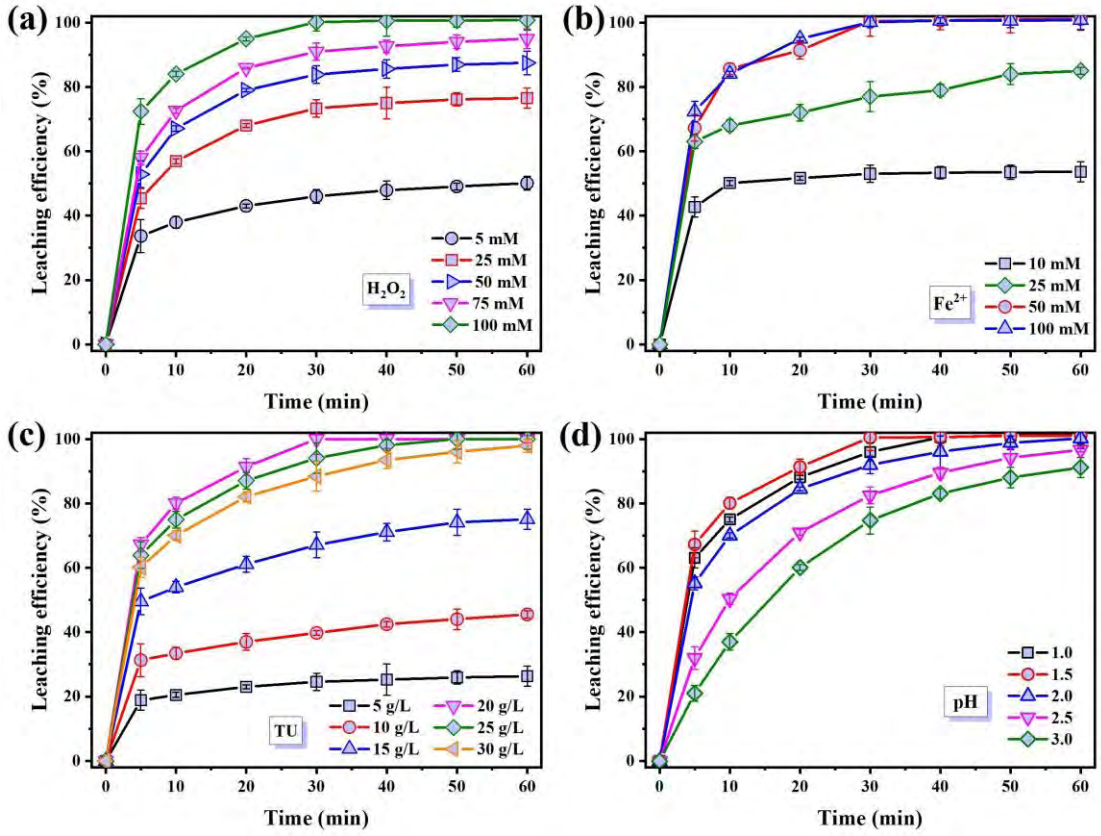

Figure 4.3 Effect of (a) H_2O_2, (b) Fe^{2+}, (c) TU concentrations, and (d) initial pH on Au leaching in the Fenton/TU system

Although the above results demonstrate the capability of the Fenton/TU system for rapid gold leaching, a key scientific issue regarding the stability of thiourea should be carefully considered. In the conventional Fe^{3+}/TU system, previous studies have highlighted two major issues associated with increasing TU consumption. On the one

hand, TU ($CS(NH_2)_2$) has the property of reduction, which can be oxidized to formamidine disulfide ($CS[(NH)(NH_2)]_2$) with a redox couple of $[CS(NH)(NH_2)]_2$/TU (E^0=0.42 V vs. SHE), as shown in Eq. (4-2) and Figure 4.4a. According to Eq. (4-3), formamidine disulfide can be protonated under acidic conditions, forming $[CS(NH_2)_2]_2^{2+}$. Thermodynamically, $[CS(NH_2)_2]_2^{2+}$ is a redundant oxidant that can degrade TU [40]. In addition, the highly dissolved Fe^{3+} ions can successively complex with TU to form some Fe^{3+}-TU complexes, e.g., $Fe[CS(NH_2)_2]^{3+}$, $Fe[CS(NH_2)_2]_2^{3+}$, and $[FeSO_4 \cdot CS(NH_2)_2]^+$ (Eqs. 4-4 to 4-6). Thus, TU is largely consumed by these side reactions [41].

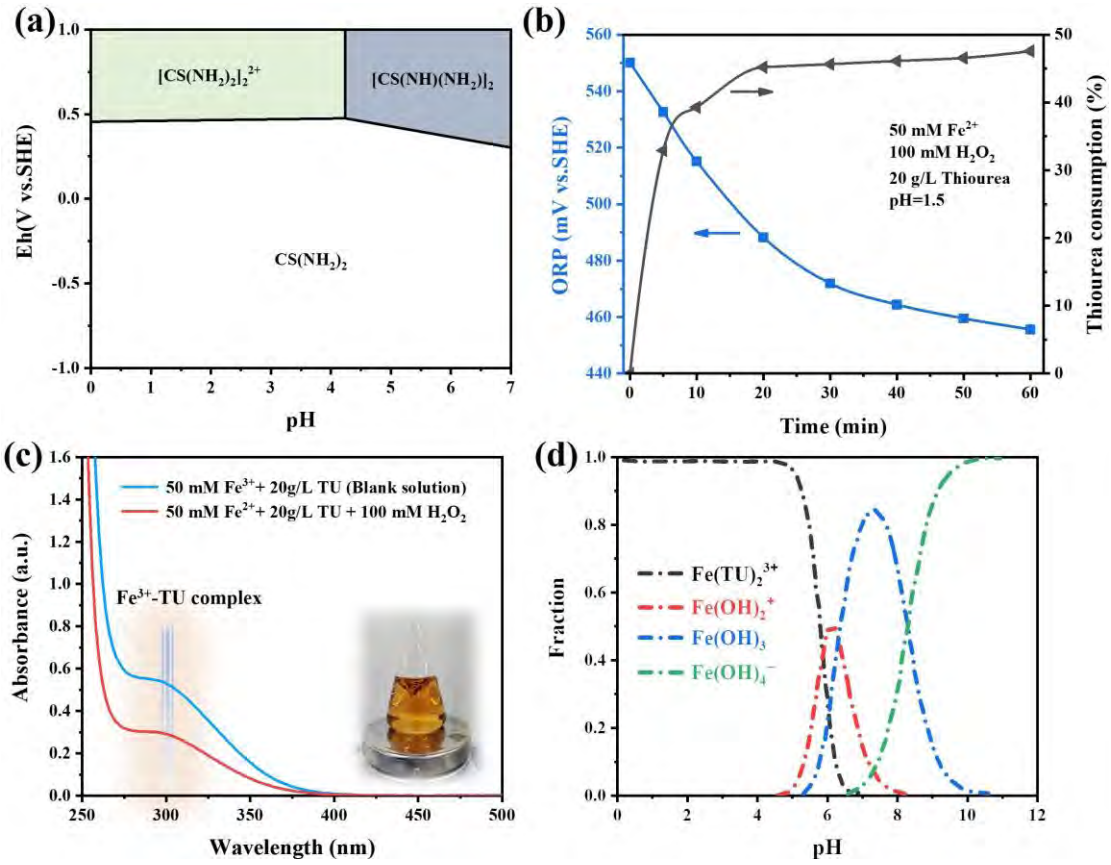

Figure 4.4 Solution characterization of the Fenton/TU system. (a) Eh-pH diagram for TU-H_2O system. (b) Variation of ORP and TU consumption during gold leaching. (c) UV-vis spectrum of the Fe^{3+}-TU complex. (d) Fe^{3+} distribution

$$2CS(NH_2)_2 \rightarrow [CS(NH)(NH_2)]_2 + 2H^+ + 2e^- \quad (4\text{-}2)$$

$$[CS(NH)(NH_2)]_2 + 2H^+ \rightarrow [CS(NH_2)_2]_2^{2+} \quad (4\text{-}3)$$

$$Fe^{3+} + CS(NH_2)_2 \rightarrow Fe[CS(NH_2)_2]^{3+} \quad (4\text{-}4)$$

$$Fe^{3+} + 2CS(NH_2)_2 \rightarrow Fe[CS(NH_2)_2]_2^{3+} \quad (4\text{-}5)$$

$$Fe^{3+} + SO_4^{2-} + CS(NH_2)_2 \rightarrow [FeSO_4 \cdot CS(NH_2)_2]^+ \quad (4\text{-}6)$$

Apparently, solution potential (ORP) not only plays a key role in gold oxidation but also closely correlates with TU stability. Here, the consumption of TU and the variation of solution potential during the optimized leaching process (50 mM Fe^{2+}, 100 mM H_2O_2, 20 g/L TU, and pH=1.5) were measured and recorded as portrayed in Figure 4.4b. Solution potential (ORP) exhibits a gradual decline from ~550 mV to ~455 mV during the entire 60 min leaching process, which is likely attributed to the continuous consumption of H_2O_2 and the concurrent variation in the concentration of the transient ROS [42]. Obviously, the high level of solution potential (＞500 mV) in the beginning 15 min causes irreversible decomposition of TU to a large degree, where the solution potential is immensely higher than the redox couple of $CS((NH)(NH_2))_2$/TU. UV-vis and speciation diagrams were adopted to study the effect of Fe ions on TU consumption. UV-vis spectra (Figure 4.4c) observed an absorbance at approximately 300 nm of the red-orange color lixiviant, which is due to the formation of Fe^{3+}-TU complex [43]. Besides, Fe^{3+} speciation diagrams (Figure 4.4d) explicitly indicated that the main species of Fe^{3+}-TU complexes exist in the substance of $Fe(TU)_2^{3+}$, which is consistent with S Örgül's results [43]. Thus, the above two reasons caused the large consumption of TU (45.6% at 30 min), which should be carefully resolved to achieve industrial application.

4.3.3 Nitrilotriacetic acid-modified Fenton oxidation for reducing thiourea consumption

Further, nitrilotriacetic acid (NTA), an easily biodegradable chelating agent, was chosen as an additive in the Fenton/TU system, forming a modified Fenton/TUNTA system [44]. A lot of work reported that NTA was an obvious choice for modifying homogeneous Fenton or Fenton-like systems, because it has sufficient coordination sites ($-NH^-$ and $-COO^-$) for Fe^{3+} ions and exhibited negligible scavenging effect on ROS. When NTA is added, the solution (with the components of Fe^{2+}, NTA, TU, and H_2O_2) gives a characteristic red color. UV-vis spectra show that the Fe^{3+}-NTA complex (absorbance at ~260 nm) is produced as the main Fe^{3+} species, rather than the Fe^{3+}-TU complex (absorbance at ~300 nm) (Figure 4.5a). In addition, the Fe^{3+} speciation diagrams (Figure 4.5b) show that the main Fe^{3+} complexes in the solution are $Fe(NTA)_2^{3-}$. Therefore, the introduction of NTA can completely avoid the TU consumption caused by the coordination of Fe^{3+} ions and TU [45].

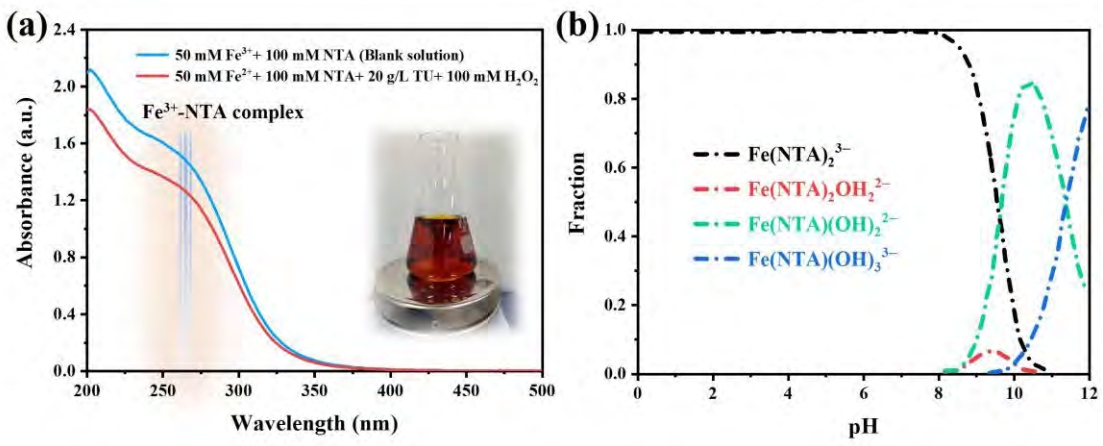

Figure 4.5 Solution characterization of the Fenton/TU/NTA system. (a) Uv-vis spectrum. (b) Fe^{3+} distribution

As shown in Figure 4.6a, the addition of NTA into the Fenton/TU system significantly lowered the level of solution potential (ORP). When the addition of NTA was increased to 100 mM, the efficiency of Au leaching remained at the highest level (100%, 30 min), while the consumption of TU gradually reduced to 30.12% (Figure 4.6b and Figure 4.6(c)). Figure 4.6d shows that pH also significantly influences the solution potential, mainly reflected in a substantial decrease with increasing pH. When the pH is below 3.5, ORP tends to be relatively high compared to higher solution pH values, resulting in faster gold leaching (100%, 60 min). Whereas, as the solution pH continues to rise, ORP significantly decreases, indicating unequivocally that the solution potential is unable to meet the requirements for gold oxidation (Figure 4.6e). Consequently, the leaching efficiency of gold becomes worse (Figure 4.6f). TU consumption in the Fenton/TU/NTA system was lowest at a solution pH of 3.5, about ~11.84%, which is obviously reduced compared to the Fenton/TU system (~45.6%).

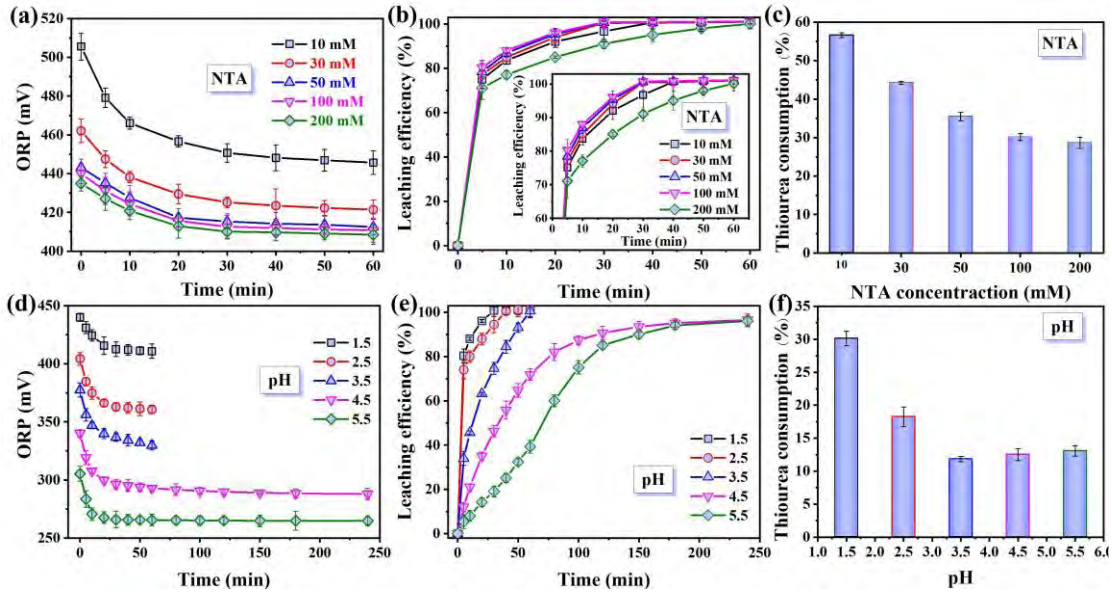

Figure 4.6 Effects of (a~c) NTA concentrations and (d~f) solution pH on ORP, Au leaching efficiency, and TU consumption

4.3.4 Mechanistic role of reactive oxygen species (ROS) in gold dissolution

Electron paramagnetic resonance (EPR) spectra were conducted to identify the reactive oxygen species (ROS), which are important for investigating the role of generated ROS for gold leaching and proposing the reaction mechanism [46]. As depicted in Figure 4.7a, the characteristic peaks of DMPO-•OH adducts, showing a 1:2:2:1 signal, were observed in the EPR spectrum in the traditional Fenton system in the absence of TU (only Fe^{2+}/H_2O_2) [47]. Conversely, the EPR spectrum showed that the peaks significantly decreased in intensity with the addition of TU and finally disappeared at a TU concentration of 20 g/L. The reason is that TU was reported to be a specific scavenger of •OH, which qualitatively inhibits the activity of •OH, as seen in Eq. (4-8) to (4-10) [48, 49]. The quenching of •OH may be beneficial to gold dissolution in this system, due to the presence of •OH (the strongest radical), which can irreversibly oxidize organics, such as TU and NTA. Additionally, Figure 4.7b illustrates an obvious characteristic peak of the DMPO-•O_2^- adduct (1:1:1:1:1 quadruple peak), which is attributed to •O_2^- in both Fenton//TU and Fenton//TU/NTA systems [50]. Furthermore, singlet oxygen ($^1O_2$) was also detected in the system as seen in the TEMPO-$^1O_2$ adduct in Figure 4.7c [51]. The above EPR results showed a high selectivity of ROS in the Fenton-TU system, where moderate •O_2^- and $^1O_2$ were the main ROS group produced, instead of •OH. Besides, the introduction of NTA into the Fenton/TU system decreased the intensity of DMPO-•O_2^- adduct, which could be a contributing factor for the reduction of ORP in the Fenton/TU/NTA system.

$$Fe^{2+} + H_2O_2 \rightarrow Fe^{3+} + OH^- + \bullet OH \quad (4\text{-}8)$$

$$SC(NH_2)_2 + \bullet OH \rightarrow SC(NH_2)_2^{\bullet -} + H^+ + e^- \quad (4\text{-}9)$$

$$SC(NH_2)_2^{\bullet -} + H^+ \rightarrow SC(NH_2)_2 \quad (4\text{-}10)$$

Chemical scavenging experiments were carried out in an attempt to explore the contribution of ROS (i.e., $\bullet O_2^-$, $^1O_2$, and •OH) to gold leaching, as illustrated in Figure 4.7d (Fenton/TU system) and Figure 4.7e (Fenton/TU/NTA system). Specifically, the addition of tertiary butanol (TBA), a qualitative indicator of •OH, had a negligible effect on gold leaching, which argues strongly against the involvement of •OH [52]. Surprisingly, the efficiency of gold leaching was significantly inhibited by p-benzoquinone (PBQ), which could have resulted from $\bullet O_2^-$ playing a remarkable role for gold leaching [53]. As well, gold leaching also visibly decreased when $^1O_2$ was inhibited by L-histamine (L-His), indicating some contribution of $^1O_2$ [54]. According to these results, it can be found that $\bullet O_2^-$ as an oxidant species primarily participated in the gold leaching process.

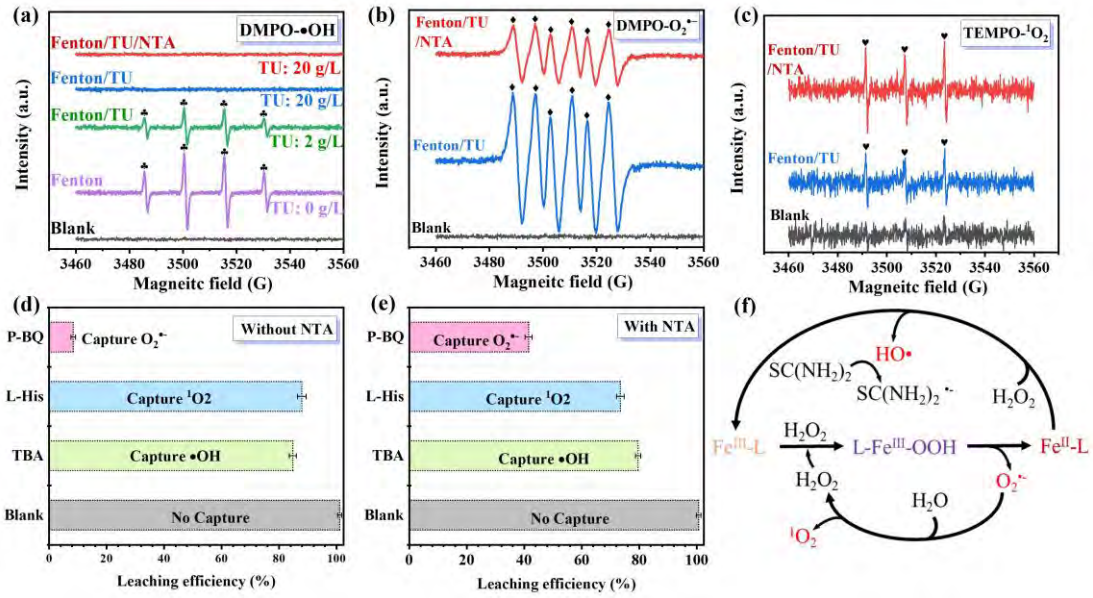

Figure 4.7 Characterization of reactive oxygen species (ROS). (a~c) EPR spectra for the DMPO-•OH, DMPO-$\bullet O_2^-$, and TEMPO-$^1O_2$ adducts. (d~e) Effect of various scavengers on Au leaching efficiency. (f) Proposed ROS generation routes

The aforementioned experiments confirm that $\bullet O_2^-$ was the primary ROS responsible for gold dissolution. However, elucidating the pathways through which it is generated remains a pertinent inquiry. According to previous studies on chelating-modified Fenton oxidation (e.g., Picolinic Acid [55], phenolic moiety [56], EDTA [57], nitrilotriacetate [58]), $\bullet O_2^-$ is easily generated by two rapid equilibrium reactions

between Fe^{3+} complex and H_2O_2 (Figure 4.7f). In the initial stage, the Fe^{3+}-Ligand complex was continuously reacted with residual H_2O_2 to form a Ligand-Fe^{3+}-OOH intermediate (Eq. 4-11). Afterwards, the high-spin Ligand-Fe^{3+}-OOH intermediate was rapidly reduced to Fe^{2+}-Ligand complex due to the weak Fe-O bond, along with the generation of $\bullet O^{2-}$ (Eq. 4-12). H_2O_2 can also utilize its oxidation ability to greatly accelerate the cycle of Fe^{2+}-Ligand to Fe^{3+}-Ligand, continuously producing the reactive species of $\bullet O^{2-}$. Consequently, the $\bullet O^{2-}$ can maintain a high concentration as the main ROS. Substantially, the formation of $^1O_2$ can inevitably occur via a chain reaction between $\bullet O^{2-}$ and H_2O, thereby inducing the co-existence of $\bullet O^{2-}$ and $^1O_2$ for efficiently oxidizing/dissolving gold (Eq. 4-13).

$$Fe^{3+}\text{-Ligand} + H_2O_2 \leftrightarrow \text{Ligand-}Fe^{3+}\text{-OOH} + H^+ \quad (4\text{-}11)$$

$$\text{Ligand-}Fe^{3+}\text{-OOH} \rightarrow Fe^{2+}\text{-Ligand} + \bullet O_2^- + H^+ \quad (4\text{-}12)$$

$$2\bullet O^{2-} + 2H_2O \rightarrow H_2O_2 + {}^1O_2 + OH^- \quad (4\text{-}13)$$

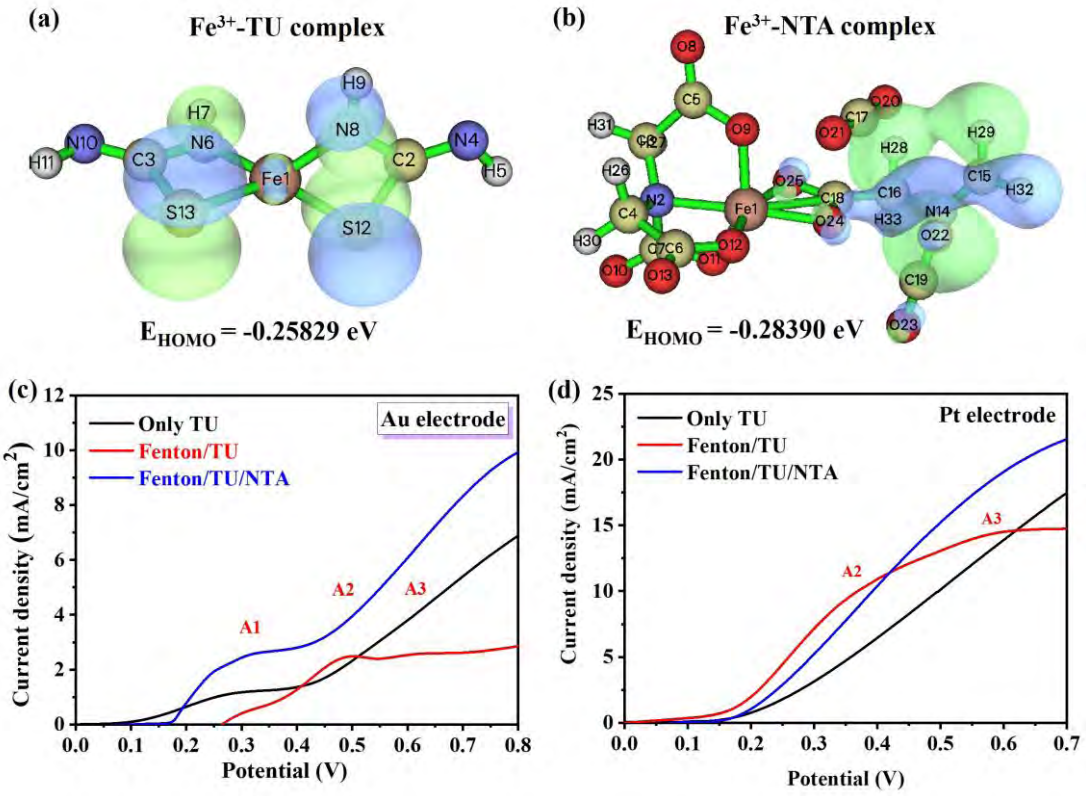

Figure 4.8 Reactivity of Fe complexes towards gold oxidation. HOMO and E_{HOMO} of (a) Fe^{3+}-TU and (a) Fe^{3+}-NTA complexes. Linear sweep voltammograms (LSV) recorded on (c) Au electrode and (d) Pt electrode

In terms of the generation pathway of $\bullet O_2^-$, the reductive step of Ligand-Fe^{3+}-OOH complex to Fe^{2+}-Ligand and $\bullet O_2^-$ is faster than the formation of Ligand-Fe^{3+}-OOH. Therefore, the first-stage reaction between the Fe^{3+} complex and H_2O_2 is the rate-determining step (Eq. 4-11), which is very relevant to the reactivity of the Fe^{3+} complex. Herein, density functional calculation (DFT) and electrochemical characterization (LSV) were used to reveal the reactivity of Fe^{3+} complexes, i.e., $Fe(NTA)_2^{3-}$ and $Fe(TU)_2^{3+}$ [59]. Here, the highest occupied molecular orbital (HOMO) indicates the ability of Fe^{3+} complexes to donate electrons to an appropriate acceptor (oxidant, H_2O_2), which is closely interrelated with the reactivity of Fe^{3+} complexes. As shown in Figures 4.8a and 4.8b**,** HOMO is localized at the lone pair orbital of N and S atoms of $Fe(TU)_2^{3+}$ complex. In contrast, for $Fe(NTA)_2^{3-}$ complex, it is centered not only on O and N atoms, but also on the π orbital of C-C bonds, showing a higher chemical stability. DFT calculations suggest the Fe^{3+}-TU complex shows a higher E_{HOMO} (-0.258294 eV) than the Fe^{3+}-NTA complex (-0.289166 eV). At a larger E_{HOMO}, the removal of electrons from the HOMO orbit of $Fe(TU)_2^{3+}$ complex to H_2O_2 is easier. Thus, $Fe(TU)_2^{3+}$ complexes have higher reactivity with H_2O_2 to form the Ligand-Fe^{3+}-OOH intermediate.

Figure 4.8c and 4.8d showcase the results of LSV using a Pt and an Au working electrode, respectively. If only TU is present, the continuously elevated current density is a result of the oxidative decomposition of the metastable TU in both ideal Pt and Au surfaces. Besides, the observed A_1 peak at ~0.3 V on the Au electrode is doubtlessly attributed to gold oxidation (Au^0 to Au^+), because it disappeared when using a Pt electrode. In the Fenton/TU system, the A2 and A3 peaks are clearly evident, whereas they are not observable in the Fenton/TU/NTA system. This different observation not only highlights the higher reactivity with H_2O_2, but also could be assigned to the faster decomposition of TU-Fe^{3+}-OOH complex [60]. These deductions seem to explain the higher $\bullet O^{2-}$ concentration (Figure 4.7b) and its greater $\bullet O^{2-}$ contribution for gold leaching (Figure 4.7d) in the Fenton/TU system. However, the Fenton/TU/NTA system appears to be more promising, because NTA regulates the generation of $\bullet O^{2-}$ into a moderate and sustainable level, which lowers TU oxidation while producing the same gold leaching.

4.3.5 Process implications and mechanistic discussion

Given the industrial availability, the effects of pulp density and stirring rate were studied in detail to obtain the best operating conditions. Typically, the gold leaching process is a fluid-solid heterogeneous reaction that depends on the viscosity of the

leaching mixture, the mass transfer rate/ion diffusion of reactants, and the contact and collision between gold and lixiviants [61, 62]. As seen in Figures 4.9a and 4.9b, Au leaching efficiency is insensitive to the variation of pulp density and stirring rate. The 100% leaching of gold can be obtained at the conditions of 125% pulp density (solids by weight). Increasing the pulp density to 200% still achieves ~86.4 % leaching of gold. Likewise, the 100% leaching of gold can be obtained at the conditions of 300 rpm under 125% pulp density. Even if the ore pulp is not stirred, 77.1% gold leaching can still be obtained. Importantly, TU consumption was reduced to 2.9 kg/t (125% pulp density and 300 rpm), which is close to the lowest level reported before (as seen in Table 4.3).

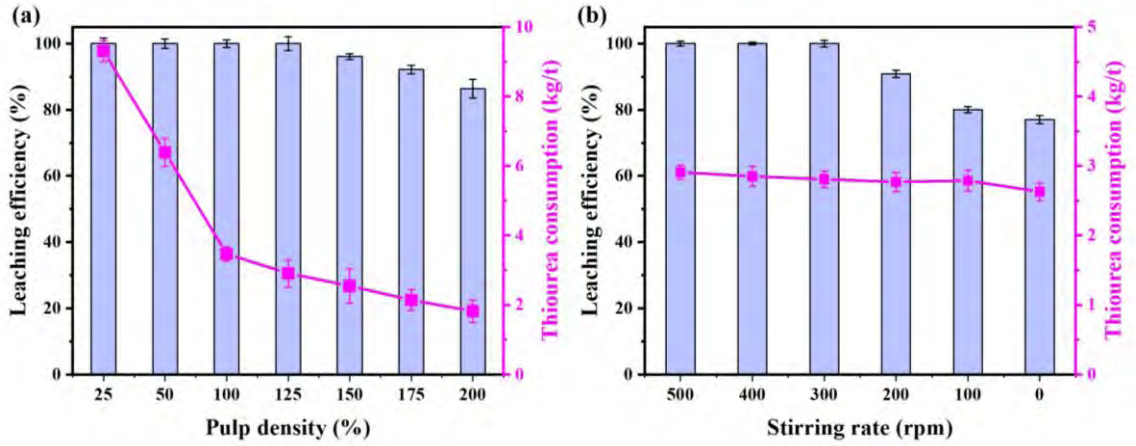

Figure 4.9 Effect of (a) pulp density and (b) stirring rate on Au leaching and TU consumption

Table 4.3 Parameters and performance of current TU systems for gold leaching

Systems	Leaching conditions	Au leaching/ TU consumption	Ref.
Fe^{3+}/TU	10 g/L TU, 5 g/L Fe^{3+}, pH＜3.0, 4 h	83%; 44.25 kg/t	[63]
H_2O_2/TU	40 mM H_2O_2, 40 g/L TU, pH=1, 60 °C, 6 h, Pulp density 20 g/L	92.6%; /	[64]
Cu^{2+}/NH_3/TU	2.5 mmol/L Cu^{2+} mol/L NH_3, 0.08 mol/L TU, L/S=3, 350 rpm, 12 h	86.6%; 18.2 kg/t	[65]
Fe^{3+}/TU/Oxalate	40 mM Fe^{3+}, 80 mM TU, pH=2, 40 °C, 6 h, 37 mM Oxalate, L/S=4	88.6%; 8.46 kg/t	[45]
Fe^{3+}/TU/Citrate	40 mM Fe^{3+}, 80 mM TU, pH=2, 40 °C, 6 h, citrate 37 mM, L/S=4:1	89.5%; 8.24 kg/t	[45]
Fe^{3+}/TU/oxalate/ jarosite	1.35 g/L Fe^{3+}, 2 g/L TU, 2 g/L oxalate, 6 g/L jarosite	87.7%; 3.7 kg/t	[66]
Fenton/TU/NTA	50 mM Fe^{2+}, 100 mM H_2O_2, 20 g/L TU, 100 mM NTA, pH=3.5, 22 °C, 30 min, Pulp density 125 %	100%; 2.9 kg/t	This work

4.4 Conclusions

In this work, a clean hydrometallurgy process for gold leaching, based on Fenton oxidation assisted by a thiourea system, was proposed. The optimum parameters for the gold leaching process were determined to be 100 mM H_2O_2, 50 mM Fe^{2+}, 20 g/L thiourea, and pH=1.5. Under these conditions, gold leaching achieved an ultra-high efficiency, rapidly leaching 100% gold from a roasted gold concentrate within 30 min. Moreover, the addition of NTA into the Fenton/thiourea system lowered the solution potential and eliminated side reactions between Fe^{3+} ions and thiourea, reducing the consumption of thiourea from 45.6% to 11.84%. Importantly, EPR analysis revealed that the moderate $\bullet O_2^-$ was the principal ROS generated from the Fenton reaction, as the strong •OH was fast quenched by thiourea. The chemical scavenging experiments show that $\bullet O_2^-$ is the main oxidative species for gold leaching, mainly generated by the reaction between Fe^{3+} complex and H_2O_2. Based on DFT calculations and LSV analysis, the addition of NTA reduced the reactivity between the Fe^{3+} complex and H_2O_2, thus regulating the generation of $\bullet O_2^-$. As a result, the consumption of thiourea is reduced while producing the same gold extraction (100%, 60 min). Apart from the above results, this system also has the capability for gold leaching under large pulp density and low stirring rate, which can be considered as a clean and efficient gold leaching process for replacing cyanidation in gold mining.

4.5 References

[1] I.S. Kwak, M.A. Bae, S.W. Won, J. Mao, K. Sneha, J. Park, M. Sathishkumar, Y.-S. Yun, Sequential process of sorption and incineration for recovery of gold from cyanide solutions: Comparison of ion exchange resin, activated carbon and biosorbent, Chem. Eng. J., 165 (2010) 440-446.

[2] Y. Ou, Y. Yang, L. Wang, K. Li, W. Gao, Y. Zhang, Q. Li, T. Jiang, A clean and efficient innovative technology for refractory sulfide gold ore: In situ gold extraction via self-generated thiosulfate, J. Cleaner Prod., 419 (2023) 138280.

[3] L. Hou, A.L. Valdivieso, P. Chen, G. Zhang, Q. Zhang, Y. Chen, S. Song, F. Jia, An electrochemical study of the dissolution behavior of gold in a novel glycine-thiosulfate system, Miner. Eng., 202 (2023) 108273.

[4] K. Dong, F. Xie, W. Wang, Y. Chang, D. Lu, X. Gu, C. Chen, The detoxification and utilization of cyanide tailings: A critical review, J. Cleaner Prod., 302 (2021) 126946.

[5] X. Huang, Z. Long, L. Wang, Z. Feng, Technology development for rare earth cleaner hydrometallurgy in China, Rare Met., 34 (2015) 215-222.

[6] S. Ju, Y. Zhang, Y. Zhang, P. Xue, Y. Wang, Clean hydrometallurgical route to

recover zinc, silver, lead, copper, cadmium and iron from hazardous jarosite residues produced during zinc hydrometallurgy, J. Hazard. Mater., 192 (2011) 554-558.

[7] L. Tang, C. Tang, J. Xiao, P. Zeng, M. Tang, A cleaner process for valuable metals recovery from hydrometallurgical zinc residue, J. Cleaner Prod., 201 (2018) 764-773.

[8] M. Huy Do, G. Tien Nguyen, U. Dong Thach, Y. Lee, T. Huu Bui, Advances in hydrometallurgical approaches for gold recovery from E-waste: A comprehensive review and perspectives, Miner. Eng., 191 (2023), e107977.

[9] G. Senanayake, The role of ligands and oxidants in thiosulfate leaching of gold, Gold Bulletin, 38 (2005) 170-179.

[10] S.S. Konyratbekova, A. Baikonurova, A. Akcil, Non-cyanide Leaching Processes in Gold Hydrometallurgy and Iodine-Iodide Applications: A Review, Miner. Process. Extr. Metall. Rev., 36 (2015) 198-212.

[11] G. Hilson, A.J. Monhemius, Alternatives to cyanide in the gold mining industry: what prospects for the future?, J. Cleaner Prod., 14 (2006) 1158-1167.

[12] B. Xu, K. Li, Q. Li, Y. Yang, X. Liu, T. Jiang, Kinetic studies of gold leaching from a gold concentrate calcine by thiosulfate with cobalt-ammonia catalysis and gold recovery by resin adsorption from its pregnant solution, Sep. Purif. Technol., 213 (2019) 368-377.

[13] W. Lin, R.W. Zhang, S.S. Jang, C.P. Wong, J.I. Hong, “Organic aqua regia”-powerful liquids for dissolving noble metals, Angew. Chem., Int. Ed., 49 (2010) 7929-7932.

[14] C. Yue, H. Sun, W.J. Liu, B. Guan, X. Deng, X. Zhang, P. Yang, Environmentally benign, rapid, and selective extraction of gold from ores and waste electronic materials, Angew. Chem., Int. Ed., 129 (2017) 9459-9463.

[15] A. Serpe, L. Marchiò, F. Artizzu, M.L. Mercuri, P. Deplano, Effective One-Step Gold Dissolution Using Environmentally Friendly Low-Cost Reagents, Chem. - Eur. J., 19 (2013) 10111-10114.

[16] M. Räisänen, E. Heliövaara, F. Al-Qaisi, M. Muuronen, A. Eronen, H. Liljeqvist, M. Nieger, M. Kemell, K. Moslova, J. Hämäläinen, K. Lagerblom, T. Repo, Pyridinethiol-Assisted Dissolution of Elemental Gold in Organic Solutions, Angew. Chem., Int. Ed., 57 (2018) 17104-17109.

[17] A. Zupanc, E. Heliövaara, K. Moslova, A. Eronen, M. Kemell, Č. Podlipnik, M. Jereb, T. Repo, Iodine-Catalysed Dissolution of Elemental Gold in Ethanol, Angew. Chem., Int. Ed., 61 (2022) e202117587.

[18] Y. Nakao, One-step syntheses of polyhalogenometal complexes by direct dissolution of the metals in halogen-halide-acetonitrile systems, Chem. Lett., 28 (1999) 433-434.

[19] L. Cau, P. Deplano, L. Marchiò, M.L. Mercuri, L. Pilia, A. Serpe, E. Trogu, New

powerful reagents based on dihalogen/N, N′-dimethylperhydrodiazepine-2, 3-dithione adducts for gold dissolution: the IBr case, Dalton Trans., 10 (2003) 1969-1974.

[20] F. Bigoli, P. Deplano, M.L. Mercuri, M.A. Pellinghelli, G. Pintus, A. Serpe, E.F. Trogu, N, N ‘-Dimethylpiperazinium-2, 3-dithione Triiodide, [Me_2Pipdt]I_3, as a Powerful New Oxidation Agent toward Metallic Platinum. Synthesis and X-ray Structures of the Reagent and the Product [Pt(Me_2Pipdt)$_2$](I_3)$_2$, J. Am. Chem. Soc., 123 (2001) 1788-1789.

[21] M.T. Räisänen, M. Kemell, M. Leskelä, T. Repo, Oxidation of elemental gold in alcohol solutions, Inorg Chem., 46 (2007) 3251-3256.

[22] M. Kamisono, T. Hanada, M. Goto, Green leaching of metallic platinum using an ionic liquid with synergistic organic acid-chlorinating agent additives, J. Chem. Eng. Jpn., 56 (2023) 2228363.

[23] Y. Chen, M. Xu, J. Wen, Y. Wan, Q. Zhao, X. Cao, Y. Ding, Z.L. Wang, H. Li, Z. Bian, Selective recovery of precious metals through photocatalysis, Nat. Sustain., 4 (2021) 618-626.

[24] Y. Chen, S. Guan, H. Ge, X. Chen, Z. Xu, Y. Yue, H. Yamashita, H. Yu, H. Li, Z. Bian, Photocatalytic dissolution of precious metals by TiO_2 through photogenerated free radicals, Angew. Chem., Int. Ed., 61 (2022) e202213640.

[25] J. Cao, Y. Chen, H. Shang, X. Chen, Q. Qiao, H. Li, Z. Bian, Aqueous photocatalytic recycling of gold and palladium from waste electronics and catalysts, ACS ES&T Eng., 2 (2022) 1445-1453.

[26] J.A. Whitehead, J. Zhang, A. McCluskey, G.A. Lawrance, Comparative leaching of a sulfidic gold ore in ionic liquid and aqueous acid with thiourea and halides using Fe(III) or HSO_5^- oxidant, Hydrometallurgy, 98 (2009) 276-280.

[27] J. Li, J. Miller, Reaction kinetics of gold dissolution in acid thiourea solution using ferric sulfate as oxidant, Hydrometallurgy, 89 (2008) 279-288.

[28] K. Li, Y. Zhang, Q. Li, X. Liu, Y. Yang, T. Jiang, Role of foreign ions in the thiourea leaching of gold, Miner. Eng., 202 (2023) 108265.

[29] J. Zhang, S. Shen, Y. Cheng, H. Lan, X. Hu, F. Wang, Dual lixiviant leaching process for extraction and recovery of gold from ores at room temperature, Hydrometallurgy, 144-145 (2014) 114-123.

[30] Y. Liu, J. Wang, Multivalent metal catalysts in Fenton/Fenton-like oxidation system: A critical review, Chem. Eng. J., 466 (2023) 143147.

[31] A.M. Nowicka, U. Hasse, M. Hermes, F. Scholz, Hydroxyl Radicals Attack Metallic Gold, Angew. Chem., 122 (2010) 1079-1081.

[32] S. Dbira, N. Bensalah, M.M. Zagho, M. Ennahaoui, A. Bedoui, Oxidative Degradation of Tannic Acid in Aqueous Solution by UV/$S_2O_8^{2-}$ and UV/H_2O_2/Fe^{2+} Processes: A Comparative Study, Appl. Sci. , 9 (2019) 156.

[33] Y. Ahmed, J. Zhong, Z. Yuan, J. Guo, Roles of reactive oxygen species in antibiotic

resistant bacteria inactivation and micropollutant degradation in Fenton and photo-Fenton processes, J. Hazard. Mater., 430 (2022) 128408.

[34] S. Zuo, Z. Guan, F. Yang, D. Xia, D. Li, Reactive oxygen species regulation and synergistic effect for effective water purification through Fenton-like catalysis on single-atom Cu–N sites, J. Mater. Chem. A, 10 (2022) 10503-10513.

[35] D.A. Ray, M. Baniasadi, J.E. Graves, A. Greenwood, S. Farnaud, Thiourea leaching: an update on a sustainable approach for gold recovery from E-waste, J. Sustain. Metall. , 8 (2022) 597-612.

[36] X.-y. Guo, L. Zhang, Q.-h. Tian, H. Qin, Stepwise extraction of gold and silver from refractory gold concentrate calcine by thiourea, Hydrometallurgy, 194 (2020) 105330.

[37] Y. Lin, X. Hu, F. Zi, Y. Chen, S. Chen, X. Li, L. Zhao, Y. Li, Synergistical thiourea and thiosulfate leaching gold from a gold concentrate calcine with copper-ammonia catalysis, Sep. Purif. Technol., 327 (2023) 124928.

[38] M.E. Poisot-Díaz, I. González, G.T. Lapidus, Electrodeposition of a silver-gold alloy (DORÉ) from thiourea solutions in the presence of other metallic ion impurities, Hydrometallurgy, 93 (2008) 23-29.

[39] Y.S. Jung, W.T. Lim, J.Y. Park, Y.H. Kim, Effect of pH on Fenton and Fenton-like oxidation, Environ. Technol., 30 (2009) 183-190.

[40] S. Zheng, Y. Wang, L. Chai, Research status and prospect of gold leaching in alkaline thiourea solution, Miner. Eng., 19 (2006) 1301-1306.

[41] J. Li, D. Miller, A review of gold leaching in acid thiourea solution, Miner. Process. Extr. M., 27 (2006), 177-214.

[42] N. Kishimoto, Y. Nakamura, M. Kato, H. Otsu, Effect of oxidation-reduction potential on an electrochemical Fenton-type process, Chem. Eng. J., 260 (2015) 590-595.

[43] S. Örgül, Ü. Atalay, Reaction chemistry of gold leaching in thiourea solution for a Turkish gold ore, Hydrometallurgy, 67 (2002) 71-77.

[44] A. De Luca, R.F. Dantas, S. Esplugas, Study of Fe(III)-NTA chelates stability for applicability in photo-Fenton at neutral pH, Appl. Catal. B Environ., 179 (2015) 372-379.

[45] K. Li, Q. Li, Y. Zhang, X. Liu, Y. Yang, T. Jiang, Improved thiourea leaching of gold from a gold ore using additives, Hydrometallurgy, 222 (2023) 106204.

[46] L. Tuo, P. Zhu, W. Song, D. Ouyang, C. Zhang, L. Liu, Boosting electro-Fenton performance by constructing a large-scale 3D-architected amorphous–nanocrystalline structure, Sustainable Mater. Technol., 37 (2023) e00667.

[47] X. Zhang, Z. Chen, X. Li, Y. Wu, J. Zheng, Y. Li, D. Wang, Q. Yang, A. Duan, Y. Fan, Promoted electron transfer in Fe^{2+}/Fe^{3+} co-doped $BiVO_4/Ag_3PO_4$ S-scheme heterojunction for efficient photo-Fenton oxidation of antibiotics, Sep. Purif. Technol., 310 (2023) 123116.

[48] M. Wasil, B. Halliwell, M. Grootveld, C. Moorhouse, D. Hutchison, H. Baum, The specificity of thiourea, dimethylthiourea and dimethyl sulphoxide as scavengers of hydroxyl radicals. Their protection of α 1-antiproteinase against inactivation by hypochlorous acid, Biochem. J., 243 (1987) 867-870.

[49] A.K. Prasad, P.C. Mishra, Scavenging of superoxide radical anion and hydroxyl radical by urea, thiourea, selenourea and their derivatives without any catalyst: A theoretical study, Chem. Phys. Lett., 684 (2017) 197-204.

[50] Q. Zhang, M. Zhang, T. Li, R. Du, G. Yu, S. Deng, FeOCl-confined activated carbon for improving intraparticle Fenton-like oxidation regeneration, J. Hazard. Mater., 442 (2023) 130026.

[51] S. Zuo, R. Guo, W. Xue, J. Shang, J. Chen, Y. Zhang, Decipher the key role of ketone toward singlet oxygen evolution in Fenton-like process for water decontamination, Appl. Catal. B Environ., 339 (2023) 123100.

[52] L. Zhang, T. Zhang, Y. Cai, Y. Zhao, S. Song, M. Quintana, Engineering sulfuric acid-pretreated biochar supporting MnO_2 for efficient toxic organic pollutants removal from aqueous solution in a wide pH range, J. Cleaner Prod., 416 (2023) 137968.

[53] Q. Qiao, Y. Chen, Y. Wang, Y. Ren, J. Cao, F. Huang, Z. Bian, Surface modification of phosphate ion to promote photocatalytic recovery of precious metals, Chin. Chem. Lett., 34 (2023) 107394.

[54] J. Gu, P. Yin, Y. Chen, H. Zhu, R. Wang, A natural manganese ore as a heterogeneous catalyst to effectively activate peroxymonosulfate to oxidize organic pollutants, Chin. Chem. Lett., 33 (2022) 4792-4797.

[55] Z. Yang, C. Shan, B. Pan, J.J. Pignatello, The Fenton Reaction in Water Assisted by Picolinic Acid: Accelerated Iron Cycling and Co-generation of a Selective Fe-Based Oxidant, Environ. Sci. Technol., 55 (2021) 8299-8308.

[56] C. Chen, Y. Wang, Y. Huang, J. Hua, W. Qu, D. Xia, C. He, V.K. Sharma, D. Shu, Overlooked self-catalytic mechanism in phenolic moiety-mediated Fenton-like system: Formation of Fe(III) hydroperoxide complex and co-treatment of refractory pollutants, Appl. Catal. B Environ., 321 (2023) 122062.

[57] Y. Gao, P. Wang, Y. Chu, F. Kang, Y. Cheng, E. Repo, M. Feng, X. Yu, H. Zeng, Redox property of coordinated iron ion enables activation of O_2 via in-situ generated H_2O_2 and additionally added H_2O_2 in EDTA-chelated Fenton reaction, Water Res., 248 (2024) 120826.

[58] H. Chen, Y. Lin, DFT study on the catalytic decomposition of hydrogen peroxide by iron complexes of nitrilotriacetate, J. Comput. Chem., 44 (2023) 2058-2072.

[59] C. Duesterberg, W. Cooper, T. Waite, Fenton-mediated oxidation in the presence and absence of oxygen, Environ. Sci. Technol., 39 (2005) 5052-5058.

[60] X. Li, M. Gao, N. Hiroyoshi, C. Tabelin, T. Taketsugu, M. Ito, Suppression of pyrite oxidation by ferric-catecholate complexes: An electrochemical study, Miner.

Eng., 138 (2019) 226-237.
[61] G. Chen, C. Jiang, R. Liu, Z. Xie, Z. Liu, S. Cen, C. Tao, S. Guo, Leaching kinetics of manganese from pyrolusite using pyrite as a reductant under microwave heating, Sep. Purif. Technol., 277 (2021) 119472.
[62] Y. Lin, X. Hu, F. Zi, Thiocyanate facilitating thiosulfate extraction of gold via inhibiting formation of passive layer, Sustainable Mater. Technol., 40 (2023), e00878.
[63] M. KAŇUCHOVÁ, A. Oravcova, M. Sisol, M. KOŠČOVÁ, Ľ. KOZÁKOVÁ, Leaching of gold from flotation waste by thiourea, Acta Montan. Slovaca, 26 (2021) 98-105.
[64] J.P. Munganyinka, J.B. Habinshuti, G.C. Komadja, P. Uwamungu, H. Tanvar, G. Ofori-Sarpong, B. Mishra, A.P. Onwualu, S. Shuey, Optimization of Gold Dissolution Parameters in Acidified Thiourea Leaching Solution with Hydrogen Peroxide as an Oxidant: Implications of Roasting Pretreatment Technology, Metals, 12 (2022) 1567.
[65] Y. Lin, Y. Chen, S. Chen, X. Hu, F. Zi, P. Yang, Facile and novel method for the recovery of gold from a calcined concentrate via copper-ammonia -thiourea system and activated carbon, Hydrometallurgy, 225 (2024) 106260.
[66] K. Li, Q. Li, T. Jiang, Y. Yang, B. Xu, R. Xu, Y. Zhang, Thiourea leaching of gold in presence of jarosite and role of oxalate, Trans. Nonferrous Met. Soc. China, 34 (2024) 322-335.

Chapter V. An electrochemical study of the gold dissolution behavior in a novel copper(II)-glycine oxidation system

5.1 Introduction

Thiosulfate leaching of gold is an alternative process to cyanidation with renowned advantages of non-toxicity, efficiency, strong ore adaptability, and without requiring consumable chemicals or energy input [1-3]. Copper is engaged in most thiosulfate systems as a catalyst, wherein success depends on the efficient redox cycling of copper between the +I and +II states. Numerous studies have reported that $Cu(NH_3)_4^{2+,}$ as copper(II) species, is necessary for catalytic gold oxidation reaction, which could speed up the gold leaching rate by 18-20 times, as shown in Eq. (5-1) [4, 5]. During this catalytic process, the $Cu(S_2O_3)_3^{5-}$ complex, in the reduced state of copper (II) ions, undergoes a reaction with dissolved oxygen to regenerate $Cu(NH_3)_4^{2+}$ complex, as described by Eq. (5-2). However, the redox potential of $Cu(NH_3)_4^{2+}/Cu(S_2O_3)_3^{5-}$ (E^0=0.22 V) is much higher than $S_4O_6^{2-}/S_2O_3^{2-}$ (E^0=0.08 V), thus the thiosulfate oxidation is also aggravated, causing huge reagent consumption, as seen in Eq. (5-3) [6]. A series of side-products from thiosulfate decomposition, such as tetrathionate ($S_4O_6^{2-}$), trithionate ($S_3O_6^{3-}$), sulfate (SO_4^{2-}), cyclo-S8, and copper/gold sulfide, can easily passivate the reaction surface of gold [7]. As a result, the gold dissolution kinetics were hugely hindered as the reaction time progressed. Moreover, the use of ammonia will bring potential environmental and toxic impacts with the emission of ammonia-nitrogen wastewater, enabling unattainable commercial applications until recently [8] [9]. Thus, the well-designed ammonia-free thiosulfate systems for gold extraction have offered opportunities to overcome these hindrances.

$$Au + 5S_2O_3^{2-} + Cu(NH_3)_4^{2+} \rightarrow Au(S_2O_3)_2^{3-} + 4NH_3 + Cu(S_2O_3)_3^{5-} \quad (5\text{-}1)$$

$$2Cu(S_2O_3)_3^{5-} + 16O_2 + 2H_2O \rightarrow 4Cu(NH_3)_4^{2+} + 4OH^- + 12S_2O_3^{2-} \quad (5\text{-}2)$$

$$2Cu(NH_3)_4^{2+} + 8S_2O_3^{2-} \rightarrow 2Cu(S_2O_3)_3^{5-} + 8NH_3 + S_4O_6^{2-} \quad (5\text{-}3)$$

Lately, the discovery of new organic ligands for copper (II) ions, such as ethylenediamine (En) [10], citrate (Cit^{3-}) [11], ethylenediaminetetraacetic acid (EDTA) [12], oxalate [13], humic acid [14], and amino acids [15] has contributed to the expansion of novel ammonia-alternative thiosulfate leaching. These organic ligands containing carboxylate or amine functional groups strongly complexed with copper(II) not only reduce the redox potential of $Cu(NH_3)_4^{2+}$ but also eliminate the side-effect of

ammonia by weakening the reactivity between free cupric ions and thiosulfate [16]. In the meantime, the redox cycling of copper species between the +I and +II states within these innovative organic ligand systems is intensified, resulting in a significant enhancement of gold extraction kinetics when compared to the conventional thiosulfate system containing ammonia [17]. The discovery that supported non-toxic amino acids (e.g., L-valine, glycine, DL-α-alanine, and L-histidine) can be excellent organic ligands for copper (II) with a reduced Cu(II)/Cu(I) redox potential, due to this reason, that contributed to promoting gold leaching efficiency and allowing thiosulfate consumption to be lowered [18].

Glycine (Gly) is one of the simplest and cheapest amino acids, which has some attractive chemical and physical properties as a ligand for transition metal ions [19,20]. Specifically, Gly as a ligand can enhance the stability of Cu(II) ions in aqueous solutions with a larger stability constant of 18.9 [21]. A fundamental thermodynamic calculation, as proposed by Wang et al., has provided evidence to suggest that Gly is a promising ligand for Cu (II) ions in the thiosulfate leaching of gold [22]. Moreover, Gly is an environmentally safe and biodegradable reagent, yet it is enzymatically destructible and is easily metabolized in most living organisms [23]. However, Gly has not yet been further used in leaching operations in thiosulfate systems for gold extraction, because the in-depth dissolution mechanism of gold and the role of the Cu (II)-glycine complex are not clear. All of these urgently require systematic research.

Electrochemical quartz crystal microbalance (EQCM), being a powerful in situ technique, was previously used to study gold dissolution in cyanide, chloride, and thiosulfate solutions containing copper and ammonia, which can directly record the mass change (sensitivity: 0.1~1 ng cm^{-2}) of gold dissolution at the electrode/electrolyte interface. Inspired by the above, a novel Gly-thiosulfate system for gold leaching was carried out, and the EQCM technique was mainly employed for the study of gold dissolution in this novel and eco-friendly system. Moreover, a series of corrosion electrochemical measurements (OCP, PDP, and EIS) and spectrum technologies (LA-ICP-MS and XPS) were used to investigate the in-depth gold dissolution mechanism and passivation behaviors. Based on the new knowledge, the effect of different forms of Cu(II)-glycine complexes (i.e., $Cu(C_2H_4NO_2)_2^0$ and $Cu(C_2H_4NO_2)_3^-$) on gold dissolution behavior in this novel Gly-thiosulfate system was in-depth discussed on the electrochemical model.

5.2 Materials and methods

5.2.1 Materials and reagents

Gold foils (99.999% Au, thickness 0.1 mm) with an area of 1 cm^2 were purchased from Zhongnuo New Materials Technology Co., Ltd (China). Analytical grade cupric sulfate pentahydrate ($CuSO_4 \cdot 5H_2O$), sodium thiosulfate ($Na_2S_2O_3$), ammonia ($NH_3 \cdot H_2O$), and glycine (Gly) were supplied by Shanghai Aladdin Biochemical Technology Co., Ltd (China). Deionized water was taken from a MilliQ purification system.

The gold concentrate sample (with particle sizes of 95% less than 0.074 mm) was obtained from the Sanmenxia province of China. A high-temperature calcination process (600 ^oC for 2 h) was first carried out to prepare the gold concentrate calcine (Au grade is 42.44 g/t). The raw gold concentrate was to liberate the encapsulated gold in the gold-bearing sulfide minerals by removing the detrimental elements (e.g., S and C) under calcination, and the remaining elements are mainly Fe, Si, Cu, and Al, as seen in Table 5.1. XRD of the gold concentrate calcine is shown in Figure 5.1, where the main mineral phases were Fe_2O_3 and SiO_2, and high-temperature products of $Cu_{0.5}Al_{2.5}S_4$.

Table 5.1 Chemical composition of the gold concentrate calcine. wt%

Elements	Au(g/t)	Fe	Si	Cu	Al	S	Pb	Ca	Zn	K	As
Content	42.44	25.57	12.77	5.34	2.67	4.34	1.80	1.63	1.41	1.02	0.68

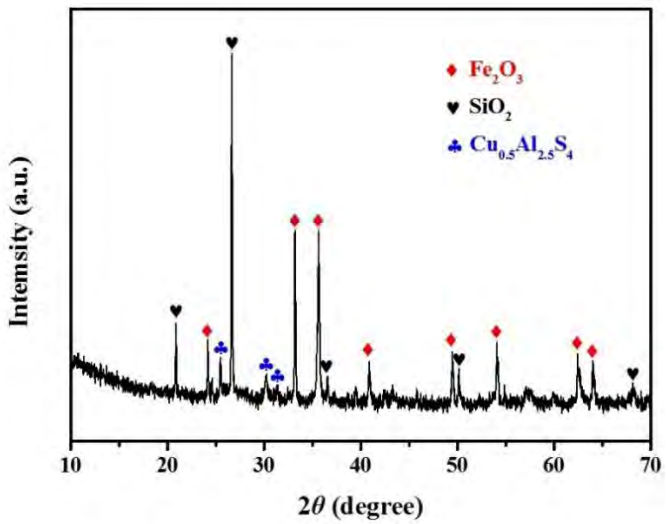

Figure 5.1 XRD pattern of the gold concentrate calcine

5.2.2 Gold leaching experiments

The leaching experiments of a gold concentrate calcine were performed in a 100

mL glass conical flask equipped with a digital mechanical stirrer (400 rpm). For the Gly-thiosulfate system, the lixiviant (50 mL) was accurately prepared by mixing 0.01 M $CuSO_4 \cdot 5H_2O$, 0.1 M $Na_2S_2O_3$, and 1.0 M Gly, with a solid-to-liquid (S/L) ratio of 1:7. Two comparative experiments were conducted under identical conditions, with one involving the substitution of glycine with ammonia (1.0 M $NH_3 \cdot H_2O$) in the lixiviant, and the other conducted without the addition of either Gly or ammonia. For each test, the initial pH of two Gly-thiosulfate lixiviants (pH 8 and pH 10.5) was adjusted by the addition of a saturated NaOH solution. The pH of the other two comparative lixiviants was controlled at 10.0. Several samples (2 mL) were taken at fixed leaching times (t=3, 6, 9 h) from the leaching slurry and filtered with a 0.22 μm pore size filter. The ore residues were fed back to the lixiviants, while the solution samples were diluted and analyzed using AAS. The concentration of thiosulfate in the obtained solution samples was measured by iodine titration. All experimental data were replicated three times to ensure accuracy and reliability.

5.2.3 Electrochemical experiments

The electrochemical dissolution of gold in the glycine-thiosulfate system was performed on CHI400E EQCM measurements (CH Instruments) at room temperature (~25 ^oC). The potential of the gold working electrode was controlled by a 3-electrode cell with a Pt counter electrode and an Ag/AgCl (0.197 V *vs.* SHE) reference electrode. The customized gold working electrode of the quartz oscillator is custom-made by coating with titanium plating followed by a gold layer (about 200 mg Au), which can be used as an active surface for testing using a 5 mL copper(II)-glycine-thiosulfate solution as electrolyte. The shift of the quartz resonance frequency (Δf) was converted into the mass change (Δm) by the Sauerbrey equation:

$$\Delta f = -2f_0^2 \, \Delta m / [A \, \mathrm{sqrt} \, (\mu\rho)] \qquad (5\text{-}4)$$

where f_0 is the resonant frequency of the crystal's fundamental mode (7.995 MHz), A is the area of the gold disk coated onto the crystal (0.196 cm^2), ρ is the crystal's density (2.684 g cm^{-3}), and μ is the shear modulus of quartz (2.947 x 10^{11} g cm^{-1} s^{-2}). The value of the calibration constant used in this work is 1.34 ng Hz^{-1}.

There are two thiosulfate solutions with different pH in the presence of $Cu(C_2H_4NO_2)_2^0$ and $Cu(C_2H_4NO_2)_3^-$) used in the studies, respectively. In detail, the anode dissolution phenomenon was tested by combining linear sweep voltammetry (LSV) and EQCM (LSV-EQCM). Moreover, Chronoamperometry (CA) coupled with

EQCM (CA-EQCM) was carried out to systematically test the electrochemical dissolution rate (EDR, μg cm^{-2} min^{-1}) calculated by the following formula:

$$EDR=\frac{\triangle m}{s\ t} \qquad (5\text{-}5)$$

Where △m (μg cm^{-2}) is the mass loss of the gold electrode before and after the reaction, s is the area of the gold coating on the electrode surface (0.196 cm^2), and t (min) is the reaction time.

The corrosive electrochemical technologies, including open circuit potential (OCP), potentiodynamic polarization (PDP), and electrochemical impedance spectroscopy (EIS), were tested using a Versa STAT4 Prastat electrochemical workstation. Gold foils with an area of 1.0 cm^2 on one side and the edges covered with wax, fixed on a platinum electrode clip, were used as the working electrode. Before tests, the active surface of gold foils was sequentially polished using sandpaper (800, 2000, and 10000 grit) and aluminum oxide polishing powder (0.3 and 0.5 μm). The reference electrode and counter electrode are consistent with the EQCM tests, and the electrolyte is a 50 mL copper (II)-Gly-thiosulfate solution. All experimental data were averaged over three tests.

5.2.4 Analytical and characterization techniques

The software of HSC Chemistry 6.0 for Windows was used to construct the Eh-pH diagrams. Atomic adsorption spectroscopy (AAS, 280Z AA, Agilent, USA) was used to determine the gold concentration in the filtrate after leaching of the gold concentrate calcine. UV-vis spectroscopy (UV-Vis, GENESYS, Thermo Fisher Scientific, UK) was used to measure the absorbance of the copper (II)-glycine complex. A scanning electron microscope (SEM, pw-100-017, Phenom, Holland) was used to characterize the morphology of gold foils after leaching. An acceleration voltage of 10 kV and back-scattered electron imaging were used in this experiment. Laser ablation inductively coupled plasma mass spectrometer (LA-ICP-MS) and X-ray photoelectron spectroscopy (XPS, Thermo ESCALAB 250XI, Thermo Fisher Scientific, UK) were used to identify the passive species of a gold foil after leaching. The XPS is equipped with a monochromatic Al-Kα X-ray source (1486.6 eV). LA-ICP-MS is equipped with a GeoLas Plus laser ablation system (LA, 193 nm ArF, Coherent, USA) and an inductively coupled plasma mass spectrometer (ICP-MS, 7700X, Agilent, USA). Density functional theory (DFT) calculations were used to better analyze the ligand exchange process during the dissolution of gold. In this part, the structures and energies

were calculated at the B3LYP level with the LANL2DZ basis set (Becke's three-parameter nonlocal-exchange functional with the nonlocal correlation of Lee et al. method) based on the GAUSSIAN 09 program [24]. To investigate the species distribution of Gly at different pH conditions, the pKa values from the literature (Michal et al., 2014) were used to construct the dissociation profiles, and the fractions of species distribution were subsequently plotted against pH levels.

5.3 Results and discussion

5.3.1 Speciation of Cu (II) - glycine complexes in thiosulfate media

It is vital to identify the forms of Cu(II) in the Gly-thiosulfate solution. According to dissociation profiles (Figure 5.2a), Gly is in the cation form (H_2Gly^+) at very acidic pH conditions (pH<2.33), and there are no active sites on the Gly molecule (NH_3^+ instead of NH_2 while COO^- remains neutral, as COOH) to coordinate with Cu(II) ions. At near neutral pH conditions (2.33 < pH < 9.57), the concentration of cation species decreased with pH increase, and Gly was presented in zwitterion forms mostly. In the zwitterion form of Gly (HGly), salt bridge bonding between the protonated amine of glycine with another COO^- site restricts the active sites for coordination with Cu(II) ions. As the pH increased to values greater than 7, anionic species (Gly^-, the deprotonated form of COOH to be a carboxylate COO^-) began to form, and when it exceeded 9.57, the predominance of these anionic species was observed. This facilitates the donation of electrons from the Gly molecules to the Cu(II) ions and the formation of Cu(II)-glycine complexes [25]. The thermodynamic data (Figure 5.2b) show two different forms of copper(II)-Gly complexes (i.e., $Cu(C_2H_4NO_2)_2^0$ and $Cu(C_2H_4NO_2)_3^-$), as Eqs. (5-6) and (5-7) [26]. Typically, the neutral $Cu(C_2H_4NO_2)_2^0$ species is predominant in solutions with relatively low pH values ranging from 4.00 to 9.14, while the anionic $Cu(C_2H_4NO_2)_3^-$ species becomes more prevalent in solutions with higher pH values ranging from 9.14 to 12.80.

$$Cu^{2+} + 2C_2H_4NO_2^- \rightarrow Cu(C_2H_4NO_2)_2^0 \quad (5\text{-}6)$$

$$Cu^{2+} + 3C_2H_4NO_2^- \rightarrow Cu(C_2H_4NO_2)_3^- \quad (5\text{-}7)$$

UV-Vis spectroscopy (Figure 5.2c) found that $Cu(C_2H_4NO_2)_2^0$ existed in pH=8 media with an absorbance of 631 nm, while an absorbance of 661 nm represents $Cu(C_2H_4NO_2)_3^-$ when the pH is increased to 10.5 [27, 28]. The stable structures of $Cu(C_2H_4NO_2)_2^0$ and $Cu(C_2H_4NO_2)_3^-$ are seen in Figure 5.2d and 5.2e, which are formed by the coordination of Cu(II) ions and oxygen atoms of -COOH in Gly molecules [29].

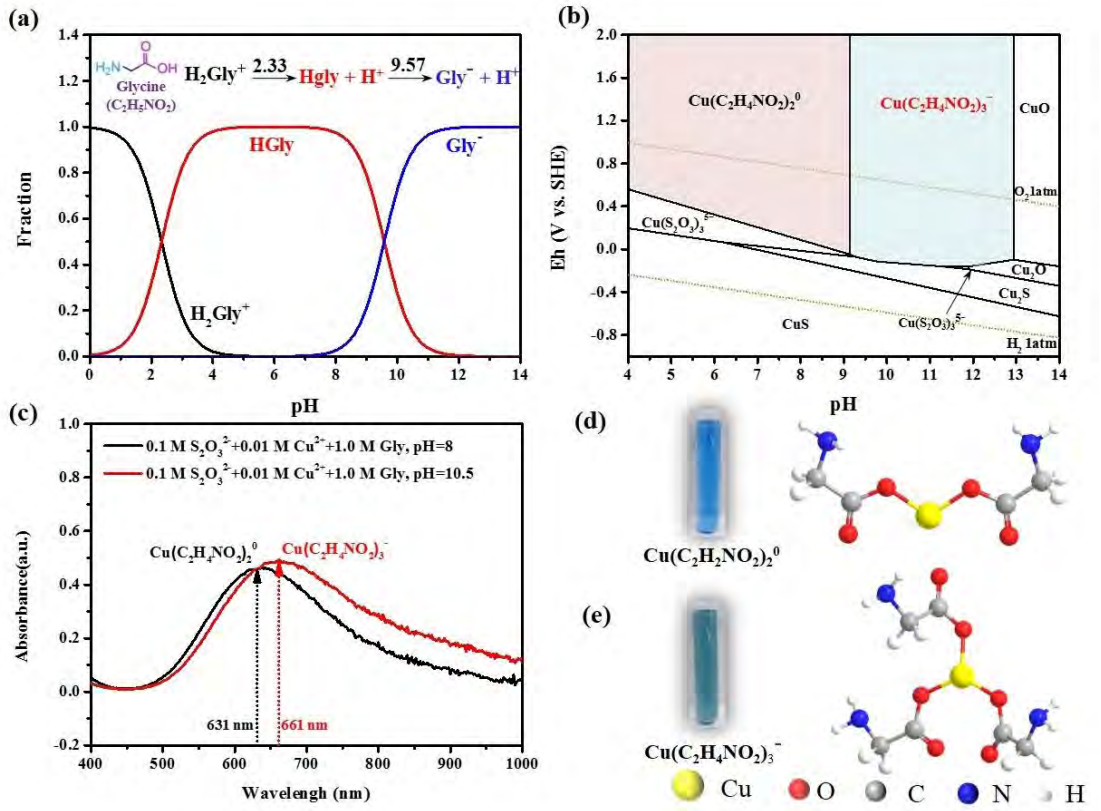

Figure 5.2 Formation of copper(II) species in Gly-thiosulfate solution. (a) Dissociation profiles of glycine. (b) Eh-pH diagram for Cu (II)-Gly-thiosulfate-water system (0.01 M Cu^{2+}, 1.0 M Gly, 0.1 M $S_2O_3^{2-}$). (c) UV-Vis spectrophotometry and (d, e) structure model for $Cu(C_2H_4NO_2)_2^0$ and $Cu(C_2H_4NO_2)_3^-$ complexes

5.3.2 Leaching of a gold concentrate calcine

The effect of Cu(II) species on the leaching of a gold concentrate calcine in thiosulfate solution, as well as the decomposition of thiosulfate, was investigated. It is noteworthy that the leaching percentage of gold in Cu(II)-Gly systems, specifically $Cu(C_2H_4NO_2)_3^-$ and $Cu(C_2H_4NO_2)_2^0$) as catalysts, are greater than the traditional Cu(II)-ammonia system (i.e., $Cu(NH_3)_4^{2+}$ as catalyst) and the system where only Cu(II) ions are present (Figure 5.3a). The gold leaching percentage of $Cu(C_2H_4NO_2)_3^-$ system at pH 10.5 reached 75.1% only 9 h of reaction, which was significantly higher than the $Cu(C_2H_4NO_2)_2^0$ system at pH 8 (62.6 %). In addition, the inclusion of Cu (II) complexes in the leaching solution inevitably promotes the consumption of thiosulfate, whereas the extent of thiosulfate consumption in the Cu(II)-Gly system is notably lower in comparison to the Cu(II)-ammonia system (Figure 5.3b). Under alkaline leaching conditions in the presence of Cu(II)-Gly complexes, the $Cu(C_2H_4NO_2)_3^-$ system exhibits a relatively low thiosulfate consumption rate, only 13.6%. Likely, this partially

consumed thiosulfate is primarily utilized for gold leaching rather than being predominantly decomposed by $Cu(C_2H_4NO_2)_3^-$.

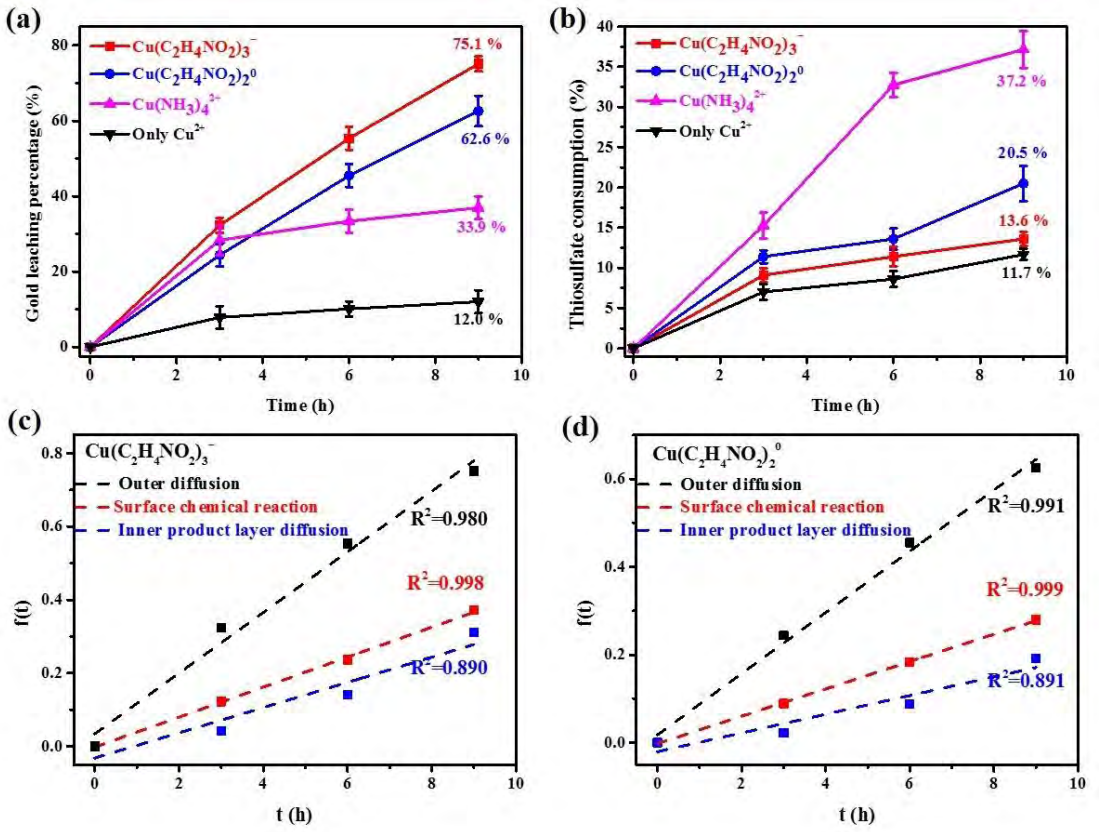

Figure 5.3 Leaching of a gold concentrate calcine catalyzed by different copper (II) species ($Cu(C_2H_4NO_2)_3^-$, $Cu(C_2H_4NO_2)_2^0$, $Cu(NH_3)_4^{2+}$ and Cu^{2+} ions): (a) gold leaching percentage and (b) thiosulfate consumption. Shrinkage core models for various control regimes: (c) $Cu(C_2H_4NO_2)_3^-$ system and (d) $Cu(C_2H_4NO_2)_2^0$ system

To determine the kinetic parameters and rate-controlling step of the gold leaching process, the well-known shrinking core model was utilized. In general, gold leaching can be described as a solid-liquid non-homogeneous reaction, and the leaching rates are controlled by one of the following several steps (Table 5.2) [30]: (1) Outer diffusion control. Movement of the leaching agent from the lixiviant to the solid product layer on the surface of the ore. (2) Surface chemical reaction control. The chemical reaction of the leaching agent ions with unreacted gold at the reaction interface. (3) Inner production layer diffusion. Diffusion of reaction products through the solid product layer from the reaction interface to the boundary layer. Where x is the reacted fraction of gold in concentrate calcine, k_r, k_c, and k_d are the apparent rate constants (h^{-1}), and t is the reaction time. As shown in Figures 5.3c and 5.3d, larger regression coefficients

(R^2) were obtained from the type of chemical surface reaction control, which indicated that the leaching process of both $Cu(C_2H_4NO_2)_3^-$ and $Cu(C_2H_4NO_2)_2^0$ systems was controlled by the chemical reaction between the gold-thiosulfate interface [31]. Besides, the apparent rate constant (k_c=0.041) of the $Cu(C_2H_4NO_2)_3^-$ system was higher than that of $Cu(C_2H_4NO_2)_2^0$ (k_c=0.031), which was defined as the more rapid gold leaching kinetic using $Cu(C_2H_4NO_2)_3^-$ as oxidant species.

Table 5.2 Time expression for the shrinking core model at various controlling steps

No.	Controlling step	Equation
1	Outer diffusion	$x = k_r t$
2	Surface chemical reaction	$1-(1-x)^{1/3} = k_c t$
3	Inner production layer diffusion	$1-3(1-x)^{2/3}+2(1-x) = k_d t$

5.3.3. Mechanistic insights into electrochemical gold dissolution

5.3.3.1. Anodic oxidation and dissolution behavior of gold

The gold-thiosulfate interface, including anodic oxidation of gold and cathodic reduction of Cu(II) processes, was first investigated with the help of CV tests (scanning speed: 1.0 mV s^{-1}). Figures 5.4a and 5.4b show the CV recorded from two thiosulfate solutions containing $Cu(C_2H_4NO_2)_2^0$ and $Cu(C_2H_4NO_2)_3^-$ complexes, respectively. The Cu(II) reduction process is a multi-step reaction in the cathodic portion, including Cu (II)/Cu (I) (C_3 peak), Cu (I)/Cu (0) (C_2 peak), and Cu (II)/Cu (0) (C_1 peak) [32]. The Cu (II)-glycine complex is the receptor of the electron from the anodic portion (gold-thiosulfate interface), which drives the oxidation of Au(0) to Au(I). In the anode process, the current peak of A_1 represents the oxidation of Cu(0) for Cu(I), which is further stripped from the electrode surface for recycling [33]. A_2 peak represents multiple mixed reactions containing gold oxidation, along with a regenerative cycle of Cu(II), and slight $S_2O_3^{2-}$ oxidation (Eq. 5-8) [34]. At higher potentials (A_3 and A_4 peaks), the current density increased due to the violent decomposition of $S_2O_3^{2-}$ to $S_4O_6^{2-}$, which further decomposed into elemental sulfur [35].

$$2S_2O_3^{2-} \rightarrow S_4O_6^{2-} + 2e^- \qquad E=0.08\ V\ (vs.\ SHE) \qquad (5\text{-}8)$$

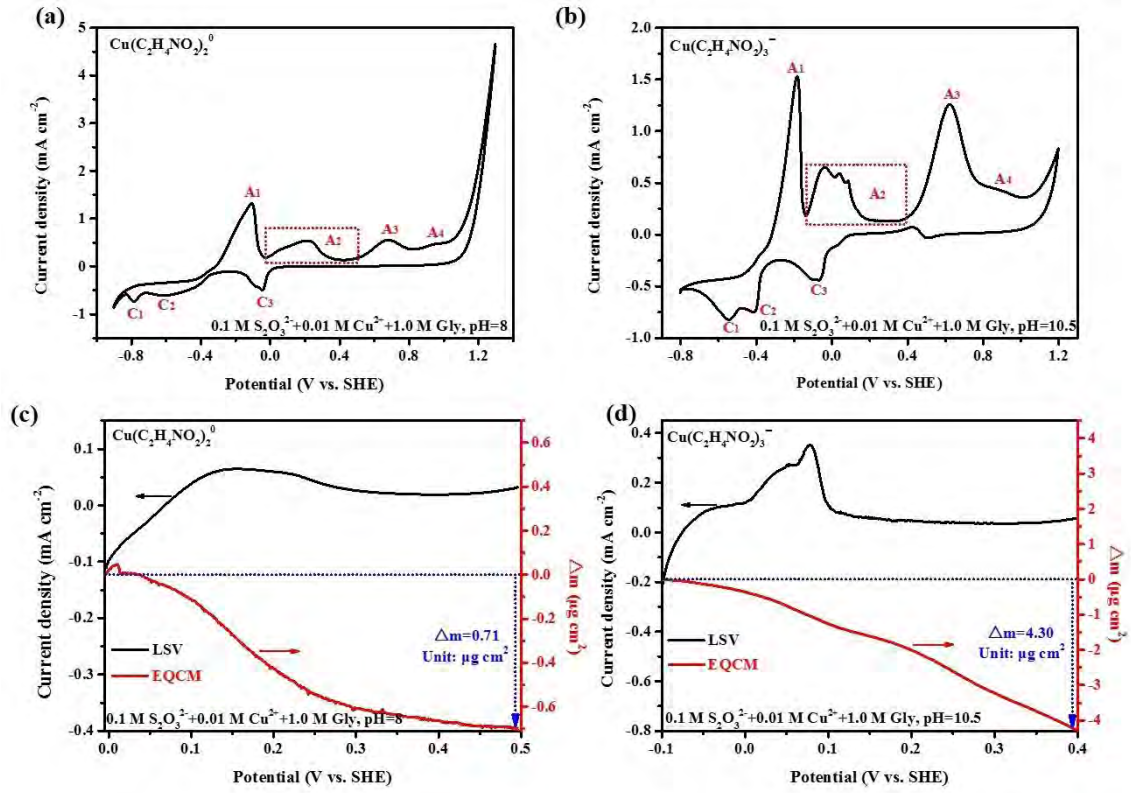

Figure 5.4 Anodic oxidation behavior of gold in Gly-thiosulfate system. (a, b) CV curves and (c, d) LSV-EQCM curves of gold dissolution catalyzed by $Cu(C_2H_4NO_2)_2^0$ and $Cu(C_2H_4NO_2)_3^-$ complexes

To further investigate the anodic dissolution behavior of gold, LSV-EQCM measurements with a scanning speed of 1.0 mV s^{-1} were conducted near the current peak of A_2 (Figures 5.4c and 5.4d). In the $Cu(C_2H_4NO_2)_2^0$ system, an obvious mass loss of 0.71 μg cm^{-2} is observed from 0.0 V to 0.5 V, where gold dissolution occurs [36, 37]. The mass loss reaches 4.30 μg cm^2 in the $Cu(C_2H_4NO_2)_3^-$ system, which is significantly higher than the $Cu(C_2H_4NO_2)_2^0$ system. Moreover, these LSV-EQCM curves did not show mass increase, indicating that voltammetry near the current peak of A_2 does not result in $S_2O_3^{2-}$ oxidation.

Here, the dissolution process of gold is described in Figure 5.5a, which was further understood by DFT and thermodynamic calculations. As previously reported, gold dissolution in thiosulfate solution in the presence of Cu(II) species can be considered an electrochemical process, which involves the oxidation of the element gold to gold ions at the anode, i.e., Au(0) to Au(I), as seen in Eq. (5-9). Thoroughly, Cu(II) ions serve as both oxidant and catalyst, enhancing the oxidation of gold by facilitating electron

transfer reactions via the reduction of Cu(II) ions at the cathode, i.e., Cu(II)→Cu(I). The oxidized gold species, in the form of Au(I), requires coordination with a ligand to be released from the unreacted gold core and enter the solution. Here, the total energy(E) of $Au(C_2H_4NO_2)_2^-$ is significantly lower than $Au(S_2O_3)_2^{3-}$ from DFT calculations (Figures 5.5b and 5.5c), which indicates that Gly may preferentially adsorb on the gold surface and first undergo a coordination reaction with Au (I) to form an $Au(C_2H_4NO_2)_2^-$ complex as the product layer, as shown in Eq. (5-10) [22].

However, thermodynamic calculations confirmed the dominant Au (I) species is $Au(S_2O_3)_2^{3-}$ rather than $Au(C_2H_4NO_2)_2^-$ in the Eh-pH diagram of the Au-glycine-thiosulphate-water solution (Figure 5.5d). In addition, since the stability constant of $Au(S_2O_3)_2^{3-}$ (logβ=24) is significantly larger than that of $Au(C_2H_4NO_2)_2^-$ (logβ=18), the complex of $Au(C_2H_4NO_2)_2^-$ can be followed a fast ligand exchange process with $S_2O_3^{2-}$ in the gold-thiosulfate interface, thus bringing Au^+ into solution as $Au(S_2O_3)_2^{3-}$, as seen in Eq. (5-11). Based on the empirical findings suggesting that the rate of gold leaching is predominantly influenced by surface chemistry reactions, the primary controlling reactions of gold dissolution can be ascribed to the oxidation of gold and the subsequent ligand exchange process.

$$Au \rightarrow Au^+ + e^- \quad (5\text{-}9)$$

$$Au^+ + 2(C_2H_4NO_2)_2^- \rightarrow Au(C_2H_4NO_2)_2^- \quad (5\text{-}10)$$

$$Au(C_2H_4NO_2)_2^- + 2S_2O_3^{2-} \rightarrow Au(S_2O_3)_2^{3-} + 2C_2H_4NO_2^- \quad (5\text{-}11)$$

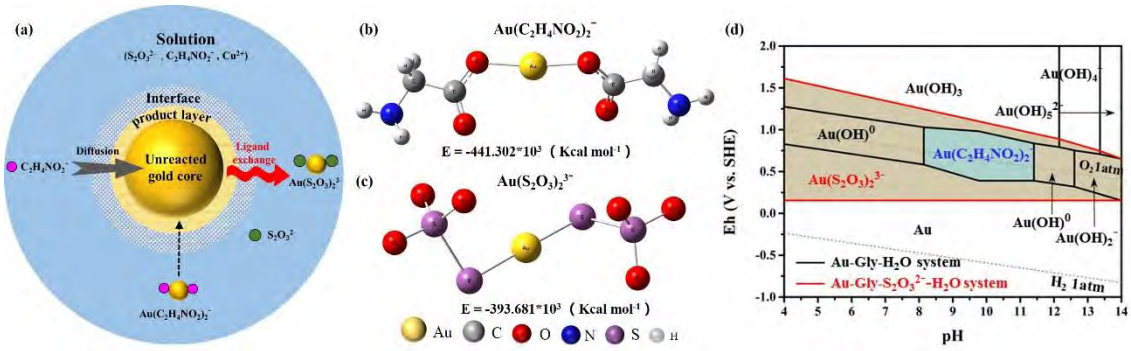

Figure 5.5 The dissolution products of gold in the Gly-thiosulfate system. (a) The proposed ligand exchange process. The optimized geometries and calculated energy of (b) $Au(C_2H_4NO_2)_2^-$ and (c) Au $(S_2O_3)_2^{3-}$. (d) Eh-pH diagram for the Au-Gly-thiosulfate-water system

5.3.3.2. Dissolution rate of gold

A series of CA-EQCM experiments, including the effect of the applied potential,

Gly concentration, and solution pH, is used to study the dissolution rate of gold in Gly-thiosulfate solution.

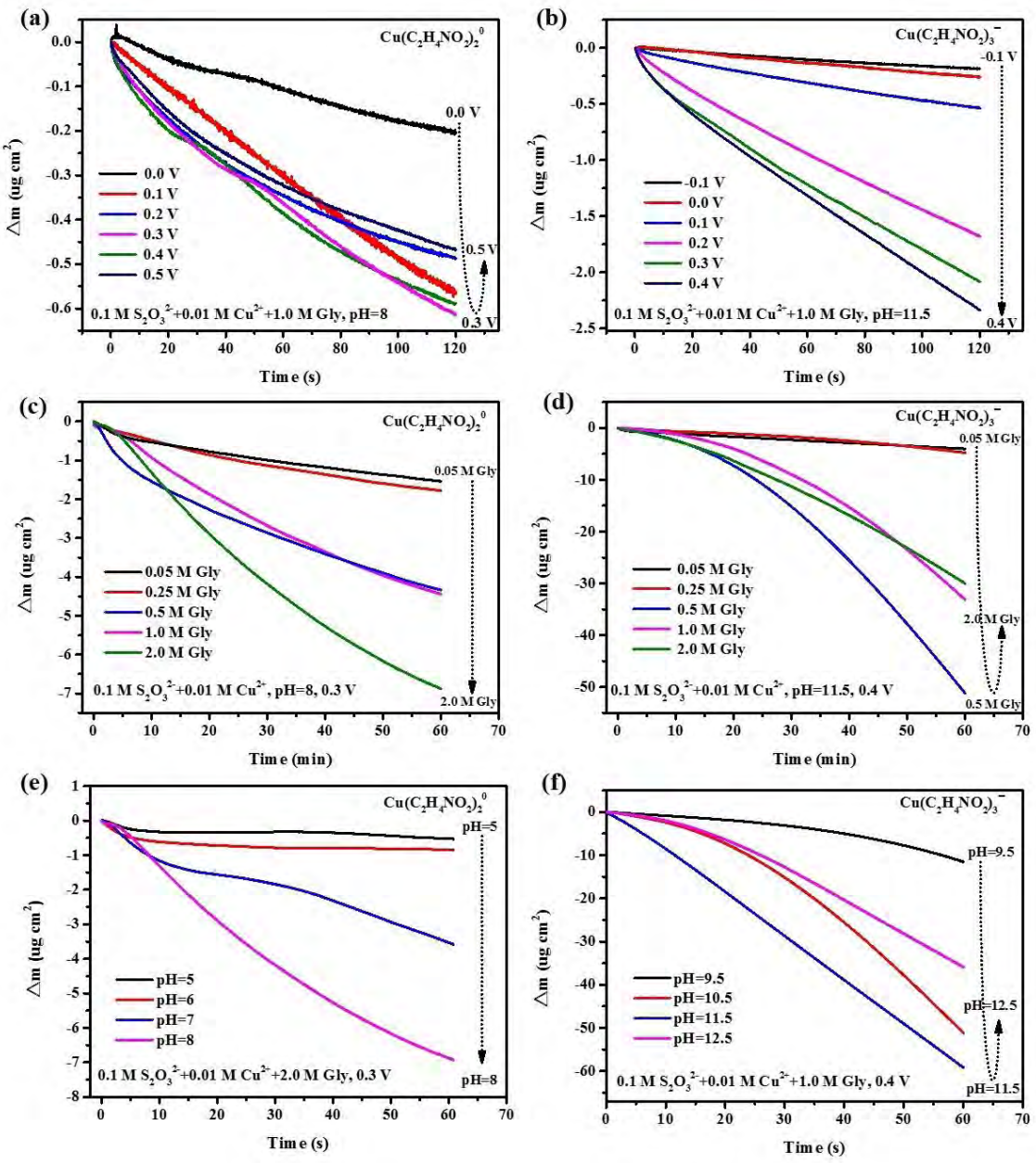

Figure 5.6 The mass loss curves of gold dissolution in Gly-thiosulfate systems: Effect of (a, b) the applied potential, (c,d) Gly concentration, and (e,f) solution pH catalyzed by $Cu(C_2H_4NO_2)_2^0$ and $Cu(C_2H_4NO_2)_3^-$ respectively

Aim to optimize the applied oxidation potential for the dissolution of the gold electrode in the subsequent EQCM tests, a thiosulfate solution in the presence of $Cu(C_2H_4NO_2)_2^0$ complex was tested in the applied potential range of 0.0 to 0.5V for 120 s. Similarly, a solution containing $Cu(C_2H_4NO_2)_3^-$ complex was conducted by

increasing the applied potential from -0.1 V to 0.4 V. Figures 5.6a and 5.6b show a significant mass loss of gold electrode, indicating that both $Cu(C_2H_4NO_2)_3^-$ and $Cu(C_2H_4NO_2)_2^0$ successfully oxidized Au (0) to Au (I) which dissolved into solution through a multi-step process ($Au(C_2H_4NO_2)_2^- \rightarrow Au(S_2O_3)_2^{3-}$). In this case, the maximum mass loss of gold electrode in the $Cu(C_2H_4NO_2)_2^0$ system is -0.61 μg cm^{-2} at 0.3 V, while in the $Cu(C_2H_4NO_2)_3^-$ system, it reaches up to -2.36 μg cm^{-2} at 0.4 V.

To investigate the maximum electrochemical dissolution rate (EDR) of gold in Gly-thiosulfate solution, the effect of Gly concentration (0.05, 0.25, 0.5, 1.0, 2.0 M) was studied at the fixed applied potential (Figures 5.6c and 5.6d). For each experimental run, the mass loss curves were tested at 0.3 V in $Cu(C_2H_4NO_2)_2^0$ and 0.4 V in $Cu(C_2H_4NO_2)_3^-$ systems for 60 min, respectively. Obviously, more Gly is beneficial for increasing the gold dissolution rate in the $Cu(C_2H_4NO_2)_2^0$ system, while the corresponding EDR is only 0.585 μg cm^{-2} min^{-1} when the Gly content goes up to 2.0 M. The gold dissolution in the $Cu(C_2H_4NO_2)_3^-$ system initially increased when the Gly content increased from 0.05 to 0.5 M, and then slightly decreased at higher Gly contents (0.5~2.0 M). The mass loss of the gold electrode at 0.5 M Gly reached 51.20 μg cm^{-2}, with a higher EDR value of 4.354 μg cm^{-2} min^{-1}.

When the applied potential and Gly concentration are kept constant, the dissolution rate of gold is mainly affected by the solution pH. Figures 5.6e and 5.6f show the mass loss curves tested at 2.0 M Gly solution for 60 min with a pH range of 5~8 ($Cu(C_2H_4NO_2)_2^0$ system) and tested at 0.5 M Gly solution with a pH range of 9.5~12.5, respectively ($Cu(C_2H_4NO_2)_3^-$ system). The catalytic performance of $Cu(C_2H_4NO_2)_3^-$ complex in an alkaline system is stronger than in a near-neutral system with $Cu(C_2H_4NO_2)_2^0$ complex. In the range of pH value from 9.5 to 11.5, the mass loss of the gold exhibits a significant enhancement with a maximum EDR of 5.032 μg cm^{-2} min^{-1}, while further increasing the solution pH to 12.5, a slight decrease of EDR is observed. Therefore, it can be concluded that the system under strongly alkaline conditions, where $Cu(C_2H_4NO_2)_3^-$ is the predominant Cu (II) species, exhibits superior catalytic performance for the gold dissolution rate.

5.3.3.3. Dissolution mechanism of gold

The corrosion electrochemical experiments (e.g., OCP, PDP, and EIS) are beneficial for understanding the dissolution mechanism of gold [38]. Especially, the combination of OCP and PDP is commonly utilized to assess the corrosion ability/tendency of metal. Figures 5.7a and 5.7b show the quasi-steady OCP curves of

a gold foil as a working electrode immersed in thiosulfate solution, including $Cu(C_2H_4NO_2)_2^0$ and $Cu(C_2H_4NO_2)_3^-$ complexes with optimized solution pH and Gly concentration from EQCM tests, respectively. As displayed in Figure 5.7a, with the increasing elapsed time (0.5 h), OCP of the $Cu(C_2H_4NO_2)_2^0$ system decreased, ranging from 0.138 to 0.115 V. In comparison, the OCP remains stable at -0.020 V in the $Cu(C_2H_4NO_2)_3^-$ system, indicating the lowest electrochemical nobility. As time progressed, the OCP of both systems increased gradually (Figure 5.7b). From a corrosion science perspective, the gold foil in $Cu(C_2H_4NO_2)_3^-$ system exhibits the most negative OCP, indicating that the gold surface is more prone to oxidation [39].

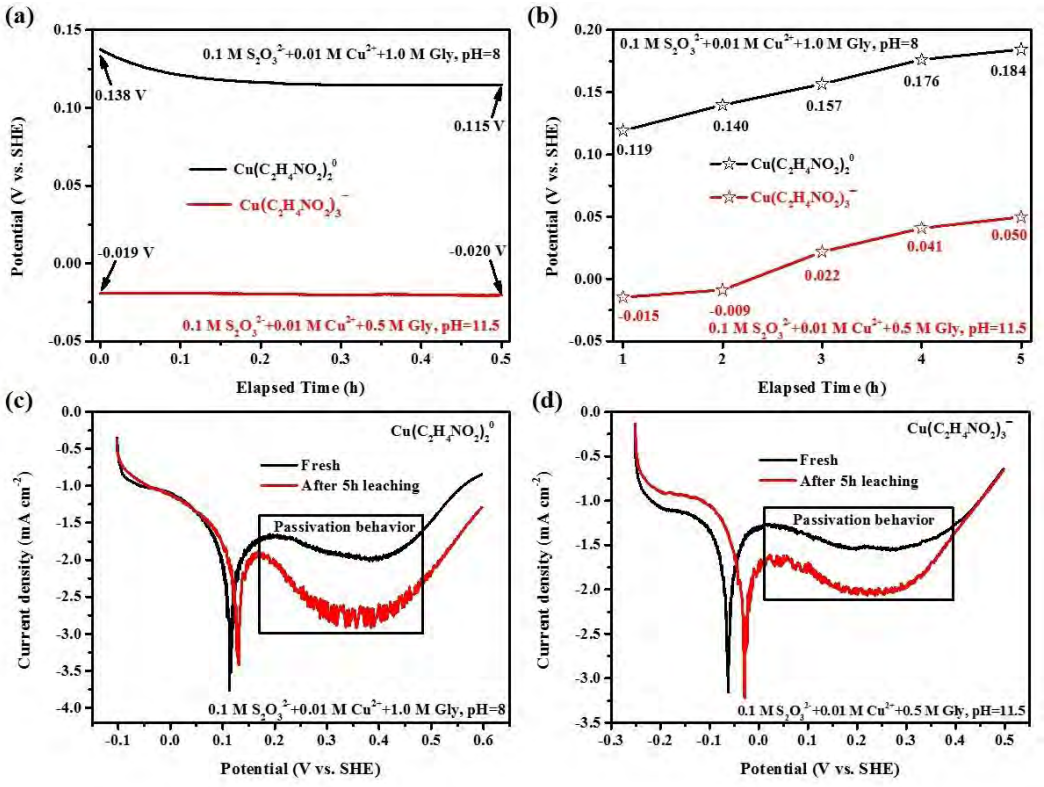

Figure 5.7 Electrochemical analysis of gold dissolution in Gly-thiosulfate systems. (a, b) OCP and (c, d) PDP curves for gold electrode tests with $Cu(C_2H_4NO_2)_2^0$ and $Cu(C_2H_4NO_2)_3^-$ complexes

Table 5.3 summarizes the corrosion potential (E_{corr}) and corrosion current density (j_{corr}), which are determined by fitting the PDP curves via a Tafel plot extrapolation method (Figures 5.7c and 5.7d; scanning speed: 0.1 mV s^{-1}). Typically, the leaching process of gold suggests that j_{corr} corresponds to the gold leaching current, and E_{corr} is the mixed potential of the lixiviant [40]. Interestingly, the E_{corr} of both systems was nearly consistent with the OCP values at the beginning state, suggesting good solution

stability [41]. The observed positive shift of E_{corr} after 5h tests reveals the dominant effect of the cathodic Cu(II) reduction (Cu(II) → Cu(I)) in facilitating the anodic oxidation of gold (Au(0) → Au(I)). The higher j_{corr} of $Cu(C_2H_4NO_2)_3^-$ system could be ascribed to the effective reduction of cupric ions in the cathodic portion, accompanied by the acceleration of elemental gold oxidation in the anode. It was widely hypothesized that the gold surfaces may have been passivated to prevent further dissolution when using Cu(II)-ammonia as catalysts/oxidant species [42]. Alongside this, an obvious passivation behavior with the current density decreases first and then tends to increase drastically at the anode curves, indicating the passivation layer breakdown and the onset of localized corrosion [43]. This phenomenon originated from the capability to receive electrons of $Cu(C_2H_4NO_2)_3^-$ complex, which is stronger than that of $Cu(C_2H_4NO_2)_2^0$ complex. In addition, the j_{corr} increased compared with the initial value in the $Cu(C_2H_4NO_2)_3^-$ system but decreased in the $Cu(C_2H_4NO_2)_2^0$ system, indicating that passivation behavior has very little impact on the gold dissolution.

Table 5.3 Fitting results of E_{corr} and j_{corr} from PDP curves

Cu(II) species	$Cu(C_2H_2NO_2)_2^0$		$Cu(C_2H_4NO_2)_3^-$	
Conditions	Fresh	After 5 h	Fresh	After 5 h
E_{corr} (V)	0.113	0.131	-0.062	-0.0223
j_{corr} (mA cm^{-2})	0.053	0.033	0.034	0.076

Electrochemical impedance spectroscopy (EIS), with a frequency range of 0.01-100 kHz, was adopted to reveal the electrochemical reaction kinetics of gold leaching during a 5 h reaction (Figures 5.8a and 5.8b). The fitting results are depicted in Figures 5.8c and 5.8d. In this case, Re represents the resistance of the solution, Rf represents the resistance of the formation of passivated substances on the gold surface, and Rct represents the resistance of the electron transfer at the reaction interface during the oxidation of Au (0) to Au (I), where electrons are received by Cu(II)-Gly complex [44]. The small Re values imply a higher ionic conductivity in the Gly-thiosulfate system. The Rct value of the $Cu(C_2H_4NO_2)_2^0$ system is significantly higher, exceeding that of the $Cu(C_2H_4NO_2)_3^-$ system by more than 10 times. Because the fitting results of the shrinking core model show that the leaching process is controlled by chemical surface reactions (section 5.3.2), it plays a significant role in improving the kinetics of gold leaching [45]. It shows that $Cu(C_2H_4NO_2)_2^0$ as a receptor makes it difficult to transfer the electrons generated by gold oxidation. Thus, the gold dissolution rate is much

slower than the $Cu(C_2H_4NO_2)_3^-$ system, as confirmed by the previous leaching and EQCM studies. Moreover, the gold surface will be passivated during long-time leaching, which is consistent with the PDP tests. In detail, the R_f value of the $Cu(C_2H_4NO_2)_3^-$ system is significantly smaller than that of the $Cu(C_2H_4NO_2)_2^0$ system, indicating that the passivation inhibition observed when using $Cu(C_2H_4NO_2)_3^-$ as catalysts for gold leaching is less pronounced.

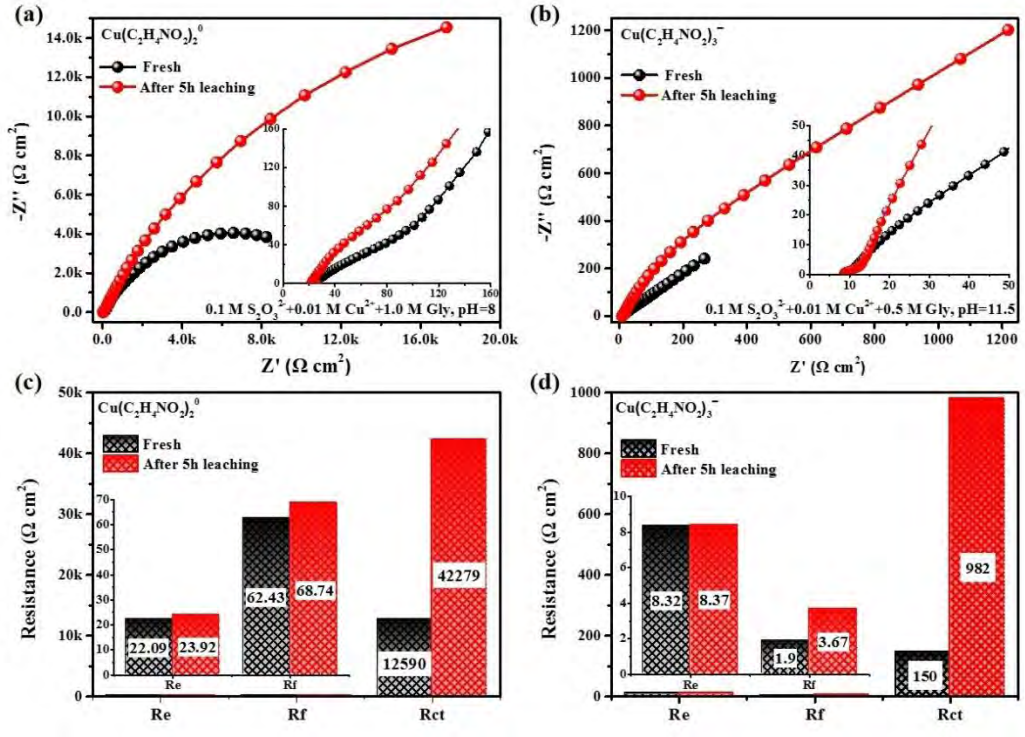

Figure 5.8 EIS results for gold electrode tests in Gly-thiosulfate systems: (a, b) EIS curves; (c,d) Values of Re, Rf, and Rct

It was inevitable that the gold dissolution kinetics would be hindered by the passivation behavior, and the passivation layer is mainly composed of sulfur-containing products such as CuS, Cu_2S, or elemental S [46, 47]. Here, the surface species of a gold foil after 5 h leaching in a Gly-thiosulfate system were identified by LA-ICP-MS, which provides accurate elemental analysis of the laser-ablated layers (less than 10 μm thick on a gold surface) [48]. As can be seen in Figure 5.9, the gold surface exhibits only minimal signals of S and Cu, suggesting a negligible formation of passivation layers resulting from thiosulfate decomposition.

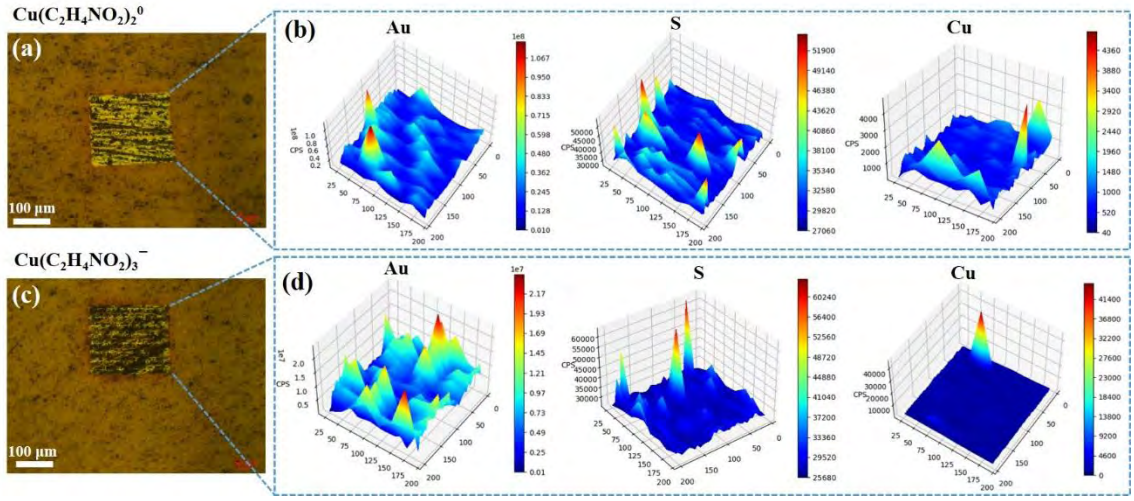

Figure 5.9 Optical microscope images and LA-ICP-MS spectra of a gold foil after 5 h leaching. (a, b) $Cu(C_2H_4NO_2)_2^0$ system (0.1 M $S_2O_3^{2-}$, 0.01 M Cu^{2+}, 2.0 M Gly and pH 8) and (c, d) $Cu(C_2H_4NO_2)_3^-$ system (0.1 M $S_2O_3^{2-}$, 0.01 M Cu^{2+}, 0.5 M Gly and pH 11.5)

We further performed XPS tests to confirm the detailed chemical composition of the passivation layer (Figure 5.10). There are two prominent peaks located at approximately 164.0 eV and 168.0 eV in S 2p spectra, which are attributed to S^{2-}, S, S_n, and SO_3^{2-}, SO_4^{2-} species [49]. In the Cu 2p spectra, the 2p3/2 peak is observed at approximately 932.5 eV, and the 2p1/2 peak appears at 952.5 eV, suggesting the presence of CuS or Cu_2S compounds [50]. However, no clear S or Cu signals were detected by XPS survey spectrums, indicating that the passivation species originating from thiosulfate is minimal [51]. Interestingly, it can be seen obvious signals of C, O, and N elements in XPS survey spectra. Several fitting peaks in the C1s spectra suggest the existence of C-C (284.8 eV), C-O/C-N (286.3 eV), and C=O (287.9 eV). Deconvolution of O 1s spectra indicated that multi-peaks are associated with C-O (533.1 eV), and O-H (531.4 eV) in the -COOH generated group. Only one predominant peak in the N 1s region (399.8 eV) was assigned to metal-N bonding (Au-N) [52, 53]. As the central carbon atom of Gly has a $-NH_2$ group and a -COOH group bonded to it, it can be concluded that the passivation species mainly originates from Gly. Numerous studies have shown that Gly as an individual lixiviant can coordinate with gold, forming an $Au(C_2H_4NO_2)_2^-$ complex [54]. As mentioned earlier, a possible ligand exchange reaction of $Au(C_2H_4NO_2)_2^-$ to Au $(S_2O_3)_2^{3-}$ can occur at the gold-solution interface (as seen in Figure 5.5a). Thus, it is believed that the formation of passivation species is mainly generated by the coordination between Gly and Au(I) ions, specifically the

formed $Au(C_2H_4NO_2)_2^-$, not stripped from the gold surface immediately, rather than thiosulfate decomposition.

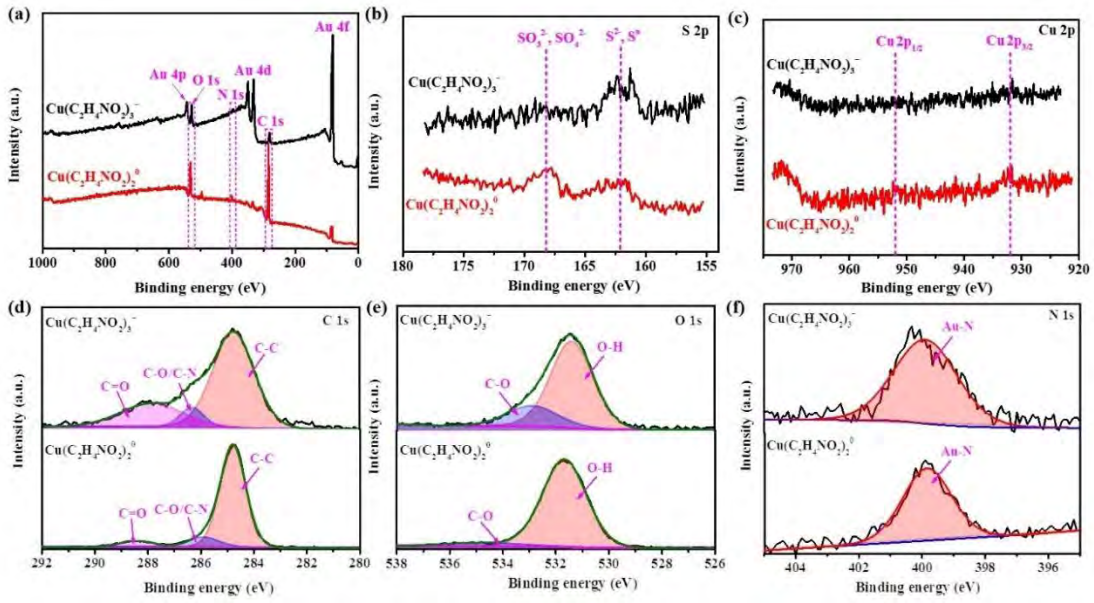

Figure 5.10 XPS spectra of a gold foil after 5 h leaching in $Cu(C_2H_4NO_2)_2^0$ and $Cu(C_2H_4NO_2)_3^-$ systems: (a) Survey spectra; (b~f) High-resolution spectra of S 2p, Cu 2p, C 1s, O 1s, and N 1s

More in-depth analysis was conducted to elucidate the mechanism of gold dissolution in the novel Gly-thiosulfate system. It is logical to believe that the gold dissolution can be driven by Cu(II)-Gly complexes, i.e., $Cu(C_2H_4NO_2)_2^0$ and $Cu(C_2H_4NO_2)_3^-$, which are sensitive to the pH of the solution. According to two electrochemical routes proposed in Figure 5.11, both Cu(II)-Gly complexes acquired electrons on the gold surface, which are directly reduced to $Cu(S_2O_3)_3^{5-}$ on the cathodic portion. In the anodic portion, Au^0 is oxidized to Au^+ which is converted to $Au(S_2O_3)_2^{3-}$ through a multi-step ligand exchange process ($Au(C_2H_4NO_2)_2^- \rightarrow Au(S_2O_3)_2^{3-}$) (see in Figure 5.5(c)). Eventually, the dissolved oxygen in the solution acts as an oxidant to convert $Cu(S_2O_3)_3^{5-}$ to Cu(II)-Gly complexes. To sum up, the strong alkaline system containing $Cu(C_2H_4NO_2)_3^-$ exhibits lower potential (OCP and corrosion potential), larger corrosion current density, and slighter passive behavior, which facilitates the redox cycling of copper ions between the +I and +II states and electron transfer during gold oxidation, resulting in an enhanced catalytic performance for gold dissolution.

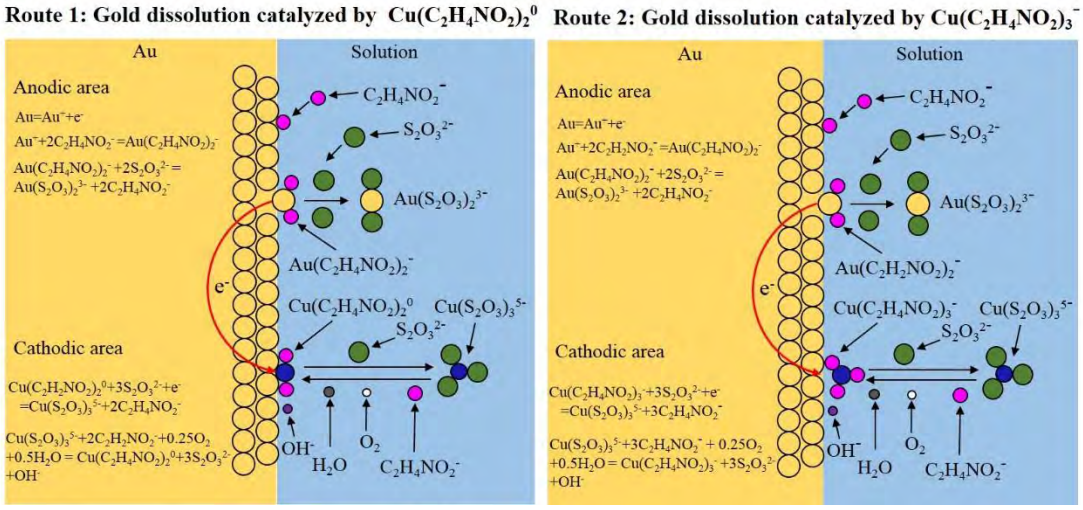

Figure 5.11 Electrochemical models of gold dissolution in the Cu(II)-glycine-thiosulfate system

Besides, the enhanced gold dissolution rate possibly benefits from the slight passive behavior of thiosulfate decomposition. As described previously, the thiosulfate can easily be consumed by $Cu(NH_3)_4^{2+}$ via a complexation with $S_2O_3^{2-}$ ($Cu(NH_3)_4S_2O_3^0$ is produced) [55]. In this study, we found that the UV-Vis absorbance of $Cu(C_2H_4NO_2)_2^0$ and $Cu(C_2H_4NO_2)_3^-$ is almost unchanged after EQCM experiments, showing a solution with good stability (Figure 5.11), which hardly coordinates with $S_2O_3^{2-}$. In other words, Cu(II)-glycine complexes are much less reactive toward thiosulfate, thereby significantly alleviating the thiosulfate composition. In addition, the OCP and E_{corr} values of the leaching system use $Cu(C_2H_4NO_2)_3^-$ as an oxidant are lower than the standard redox potential of $S_4O_6^{2-}/S_2O_3^{2-}$ (0.08 V), thus the excess oxidation of thiosulfate is limited [56].

5.4 Conclusions

In this work, an electrochemical investigation into gold leaching in a novel and eco-friendly Gly-thiosulfate system was conducted. The gold dissolution behavior from EQCM studies was primarily affected by the forms of Cu(II)-Gly complexes acting as catalysts/oxidant species. Specifically, $Cu(C_2H_4NO_2)_3^-$ complex in a strong alkaline system exhibits superior catalytic capability for gold dissolution compared to $Cu(C_2H_4NO_2)_2^0$ complex in a near-natural pH solution. A rapid dissolution rate of 5.032 μg cm^{-2} min^{-1} was obtained in the $Cu(C_2H_4NO_2)_3^-$ system under specific conditions, including an applied potential of 0.4 V, a Gly concentration of 0.5 M, and a solution pH of 11.5. Such excellent performance of the $Cu(C_2H_4NO_2)_3^-$ system was further

understood via corrosion electrochemistry (OCP, PDP, and EIS) and spectrum technologies (LA-ICP-MS and XPS). The results demonstrate that the $Cu(C_2H_4NO_2)_3^-$ system exhibits lower corrosion potential, slightly passivated behavior, and rapid electron transfer compared with the $Cu(C_2H_4NO_2)_2^0$ system. In addition, it is worth noting that the passivation species observed on the gold surface is primarily attributed to the coordination between glycine and Au (I) ions rather than sulfur-containing products resulting from thiosulfate decomposition, which has a minimal negative influence on gold dissolution.

5.5 References

[1] Y. Zhang, B. Xu, M. Cui, Q. Li, X. Liu, T. Jiang, X. Lyu, Thiosulfate leaching of gold catalyzed by hexaamminecobalt(III): Electrochemical behavior and mechanisms, Electrochimica Acta 399 (2021).

[2] Y. Chen, M. Xu, J. Wen, Y. Wan, Q. Zhao, X. Cao, Y. Ding, Z.L. Wang, H. Li, Z. Bian, Selective recovery of precious metals through photocatalysis, Nature Sustainability 4 (2021) 618-626.

[3] P. Chen, J. Ni, Y. Liang, B. Yang, F. Jia, S. Song, Piezo-photocatalytic reduction of Au(I) by defect-rich MoS_2 nanoflowers for efficient gold recovery from a thiosulfate solution, ACS Sustainable Chemistry & Engineering 9 (2020) 589−598.

[4] F. Xie, J. Chen, J. Wang, W. Wang, Review of gold leaching in thiosulfate-based solutions, Transactions of Nonferrous Metals Society of China 31 (2021) 3506-3529.

[5] Y. Liang, W. Zhan, Y. Yuan, N. Zamora-Romero, F. Jia, B. Yang, Z. Nasrddinov, J.L. Arauz-Lara, S. Song, Manganese and oxygen dual-doping MoS2 boosts reduction and adsorption activity toward efficient recovery of gold(I) from thiosulfate solutions, Journal of Alloys and Compounds 928 (2022) 167185.

[6] X. Liu, B. Xu, Y. Zhang, Q. Li, Y. Yang, Y. He, Thiosulphate leaching of gold in the $Cu–NH_3–S_2O_3^{2-}–H_2O$ system: An updated thermodynamic analysis using predominance area and species distribution diagrams, Minerals Engineering 151 (2020) 106336.

[7] Y. Zia, M. Abdollahy, Gold passivation by sulfur species: A molecular picture, Minerals Engineering 134 (2019) 215-221.

[8] Y. Zhang, B. Xu, Y. Zheng, Q. Li, Y. Yang, X. Liu, X. Lyu, Hexaamminecobalt(III) catalyzed thiosulfate leaching of gold from a concentrate calcine and gold recovery from its pregnant leach solution via resin adsorption, Minerals Engineering 171 (2021) 107079.

[9] H. Li, A. Ma, C. Srinivasakannan, L. Zhang, S. Li, S. Yin, Investigation on the recovery of gold and silver from cyanide tailings using chlorination roasting process, Journal of Alloys and Compounds 763 (2018) 241-249.

[10] Q. Wang, X. Hu, F. Zi, P. Yang, Y. Chen, C. Shuliang, Environmentally friendly extraction of gold from refractory concentrate using a copper – ethylenediamine – thiosulfate solution, Journal of Cleaner Production 214 (2019) 860-872.

[11] J. Wang, F. Xie, W. Wang, Y. Bai, Y. Fu, Y. Chang, Leaching of gold from a free milling gold ore in copper-citrate-thiosulfate solutions at elevated temperatures, Minerals Engineering 155 (2020) 106476.

[12] D. Feng, J. Van Deventer, Thiosulphate leaching of gold in the presence of ethylenediaminetetraacetic acid (EDTA), Minerals Engineering 23 (2010) 143-150.

[13] Y. Zhang, Q. Li, X. Liu, A thermodynamic analysis on thiosulfate leaching of gold under the catalysis of Fe^{3+}/Fe^{2+} complexes, Minerals Engineering 180 (2022) 107511.

[14] B. Xu, Y. Yang, Q. Li, X. Zhang, G. Li, Effect of common associated sulfide minerals on thiosulfate leaching of gold and the role of humic acid additive, Hydrometallurgy 171 (2017) 44-52.

[15] D. Feng, J. Van Deventer, The role of amino acids in the thiosulphate leaching of gold, Minerals Engineering 24 (2011) 1022-1024.

[16] O. Sitando, G. Senanayake, X. Dai, A. Nikoloski, P. Breuer, A review of factors affecting gold leaching in non-ammoniacal thiosulfate solutions including degradation and in-situ generation of thiosulfate, Hydrometallurgy 178 (2018) 151-175.

[17] C. Sun, X. Zhang, J. Kou, Y. Xing, A review of gold extraction using noncyanide lixiviants: Fundamentals, advancements, and challenges toward alkaline sulfur-containing leaching agents, International Journal of Minerals, Metallurgy and Materials 27 (2020) 417-431.

[18] H. Li, Z. Deng, E. Oraby, J. Eksteen, Amino acids as lixiviants for metals extraction from natural and secondary resources with emphasis on glycine: A literature review, Hydrometallurgy 216 (2023) 106008.

[19] E.A. Oraby, J.J. Eksteen, The selective leaching of copper from a gold–copper concentrate in glycine solutions, Hydrometallurgy 150 (2014) 14-19.

[20] S. Aksu, F. Doyle, Electrochemistry of Copper in Aqueous Glycine Solutions, Journal of The Electrochemical Society 148 (2001) B51-B57.

[21] H.N. Aliyu, J. Na'Aliya, Potentiometric studies on essential metal (II) amino acid complexes, Int. Res. J. Pharm. 2 (2012) 76-80.

[22] J. Wang, R. Wang, Y. Pan, F. Liu, Z. Xu, Thermodynamic analysis of gold leaching by copper-glycine-thiosulfate solutions using Eh-pH and species distribution diagrams, Minerals Engineering 179 (2022) 107438.

[23] S. Aksu, The role of complexing agents in the chemical-mechanical planarization of copper, J. Electrochem. Soc. 149 (2002) 352-361.

[24] C. Wang, G. Lin, J. Zhao, S. Wang, L. Zhang, Y. Xi, X. Li, Y. Ying, Highly selective

recovery of Au(III) from wastewater by thioctic acid modified Zr-MOF: Experiment and DFT calculation, Chemical Engineering Journal 380 (2020) 122511.

[25] M. Borkovec, G.J.M. Koper, B. Spiess, The intrinsic view of ionization equilibria of polyprotic molecules, New Journal of Chemistry 38 (2014) 5679-5685.

[26] E.A. Oraby, J.J. Eksteen, Gold leaching in cyanide-starved copper solutions in the presence of glycine, Hydrometallurgy 156 (2015) 81-88.

[27] Y. Zhang, B. Xu, M. Cui, Q. Li, X. Liu, X. Lyu, Thiosulfate leaching of gold catalyzed by hexaamminecobalt(III): Electrochemical behavior and mechanisms, Electrochimica Acta 399 (2021) 139393.

[28] J. Wang, F. Xie, W. Wang, Y. Bai, Y. Fu, D. Dreisinger, Eco-friendly leaching of gold from a carbonaceous gold concentrate in copper-citrate-thiosulfate solutions, Hydrometallurgy 191 (2019) 105204.

[29] B. Ivanova, M. Spiteller, 3D structural analysis of copper (II) complex of glycine–experimental mass spectrometric and theoretical quantum chemical approach, Journal of Molecular Structure 1179 (2019) 192-204.

[30] M. Saeedi, N. Sadeghi, E.K. Alamdari, Modeling of Au Chlorination Leaching Kinetics from Copper Anode Slime, Mining, Metallurgy & Exploration 38 (2021) 2559-2568.

[31] R. Wang, L. Zhang, C. Zhang, J. Wang, J. Guan, Z. Jian, Y. Bu, Selective extraction of precious metals in the polar aprotic solvent system: Experiment and simulation, Waste Management 153 (2022) 1-12.

[32] I. Korolev, S. Spathariotis, K. Yliniemi, B. Wilson, A. Abbott, M. Lundström, Mechanism of selective gold extraction from multi-metal chloride solutions by electrodeposition-redox replacement, Green Chemistry 22 (2020) 3615-3625.

[33] Y. Nie, L. Yang, Q. Wang, C. Shi, F. Zi, H. Yu, Connection between gold dissolution in thiosulfate leaching and Cu(II) complexes during the cathodic process, Electrochimica Acta 328 (2019) 135079.

[34] A.G. Zelinsky, RDE study of thiosulfate oxidation on gold, Journal of Electroanalytical Chemistry 735 (2014) 111-114.

[35] M. Soleymani, L. Li, F. Sadri, A. Ghahreman, The electrochemical catalytic role of Pb^{2+} in thiosulfate gold oxidation process, Minerals Engineering 184 (2022) 107676.

[36] A.G. Zelinsky, EQCM study of the dissolution of gold in thiosulfate solutions, Hydrometallurgy 138 (2013) 79-83.

[37] A.G. Zelinsky, Anode current on gold in mixed thiosulfate-sulfite electrolytes, Electrochimica Acta 154 (2015) 315-320.

[38] S. Cherevko, A.A. Topalov, A.R. Zeradjanin, I. Katsounaros, K. Mayrhofer, Gold dissolution: towards understanding of noble metal corrosion, Rsc Advances 3 (2013) 16516-16527.

[39] M. Soleymani, F. Sadri, A. Ghahreman, Effect of mixing acidic and alkaline pressure oxidation discharges with different ratios on gold thiosulfate leaching efficiency, Hydrometallurgy 205 (2021) 105744.

[40] J. Baron, G. Szymanski, J. Lipkowski, Electrochemical methods to measure gold leaching current in an alkaline thiosulfate solution, Journal of Electroanalytical Chemistry 662 (2011) 57-63.

[41] A.D. Bas, E. Ghali, Y. Choi, A review on electrochemical dissolution and passivation of gold during cyanidation in presence of sulphides and oxides, Hydrometallurgy 172 (2017) 30-44.

[42] A.D. Bas, W. Zhang, E. Ghali, Y. Choi, A study of the electrochemical dissolution and passivation phenomenon of roasted gold ore in cyanide solutions, Hydrometallurgy 158 (2015) 1-9.

[43] C. Pan, M. Niu, R. Cui, L. Li, X. You, X. Sun, I. Epstein, Q. Gao, Mesoscopic Pitting Oscillation-Induced Periodic Anodic Layer Electrodissolution of Au(111), Journal of Physical Chemistry Letters 12 (2021) 12062–12066.

[44] M. Mohammadi, L. Choudhary, I.M. Gadala, A. Alfantazi, Electrochemical and passive layer characterizations of 304L, 316L, and duplex 2205 stainless steels in thiosulfate gold leaching solutions, Journal of The Electrochemical Society 163 (2016) C883.

[45] K. Ljubetic, K.M. Deen, W. Liu, Kinetic limitations of gold leaching in ferric chloride media Part II: Potentiodynamic polarization and electrochemical impedance spectroscopy, Minerals Engineering 178 (2022) 107433.

[46] S. Smith, C. Zhou, J. Baron, Y. Choi, J. Lipkowski, Elucidating the interfacial interactions of copper and ammonia with the sulfur passive layer during thiosulfate mediated gold leaching, Electrochimica Acta 210 (2016) 925-934.

[47] J. Baron, J. Mirza, E. Nicol, S. Smith, J. Leitch, Y. Choi, J. Lipkowski, SERS and electrochemical studies of the gold–electrolyte interface under thiosulfate based leaching conditions, Electrochimica Acta 111 (2013) 390.

[48] R. Sultana, L.F. Greenlee, The implications of pulsating anode potential on the electrochemical recovery of phosphate as magnesium ammonium phosphate hexahydrate (struvite), Chemical Engineering Journal 459 (2023) 141522.

[49] R. Woods, G. Hope, K. Watling, M. Jeffrey, A Spectroelectrochemical Study of Surface Species Formed in the Gold/Thiosulfate System, Journal of The Electrochemical Society 153 (2006) D105.

[50] Y. Nie, H. Chi, F. Zi, X. Hu, H. Yu, S. He, The effect of cobalt and nickel ions on gold dissolution in a thiosulfate-ethylenediamine (en)-Cu^{2+} system, Minerals Engineering 83 (2015) 205-210.

[51] E. Nicol, J. Baron, J. Mirza, J. Leitch, Y. Choi, J. Lipkowski, “Surface-enhanced Raman spectroscopy studies of the passive layer formation in gold leaching from thiosulfate solutions in the presence of cupric ion”, Journal of Solid State Electrochemistry 18 (2013) 1469-1484.

[52] X. Xiao, H. Wang, W. Bao, P. Urbankowski, L. Yang, Y. Yang, K. Maleski, L. Cui, S.J. Billinge, G. Wang, Two-dimensional arrays of transition metal nitride nanocrystals, Advanced Materials 31 (2019) 1902393.

[53] Y.V. Butenko, L. Alves, A. Brieva, J. Yang, S. Krishnamurthy, L. Šiller, X-ray induced decomposition of gold nitride, Chemical physics letters 430 (2006) 89-92.

[54] A. Chipman, A. Gouranourimi, K. Farshadfar, A. Olding, B.F. Yates, A. Ariafard, A computational mechanistic investigation into reduction of gold (III) complexes by amino acid glycine: A new variant for amine oxidation, Chemistry–A European Journal 24 (2018) 8361-8368.

[55] X. Liu, B. Xu, Y. Yang, Q. Li, Y. He, Thermodynamic analysis of ammoniacal thiosulphate leaching of gold catalysed by Co(III)/Co(II) using E h -pH and speciation diagrams, Hydrometallurgy 178 (2018) 240-249.

[56] G. Senanayake, X. Zhang, Gold leaching by copper (II) in ammoniacal thiosulphate solutions in the presence of additives. Part II: Effect of residual Cu (II), pH and redox potentials on reactivity of colloidal gold, Hydrometallurgy 115 (2012) 21-29.

Chapter VI. Pentetic acid/ammonia cooperatively stabilizes Cu(II) as an efficient oxidant for green thiosulfate leaching of gold

6.1 Introduction

Worldwide, cyanidation is the most proven hydrometallurgical technique for gold extraction in both mining and waste resource recycling industries [1]. Despite the advantages of a well-established leaching system, straightforward operating parameters, and cost-effective reagents, there is growing public concern over the use of cyanide, one of the most toxic chemicals [2]. Advances in green hydrometallurgy have identified that thiosulfate is the most promising alternative to cyanide, with the remarkable advantage of non-toxicity [3, 4]. In principle, the gold dissolution process in cyanide and thiosulfate systems is similar, both converting elemental gold particles into oxidized Au(I) ions in solution: $Au(CN)_2^-$ (logk=38.3) for cyanide and $Au(S_2O_3)_2^{3-}$ (logk=26.5) for thiosulfate, respectively [5]. The key difference is that thiosulfate leaching requires an oxidant to accelerate the gold dissolution rate and improve the redox potential for $Au(S_2O_3)_2^{3-}$ stabilization, while cyanidation only relies on oxygen due to the ultra-high complex stability [6]. Therefore, the development of efficient oxidation systems is a critical scientific problem and a research hotspot in gold leaching using thiosulfate [7].

Designing oxidation systems for thiosulfate leaching of gold is emerging as a focal point of research in the areas of hydrometallurgy, electrochemistry, and solution chemistry [8]. In terms of oxidant selection, transition metals (iron [9], nickel [10], cobalt [11], and copper [12]) with oxidation states have been claimed as particularly suitable for catalyzing gold dissolution. Among them, the Cu(II) oxidation system is most widely studied with some advantages [13, 14]: (i) Cu(II) is relatively stable across a wide range of pH conditions and does not precipitate in alkaline thiosulfate solutions. (ii) Cu(II) is the most common oxidation state (+II) of copper and exhibits excellent catalytic oxidation performance. (iii) Cu(II) is inexpensive and readily available; for example, it can be easily introduced into the aqueous solution by dissolving commercial $CuSO_4{\cdot}5H_2O$. Adding Cu(II) ions as oxidants to the thiosulfate system obviously accelerates gold dissolution, yielding at least ten times higher leaching than pure thiosulfate. However, some side reactions are inevitable, making the leaching process less attractive for industrialization. (i) Cu(II) ions is easy coordinate with $S_2O_3^{2-}$, forming the $Cu(S_2O_3)_2^{2-}$; (ii) The oxidizing properties of Cu(II) is relative high, which can degrade $S_2O_3^{2-}$ into some by-products, such as tetrathionate ($S_4O_6^{2-}$), trithionate ($S_3O_6^{3-}$), sulfate (SO_4^{2-}), cyclo-S_8, and copper sulfide. (iii) Gold dissolution is

passivated by the buildup of sulfur-containing coatings on the gold surface. (iv) Cu(II) ions are easily reduced, resulting in insufficient oxidant during the long leaching period.

Numerous research activities reported that ammonia (NH_3) can act as a stabilizer for Cu(II) ions by forming the $Cu(NH_3)_4^{2+}$ complex [15]. This strategy not only prevents the coordination between Cu(II) and $S_2O_3^{2-}$, but also maintains a high concentration of Cu(II) oxidant throughout the long leaching period [16]. The role of $Cu(NH_3)_4^{2+}$ in the oxidation of metallic gold to aurous $Au(S_2O_3)_2^{3-}$ ions is shown in the reaction (Eq. 6-1). Nevertheless, the application of the copper-ammonia-thiosulfate system is not commercially achieved because of the following limitations [17, 18]: (i) $Cu(NH_3)_4^{2+}$ has strong oxidation capability, which can inevitably oxidize $S_2O_3^{2-}$ ions. (ii) The volatilization of NH_3 causes $Cu(NH_3)_4^{2+}$ to dissociate into free copper ions during the long-time leaching period, which can react with thiosulfate ions. (iii) The amount of NH_3 used in the leaching operation is very high (> 1.0 mol/L), making it uneconomic and causing health problems for the public.

$$Au + 5S_2O_3^{2-} + Cu(NH_3)_4^{2+} = Au(S_2O_3)_2^{3-} + 4NH_3 + Cu(S_2O_3)_3^{5-} \quad (6\text{-}1)$$

To address these issues, enormous non-toxic or less-toxic organic ligands have been introduced into the thiosulfate leaching as more efficient stabilizers for Cu(II) oxidant. Examples of such organic ligands include ethylenediamine (En) [19], citrate (Cit^{3-}) [20], ethylenediaminetetraacetic acid (EDTA) [21], ethydiaminedhephen acetic (EDDHA) [22], carboxymethyl cellulose (CMC) [23], amino acids [24], and so on. This innovation effectively reduced the demand for NH_3, adding to the burgeoning green thiosulfate leaching based on low-NH_3 or NH_3-free systems. For instance, Feng and van Deventer reported that EDTA as an additive reduces the redox equilibrium potential of the catalytic Cu(II)/Cu(I) complex, hence reducing the mixed solution potential and the thiosulfate consumption [25]. Our early work introduces the ethydiaminedhephen acetic (EDDHA) into the leaching system, making the leaching system stale with almost no passivation [22]. Concededly, the advantage of low thiosulfate consumption of these novel organic ligand-based systems is promising for the development of green thiosulfate leaching. However, the leaching kinetics are largely inhibited by the ultrahigh stability of the Cu(II) complex, which lacks sufficient oxidation capability for oxidizing metallic gold to gold ions [26]. Therefore, to achieve satisfactory gold leaching within a relatively short time, the deficit of oxidation capability of these organic ligand-based systems must be deeply considered, in addition to pursuing low thiosulfate consumption.

Pentetic acid, also known as diethylenetriaminepentaacetic acid (DTPA), a non-toxic, eco-friendly, and inexpensive organic ligand, can effectively chelate with Cu(II) ions, using abundant carboxylic acid (-COOH) and amine (-NH_2) as coordination sites [27]. This work first proposed using DTPA as a stabilizer for Cu(II) oxidant, aiming to form a stable and efficient thiosulfate system for the green leaching of gold. Specifically, three thiosulfate systems were designed to explore the cooperative contribution of NH_3 in improving gold leaching performance, with an emphasis on the improvement of oxidation capability of the Cu(II)-DTPA complex: (i) $(NH_4)_2S_2O_3$ system, (ii) $Na_2S_2O_3$ with $(NH_4)_2SO_4$ system, and (iii) $Na_2S_2O_3$ with NH_4OH system. Besides, more effects were concerned about the role of DTPA in maintaining system stability, reducing thiosulfate consumption, and mitigating passivation issues by controlling the amount of DTPA added. Furthermore, other operation parameters, including the adding dosages of Cu(II) and thiosulfate, liquid-solid ratio (L/S), as well as stirring speed (rpm), were comprehensively optimized. It provides some valuable guidance for the facile design of green thiosulfate leaching systems for industrialized gold extraction.

6.2 Materials and methods

6.2.1 Materials and reagents

A multi-stage pretreated concentrate provided by Jinyuan Mining Co., Ltd. (Henan Province, China) was used as the raw material in this work. Although it was obtained from the same company as the gold ore used in Chapter IV, it belonged to a different batch and was therefore re-characterized before use. This material was a flotation concentrate that had undergone two-stage roasting to expose gold, followed by sulfuric acid leaching for copper removal. It contains 44.2 g/t Au (determined by fire assay) and a high content of iron and silicon oxide, and a small amount of other metallic oxides (Table 6.1). Figure 6.1(a) presents a fine particle size of the sample, with 68.65% below 38 um. As shown in Figure 6.1b, the X-ray diffraction (XRD) pattern established that quartz (SiO_2), hematite (Fe_2O_3), and gypsum ($S_{4.00}Ca_{4.00}O_{24.00}$) are abundant mineral phases. SEM-EDS found small gold particles in the porous channels of hematite, in the form of a half-exposed phase (Figure 6.1(c)). Cyanidation can achieve a gold leaching percentage as high as near 95% from this sample in the plant. Therefore, the exposed gold phase and the satisfactory gold leaching by cyanide make it a suitable standard for evaluating gold leaching efficiency in this research.

Table 6.1 Chemical composition of the pretreated gold concentrate (a: g/t)

Element	FeO	SiO_2	Al_2O_3	S	CaO	K_2O	PbO	Na_2O	Au[a]
Content/%	36.53	31.54	6.15	5.33	2.81	2.18	1.59	1.16	44.2

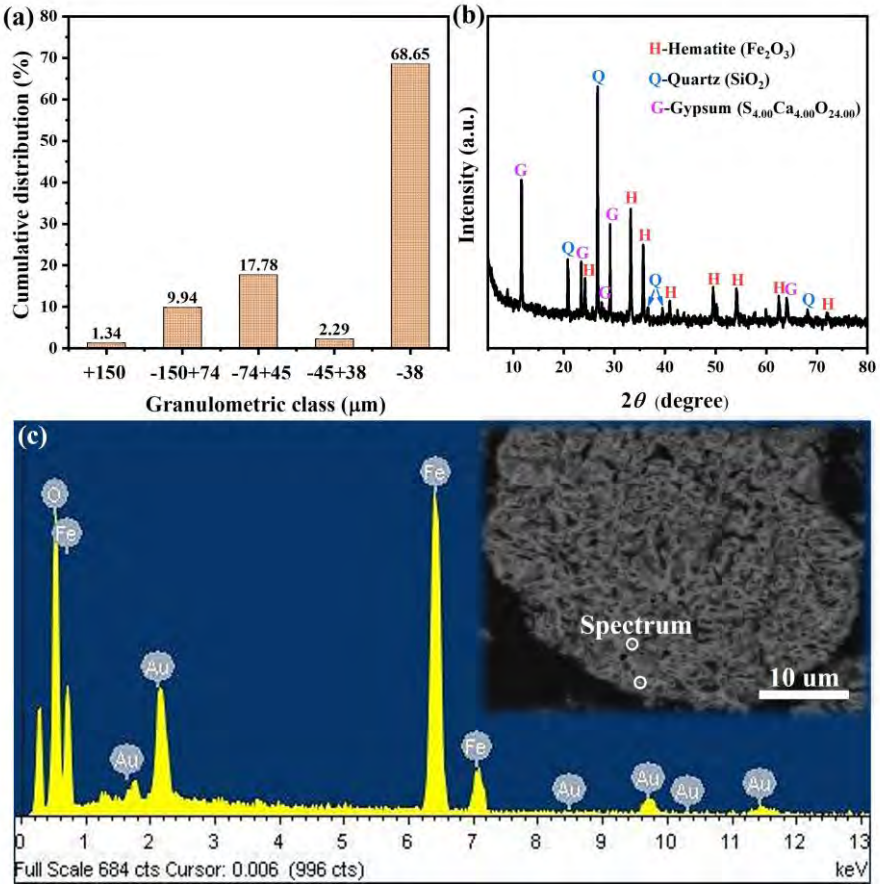

Figure 6.1 Characterization of the pretreated gold concentrate. (a) Particle size distribution. (b) XRD spectrogram. (c) Scanning Electron Microscope (SEM) images and Energy Dispersive Spectroscopy (EDS) images of gold particles in hematite

Analytical grade reagents, including $(NH_4)_2S_2O_3$, $Na_2S_2O_3{\cdot}5H_2O$, pentetic acid (diethylenetriaminepentaacetic acid), $CuSO_4{\cdot}5H_2O$ (Cu(II)), $(NH_4)_2SO_4$, and $NH_3{\cdot}H_2O$ utilized in the following experiments were purchased from Sigma-Aldrich. Unless otherwise specified, NTS represents $(NH_4)_2S_2O_3$, TS represents $Na_2S_2O_3$, DTPA represents pentetic acid, and Cu(II) represents $CuSO_4$. All solutions were prepared using DI water with a resistivity of 18.25 MΩ cm.

6.2.2 Analysis and preparation of Cu(II)-DTPA complex solution

Pentetic acid (DTPA) is a topically aminopolycarboxylic acid consisting of a diethylenetriamine backbone with five carboxymethyl groups (-COOH). Figure 6.2a shows the acid dissociation curves of carboxymethyl groups in DTPA based on the pKa

values presented in Table 6.2 [28]. Under alkaline conditions, the penta-anion $DTPA^{5-}$ predominates as an octadentate ligand, utilizing both nitrogen and $-COO^-$ groups as coordination sites. Early characterization work presented the potential complexes between Cu(II) and DTPA are $CuDTPA^{3-}$, $CuHDTPA^{2-}$, CuH_2DTPA^-, CuH_3DTPA, and Cu_2DTPA^- [29]. Based on the proposed stability constants of these complexes, the species distribution of Cu(II) in neutral and alkaline conditions is mainly in the form of $CuDTPA^{3-}$ (Figure 6.2b), which can be verified by the UV-vis spectroscopy of Cu-DTPA complex at different pH (Figure 6.2c). Besides, UV-vis spectroscopy also confirmed the stable 1:1 structure of the complex (Figure 6.2d). Figure 6.2e presents the well-known structure model of the $CuDTPA^{3-}$ complex, which binds in a hexadentate manner utilizing the three amine centers and three of the five carboxylates, forming the highly stable chelate [30, 31].

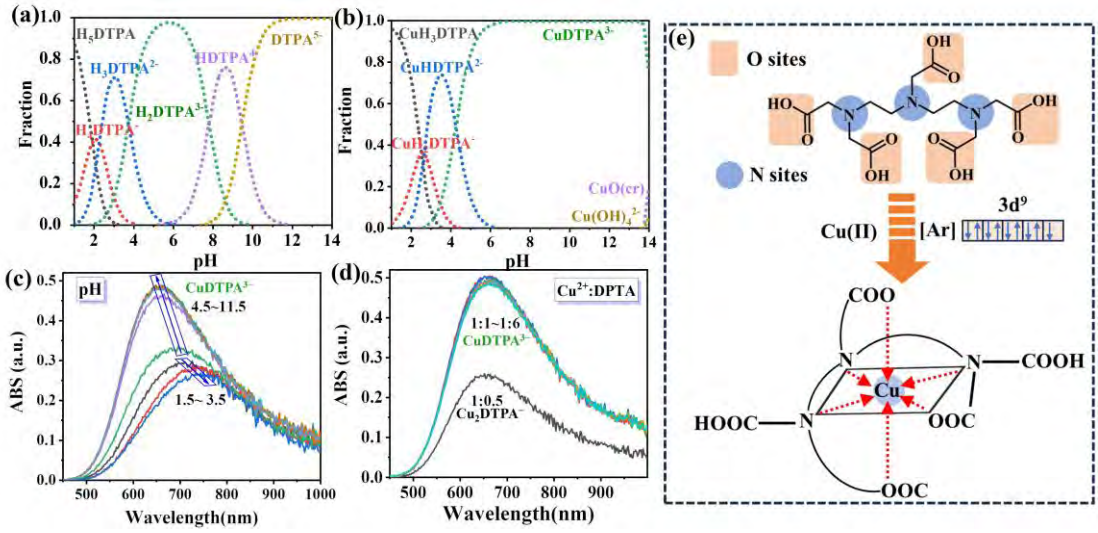

Figure 6.2 Coordination behavior analysis between Cu(II) and DTPA. (a) Acid dissociation curves of DTPA. (b) Species distribution of Cu(II) at different pH. Uv-vis spectroscopy under (d) pH varies from 1.5 to 11.5 and (c) the mole ratios of Cu(II) to DTPA from 1:0.5 to 1:6. (e) Coordination structure of Cu(II)-DTPA complex

Table 6.2 Acid dissociation constants and Cu(II) stability constants for DTPA

Reaction	pKa	Reaction	log K_{eq}
$H^+ + DTPA^{5-} = HDTPA^{4-}$	10.48	$Cu^{2+} + DTPA^{5-} = CuDTPA^{3-}$	21.42
$2H^+ + DTPA^{5-} = H_2DTPA^{3-}$	8.60	$Cu^{2+} + H^+ + DTPA^{5-} = CuHDTPA^{2-}$	26.22
$3H^+ + DTPA^{5-} = H_3DTPA^{2-}$	4.28	$Cu^{2+} + 2H^+ + DTPA^{5-} = CuH_2DTPA^-$	29.18
$4H^+ + DTPA^{5-} = H_4DTPA^-$	2.60	$Cu^{2+} + 3H^+ + DTPA^{5-} = CuH_3DTPA$	31.74
$5H^+ + DTPA^{5-} = H_5DTPA$	2.00	$2Cu^{2+} + DTPA^{5-} = Cu_2DTPA^-$	28.21

Supported by these fundamental characteristics, the $CuDTPA^{3-}$ solution is

prepared as follows. First, a certain amount of DTPA is added to deionized water. Next, NaOH is gradually added to the solution to facilitate the dissolution of DTPA, forming the dissociated $DTPA^{5-}$ anion. The solution is stirred for 10 min after each addition of NaOH. Once the DTPA is completely dissolved, the pH of the solution is adjusted to 10.5. Finally, a specific concentration of copper sulfate is added to the solution to form a blue Cu(II)-DTPA solution (mainly containing the $CuDTPA^{3-}$ complex). This solution is very stable at room temperature and was used as a stock liquor for the following gold ore leaching tests.

6.2.3 Gold leaching procedures

Leaching tests were conducted in a 250 mL glass conical flask using mechanical agitation at ambient temperature and atmospheric pressure. Initially, the leaching reagent, either $(NH_4)_2S_2O_3$ or $Na_2S_2O_3$ (with NH_4OH or $(NH_4)_2SO_4$), was added to the 200 mL Cu(II)-DTPA solution (pre-prepared as described in section 2.2). Subsequently, a predetermined amount of gold ore was added to the solution to form a pulp, based on a specified liquid-to-solid ratio (L/S). After adjusting the pH to a desired level with saturated NaOH solution, the leaching reaction commenced. Over a total leaching time of 12 h, filtered aqueous samples were taken at fixed intervals (t = 1, 3, 6, 9, and 12 h), diluted, and analyzed to determine Au leaching efficiency (η).

$$\eta = \frac{C\,V}{m\,\beta} \times 100\% \tag{6-2}$$

Where η (%) is the leaching percentage of gold; C (mg/L) is the concentration of gold ions in filtrate; V (mL) is the volume of leaching solution; m (g) is the weight of gold ore, and β (g/t) is the grade of the gold ore.

6.2.4 Analytical and characterization techniques

The leached gold in filtrates was determined by atomic adsorption spectroscopy (AAS, 280Z AA, Agilent, USA). The mineral phases of pyrite samples were identified by X-ray diffraction (XRD, D8 Advance, Bruker, Japan). The concentration of thiosulfate (NTS and TS) in filtrates was analyzed by a modified iodimetry titration with starch as an indicator [32]. The formation of the Cu(II) complex was measured by ultraviolet-visible spectroscopy (UV-vis, GENESYS, Thermo Fisher Scientific, USA). Medusa-Hydra software was used to construct the distribution diagram of Cu(II) species. XRD and Fourier transform infrared spectroscopy (FTIR, PerkinElmer 1725x, USA) were employed to characterize the effects of NH_3 on the structural features of the Cu(II)-DTPA complex. A scanning electron microscope (SEM, pw-100-017, Phenom,

Holland), equipped with an energy dispersive spectroscopy (EDS), was utilized to characterize the phase of the gold particle in gold ore and the surface states of gold sheets after leaching. To provide information on the frontier molecular orbital (FMO) and the corresponding energy levels (E_{HOMO} and E_{LUMO}) for Cu(II) complexes, density functional theory (DFT) calculations were performed on GAUSSIAN 09 software based on the B3LYP functional and def2SVP basis set. Cyclic voltammetry (CV) curves were conducted on an electrochemical workstation (CHI400E, Shanghai Chenhua, China) to analyze the redox properties of Cu(II) complexes and the gold leaching mechanism, utilizing a Pt electrode and an Au electrode, respectively. The solution potential (ORP) of lixiviants was determined by a pH/ion concentration meter (YHBJ-262, Shanghai INESA Scientific, China) equipped with an ORP electrode (vs. SHE).

6.3 Results and discussion

6.3.1 Comparative thiosulfate leaching using DTPA chelated Cu(II) as oxidant

6.3.1.1 Ammonium thiosulfate (NTS) leaching

Figure 6.3a first compared the effect of thiosulfate salts on the gold leaching performance of the pretreated gold concentrate, under the same Cu(II)-DTPA oxidation system. Obviously, the types of thiosulfate salts have a significant impact on the extraction behavior of gold. The main manifestation is that gold leaching in the sodium thiosulfate (TS) system is very slow. Although the concentration of $Na_2S_2O_3$ is increased to 300 mM, only ~32.2% of gold can be leached after 60 h. In comparison, 96.1% of gold can be rapidly leached from this gold ore within 12 h when a smaller amount of $(NH_4)_2S_2O_3$ (NTS) is employed as the leaching reagent, demonstrating faster leaching kinetics and higher leaching efficiency. As is well-known, thiosulfate leaching of gold is closely correlated with solution potential (ORP), which also impacts thiosulfate consumption [33]. As depicted in Figure 6.3b, the solution potential (ORP) of the NTS system is significantly higher than that of the TS system, likely explaining the improved gold leaching.

Figure 6.3c and 6.3d illustrate the influence of the initial pH on gold leaching efficiency, solution potential (ORP), and thiosulfate consumption. At a fixed pH value of 8.5, the solution potential (ORP) remains relatively low, approximately 208 mV, which correlates with the poorest gold leaching efficiency (33.9%) and the lowest thiosulfate degradation (6.8%) observed. The solution potential (ORP) is highly sensitive to variations in pH values [34], exhibiting an upward trend as the pH elevates.

At pH 10.5, the gold leaching efficiency and thiosulfate consumption surprisingly increase to 96.1% and 16.9%, respectively. This increase may well be associated with the elevated level of solution potential (ORP), indicating a high oxidation capacity of the leaching system.

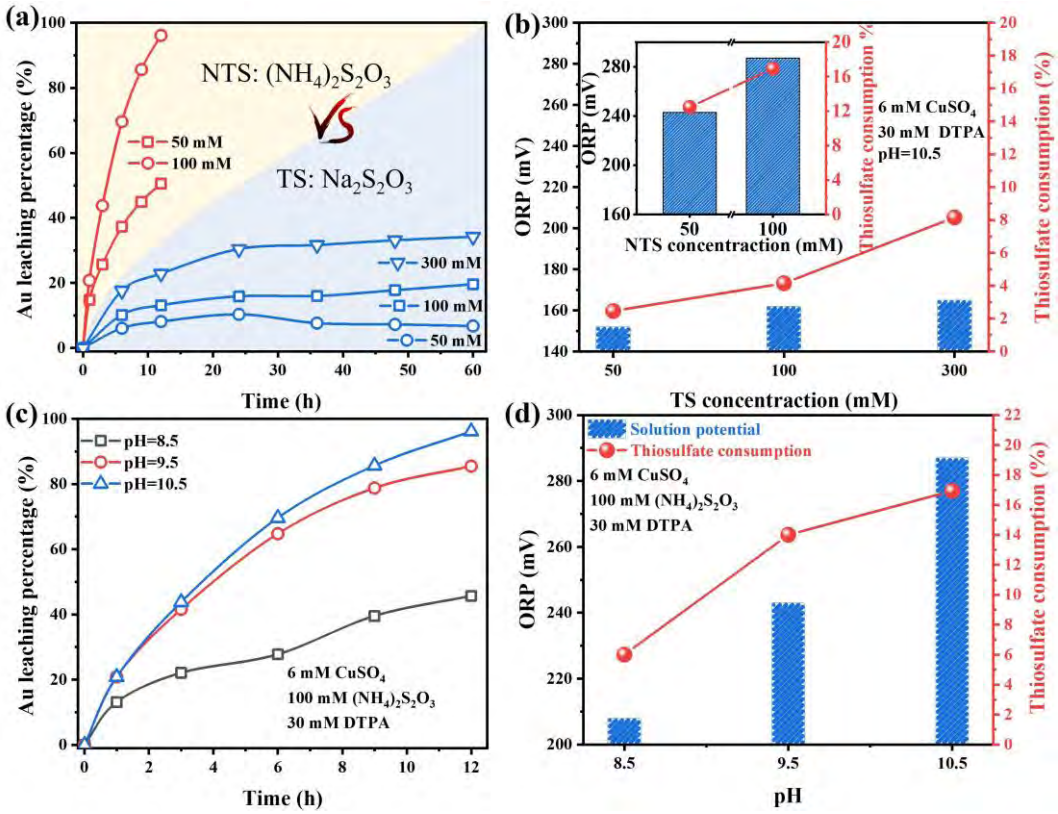

Figure 6.3 (a, b) Effects of thiosulfate (NTS and TS) concentrates and (c, d) pH on gold leaching, solution potential (ORP), and thiosulfate consumption

6.3.1.2 Sodium thiosulfate (TS) leaching with addition of $(NH_4)_2SO_4$

Here, sodium thiosulfate (TS) leaching of the gold ore with the addition of $(NH_4)_2SO_4$ was given as a control system, also using $CuDTPA^{3-}$ complex as oxidant. As shown in Figure 6.4a, in the range from 25 mM to 100 mM of $(NH_4)_2SO_4$ addition, the gold leaching efficiency was significantly increased from 42.3% to 97.3%. This improvement is attributed to solution potential (ORP), which is improved by the higher concentration of $(NH_4)_2SO_4$ (Figure 6.4b). Interestingly, the gold leaching efficiency and ORP decrease with the gradual decrease of pH from 10.5 to 8.5 (Figure 6.4c and 6.4d), which is similar to the efficiency of $(NH_4)_2S_2O_3$ (NTS) leaching. Compared with the chemical structure of $(NH_4)_2SO_4$, $(NH_4)_2S_2O_3$ can also provide an equivalent amount of NH_4^+ into the solution, forming the same chemical solution system. Clearly, the similar leaching results of the gold ore using the NTS system (Figure 6.3) and the

TS system with $(NH_4)_2SO_4$ (Figure 6.4) demonstrated the critical role of NH_4^+ ions.

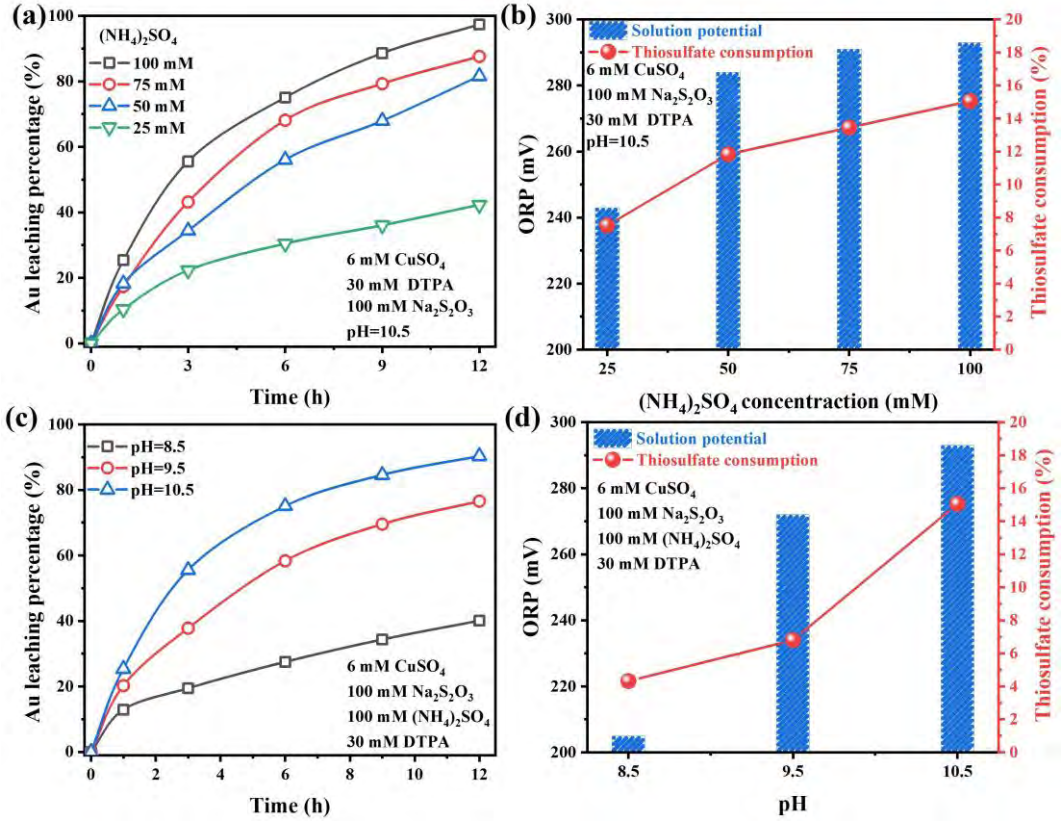

Figure 6.4 Effect of (a, b) $(NH_4)_2SO_4$ concentrations and (c, d) pH on gold leaching, solution potential (ORP), and thiosulfate consumption

6.3.1.3 Sodium thiosulfate (TS) leaching with addition of NH_4OH

To understand the function mechanism of NH_4^+ ions, attention must be paid to their solution perspectives. It is not difficult to find that NH_3 is the conjugate base of the acid NH_4^+ ions, indicating that NH_4^+ is easily formed when NH_3 accepts a proton (H^+) from the acid, as shown in equilibrium Eqs. (6-3) and (6-4) (pka=9.24) [35]. Therefore, NH_4^+ would gradually translate into NH_3 as the pH of the solution increases.

$$NH_{3(aq)} + H^+ \leftrightarrow NH_4^+ \quad (6\text{-}3)$$

$$NH_4^+ + OH^- \leftrightarrow NH_{3(aq)} + H_2O \quad (6\text{-}4)$$

To verify the effect of this equilibrium on gold leaching, a control TS system with the addition of NH_4OH was studied at pH 10.5. Noticeably, the gold leaching efficiency gradually increased with the addition of NH_4OH (Figure 6.5a). When the concentrations of NH_4OH reached 200 mM, the gold leaching efficiency reached 94.3%, which is the same as the above-mentioned two systems (Figures 6.3 and 6.4). Besides, the contribution of NH_4OH for gold leaching can be easily observed by regulating the pH

of the slurry. The variation in pH over the range of 8.5 to 10.5 results in a significant increase in gold leaching efficiency, from 33.9% to 94.3% (Figure 6.5c). The lowest gold leaching rate occurs at pH 8.5, which may be attributed to the decreased stability and concentration of NH_3 (NH_4^+ dominating). For comparison, when the pH rises above 9.5, the stability regions of NH_3 gradually extend (NH_4^+/NH_3 co-exist), and almost all NH_3 exists at pH 10.5 (NH_3 dominant). From Figure 6.5b and Figure 6.5d, as the concentration of NH_3 increases, so does the solution potential (ORP), resulting in higher gold leaching efficiency and thiosulfate consumption. This provides strong evidence that NH_3 increases the oxidizing properties of the Cu(II)-DTPA-$S_2O_3^{2-}$ leaching system.

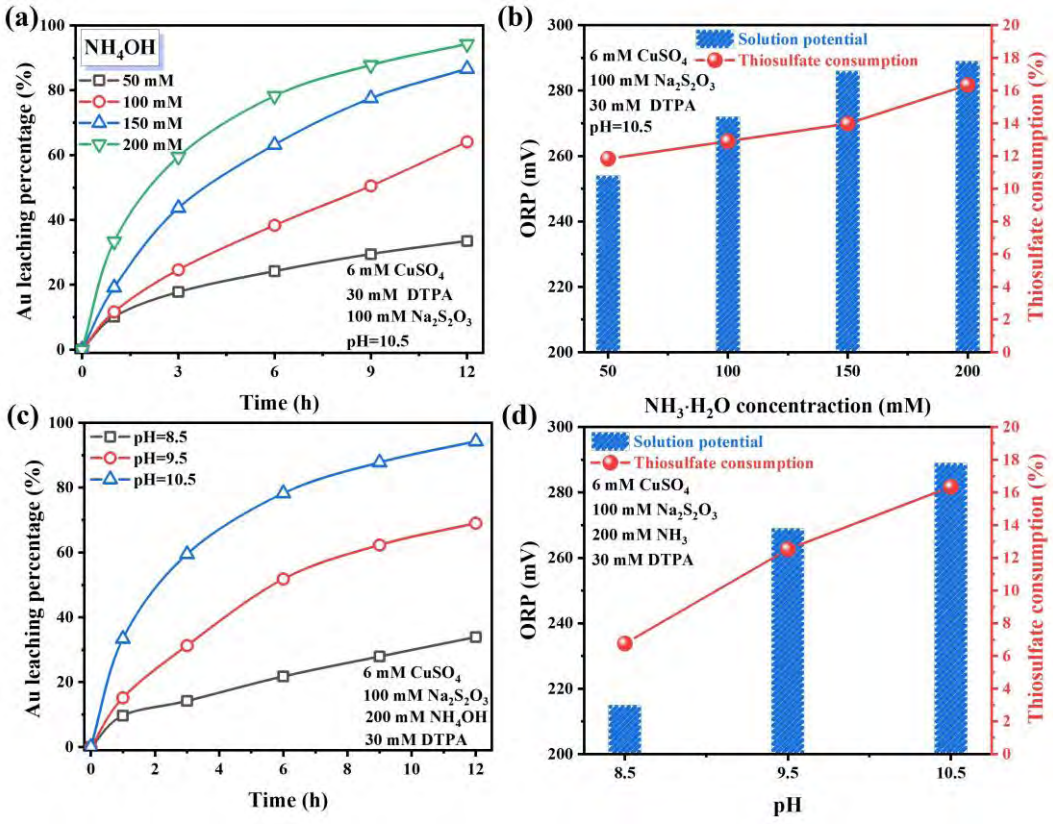

Figure 6.5 Effect of (a, b) NH_4OH concentrations and (c, d) pH on gold leaching, solution potential (ORP), and thiosulfate consumption

6.3.2 Mechanistic role of ammonia for enhancing gold leaching

As previously stated, the increase in solution potential (ORP) in the Cu(II)-DTPA oxidation system is due to the cooperative role of NH_3, which is crucial for gold leaching. Using Cu(II) as oxidant, the solution potential (ORP) is determined by the potential of the redox couple of Cu(I) complex/Cu(II) complex, i.e., $E^{\theta}_{Cu(I)/Cu(II)}$, which can be calculated by Eq. (6-5) [36]. To a wide recognition, the most stable reduction

product of the Cu(I) complex in the thiosulfate leaching system is $Cu(S_2O_3)_3^{5-}$ (Eq. 6-6) [22]. Therefore, the potential of $E^{\theta}_{Cu(II)/Cu(I)}$ is dependent on the stability of the Cu(II) complex [37]. Figure 6.6a gives a possible ion composition of the leaching solution, which consists of $CuSO_4$, DTPA, and $(NH_4)_2S_2O_3$. Cupric sulfate ($CuSO_4$) is used to provide catalytic Cu(II) ions, which are stabilized by $DTPA^{5-}$ to form the stable $CuDTPA^{3-}$ complex. Sulfate ions (SO_4^{2-}), dissociated from $CuSO_4$, remain stable and standalone. Importantly, one molecule of $(NH_4)_2S_2O_3$ dissociates to produce two NH_4^+/NH_3 and one $S_2O_3^{2-}$. Theoretically, NH_3 and $S_2O_3^{2-}$ both are ligands for Cu(II) ions, preferentially forming $Cu(NH_3)_4^{2+}$ and $Cu(S_2O_3)_2^{2-}$ complexes (Eqs. 6-7 and 6-8), respectively. Thus, the stability of $CuDTPA^{3-}$ complex in the presence of NH_3 and $S_2O_3^{2-}$ ions should be carefully considered.

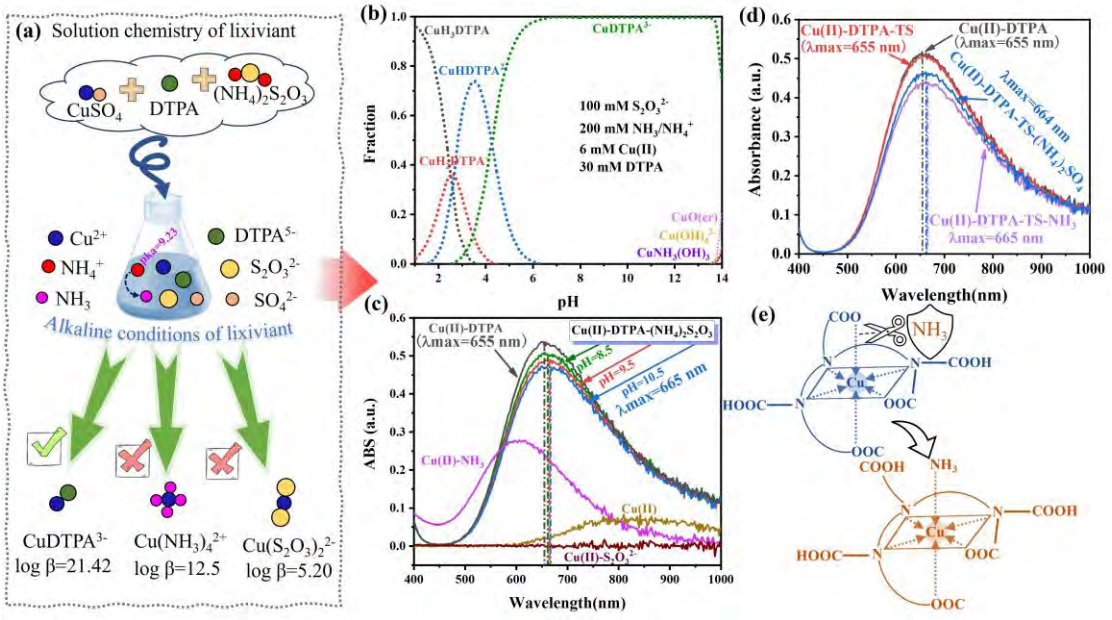

Figure 6.6 Solution chemistry of the leaching system. (a) Ion composition, (b) Cu(II) species distribution diagrams, (c~d) Uv-vis spectroscopy. (e) Effect of NH_3 on the structure of Cu(II)-DTPA complex

$$E^{\theta}_{Cu(II)/Cu(I)} = E^{\theta}_{Cu^{2+}/Cu^{+}} + 0.0591\log[\beta_{Cu(I)}/\beta_{Cu(II)}] \quad (6\text{-}5)$$

$$Cu^{+} + 3S_2O_3^{2-} = Cu(S_2O_3)_3^{5-} \quad (6\text{-}6)$$

$$Cu^{2+} + 4NH_3 = Cu(NH_3)_4^{2+} \quad (6\text{-}7)$$

$$Cu^{2+} + 2S_2O_3^{2-} = Cu(S_2O_3)_2^{2-} \quad (6\text{-}8)$$

Figure 6.6b calculated the Cu(II) species distribution across a pH range of 1.0 to 14.0 in the presence of DTPA, $S_2O_3^{2-}$, and NH_3/NH_4^+ ions. The results show

conclusively that $CuDTPA^{3-}$ is dominant under alkaline conditions. Further evidence for the formation of the $CuDTPA^{3-}$ complex was obtained through UV/Vis spectrophotometry (Figure 6.6c), presenting distinct peak locations at ~655 nm, which is different from $Cu(NH_3)_4^{2+}$. Besides, the addition of sodium thiosulfate (TS) does not affect the peak of $CuDTPA^{3-}$. Interestingly, in the presence of NH_3, the absorption peak of the $CuDTPA^{3-}$ complex varies (Figure 6.6d), exhibiting a decrease in intensity and a slight redshift in its location [38]. A similar phenomenon has been reported by Zhao et al., explaining the formation of a mixed-ligand Cu(II) complex, i.e., $[Cu(TEA)(NH_3)_3]^{2+}$, as an oxidant for thiosulfate leaching [39]. In detail, the coordination sites located on the terminal axis of six-coordinated Cu(II) complexes are inherently unstable and prone to substitution. NH_3 acts as a nucleophile, enabling it to efficiently perturb the structure of the complexes with multiple coordination sites [40]. This ability allows NH_3 to form mixed-ligand complexes, such as $[Cu(Ida)(NH_3)]$, $[Cu(mad)(NH_3)]$, $[Cu(NTA)(NH_3)]^-$, $[Cu(gly)(NH_3)]^+$, and so on. Based on this inference, it is likely that a $[Cu(DTPA)(NH_3)]^{3-}$ complex, incorporating mixed ligands of DTPA and NH_3, is probably formed (Figure 6.6e).

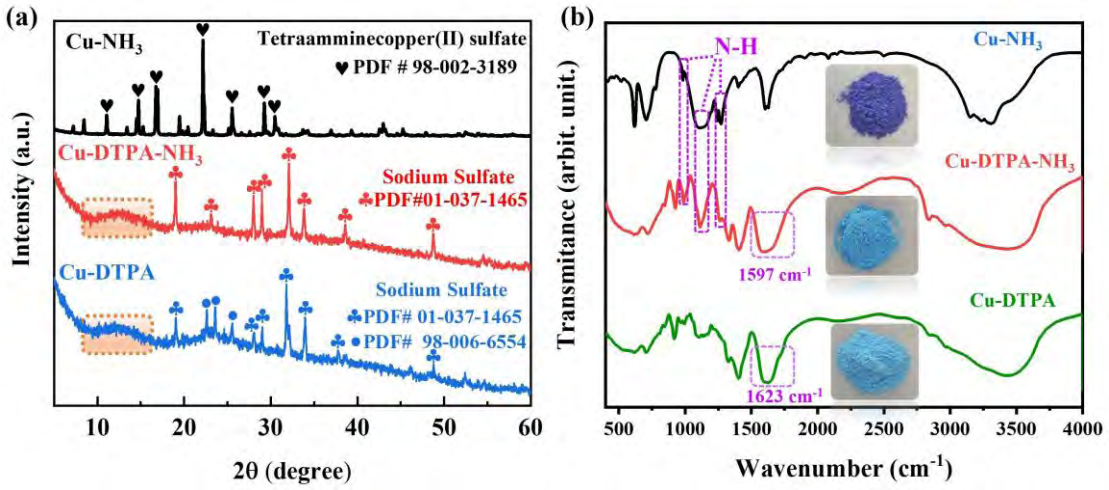

Figure 6.7 Characterization of the structure of Cu-NH_3, Cu-DTPA, and Cu-DTPA-NH_3 complexes. (a) XRD patterns. (b) FTIR spectroscopy

To demonstrate the effect of NH_3 on the formation of the Cu(II) complex, Cu(II)-NH_3, Cu(II)-DTPA, and Cu(II)-DTPA-NH_3 complexes were crystallized by adding ethyl alcohol to the corresponding solution, and the solid products obtained through freeze drying were then analyzed using X-ray diffraction (XRD) and Fourier-transform infrared spectroscopy (FTIR). As seen in Figure 6.7a, the XRD patterns of Cu(II)-DTPA and Cu(II)-DTPA-NH_3 samples are almost identical but differ from that of the Cu-NH_3 sample, indicating that tetraamminecopper(II) sulfate (i.e., $Cu(NH_3)_4^{2+}$) does not exist

independently. Apart from the signal of sodium sulfate, the broad peak located at 10~15° potentially suggests that the amorphous structure of both $[Cu(DTPA)]^{3-}$ and $[Cu(DTPA)(NH_3)]^{3-}$. Figure 6.7b shows similar FTIR spectra for Cu(II)-DTPA and Cu(II)-DTPA-NH_3 samples in the range of 1200 cm^{-1} to 4000 cm^{-1}, proving the structural similarity of the corresponding complexes. A slight difference is observed in the carboxylate-metal bond area, with a peak at 1623 cm^{-1} in Cu(II)-DTPA and 1597 cm^{-1} in Cu(II)-DTPA-NH_3. A correlation between the bond character and the absorption band has also been reported in various kinds of literature, with higher frequencies being associated with more covalent carboxylate-metal bonds [41, 42]. Compared with Cu(II)-NH_3 and Cu(II)-DTPA-NH_3 samples, some N-H bond vibrations appeared at the same location, raised at 1113 cm^{-1}, 1241 cm^{-1}, and 1271 cm^{-1}, which are reported characteristic vibrations of NH_3 in cupric ammine compound [43]. However, these bond peaks barely existed in Cu-DTPA. These results indicate that the NH_3 molecule is probably incorporated into the structure of $[Cu(DTPA)]^{3-}$, forming $[Cu(DTPA)(NH_3)]^{3-}$.

It is hypothesized that the structure modification of $[Cu(DTPA)]^{3-}$ by NH_3 changed its chemical reactivity, which is closely related to the oxidation capability of Cu(II) complex. To prove this, cyclic voltammetry (CV) curves and DFT simulation were used to characterize $[Cu(DTPA)]^{3-}$ and $[Cu(DTPA)(NH_3)]^{3-}$. As depicted in Figure 6.8a, two pairs of redox peaks (A_1/C_1 and A_2/C_2) are distinctly detected in Cu(II) solution containing DTPA alone, which are attributed to the stepwise oxidation-reduction of $[Cu(DTPA)]^{3-}$ complex involving Cu(II), Cu(I), and Cu(0) species. Comparatively, when DTPA and NH_3 are co-present in the Cu(II) solution, only one pair of redox peaks appeared (A_1/C_1), as shown in Figure 6.8b. This shift indicates that redox reaction easily occurred from multi-steps to a single-step process, demonstrating the improved redox property of $[Cu(DTPA)(NH_3)]^{3-}$ complex [44,45].

Besides, the frontier molecular orbital analysis (FMOs) indicates that the chemical reactivity of molecules is dependent on the energy gap (ΔE) between E_{HOMO} and E_{LUMO} (Figure 6.8c and 6.8d) [46,47]. The energy gap (ΔE) of the oxidation system of Cu(II)-DTPA-NH_3 (4.298 eV) is smaller than that of Cu(II)-DTPA (5.315 eV). This result predicts a more stable coordination of the chelated $[Cu(DTPA)]^{3-}$ complex. When NH_3 is integrated into the structure of $[Cu(DTPA)]^{3-}$, complex formation destabilizes the overall system, and the final structure gains some reactive behavior, accepting electrons and reaching a relatively stable excited state [48]. Based on these evaluations, the oxidation system of Cu(II)-DTPA in the presence of NH_3 exhibits higher chemical reactivity. This is likely the dominant factor contributing to the elevated solution

potential (ORP) of the oxidation system, resulting in superior oxidation activity and enhanced catalytic performance for gold leaching.

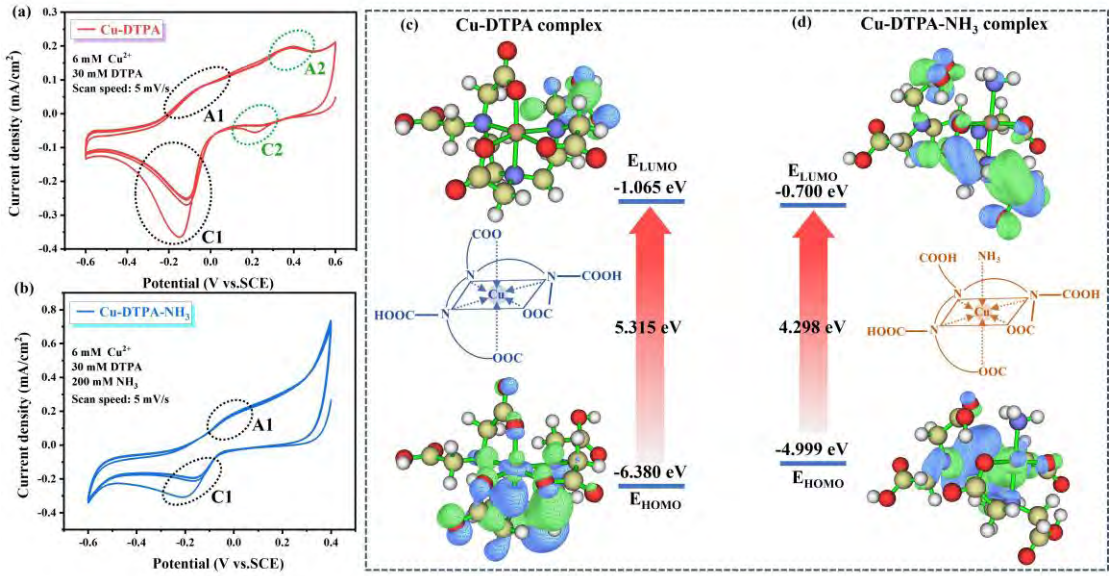

Figure 6.8 Reactivity analysis of different Cu(II) complexes with gold oxidation. Cyclic voltammetry (CV) curves of (a) Cu(II)-DTPA system and (b) Cu(II)-DTPA-NH_3 system recorded on a Pt electrode. The frontier molecular orbital (FMO) and energy values of (c) Cu(II)-DTPA and (d) Cu(II)-DTPA-NH_3 complexes

It is widely considered that gold thiosulfate leaching is an electrochemical process, involving gold oxidation/dissolution in anodic area and Cu(II) reduction/regeneration in cathodic area. Figure 6.9 proposed an electrochemical mechanism model of gold thiosulfate leaching using the proposed novel system (a $Cu[(DTPA)(NH_3)]^{3-}$ complex as oxidant), along with a Cyclic voltammetry (CV) curve recorded on a gold electrode. As seen in the CV curve, the anodic reaction only contains a broad peak at a potential range of -0.15 V to 0.0 V, indicating an oxidative dissolution process of gold (Au^+ to $Au(S_2O_3)_2^{3-}$), as shown in Eqs. (6-9) and (6-10) [49]. An obvious cathodic peak arising at a potential of ~0.2 V, clears a reduction reaction of the Cu(II) complex to $Cu(S_2O_3)_3^{5-}$ (as Cu(I) species) in the cathodic area, as shown in Eqs. (6-11) and (6-12) [50]. In summary, Au^+, oxidized by $Cu[(DTPA)(NH_3)]^{3-}$, is combined with $S_2O_3^{2-}$ to form $Au(S_2O_3)_2^{3-}$, and the generated $Cu(S_2O_3)_3^{5-}$ is oxidized by O_2 to get $Cu[(DTPA)(NH_3)]^{3-}$ and forms a redox cycle (Eq. 6-13) [51].

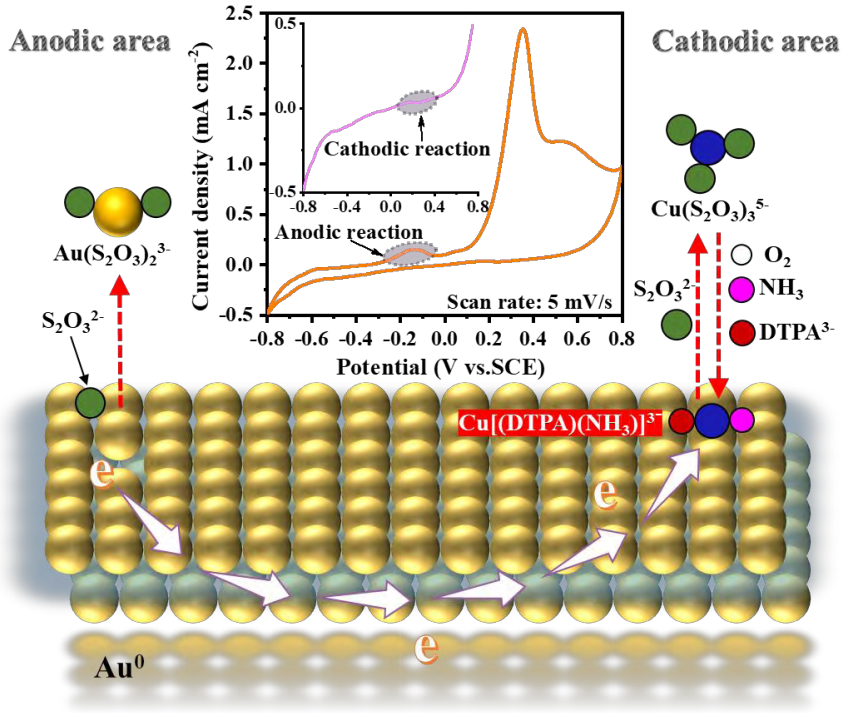

Figure 6.9 Mechanism model of gold leaching by ammonium thiosulfate in the Cu(II)-DTPA oxidation system. Cyclic voltammetry (CV) curve recorded on an Au electrode under conditions of 100 mM $(NH_4)_2S_2O_3$, 6 mM Cu(II), 30 mM DTPA, and pH=10.5

Anodic area:

$$Au = Au^{+} + e \quad (6\text{-}9)$$

$$Au^{+} + 3S_2O_3^{2-} = Au(S_2O_3)_2^{3-} + 2e \quad (6\text{-}10)$$

Cathodic area:

$$Cu^{2+} + e = Cu^{+} \quad (6\text{-}11)$$

$$Cu[(DTPA)(NH_3)]^{3-} + 3S_2O_3^{2-} + e = Cu(S_2O_3)_3^{5-} + NH_3 + DTPA^{5-} \quad (6\text{-}12)$$

Total reaction:

$$Au + 5S_2O_3^{2-} + Cu[(DTPA)(NH_3)]^{3-} = Au(S_2O_3)_2^{3-} + Cu(S_2O_3)_3^{5-} + NH_3 + DTPA^{5-} \quad (6\text{-}13)$$

6.3.3 Effect of DTPA on thiosulfate stability and surface passivation

More recent efforts have focused on reducing thiosulfate consumption to lower the production costs. The effect of DTPA concentrations (0, 6, 18, 30 mM) on gold leaching and thiosulfate consumption in the above-mentioned three leaching systems is displayed in Figure 6.10.

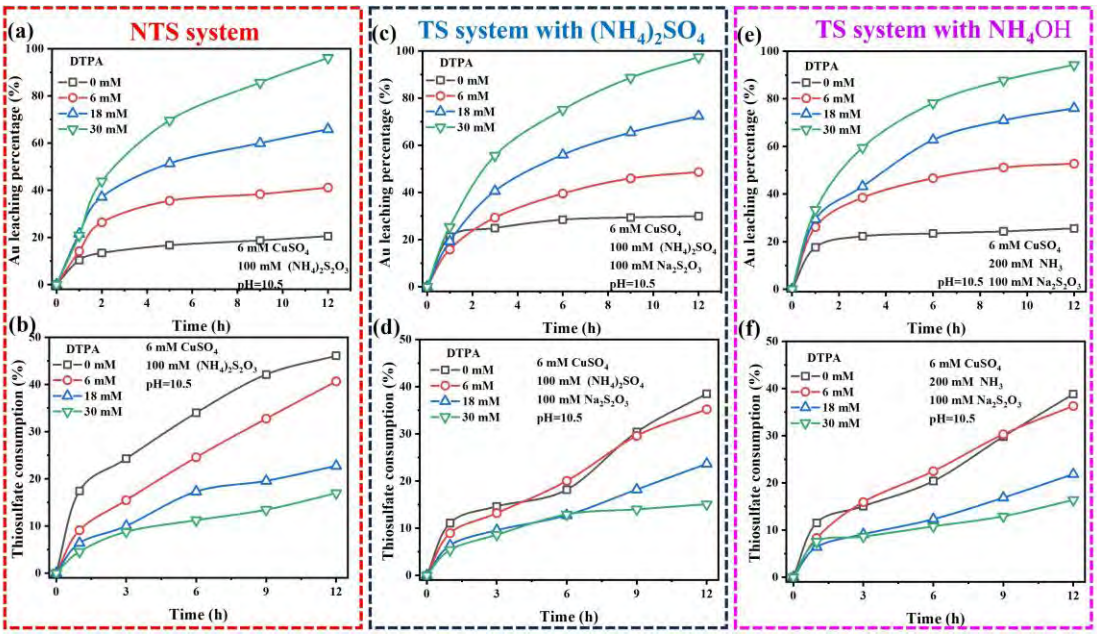

Figure 6.10 Effect of DTPA concentrations on gold leaching from the pretreated gold concentrate and corresponding thiosulfate consumption. (a, b) $(NH_4)_2S_2O_3$ (NTS) system, (c, d) NaS_2O_3 (TS) system with $(NH_4)_2SO_4$, and (e, f) NaS_2O_3 (TS) system with NH_4OH

In the absence of DTPA (0 mM), the oxidant present in the solution is likely in the form of $Cu(NH_3)_4^{2+}$ complex. In this condition (200 mM NH_3/NH_4^+), the $Cu(NH_3)_4^{2+}$ complex is unstable and will quickly reduce or precipitate, resulting in a lack of the Cu(II) oxidant. Besides, the abundant free Cu(II) ions could rapidly decompose thiosulfate ions. Therefore, the gold leaching in this condition is very low (less than 30%), and the consumption of thiosulfate is very large (higher than 50%). Obviously, the gold leaching increases with the increase of DTPA concentrations. When the DTPA is above 6 mM, DTPA preferentially coordinates with Cu(II) to form a stable $CuDTPA^{3-}$ complex, and NH_3 also participates in the coordination to increase its oxidation reactivity. Increasing the concentration of DTPA to 30 mM, the consumption of thiosulfate was reduced to ~10%, a near five-fold decrease compared with 6 mM DTPA.

To explain the beneficial role of DTPA, the solution variation of lixiviant containing 6 mM DTPA and 30 mM DTPA was comparably studied. As can be seen from Figures 6.11a and 6.11b, the color of the lixiviant containing 6 mM DTPA turns from blue to white after 12 h of leaching, while no significant changes occur in the contrasted 30 mM DTPA condition. The solution sample was further analyzed by Uv-vis spectrophotometry (Figure 6.11c). Obviously, both systems exhibit a similar intensity of the absorption peak of the Cu(II)-DTPA complex at the beginning. After 12

h of leaching, the intensity of the absorption peak of $CuDTPA^{3-}$ complex decreases significantly under the 6 mM DTPA condition compared to the 30 mM DTPA condition. The difference in solution color and absorption peak of Cu(II)-DTPA complex indicates that the excess addition of DTPA (30 mM) is good to stabilize the Cu(II) oxidation system, which can also be demonstrated by the less decay of solution potential (ORP), as shown in Figure 6.11d. Besides, the variation of pH during the leaching process was recorded (Figure 6.11e). The decision of pH is due to free Cu(II) ions consuming OH^- and $S_2O_3^{2-}$ oxidation to produce H^+ (Eqs. 6-14 to 6-19**)** [52, 53]. The results provide strong evidence for the beneficial role of DTPA in stabilizing the leaching system.

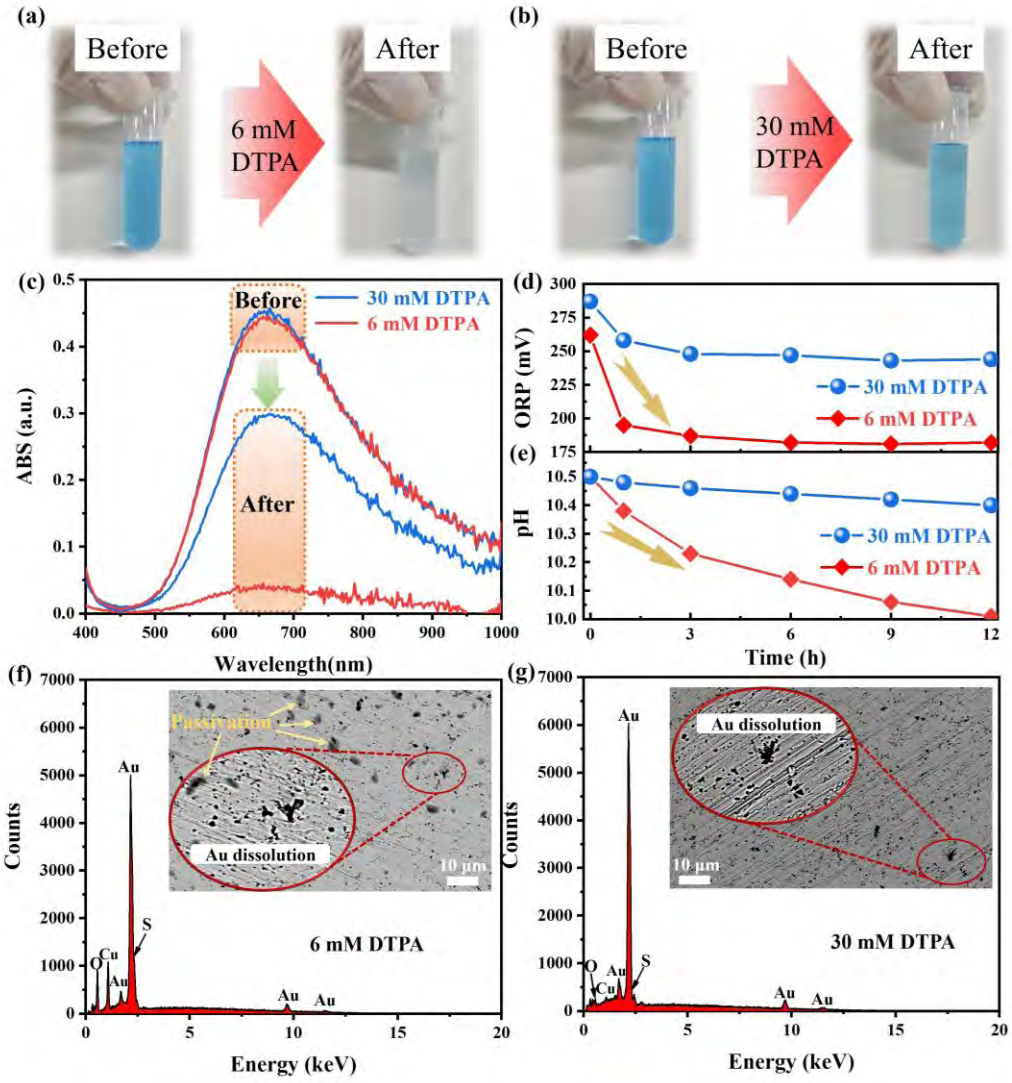

Figure 6.11 Compare the leaching systems containing 6 mM DTPA and 30 mM DTPA. The changes in (a, b) solution color, (c) Uv-vis spectroscopy, (d) solution potential (ORP) and (e) pH during gold ore leaching. (f, g) SEM-EDS images of gold

sheets after leaching. (100 mM $(NH_4)_2S_2O_3$, 6 mM Cu(II), pH=10.5)

$$Cu^{2+} + H_2O = 2H^+ + CuO \quad (6\text{-}14)$$

$$Cu^{2+} + 2OH^- = Cu(OH)_2 \quad (6\text{-}15)$$

$$Cu^{2+} + 4OH^- = Cu(OH)_4^{2-} \quad (6\text{-}16)$$

$$Cu^{2+} + S_2O_3^{2-} + H_2O = CuS + SO_4^{2-} + 2OH^- \quad (6\text{-}17)$$

$$S_2O_3^{2-} + H_2O + 1/2O_2 = S_4O_6^{2-} + S^{2-} + 6H^+ \quad (6\text{-}18)$$

$$4S_4O_6^{2-} + 6OH^- = 5S_2O_3^{2-} + 2S_3O_6^{2-} + 3H_2O \quad (6\text{-}19)$$

Furthermore, pure gold sheets leached with lixiviant containing 6 mM DTPA and 30 mM DTPA were analyzed using SEM-EDS. As seen in Figure 6.11f and Figure 6.11g, numerous holes appeared on the surfaces of gold sheets, indicating gold dissolution. Differently, many dark spots only appeared on the surface of the gold sheet leached with the lixiviant containing 6 mM DTPA. EDS analysis indicated the components of the dark spots were Cu, O, and S, suggesting the formation of porous layers of copper oxides and copper sulfides, which constitute a passivation layer [54]. At 6 mM DTPA, a relatively high concentration of NH_3 (200 mM) compared with 6 mM DTPA reduced the stability of the $CuDTPA^{3-}$ complex, potentially leading to the release of free Cu(II) ions. The copper oxide species is produced by the precipitation of Cu(II) ions (Eqs. 6-14 and 6-15), while the copper sulfide species is generated as a consequence of the side reactions between Cu(II) ions and thiosulfate ions (Eq. 6-17). The results make a point that excess DTPA has a role in eliminating passivation, which is fatal to gold dissolution.

Concisely, once the passivation layer forms on the surface of the exposed gold particles, it disrupts the diffusion of leaching agents to the gold surface and the diffusion of the oxidized Au(I) products into the solution, thereby slowing the gold dissolution rate. Based on this reason, many works reported that the traditional thiosulfate leaching of gold is a diffusion-controlled process (i.e., $Cu(NH_3)_4^{2+}$ as oxidant). According to the shrinking core model (SCM), a heterogeneous reaction process may be controlled by surface chemical reaction (Eq. 6-20), diffusion of the reagent through the product layer (Eq. 6-21), or both the interface transfer and diffusion across the product layer (Eq. 6-22) [55, 56].

$$1- (1-x)^{1/3} = k_a t \quad (6\text{-}20)$$

$$1-3(1-x)^{2/3} + 2(1-x) = k_b t \quad (6\text{-}21)$$

$$1/3\ln(1-x)-[1-(1-x)^{-1/3}] = k_c t \quad (6\text{-}22)$$

where x is the dissolution efficiency of pyrite at any time (t), and kr and kd are rate constants for the chemical reaction and diffusion control, respectively.

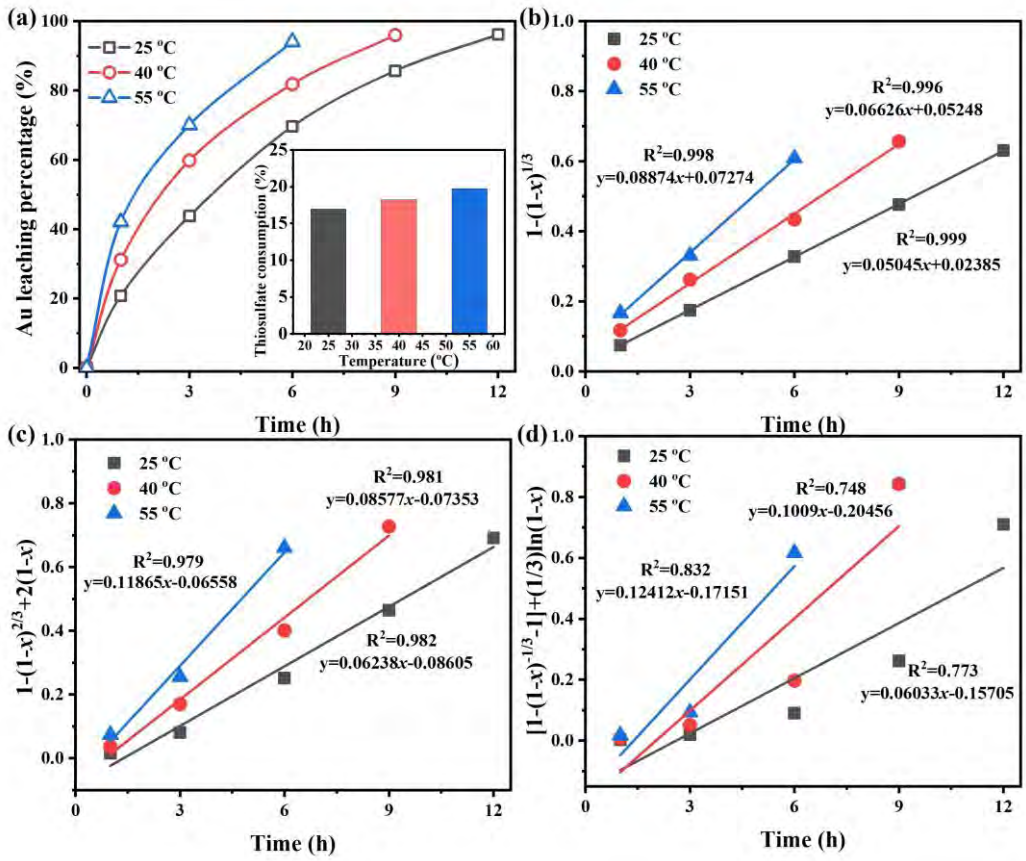

Figure 6.12 Leaching kinetics analysis. (a) Effect of temperatures (25 °C, 40 °C, and 55 °C) on gold leaching from the pretreated gold concentrate. The fitting results of gold leaching rates based on the shrinking core (SCM) model: (b) chemical reaction control (Eq. 6-20), (c) diffusion control (Eq. 6-21), and (d) mix control (Eq. 6-22). (100 mM $(NH_4)_2S_2O_3$, 6 mM Cu(II), 30 mM DTPA, pH=10.5, L/S=4)

To make a deeper understanding of the interaction mechanism, the kinetic fitting of gold ore leaching at various temperatures was analyzed. The increase in temperature accelerated the rate of gold leaching from 12 h at 25 °C k to 6 h at 55 °C, without a significant increase in the consumption of thiosulfate (Figure 6.12a). The fitting curves of these kinetic models (SCM) are shown in Figures 6.12b to 6.12d, and the linear fitting parameters are listed together. Obviously, R^2 of the chemical reaction (Figure 6.12b) at the temperatures of 25 °C, 40 °C, and 55 °C were 0.9917, 0.9950, and 0.8996, respectively, which is larger than the other two models. Based on these results, experimental data showed that the leaching process was mainly controlled by the chemical reaction model. It could indicate that the interface transfer of leaching agents is not a major factor, and the dissolution of oxidized gold was not affected by the passivation layer [57, 58].

6.3.4 Optimizing the gold leaching process from the pretreated gold concentrate

The operation parameters of gold leaching from the pretreated gold concentrate in an ammonium thiosulfate (NTS) system using $CuDTPA^{3-}$ complex as an oxidant were further optimized. As shown in Figure 6.13a, the gold leaching percentage decreased with the decrease in $(NH_4)_2S_2O_3$ concentration. Under a low input of $(NH_4)_2S_2O_3$, the concentrations of $S_2O_3^{2-}$ and NH_3/NH_4^+ are both deficient. In other words, the complexation and oxidation capability of the leaching solution were also reduced, thus resulting in poor gold leaching. For Cu(II), adding (Figure 6.13b), in the range from 4 mM to 5 mM, the gold leaching performance stays the same. Considering the consumption of thiosulfate, 4 mM Cu(II) is enough. Liquid-to-solid ratio (L/S) and stirring speed are important operation parameters for the viscosity of pulp, the mass transfer rate/ion diffusion of reactants, and the contact and collision between gold and lixiviants [59]. Noticeably, maintaining the L/S ratio at 4 and reducing the stirring speed to 300 rpm can sustain high levels of gold extraction (Figures 6.13c and 6.13d).

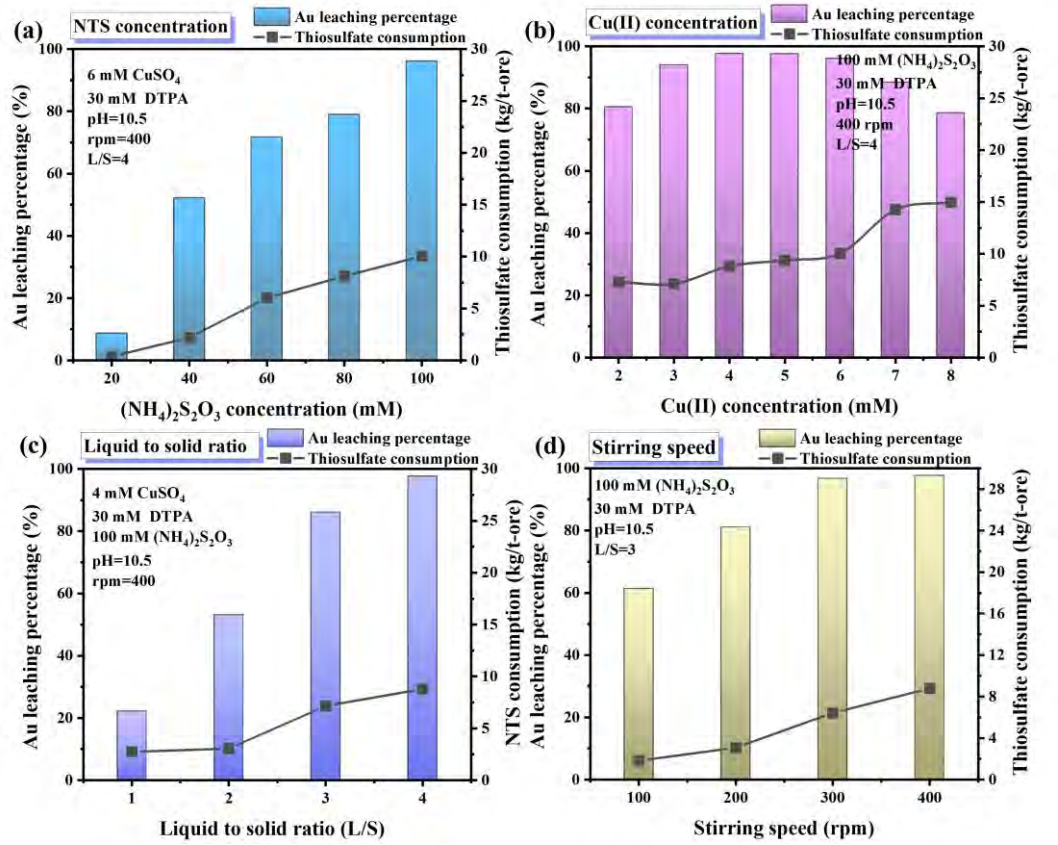

Figure 6.13 Optimization of gold leaching parameters. Effects of (a) $(NH_4)_2S_2O_3$ (NTS), (b) Cu(II), (c) liquid-to-solid ratio (L/S), and (d) stirring speed (rpm) on gold leaching from the pretreated gold concentrate and corresponding thiosulfate

consumption

Based on the above experiments, an optimal leaching process was optimized:100 mM $(NH_4)_2S_2O_3$, 4 mM Cu(II), 30 mM DTPA, pH 10.5, an L/S ratio of 4, and a stirring speed of 300 rpm. Under this condition, 97.8% of gold can be leached from the pretreated gold concentrate, with low consumption of thiosulfate of 8.8 kg/t-ore.

The above experiments optimized the best conditions for ammonium thiosulfate (NTS) leaching, where NH_3 was self-generated by $(NH_4)_2S_2O_3$ through an NH_4^+ to NH_3 pathway. Under the same operation parameters, gold leaching performance from the same gold ore was further investigated by using sodium thiosulfate (TS), and NH_3 was supplied by the addition of equivalent ammonium salts. As depicted in Figure 6.14a, gold leaching percentages using NH_4OH, $(NH_4)_2SO_4$, CH_3COONH_4, and NH_4Cl as additives were 92.4 %, 94.9 %, 96.4 %, and 94.0 %, with the same thiosulfate consumption of 11.7 kg/t-ore, 9.3 kg/t-ore, 12.8 k/t-ore, and 12.6 kg/t-ore, respectively.

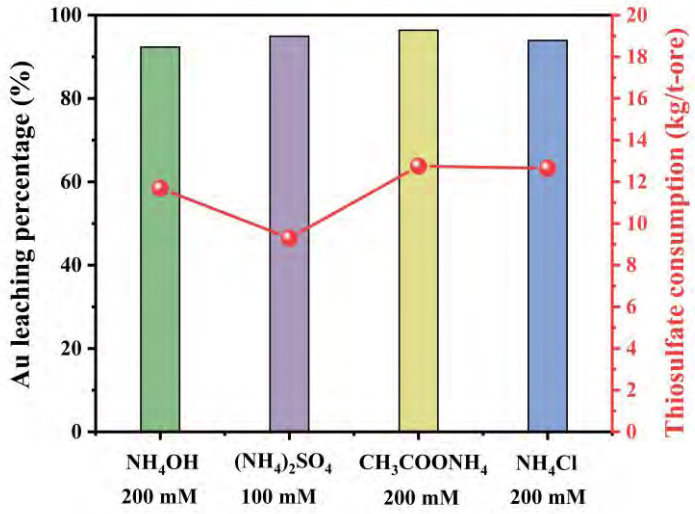

Figure 6.14 Effect of ammonium salts as additives on sodium thiosulfate (TS) gold leaching. Gold leaching efficiency of the pretreated gold concentrate and corresponding thiosulfate consumption. (100 mM $Na_2S_2O_3$, 4 mM $CuSO_4$, 30 mM DTPA, pH 10.5, L/S 4, 300 rpm).

6.4. Conclusions

In the key indicators of thiosulfate leaching, a stable Cu(II) oxidation system is important for both efficient gold extraction and low thiosulfate consumption. This work demonstrates that pentetic acid (DTPA) can effectively stabilize Cu(II) oxidant based

on the stable-chelated $CuDTPA^{3-}$ complex. On the one hand, comparative leaching using a $(NH_4)_2S_2O_3$ system, a $Na_2S_2O_3$ with $(NH_4)_2SO_4$ system, and a $Na_2S_2O_3$ with NH_4OH system demonstrated the important role of NH_3 in improving the oxidation performance of the $CuDTPA^{3-}$ oxidant. The mechanism of NH_3 was studied using Uv-vis spectroscopy, XRD, and FT-IR spectroscopy, cyclic voltammetry (CV), and DFT calculations, revealing that NH_3 contributes to the formation of a mixed $[Cu(DTPA)(NH_3)]^{3-}$ complex with enhanced chemical reactivity. On the other hand, DTPA presents a significant effect on the stability of the leaching system. An excess addition of DTPA can improve gold leaching efficiency, reduce thiosulfate consumption, and mitigate passivation issues. Furthermore, the operating parameters for $(NH_4)_2S_2O_3$ leaching of the pretreated gold concentrate were optimized. Under the condition of 100 mM $(NH_4)_2S_2O_3$, 4 mM Cu(II), 30 mM DTPA, pH 10.5, L/S ratio of 4, and a stirring speed of 300 rpm, 97.7% gold can be leached with a thiosulfate consumption of only 8.8 kg/t. Importantly, the practical operation process can be facilely designed using other leaching chemicals such as $Na_2S_2O_3$ with the addition of a low amount of NH_4OH or various ammonium salts like $(NH_4)_2SO_4$, CH_3COONH_4, and NH_4Cl. This study provides valuable insights for advancing the commercial viability of environmentally friendly gold leaching processes.

6.5 References

[1] H. Guo, S. Wang, Y. Nie, J. Chen, Q. Wang, Improving the cementation effect of copper on gold in thiosulfate solution by pre-regulating the existing form of Cu^{2+}, J. Ind. Eng. Chem. 130 (2024) 483-493.

[2] V.H. Ha, J. Lee, J. Jeong, H.T. Hai, M.K. Jha, Thiosulfate leaching of gold from waste mobile phones, J. Hazard. Mater. 178 (2010) 1115-1119.

[3] J. Xiong, Y. Zhou, B. Ren, Z. Zhang, Y. Zhang, J. Zhang, J. Chang, X. Yang, S. Wang, Protonated covalent organic frameworks for green and effective recovery of Au(I) from thiosulfate solutions: Performance, DFT calculations, and mechanism insights, Sep. Purif. Technol. 353 (2025) 128329.

[4] Z. Dong, T. Jiang, B. Xu, Y. Yang, Q. Li, An eco-friendly and efficient process of low potential thiosulfate leaching-resin adsorption recovery for extracting gold from a roasted gold concentrate, J. Cleaner Prod. 229 (2019) 387-398.

[5] G. Hilson, A.J. Monhemius, Alternatives to cyanide in the gold mining industry: what prospects for the future?, J. Cleaner Prod. 14 (2006) 1158-1167.

[6] G. Senanayake, The role of ligands and oxidants in thiosulfate leaching of gold, Gold Bull. 38 (2005) 170-179.

[7] B. Xu, Y. Nie, X. Feng, Q. Wang, Dissolution patterns of gold on various structural surfaces in thiosulfate solutions: The effect of interface adsorption on thiosulfate

oxidation and gold atom dissociation, Electrochim. Acta 497 (2024) 144602.
[8] M. Aazami, G.T. Lapidus, A. Azadeh, The effect of solution parameters on the thiosulfate leaching of Zarshouran refractory gold ore, Int. J. Miner. Process. 131 (2014) 43-50.
[9] I. Chandra, M.I. Jeffrey, A fundamental study of ferric oxalate for dissolving gold in thiosulfate solutions, Hydrometallurgy 77 (2005) 191-201.
[10] B. Xu, K. Li, Z. Dong, Y. Yang, Q. Li, X. Liu, T. Jiang, Eco-friendly and economical gold extraction by nickel catalyzed ammoniacal thiosulfate leaching-resin adsorption recovery, J. Cleaner Prod. 233 (2019) 1475-1485.
[11] Y. Zhang, B. Xu, Y. Zheng, Q. Li, Y. Yang, X. Liu, T. Jiang, X. Lyu, Hexaamminecobalt(III) catalyzed thiosulfate leaching of gold from a concentrate calcine and gold recovery from its pregnant leach solution via resin adsorption, Miner. Eng. 171 (2021) 107079.
[12] M.G. Aylmore, D.M. Muir, Thiosulfate leaching of gold-A review, Miner. Eng. 14 (2001) 135-174.
[13] E. Molleman, D. Dreisinger, The treatment of copper–gold ores by ammonium thiosulfate leaching, Hydrometallurgy 66 (2002) 1-21.
[14] X.M. Zhang, G. Senanayake, A Review of Ammoniacal Thiosulfate Leaching of Gold: An Update Useful for Further Research in Non-cyanide Gold Lixiviants, Miner. Process. Extr. Metall. Rev. 37 (2016) 385-411.
[15] Y. Yang, W. Gao, B. Xu, Q. Li, T. Jiang, Study on oxygen pressure thiosulfate leaching of gold without the catalysis of copper and ammonia, Hydrometallurgy 187 (2019) 71-80.
[16] Z. Liu, X. Guo, Q. Tian, L. Zhang, A systematic review of gold extraction: Fundamentals, advancements, and challenges toward alternative lixiviants, J. Hazard. Mater. 440 (2022) 129778.
[17] F. Xie, J.-n. Chen, J. Wang, W. Wang, Review of gold leaching in thiosulfate-based solutions, Trans. Nonferrous Met. Soc. China 31 (2021) 3506-3529.
[18] G. Senanayake, Gold leaching by thiosulphate solutions: a critical review on copper(II)–thiosulphate–oxygen interactions, Miner. Eng. 18 (2005) 995-1009.
[19] Q. Wang, X. Hu, F. Zi, P. Yang, Y. Chen, S. Chen, Environmentally friendly extraction of gold from refractory concentrate using a copper – ethylenediamine – thiosulfate solution, J. Cleaner Prod. 214 (2019) 860-872.
[20] J. Wang, F. Xie, W. Wang, Y. Bai, Y. Fu, Y. Chang, Leaching of gold from a free milling gold ore in copper-citrate-thiosulfate solutions at elevated temperatures, Miner. Eng. 155 (2020) 106476.
[21] D.M. Puente-Siller, J.C. Fuentes-Aceituno, F. Nava-Alonso, A kinetic–thermodynamic study of silver leaching in thiosulfate–copper–ammonia–EDTA solutions, Hydrometallurgy 134-135 (2013) 124-131.
[22] G. Zhang, L. Hou, P. Chen, Q. Zhang, Y. Chen, N.Z. Zainiddinovich, C. Wu, L.V.

Alejandro, F. Jia, Efficient and stable leaching of gold in a novel ethydiaminedhephen acetic-thiosulfate system, Miner. Eng. 209 (2024) 108639.

[23] D. Feng, J.S.J. van Deventer, Thiosulphate leaching of gold in the presence of carboxymethyl cellulose (CMC), Miner. Eng. 24 (2011) 115-121.

[24] D. Feng, J.S.J. van Deventer, The role of amino acids in the thiosulphate leaching of gold, Miner. Eng. 24 (2011) 1022-1024.

[25] D. Feng, J.S.J. van Deventer, Thiosulphate leaching of gold in the presence of ethylenediaminetetraacetic acid (EDTA), Miner. Eng. 23 (2010) 143-150.

[26] L. Hou, A.L. Valdivieso, A. Robledo-Cabrera, N.Z. Zainiddinovich, C. Wu, S. Song, F. Jia, Stepwise oxidation of refractory pyrite using persulfate for efficient leaching of gold and silver by an eco-friendly copper(II)-glycine-thiosulfate system, Powder Technology 448 (2024) 120323.

[27] T.V. Popova, N.V. Shcheglova, Comparative Study of the Formation of Heterometallic Diethylenetriaminpentaacetates of Cobalt(II), Nickel(II), and Copper(II) in Aqueous Solutions, Russ. J. Phys. Chem. A 96 (2022) 1170-1174.

[28] V.M. Vulava, A. Torrents, B.R. James, Copper solubility in Myersville B horizon soil in the presence of DTPA, Soil Sci. Soc. Am. J. 61 (1997) 44-52.

[29] W.W. Xie, P.R. Tremaine, Thermodynamics of Aqueous Diethylenetriaminepentaacetic Acid (DTPA) Systems: Apparent and Partial Molar Heat Capacities and Volumes of Aqueous H_2DTPA^{3-}, $DTPA^{5-}$, $CuDTPA^{3-}$, and Cu_2DTPA^{-} from 10 to 55°C, J. Solution Chem. 28 (1999) 291-325.

[30] V.L. Silva, R. Carvalho, M.P. Freitas, C.F. Tormena, W.C. Melo, Spectrometric and theoretical investigation of the structures of Cu and Pb/DTPA complexes, Struct. Chem. 18 (2007) 605-609.

[31] R.E. Sievers, J.C. Bailar Jr, Some metal chelates of ethylenediaminetetraacetic acid, diethylenetriaminepentaacetic acid, and triethylenetetraminehexaacetic acid, Inorg. Chem. 1 (1962) 174-182.

[32] Y. Ou, Y. Yang, K. Li, W. Gao, L. Wang, Q. Li, T. Jiang, Eco-friendly and low-energy innovative scheme of self-generated thiosulfate by atmospheric oxidation for green gold extraction, J. Cleaner Prod. 387 (2023) 135818.

[33] B. Xu, Y. Yang, Q. Li, T. Jiang, X. Zhang, G. Li, Effect of common associated sulfide minerals on thiosulfate leaching of gold and the role of humic acid additive, Hydrometallurgy 171 (2017) 44-52.

[34] Z. Tian, H. Li, Q. Wei, W. Qin, C. Yang, Effects of redox potential on chalcopyrite leaching: An overview, Miner. Eng. 172 (2021) 107135.

[35] E. Reyes-Sandoval, J.C. Fuentes-Aceituno, Maximization of the silver recovery with the “monoethanolamine-copper-ammonium sulfate” novel system. A step towards the development of a less toxic leaching technology, Hydrometallurgy 173 (2017) 22-31.

[36] X. Liu, T. Jiang, B. Xu, Y. Zhang, Q. Li, Y. Yang, Y. He, Thiosulphate leaching of

gold in the Cu–NH_3–$S_2O_3^{2-}$–H_2O system: An updated thermodynamic analysis using predominance area and species distribution diagrams, Miner. Eng. 151 (2020) 106336.

[37] B. Xu, J. Wu, Z. Dong, S. Zhong, X. Liu, T. Jiang, Solution circulation for green and sustainable gold extraction with an integrated low potential thiosulfate leaching-resin adsorption recovery process, Sep. Purif. Technol. 353 (2025) 128535.

[38] G. Alvarado-Macías, J.C. Fuentes-Aceituno, F. Nava-Alonso, Silver leaching with the thiosulfate–nitrite–sulfite–copper alternative system, Hydrometallurgy 152 (2015) 120-128.

[39] H. Zhao, H. Yang, X. Chen, G. Chen, L.-L. Tong, Z. Jin, Effect of Triethanolamine as a New and Efficient Additive on Thiosulfate-Copper-Ammonia System Leaching of Gold, JOM 72 (2019) 946–952.

[40] H. Zhao, H. Yang, W. Shi, L. Lu, P. Ma, H. Li, X. Chen, Effect of an additive TEA on thiosulfate leaching of low sulfur gold concentrate, J. Phys.: Conf. Ser. 1347 (2019) 012118.

[41] F. Wan, L. Wang, W. Xu, C. Li, Y. Li, C. Zhang, L. Jiang, Binuclear gadolinium(III) complex based on DTPA and 1,3-bis(4-aminophenyl)adamantane as a high-relaxivity MRI contrast agent, Polyhedron 145 (2018) 141-146.

[42] L. Guglielmero, A. Mero, A. Mezzetta, G. Tofani, F. D'Andrea, C.S. Pomelli, L. Guazzelli, Novel access to ionic liquids based on trivalent metal–EDTA complexes and their thermal and electrochemical characterization, J. Mol. Liq. 340 (2021) 117210.

[43] M. Trpkovska, B. Šoptrajanov, Tetraamminecopper(II) molybdate and tetraamminecopper(II)tungstate: a Fourier-transform infrared study, J. Mol. Struct. 408-409 (1997) 345-348.

[44] J.L. Deutsch, D.B. Dreisinger, Silver sulfide leaching with thiosulfate in the presence of additives Part I: Copper–ammonia leaching, Hydrometallurgy 137 (2013) 156-164.

[45] Y. Nie, L. Yang, Q. Wang, C. Shi, F. Zi, H. Yu, Connection between gold dissolution in thiosulfate leaching and Cu(II) complexes during the cathodic process, Electrochim. Acta 328 (2019) 135079.

[46] L. Hu, X. Zhang, H. Wang, J. Zhang, R. Xia, J. Cao, G. Pan, Experimental and density functional theory study of complexing agents on cobalt dissolution in alkaline solutions, Electrochim. Acta 375 (2021) 137977.

[47] D.S. El Sayed, T.E. Khalil, H.A. Elbadawy, Rational and experimental investigation of antihypotensive midodrine-Fe(III) complex: Synthesis, spectroscopy, DFT, biological activity and molecular docking, Journal of Molecular Structure 1311 (2024) 138421.

[48] J. Wu, B. Xu, X. Liu, Z. Dong, T. Jiang, Development of a novel cobalt-glycine

catalyzed thiosulfate system by DFT calculation for eco-friendly and efficient gold extraction, Sep. Purif. Technol. 354 (2025) 128959.

[49] P.L. Breuer, M.I. Jeffrey, An electrochemical study of gold leaching in thiosulfate solutions containing copper and ammonia, Hydrometallurgy 65 (2002) 145-157.

[50] S. Zhang, M.J. Nicol, An electrochemical study of the dissolution of gold in thiosulfate solutions. Part II. Effect of Copper, J. Appl. Electrochem. 35 (2005) 339-345.

[51] L. Hou, A. López Valdivieso, P. Chen, G. Zhang, Q. Zhang, Y. Chen, S. Song, F. Jia, An electrochemical study of the dissolution behavior of gold in a novel glycine-thiosulfate system, Miner. Eng. 202 (2023) 108273.

[52] O. Sitando, G. Senanayake, X. Dai, A.N. Nikoloski, P. Breuer, A review of factors affecting gold leaching in non-ammoniacal thiosulfate solutions including degradation and in-situ generation of thiosulfate, Hydrometallurgy 178 (2018) 151-175.

[53] H. Yu, F. Zi, X. Hu, J. Zhong, Y. Nie, P. Xiang, The copper–ethanediamine–thiosulphate leaching of gold ore containing limonite with cetyltrimethyl ammonium bromide as the synergist, Hydrometallurgy 150 (2014) 178-183.

[54] M.I. Jeffrey, K. Watling, G.A. Hope, R. Woods, Identification of surface species that inhibit and passivate thiosulfate leaching of gold, Miner. Eng. 21 (2008) 443-452.

[55] Y. Lin, X. Hu, F. Zi, Thiocyanate facilitating thiosulfate extraction of gold via inhibiting formation of passive layer, Sustainable Mater. Technol. 40 (2024) e00878.

[56] Q. Meng, X. Yan, G. Li, Eco-friendly and reagent recyclable gold extraction by iodination leaching-electrodeposition recovery, J. Cleaner Prod. 323 (2021) 129115.

[57] E. Mohammadi, M. Pourabdoli, M. Ghobeiti-Hasab, A. Heidarpour, Ammoniacal thiosulfate leaching of refractory oxide gold ore, Int. J. Miner. Process. 164 (2017) 6-10.

[58] N.P. Baloyi, J.M. Nseke, M.E. Makhatha, Application of response surface methodology (RSM) for simultaneous optimization of kinetic parameters affecting gold leaching in thiosulfate based media: a statistical approach, J. Chem. 2022 (2022) 8348167.

[59] L. Hou, A.L. Valdivieso, Y. Chen, P. Chen, N.Z. Zainiddinovich, C. Wu, S. Song, F. Jia, A highly efficient clean hydrometallurgy process for gold leaching in a Fenton oxidation assisted thiourea system, Sustainable Mater. Technol. 40 (2024) e00975.

Chapter VII. Dissolution mechanism of gold in a high-valent Cu(III)-assisted iodide system: Towards eco-friendly and fast gold oxidative leaching from ore and e-waste

7.1 Introduction

Gold (Au), one of the most ancient treasures on earth, has held an unparalleled place in human civilization for millennia, and is gradually expanding its role as a critical material to modern industries [1]. Given limited raw resources and rising demand, both extraction from primary ores and recycling from secondary urban e-waste streams are viable options for securing gold supply [2, 3]. Historically, the method of gold extraction has been dominated by direct cyanidation, yet the requisite lixiviant, cyanide (CN^-), is acutely toxic with serious environmental concerns [4].

Driven by clean production initiatives, fostering the utilisation of green lixiviants, such as thiourea ($CS(NH_2)_2$), thiocyanate (SCN^-), thiosulfate ($S_2O_3^{2-}$), and halides (Cl^-, Br^-, and I^-), offers a blueprint for advancing eco-friendly gold hydrometallurgical extraction and separation. Among these lixiviants, systems based on $CS(NH_2)_2$, Cl^-, Br^-, and SCN^- have been widely applied under highly acidic conditions (pH＜2), achieving high gold recovery and fast leaching kinetics [5]. While typically less toxic than CN^-, these lixiviants also pose significant challenges, such as high corrosivity toward metallurgical equipment and poor selectivity, which are often regarded as industrially undesirable [6]. Researchers have long recognized that $S_2O_3^{2-}$ is a better lixiviant due to its ability to operate effectively under alkaline conditions (pH 8-11). However, in many cases, the instability of $Cu(NH_3)_4^{2+}$, an essential oxidant, leads to irreversible side reactions resulting in high reagent consumption [7]. Evidence indicates that iodide (I^-) enables efficient gold leaching from primary ore (e.g., carbonaceous ores, sulphide ore, and polymetallic ores) and even from secondary electronic waste under near-neutral pH [8, 9]. Thanks to this, iodide provides a promising leaching system for gold extraction that is simple, safe, and well-aligned with the 12 principles of sustainable hydrometallurgy [10].

Iodide leaching typically employs an I^-/I_2 redox couple, where dissolved I_2 reacts with I^- to form triiodide (I_3^-), the key oxidant for Au dissolution, as Eqs. (7-1)-(7-3) [11]. However, directly using solid I_2 is impractical for metallurgical leaching: (i) it has poor solubility and requires a high amount of iodide to assist it in dissolving; (ii) it can

easily volatilize at ambient temperature, complicating process control and leading to serious side effects; and (iii) it is expensive; a kilogram of iodine has been traded at a price above 60 euros/kg, placing it among the most expensive basic chemicals.

$$I_{2(l)} + I^- \rightarrow I_3^- \quad (7\text{-}1)$$

$$2Au + I^- + I_3^- \rightarrow 2AuI_2^- \quad (7\text{-}2)$$

$$2Au + I_3^- \rightarrow 2AuI_4^- + I^- \quad (7\text{-}3)$$

Taking these factors into account, many efforts have focused on using alternatives to direct solid I_2 dosing. One promising strategy is using iodide-oxidizing bacteria, such as *A. baumannii, R. tolerans,* and *R. mucosus*, to in situ convert I^- to liquid I_2, which enables gold extraction from sulphide ores and e-waste [12-14]. However, these biocatalysts typically require an extra electron acceptor (e.g., H_2O_2), and always suffer from long cultivation periods and limited process controllability [15]. In recent years, chemical catalytic oxidation based on persulfate ($S_2O_8^{2-}$) has been regarded as a huge leap [16]. According to Eqs. (7-4) and (7-5), free radicals ($SO_4^{\bullet-}$) generated from $S_2O_8^{2-}$ can directly activate I^- to $I_{2(l)}$, which further convert into I_3^- spontaneously (Eq. (7-1)). This finding definitely provides intriguing scientific insights, yet generating $SO_4^{\bullet-}$ radical is nontrivial and always requires external energy input (e.g., light, heat, ultrasound, etc.) [17, 18].

$$S_2O_8^{2-} \rightarrow 2\ SO_4^{\bullet-} \quad (7\text{-}4)$$

$$2SO_4^{\bullet-} + 2I^- \rightarrow I_{2(l)} + 2SO_4^{2-} \quad (7\text{-}5)$$

$$Cu(III) + I^- \rightarrow I^{\bullet} + Cu(II) \quad (7\text{-}6)$$

$$I^{\bullet} \rightarrow I_{2(l)} \quad (7\text{-}7)$$

Interestingly, early studies reported that high-valent Cu(III), in the form of a periodate complex, is capable of catalytically oxidizing I^- to $I_{2(l)}$, as Eqs (7-6) and (7-7) [19, 21]. This reaction has no need for any external energy input and can proceed over a wide pH range, which has been applied to the recovery of critical metals such as americium [22] and mercury [23]. Inspired by this, this exploratory study aligns with the principles of clean gold production by, for the first time, employing Cu(III) to assist iodide gold leaching. First of all, the thermodynamic feasibility of the proposed high-valent Cu(III) oxidation system for driving iodide gold leaching was evaluated using Eh-pH diagrams. Secondly, key operational parameters, including Cu(III)/KI concentrations, pH, liquid-to-solid ratio, and agitation speed, were systematically optimized using gold ore and e-waste. We further conducted a comprehensive solution

chemistry analysis to identify the dominant oxidants and clarify their roles in the oxidative dissolution of gold. Finally, leachate reuse and adsorption recovery of leached gold using commercial activated carbon are further assessed, aiming to provide practical guidance for environmentally friendly iodide gold extraction.

7.2 Materials and methods

7.2.1 Materials and reagents

One of the Au-bearing materials used in this chapter was a multi-stage pretreated gold concentrate, hereafter referred to as ore. Although it was obtained from the same company as the samples used in Chapters IV and VI, namely Jinyuan Mining Co., Ltd. (Henan Province, China), it was collected at a different time and was therefore re-characterized before use. The other was an e-waste sample consisting of waste mobile phone printed circuit boards (PCBs, hereafter referred to as e-waste). Before leaching, the e-waste was shredded, ground to a particle size below 100 μm, and washed with HNO_3, followed by rinsing and drying. X-ray fluorescence (XRF, PANalytical B.V., Netherlands) was used to determine their chemical composition. As shown in Table 7.1, the ore mainly contains Fe (57.17 wt%) and Si (24.21 wt%), while Si (70.59 wt%) and Br (14.56 wt%) are the predominant elements in e-waste. The Au grade was 44.5 g/t for the gold ore sample (fire assay) and 70.6 g/t for the e-waste (ICP-OES after aqua regia digestion) [24, 25].

Table 7.1 Elemental composition of the gold ore and e-waste (wt%; Au in g/t)

Element	Fe	Si	Al	S	K	Ca	Ti	Br	Ba	Pb	Au[a]
gold ore	57.17	24.21	5.21	3.17	2.07	2.57	0.50	/	/	2.97	44.5
e-waste	0.89	70.59	3.26	0.45	0.08	5.25	0.95	14.56	3.27	/	70.6

X-ray diffraction (XRD, Rigaku, Japan) analysis confirmed that the gold ore contained Fe_2O_3 (hematite), SiO_2 (quartz), and $CaSO_4$ (gypsum), with the brick-red color and high Fe content indicating hematite as the main phase (Figure 7.1a). XRD pattern of the e-waste shows a broad halo in the 10°–35° region, suggesting a significant amorphous contribution. Together with the high Si content from chemical analysis, this feature is consistent with the presence of Si-rich amorphous phases, potentially including amorphous silica (Figure 7.1b) [26].

A scanning electron microscope (SEM, pw-100-017, Phenom, Holland), equipped with an energy dispersive spectroscopy (EDS), was used to detect the liberation of gold in samples. As shown in Figure 7.1c, gold was found to exist as independent and small

particles within the porous hematite, though the presence of larger visible gold particles cannot be ruled out in this gold ore sample. In general cases, the higher the degree of liberation of the gold particles in the materials, the more effective the leaching rate will be. For the e-waste sample, Au is expected to be readily leached because it is mainly present as a surface-plated layer on PCBs contact features (Figure 7.1d).

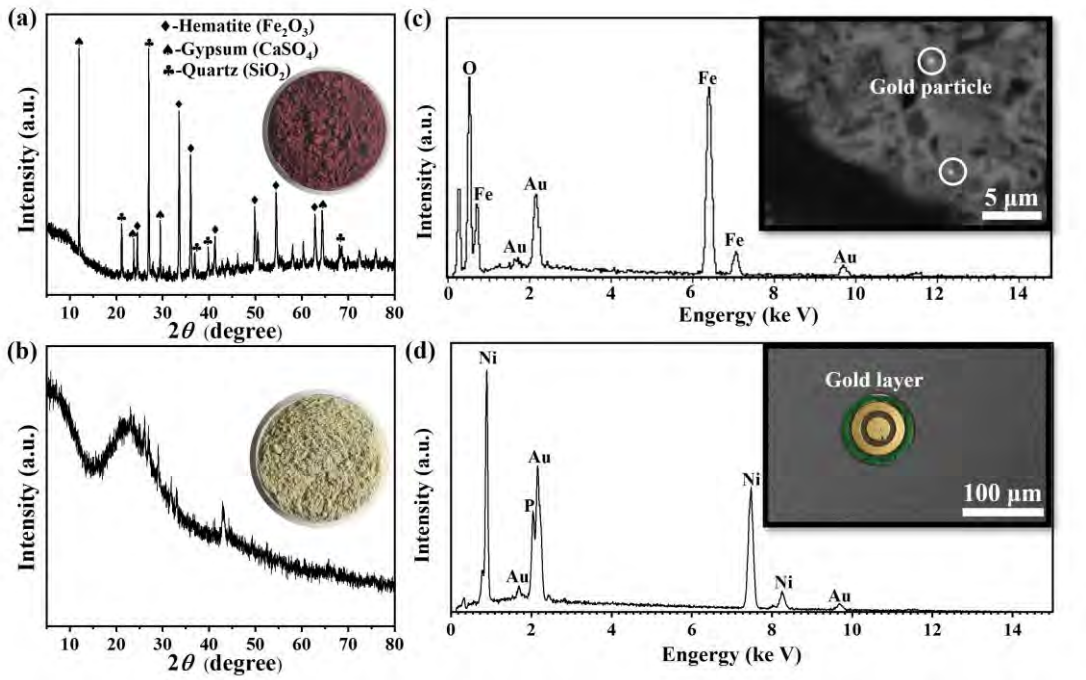

Figure 7.1 Characterization of gold-bearing feedstocks. (a, b) XRD patterns and (c, d) SEM-EDS spectra of the gold ore (top) and e-waste (bottom)

Analytical grade of copper sulfate pentahydrate ($CuSO_4•5H_2O$), potassium persulfate ($K_2S_2O_8$), potassium periodate (KIO_4), and potassium hydroxide (KOH) were used for the preparation of Cu(III) periodate, which were all supplied by Sigma Aldrich, China. Potassium iodide (KI, Sinopharm, China) was used as a gold lixiviant. Starch (Sinopharm, China) was used as a probe for detecting iodide derivatives (I_3^- and I_2) in solution. Nitric acid (HNO_3, Sinopharm, China) was used for e-waste pre-treatment. Granular activated carbon (20-40 mesh, Zhengzhou Yihang Water Purification Materials Co., Ltd.) was ground to less than 75 μm ahead of gold adsorption experiments. All solutions were prepared using deionized (DI) water.

7.2.2 Preparation of Cu(III) periodate solution

The stock solution of the Cu(III) periodate complex was prepared by oxidizing Cu(II) in an alkaline medium in the presence of KIO_4. Firstly, 8.00 g of KOH was

dissolved in 80 mL of DI water, after which 2.87 g of KIO_4 was added to the solution with continuous stirring to ensure complete dissolution (Solution A). Subsequently, 1.56 g of $CuSO_4 \cdot 5H_2O$ was dissolved in 20 mL of DI water (Solution B). Solution B was then added dropwise to Solution A while stirring, resulting in a dark-green Solution C. Solution C was then heated to 90°C with stirring, and 1.00 g of $K_2S_2O_8$ was added in small portions step by step; then, it was gently boiled for additional 20 min to ensure a complete decomposition of $S_2O_8^{2-}$, eventually yielding a dark brown solution (insert of Figure 7.2). This solution was cooled down and stored in a sealed glass bottle at room temperature.

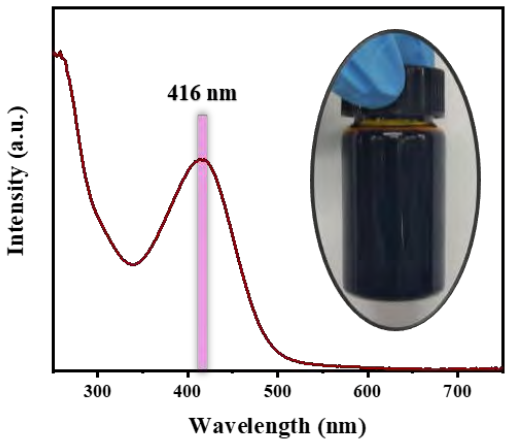

Figure 7.2 UV-vis absorption spectrum of the as-prepared Cu(III) solution

The ultraviolet and visible spectrophotometer (UV-vis, GENESYS, Thermo Fisher Scientific, USA) was used to confirm the successful synthesis of Cu(III) periodate. As seen in Figure 7.2, the obtained solution shows a broad absorption band at 416 nm, consistent with previous reports of the high-valent Cu(III) periodate complex [27] [28].

7.2.3 Gold extraction procedures

7.2.3.1 Gold leaching procedure

Magnetic stirring was used for leaching gold from both ore and e-waste, which were carried out in a 150 mL beaker, at room temperature under ambient atmosphere. The powder of gold-bearing materials was first added to 100 mL of DI water, forming a pulp by stirring. Then Cu(III) solution was dropped into it, and the pH was immediately adjusted to the preset value using 10% H_2SO_4. Finally, solid KI was added to the pulp to start the leaching reaction. The leaching durations were 60 min for gold ore and 20 min for e-waste, respectively. At each time interval, 1 mL leachate was taken and diluted with DI water to analyse Au leaching efficiency (η, %) by atomic absorption

spectroscopy (AAS, 280Z AA, Agilent, USA), as shown in Eq. (7-8). To minimize experimental error, all tests were performed in triplicate and reported as the mean value.

$$\eta = \frac{V C_1}{M \beta} \times 100\% \quad (7\text{-}8)$$

Where V (mL) and C_1 (mg/L) are the leachate volume and Au concentration therein, respectively; m (g) and β (g/t) are the mass and Au grade of ore and e-waste, respectively.

7.2.3.2 Multi-cycle leaching procedure

Using Section 7.3.2's optima, this work conducted five consecutive gold-leaching cycles for ore (3% Cu(III), 40 mM KI, pH 5.5, L/S 2, 200 rpm, 60 min) and e-waste (1% Cu(III), 20 mM KI, pH 5.5, L/S 8, 300 rpm, 20 min). After each leach, the slurry was filtered to obtain the filtrate, which was allowed to be reused to leach fresh Au-bearing feeds without any reagent supplementation. To offset leachate loss during filtration, the mass of fresh solids was adjusted in later cycles to keep L/S constant. The leached solid residues from each cycle were thoroughly washed and dried for gold content analysis (fire assay):

$$A = \frac{m_0 \beta - m_1 \gamma}{m_0 \beta} \times 100\% \quad (7\text{-}9)$$

Where β (g/t) and γ (g/t) are the Au grades of the feed (gold ore or e-waste) and its leached residue, and m_0 (g) and m_1 (g) are their respective masses.

7.2.3.3 Gold recovery procedure

The coconut shell activated carbon was used in this study for leached gold adsorption. Before the adsorption test, it was washed with 2 M HCl followed by hot distilled water and dried at 70 °C for 24 h. After completion of the cycled gold leaching process, activated carbon, with a dose of 1 g/L, was directly added to the filtered solution for gold adsorption recovery. During the adsorption test (120 min), 1 mL of solution was taken at distinct times to analyze the gold concentration by AAS. The recovery rate of gold adsorption onto the activated carbon (Y, %) was calculated using Eq. (7-10).

$$Y = \frac{C_0 - C_t}{C_0} \times 100\% \quad (7\text{-}10)$$

Where C_0 is the initial Au concentration and C_t is the Au concentration at time t in the leaching solution, both expressed in mg/L.

7.2.4 Solution characterization and thermodynamic/DFT analysis

Ultraviolet-visible spectroscopy (UV-vis, GENESYS, Thermo Fisher Scientific, USA) was used to measure the formation of oxidative species in solution (e.g., Cu(III) periodate, I_3^-, and $I_{2(l)}$). X-ray photoelectron spectroscopy (XPS, PHI5000, ULVAC PHI, Japan) was carried out to characterize the chemical state of gold in the leachate. Electrochemical measurements were conducted to characterize the anodic dissolution behavior of gold in solution, using a CHI400E electrochemical workstation equipped with a Quartz Crystal Microbalance (QCM). A gold-coated quartz crystal electrode, a platinum electrode, and a saturated calomel electrode (SCE) were employed as the working, counter, and reference electrodes, respectively. The Cu(III)/KI leaching solution was used as the electrolyte, and all potentials were reported versus the standard hydrogen electrode (SHE).

HSC Chemistry software was used to construct Eh-pH diagrams for Au-H_2O, Au-I-H_2O, and I-H_2O systems. Density functional theory (DFT) calculations were performed using the Materials Studio program and were carried out at the GGA/BLYP level with effective core potentials (ECPs) for core treatment and a double numerical plus polarization (DNP) basis set. Geometry optimizations used convergence criteria of 5×10^{-3} Å (displacement), 2×10^{-3} Hartree Å^{-1} (force), 2×10^{-5} Hartree (energy), and 1×10^{-5} Hartree (SCF), with a 4 Å orbital cutoff.

7.3 Results and discussion

7.3.1 Thermodynamic feasibility assessment of the Cu(III)/KI system

In the field of extractive metallurgy, Eh-pH diagrams are very useful to predict thermodynamically stable species and feasible reaction pathways [29]. Firstly, an Eh-pH diagram for the Au-H_2O system (Figure 7.3a) was constructed, and the diagram indicates that metallic gold is insoluble in aqueous media without any complexing agents. Theoretically, $Au(OH)_2^-$ can form under sufficient alkalinity and potentials, while it is only an intermediate product that cannot stably exist [30]. With I^- as a ligand, the Eh-pH diagram for the Au-I-H_2O system (Figure 7.3b) indicates that metallic gold can be dissolved as AuI_2^- and AuI_4^- ions (Eqs. 7-11 and 7-12) [31]. Both Au(I) and Au(III) complexes are stable enough over a wide pH range from acidic to alkaline conditions (pH < 11.48). Besides, the addition of I^- distinctly lowered the potential for the formation of these soluble gold species, which provided a possibility for gold leaching, as the higher the potential, the harder the dissolution of gold. Nonetheless,

lines ① and ② show that the formation of AuI_2^- (E^0 = 0.40 V) and AuI_4^- (E^0 = 0.65 V) still requires a minimum potential, which means a suitable oxidizing atmosphere is still needed [32].

$$Au + 2I^- \rightarrow AuI_2^- + e^- \quad (7\text{-}11)$$

$$Au + 4I^- \rightarrow AuI_4^- + 3e^- \quad (7\text{-}12)$$

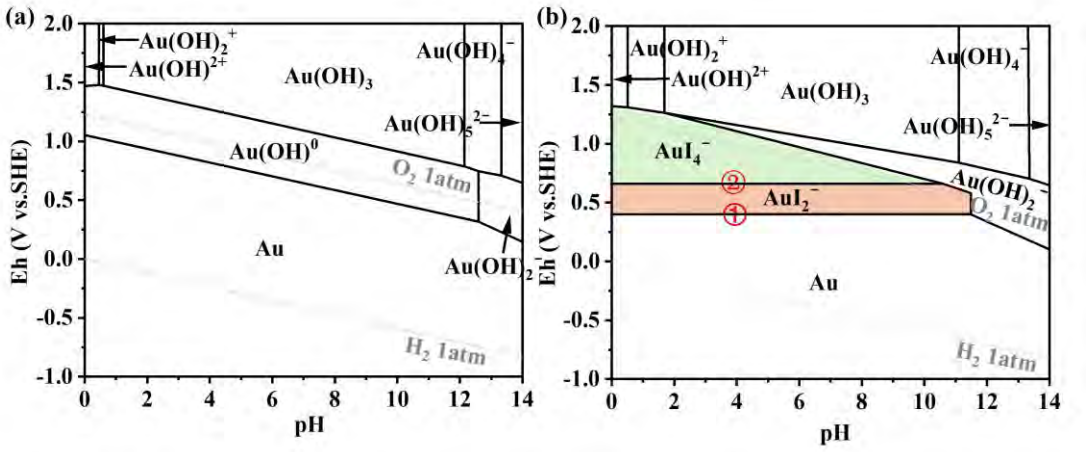

Figure 7.3 Eh-pH diagrams of (a) Au-H_2O system and (b) Au-I-H_2O system

Herein, the +III oxidation state of copper itself exhibits a higher potential ($E^0_{Cu(III)/Cu(II)}$ = 2.4 V) than that required for the formation of both AuI_2^- and AuI_4^- ions [28]. Besides, according to Eqs. (7-6) and (7-7), Cu(III) periodate is capable of oxidizing I^- to $I_{2(l)}$. Accordingly, once soluble $I_{2(l)}$ is formed, the more powerful species of I_3^- can also be formed simultaneously (Eq. 7-1). Therefore, the Cu(III)/KI system may contain multi-oxidants, such as high-valent Cu(III) periodate, $I_{2(l)}$, and I_3^-, that are thermodynamically capable of oxidizing and dissolving gold.

7.3.2 Optimization of gold leaching parameters for ore and e-waste

7.3.2.1 Effect of Cu(III) dosage and KI concentration

Figure 7.4a and Figure 7.4b show how Cu(III) periodate affects Au leaching. In the absence of Cu(III) periodate, negligible Au dissolution was observed, which is expected because Au cannot dissolve in iodide solution without an oxidant [33, 34]. Adding Cu(III) periodate markedly increased leaching, which corroborates the thermodynamic analysis that Cu(III) periodate is powerful enough. A maximum gold leaching percentage of 95.3% was achieved for gold ore when the concentration of Cu(III) was increased to 3 vol%. For e-waste, gold leaching sharply increased up to a maximum of 97.9% at 1 vol% Cu(III). Continuing to increase the concentration of Cu(III), there was no serious variation in leaching percentage. Having said that, the

improved leaching rate is likely attributable to homogeneous redox reactions between high-valent Cu(III) and I^- that generate additional oxidants (e.g., $I_{2(l)}$ and I_3^-).

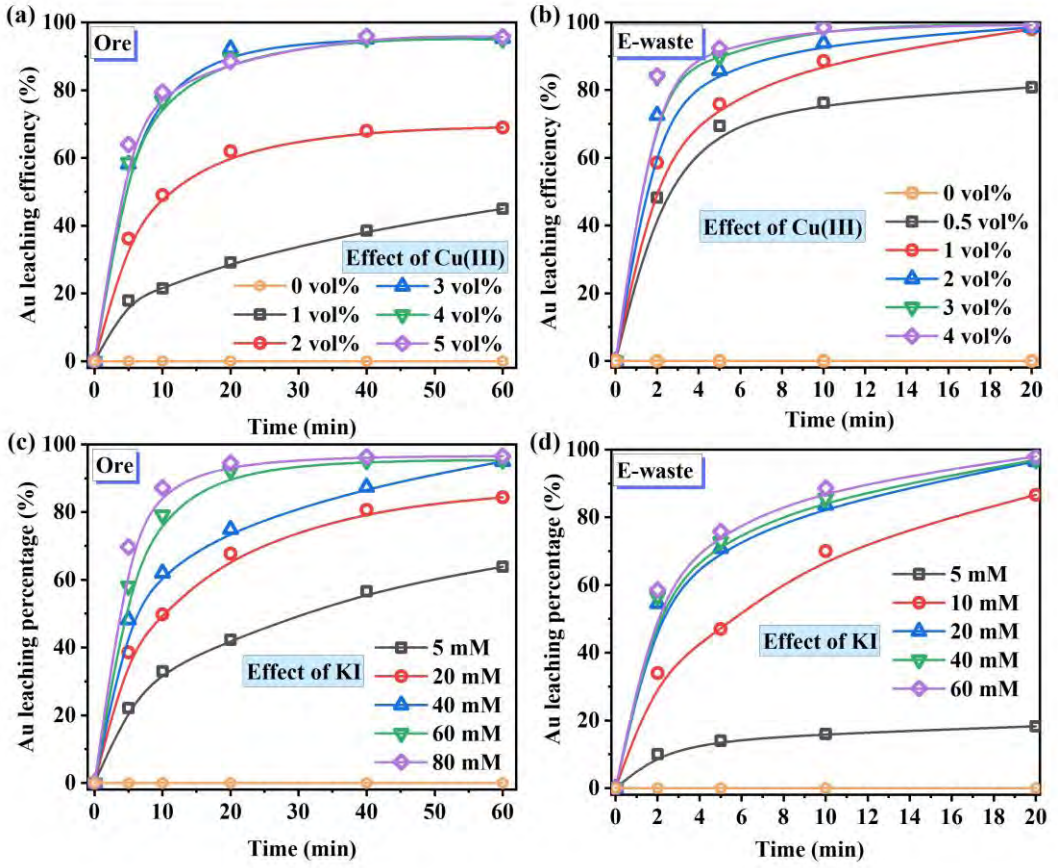

Figure 7.4 Effects of (a, b) Cu(III) dosage and (c, d) KI concentration on Au leaching efficiency. Other conditions: pH 7.0, liquid-to-solid ratio 4:1, and agitation speed 400 rpm for gold ore; pH 7.0, liquid-to-solid ratio 10:1, and agitation speed 400 rpm for e-waste.

Figure 7.4c and Figure 7.4d show the effect of KI on gold leaching from ore and e-waste, respectively. Similarly, when the system was pure Cu(III), gold dissolution was negligible. Once KI was added, the efficiency of gold leaching increased, yielding a maximum percentage of 94.9% and 96.5% with a KI molarity of 40 mM for gold ore and 20 mM for e-waste, respectively. Generally speaking, KI mainly supplies I^- for complexing with oxidized Au ions, but given the very low content of gold in the ore and e-waste, the consumption of I^- to produce Au-iodide species is insignificant [35]. So, maintaining a higher I^- level than stoichiometric is mainly used to avoid their dissociation [36]. Moreover, the vast majority of I^- could be used to maintain the system in a highly oxidized environment, if iodide derivatives $I_{2(l)}$ and I_3^- actually exist.

7.3.2.2 Effect of pH

Variations in pH always affect the activities of protons and hydroxide ions, which in turn affect the speciation and thermodynamic stability of species [37]. Here, gold leaching tests under a wide pH range from 1.5 to 12.5 were investigated. As presented in Figure 7.5, gold leaching was achieved at wide pHs (4.0-10.0), showing both fast leaching kinetics and high leaching percentage. As pH fell to a highly acidic condition (pH 1.5), gold leaching did not proceed, likely because periodate detaches from Cu(III) and is protonated, making Cu(III) reduction very quick [22]. Gradually rising pH to alkaline (pH 10), gold leaching can be achieved, but the curves are likely characterized by parabolic to linear, indicating that leaching kinetics slowed down. The main reason for this change is possibly due to the instability of I_3^- and $I_{2(l)}$ under highly alkaline environments, where these oxidizing species can quickly disproportionate to IO_3^- [38]. Likewise, as pH reached an ultra-high alkaline condition (pH 12.5), gold leaching efficiency also declined precipitously, possibly due to the Au-iodide species precipitating as solid products (e.g., AuO_2 and $Au(OH)_3$). Thus, pH 5.5 was selected, achieving 96.3% and 98.0% Au leaching from ore and e-waste, respectively.

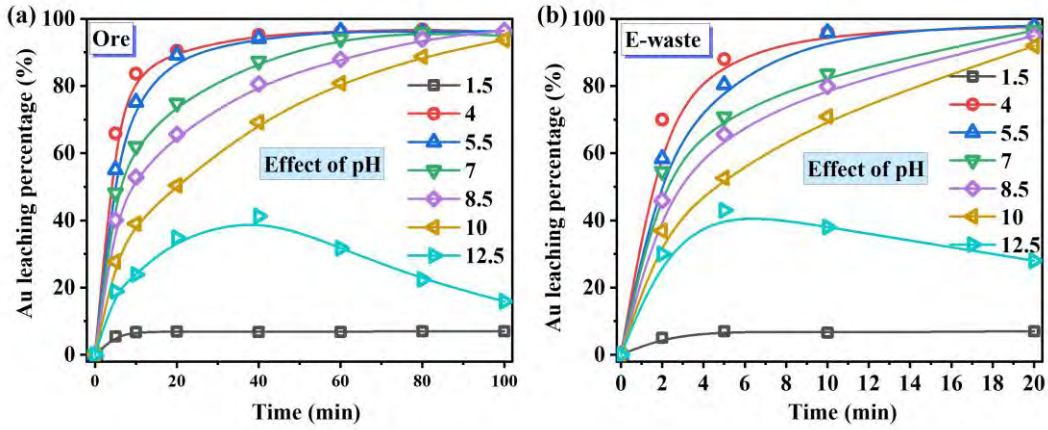

Figure 7.5 Effect of pH on Au leaching efficiency. Other conditions: 3 vol% Cu(III), 40 mM KI, liquid-to-solid ratio 4:1 and agitation speed 400 rpm for gold ore; 1 vol% Cu(III), 20 mM KI, liquid-to-solid ratio 10:1 and agitation speed 400 rpm for e-waste.

7.3.2.3 Effect of liquid-solid ratio and agitation speed

In the heterogeneous ore leaching process, the liquid-solid ratio (L/S) and agitation speed (rpm) should be controlled at a minimum level to increase the processing capacity, decrease the reagent consumption, and save energy [39]. As shown in Figure 7.6a, decreasing L/S from 4 to 2 did not significantly affect Au leaching from the ore. In the

case of e-waste, satisfactory leaching can be achieved when L/S was set to 8 (Figure 7.6b). Further reducing L/S decreased leaching efficiency for both ore and e-waste. That is because lower L/S could increase pulp viscosity as well, thereby hindering reagent diffusion to gold surfaces and slowing dissolution kinetics. As seen in Figure 7.6c and Figure 7.6d, agitation is necessary due to only a very poor Au leaching occurring without stirring; while 94.1% and 96.6% leaching efficiency can be obtained when agitation speeds are higher than 200 rpm for ore and 300 rpm for e-waste, respectively. By contrast, e-waste requires a higher L/S and agitation speed, likely due to its relatively low apparent density, which increases diffusional resistance.

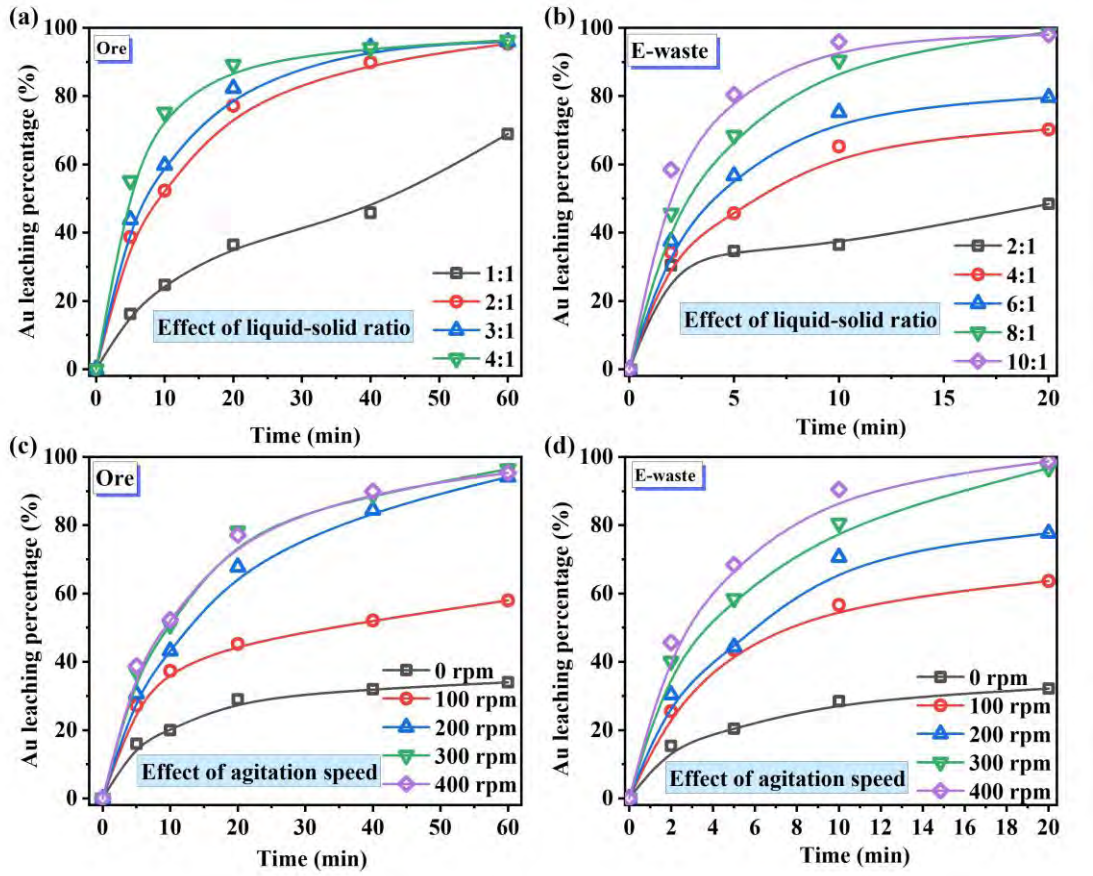

Figure 7.6 Effect of (a, b) liquid-solid ratio (L/S) and (c, d) agitation speed (rpm) on Au leaching efficiency. Other conditions: 3 vol% Cu(III), 40 mM KI and pH 5.5 for gold ore; 1 vol% Cu(III), 20 mM KI and pH 5.5 for e-waste.

In summary, the optimal gold leaching conditions are 3 vol% Cu(III), 40 mM KI, pH 5.5, L/S 2, 200 rpm for gold ore and 1 vol% Cu(III), 20 mM KI, pH 5.5, L/S 8, 300 rpm for e-waste, achieving gold leaching efficiencies of 94.1% and 96.6%, respectively.

7.3.3 Mechanistic insights into Cu(III)/KI-mediated gold dissolution

7.3.3.1 Speciation of Cu(III) under different pH

As a weak acid, periodate does not exist as IO_6^{5-} in actual solution; instead, four types of protonated forms (e.g., H_5IO_6, $H_4IO_6^-$, $H_3IO_6^{2-}$, and $H_2IO_6^{3-}$) may generally arise with respect to pH variation. Here, the speciation of periodate was plotted to provide insight into the forms of Cu(III) periodate (Figure 7.7a). There are H_5IO_6 and $H_4IO_6^-$ at pH below 8.36, $H_3IO_6^{2-}$ and $H_2IO_6^{3-}$ at pH above 8.36 [40]. $H_3IO_6^{2-}$ is widely considered the ligand for Cu(III) at strong alkalinity, forming diperiodatocuprate(III) (DPC), $[Cu(H_3IO_6)_2]^-$ (Eq. (7-13)), supported by the characteristic electronic absorption for the pH 13.6 sample in the UV-vis spectrum (Figure 7.7b). Upon decreasing pH, the bidentate $H_3IO_6^{2-}$ ligand is partially displaced by water to yield the diaquomonoperiodatocuprate(III) (MPC), $[Cu(H_3IO_6)(H_2O)_2]^-$ (Eq. (7-14)), reflected by the corresponding spectral shift at pH 10 [41]. Further pH decrease to acid leaves the UV-vis peak position unchanged, consistent with an MPC, while the intensity decreases due to reduction. The structures of DPC and MPC are shown in Figure 7.7(c).

$$[Cu(H_2IO_6)_2]^- + 2H_2O \rightarrow [Cu(H_3IO_6)_2]^- + 2OH^- \quad (7\text{-}13)$$

$$[Cu(H_3IO_6)_2]^- + 2H_2O \rightarrow [Cu(H_3IO_6)(H_2O)_2]^+ + H_3IO_6^{2-} \quad (7\text{-}14)$$

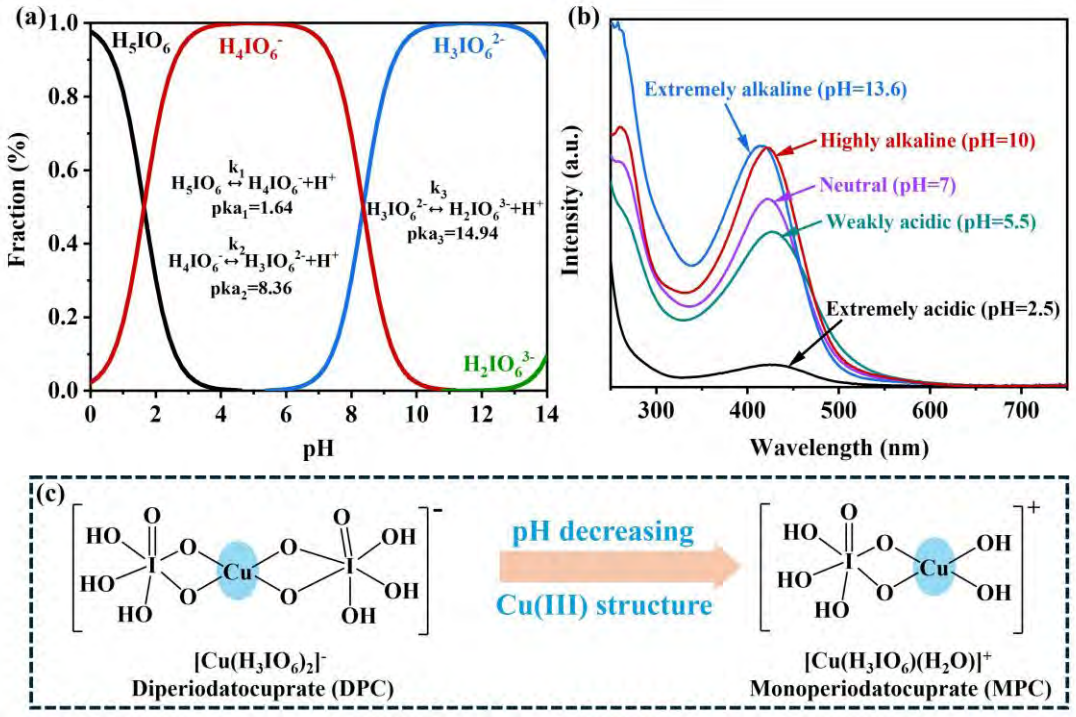

Figure 7.7 Speciation of Cu(III) under different pH. (a) Distribution of periodate species over pH 0-14. (b) UV-vis spectra of Cu(III) periodate at different pHs. (c)

Structure evolution of Cu(III) periodate with decreasing pH

7.3.3.2 Identification of reactive oxidants

As a typical oxidative leaching process, understanding the leaching mechanism requires linking Au dissolution to active species of oxidants. The Cu(III)/KI system looks simple, but the redox chemistry between Cu(III) and I^- would render the process complicated [19]. As concluded earlier, this system revealed a pronounced effect of pH on gold leaching (Figure 7.5), with clear differences from acidic to alkaline conditions. Accordingly, we hypothesized that the dissolution behaviour of gold in the Cu(III)/KI solutions is pH-dependent, which was tested by observing the difference between pH 5.5 (weakly acidic) and pH 10.0 (highly alkaline). As shown in Figure 7.8a, the solution at pH 10 is accompanied by a colour fade during 120 min reaction; in contrast, there's almost no change at pH 5.5 (Figure 7.8b). Interestingly, precipitates appeared in both solutions after a standing period. After filtration and drying, green $Cu(IO_3)_2$ were collected (Figures 7.8c and 7.8d) [42], which ought to be the reduction product of Cu(III). Here, IO_3^- likely produced from a side reaction between protonated periodate (H_3IO_6) and I^-, with its occurrence increasing as pH decreases (Eq. (7-15)).

$$3H_3IO_6 + I^- + 3H^+ \rightarrow 4IO_3^- + 6H_2O \quad (15)$$

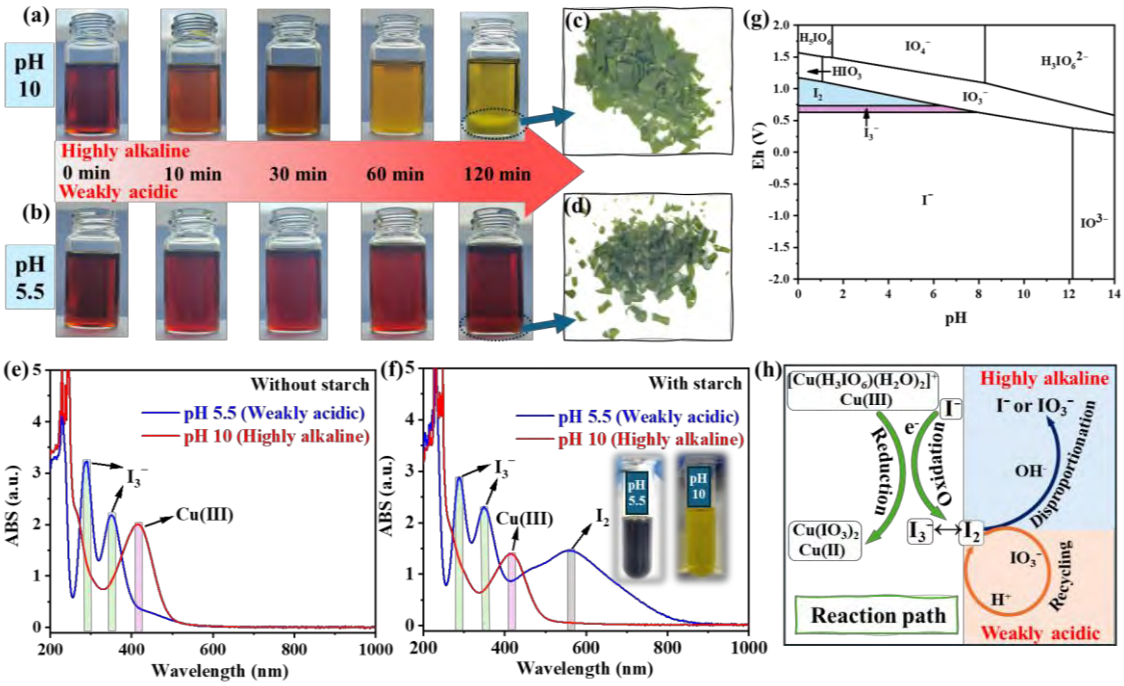

Figure 7.8 Characterization of the Cu(III)/KI solution at pH 5.5 and 10. (a, b) color change; (c, d) reduction products of Cu(III); (e, f) UV-vis spectra; (g) Eh-pH diagram

of the I-H_2O system; (h) proposed formation pathway of oxidative species

Further on, the detection of reactive oxidants was carried out on the UV-vis spectrum. At pH 5.5, the characteristic Cu(III)-periodate absorption diminished after reaction, accompanied by the appearance of new absorption features (around 290 and 350 nm), consistent with the formation of I_3^- (Figure 7.8e) [43]. When starch was added as an indicator, the solution turned dark blue, and an additional absorption band appeared at around 560 nm (Figure 7.8f), supporting the presence of $I_{2(l)}$ capable of forming a starch-iodine complex [44]. In contrast, at pH 10.0, the spectrum remained dominated by the Cu(III)-periodate feature with or without starch (416 nm), indicating that iodine-based oxidants (i.e., I_3^- and $I_{2(l)}$) are not persistent under strongly alkaline conditions. This observation is consistent with the Eh-pH diagram analysis of the I-H_2O system (Figure 7.8g) [45].

Based on the above analysis, the reactive oxidant in the Cu(III)/KI system becomes clear, as illustrated in Figure 7.8h. When KI is added to the Cu(III) solution, a redox reaction occurs in which high-valent Cu (III) is reduced to Cu(II) by gaining electrons, while I^- is simultaneously oxidized to $I_{2(l)}$ by losing electrons (Eqs. 7-16 and 7-17). Although $I_{2(l)}$ can theoretically form and convert to I_3^-, under highly alkaline conditions, $I_{2(l)}$ would likely react with OH^- to form I^- or IO_3^- by disproportionation (Eq. 7-18). However, as pH decreases, $I_{2(l)}$ and I_3^- remain stable and co-exist, as described by Eqs. (7-19) and (7-20).

$$Cu^{3+} + 2I^- \rightarrow Cu^{2+} + I_2 \quad (7\text{-}16)$$

$$[Cu(H_3IO_6)(H_2O)_2]^+ + 3I^- \rightarrow I_2 + Cu(IO_3)_2 + 7OH^- \quad (7\text{-}17)$$

$$3I_2 + 6OH^- \rightarrow 5I^- + IO_3^- + 3H_2O \quad (7\text{-}18)$$

$$5I_2 + IO_3^- + 6H^+ \rightarrow 3I_2 + 3H_2O \quad (7\text{-}19)$$

$$IO_3^- + 8I^- + 6H^+ \rightarrow 3I_3^- + 3H_2O \quad (7\text{-}20)$$

7.3.3.3 Chemical reaction pathway of Au oxidative dissolution

EQCM was widely used to observe Au oxidation by in situ recording the mass change of the Au-coated quartz electrode during anodic polarization [46]. Here, anodic oxidation curves of gold electrodes were measured by a Linear sweep voltammetry (LSV) method (Figures 7.9a and 7.9b), while Figures 7.9c and 7.9d depict the corresponding mass changes. It pointed out that two distinct mass-loss regions were observed, concurrent with sharp increases in current density, which are attributed to the oxidation of metallic Au(0) to Au(I) and Au(III), respectively [47] [48]. However, the mass decrease occurred at a lower potential in a given Cu(III)/KI system of pH 5.5

compared to pH 10. The reason behind this denotes that the gold oxidation process is more favourable at the lower pH (5.5), where the active oxidant was proved to be iodide derivatives (i.e., I_3^- and $I_{2(l)}$) instead of Cu(III).

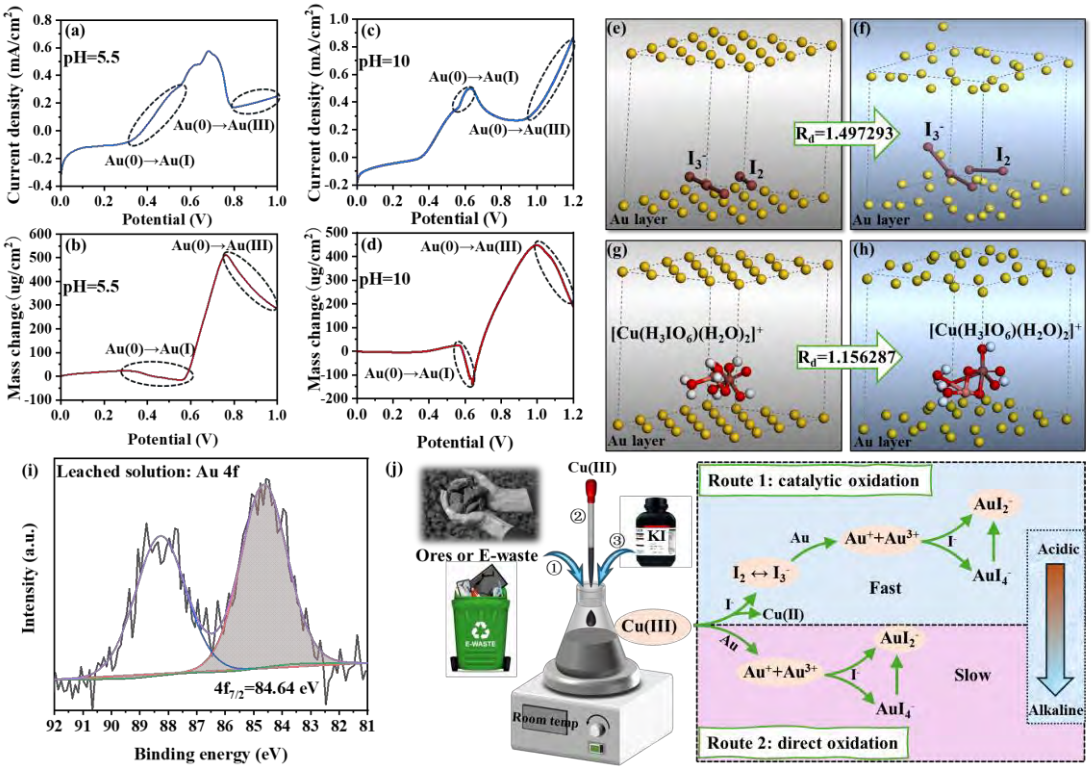

Figure 7.9 Characterization of gold oxidation behavior in the Cu(III)/KI system at pH 5.5 and 10. (a-d) anodic current density and EQCM mass response as a function of potential; (e-h) initial and optimized adsorption configurations of Cu(III) and $I_3^-/I_{2(l)}$ on gold surface; (i) Au 4f XPS spectra of the leachate; (j) proposed Au oxidation pathways

DFT calculations have been previously applied to investigate Au oxidation [49]. Figure 7.9e shows the adsorption structures of Cu(III) on the Au surface model (25 Au atoms), and Figure 7.9g shows the co-adsorption structure of I_3^- and $I_{2(l)}$, respectively. To quantify the extent of surface relaxation induced by different oxidants, the average relaxation descriptor Rd for the surface Au atoms was calculated using Eq. (7-21), which has been proposed as a useful metric for comparing oxidant-Au interfacial reactivity [50]. As shown in Figures 7.9f and 7.9h, geometry optimization leads to appreciable relaxation of the surface Au atoms, as reflected by the changes in their Cartesian coordinates. Notably, the $I_3^-/I_{2(l)}$ system exhibits a larger R_d value than the Cu(III) system, indicating a stronger perturbation of the Au surface. This trend is consistent with the experimental observation that $I_3^-/I_{2(l)}$ play a more dominant role in

promoting Au oxidation under the corresponding conditions. The smaller size of $I_3^-/I_{2(l)}$ may allow a closer approach to surface sites and stronger interfacial coupling, thereby facilitating charge transfer and accelerating Au oxidation, whereas the bulky Cu(III) (i.e., diaquomonoperiodatocuprate(III)) may experience steric hindrance when approaching the Au surface [51].

$$R_d = \frac{1}{n}\sum_{i=1}^{n}\sqrt{(x_i^* - x_i)^2+(y_i^* - y_i)^2+(z_i^* - z_i)^2} \quad (7\text{-}21)$$

Where (*xi*, *yi*, *zi*) and (*xi**, *yi**, *zi**) are the Cartesian coordinates of the i-th Au atom (i=1, 2,…, n) in the adsorption structure before and after geometry optimization, respectively, and n=25.

In most iodide leaching processes, Au(I) and Au(III) are both possible forms; thus, the speciation of gold in leachate was further identified using XPS. The Au4f 7/2 peak appeared at 84.48 eV, consistent with Au(I) complex, i.e., AuI_2^- (Figure 7.9i) [52]. Under typical leaching conditions, it is difficult to obtain the ultra-high potential required for the formation of Au(III) complex (i.e., AuI_4^-) without specific temperature, pressure, and acidity [53]. Besides, if the potential is not high enough, AuI_4^- will easily undergo a disproportionation reaction to form colloidal $AuI_{(s)}$, which exists only as an intermediate in aqueous solution and will quickly react with I^- to form AuI_2^- (Eqs. 7-22 and 7-23). So, Au is predominantly present as AuI_2^- in the leachate.

$$AuI_4^- \rightarrow AuI_{(s)} + Au + I_3^- \quad (7\text{-}22)$$

$$AuI_{(s)} + I^- \rightarrow AuI_2^- \quad (7\text{-}23)$$

As pointed out above, a possible mechanism model for gold leaching in the Cu(III)/KI system was enunciated in Figure 7.9j. At acid and near-neutral conditions, high-valent Cu(III) can function as a catalyst for the in situ generation of I^- derivatives, i.e., I_3^- and $I_{2(l)}$, which co-exist as the powerful oxidant for gold dissolution (Route 1). At alkaline conditions, Cu(III) itself is the active oxidant for gold dissolution (Route 2). In general, both oxidation pathways can achieve gold leaching from gold ore or e-waste samples, producing AuI_2^- as the final product. Since I_3^- and $I_{2(l)}$ are relatively more proficient oxidants here, it was established that a weakly acidic pH was ideally required for effective gold leaching.

7.3.4 Process limitations and industrial implications

Although this is only an exploratory study, this work also made some efforts to reuse the leaching solution and recover the leached AuI_2^- ions. As shown in Figure 7.10a, five repetitions of gold leaching from ore and e-waste were started under

optimized conditions (section 7.3.2). In each cycle, the filtered leachate was directly used to leach fresh ore or e-waste without any supplementary reagents. Notably, the Cu(III)/KI system maintained gold leaching efficiencies higher than 90% over three consecutive cycles. Such repeated use of the solution without additional reagents demonstrates good sustainability. As shown in Figure 7.10b, commercial activated carbon achieved very high efficiencies of gold recovery of 98.5% and 99.3% from triply cycled ore and e-waste leachates, respectively, demonstrating that conventional gold adsorbent is well-suited for use in our system. Finally, in actual operation, the recommended workflow is to apply the leaching solution to three leaching runs, then conduct one gold recovery operation.

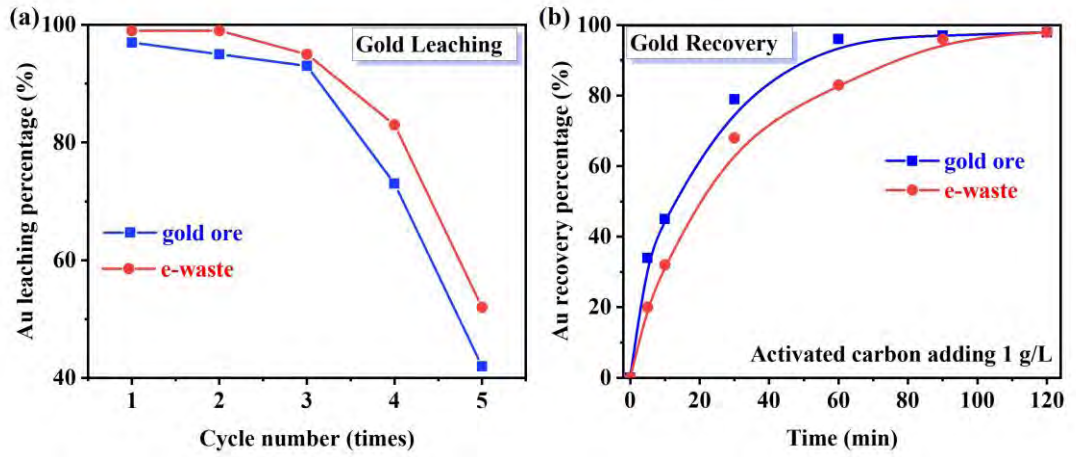

Figure 7.10 Multi-cycle leaching and activated carbon recovery of gold ions. (a) Multi-cycle leaching under: 3 vol% Cu(III), 40 mM KI, pH 5.5, liquid-solid ratio 2:1, agitation speed 200 rpm, and 60 min for gold ore and 1 vol% Cu(III), 20 mM KI, pH 5.5, liquid-solid ratio 8:1, agitation speed 300 rpm, and 20 min for e-waste. (b) Activated carbon recovery of gold ions from three-times cycled ore and e-waste leaching solution.

We observed that leaching efficiency decreased after the third cycle, primarily due to the insufficient supply of oxidative species, namely the precipitation of Cu(III) into insoluble Cu(II) irreversibly, and the loss of $I_3^-/I_{2(l)}$ through unavoidable adsorption onto ore and e-waste. From a sustainable hydrometallurgy perspective, this is suboptimal. Our next phase of work will focus on closed-loop regeneration of Cu(III) and the $I_3^-/I_{2(l)}$ couple to ensure better life-cycle sustainability.

7.4 Conclusions

In summary, our results indicate that high-valent Cu(III) periodate alleviates the

main drawback of iodide gold leaching, namely the high reliance on added iodine. The following observations and conclusions are made: (i) Under the optimized conditions, the Cu(III)/KI system achieved 94.1% Au leaching from ore (3 vol% Cu(III), 40 mM KI, pH 5.5, L/S 2, 200 rpm, 60 min) and 96.6% from e-waste (1 vol% Cu(III), 20 mM KI, pH 5.5, L/S 8, 300 rpm, 20 min). (ii) The function mechanism of Cu(III) periodate is highly pH-dependent, serving as the active oxidant in alkaline media, whereas at lower pH it acts catalytically to generate more efficient I_3^-. (iii) This eco-friendly system can sustainably reuse leachate and enables the recovery of leached AuI_2^- using commercial activated carbon, thereby offering a promising alternative and paving the way for green gold extraction.

7.5 References

[1] M. Mann, T.P. Nicholls, H.D. Patel, L.S. Lisboa, J.M.M. Pople, L.N. Pham, M.J.H. Worthington, M.R. Smith, Y. Yin, G.G. Andersson, C.T. Gibson, L.J. Esdaile, C.E. Lenehan, M.L. Coote, Z. Jia, J.M. Chalker, Sustainable gold extraction from ore and electronic waste, Nat. Sustainability 8 (2025) 947-956.

[2] Y. Chen, M. Xu, J. Wen, Y. Wan, Q. Zhao, X. Cao, Y. Ding, Z.L. Wang, H. Li, Z. Bian, Selective recovery of precious metals through photocatalysis, Nat. Sustainability 4 (2021) 618-626.

[3] X. Jin, J. Li, C. Li, L. Chen, X. Wang, W. Shi, J. Xiong, R. Zhang, W. Guo, D. Yin, Efficient and selective gold recovery from practical e-waste and electroplating wastewater using protein crystals, Resour., Conserv. Recycl. 222 (2025) 108450.

[4] J. Wang, F. Faraji, J. Ramsay, A. Ghahreman, A review of biocyanidation as a sustainable route for gold recovery from primary and secondary low-grade resources, J. Cleaner Prod. 296 (2021) 126457.

[5] Z. Liu, X. Guo, Q. Tian, L. Zhang, A systematic review of gold extraction: Fundamentals, advancements, and challenges toward alternative lixiviants, J. Hazard. Mater. 440 (2022) 129778.

[6] G. Hilson, A.J. Monhemius, Alternatives to cyanide in the gold mining industry: what prospects for the future?, J. Cleaner Prod. 14 (2006) 1158-1167.

[7] F. Xie, J. Chen, J. Wang, W. Wang, Review of gold leaching in thiosulfate-based solutions, Trans. Nonferrous Met. Soc. China 31 (2021) 3506-3529.

[8] Q. Meng, X. Yan, G. Li, Eco-friendly and reagent recyclable gold extraction by iodination leaching-electrodeposition recovery, J. Cleaner Prod. 323 (2021) 129115.

[9] M. Sahin, A. Akcil, C. Erust, S. Altynbek, C.S. Gahan, A. Tuncuk, A Potential Alternative for Precious Metal Recovery from E-waste: Iodine Leaching, Sep. Sci. Technol. 50 (2015) 2587-2595.

[10] K. Binnemans, P.T. Jones, The Twelve Principles of Circular Hydrometallurgy, J. Sustain. Metall. 9 (2023) 1-25.

[11] S.S. Konyratbekova, A. Baikonurova, G.A. Ussoltseva, C. Erust, A. Akcil, Thermodynamic and kinetic of iodine–iodide leaching in gold hydrometallurgy, Trans. Nonferrous Met. Soc. China 25 (2015) 3774-3783.
[12] S. Anusaraporn, R. Dolphen, P. Thiravetyan, S. Farnaud, Influence of biogenic iodide-iodine lixiviant and laccase enzyme produced by two-step conditioning of Acinetobacter baumannii on gold, copper, and nickel bioleaching from gold fingers in used card edge connectors, J. Environ. Chem. Eng. 13 (2025) 115567.
[13] K. Kudpeng, T. Bohu, C. Morris, P. Thiravetyan, A.H. Kaksonen, Bioleaching of Gold from Sulfidic Gold Ore Concentrate and Electronic Waste by Roseovarius tolerans and Roseovarius mucosus, Microorganisms 8 (2020) 1783.
[14] S.Y. Khaing, Y. Sugai, K. Sasaki, M.M. Tun, Consideration of Influential Factors on Bioleaching of Gold Ore Using Iodide-Oxidizing Bacteria, Minerals 9 (2019) 274.
[15] S.Y. Khaing, Y. Sugai, K. Sasaki, Gold Dissolution from Ore with Iodide-Oxidising Bacteria, Sci. Rep. 9 (2019) 4178.
[16] Q. Wang, T. Liu, Y. Chen, S. Chen, X. Qin, Y. Nie, F. Zi, Eco-friendly and economical extraction of gold from a refractory gold ore in iodide solution using persulfate as the oxidant, Hydrometallurgy 198 (2020) 105502.
[17] L. Hou, A.L. Valdivieso, A. Robledo-Cabrera, N.Z. Zainiddinovich, C. Wu, S. Song, F. Jia, Stepwise oxidation of refractory pyrite using persulfate for efficient leaching of gold and silver by an eco-friendly copper(II)-glycine-thiosulfate system, Powder Technol. 448 (2024) 120323.
[18] A. Ding, M. Li, C. Liu, T. Chee, Q. Yan, L. Lei, C. Xiao, Recovering palladium and gold by peroxydisulfate-based advanced oxidation process, Sci. Adv. 10 (2024) eadm9311.
[19] S. Nadimpalli, J. Padmavathy, K.K.M. Yusuff, Determination of the nature of the diperiodatocuprate(III) species in aqueous alkaline medium through a kinetic and mechanistic study on the oxidation of iodide ion, Transition Met. Chem. 26 (2001) 315-321.
[20] P.B.A. Vrkljan, J. Bauer, V. Tomisic, Kinetics and Mechanism of Iodide Oxidation by Iron(III): A Clock Reaction Approach, J. Chem. Educ. 85 (2008) 1123.
[21] N. Sridevi, K. Yusuff, Kinetics and mechanism of oxidation of iodide by diperiodatoargentate (III), Indian J. Chem. 35A (1996) 894-896.
[22] K. McCann, D.M. Brigham, S. Morrison, J.C. Braley, Hexavalent Americium Recovery Using Copper(III) Periodate, Inorg. Chem. 55 (2016) 11971-11978.
[23] Y. Zhao, F. Xue, T. Ma, Experimental study on Hg0 removal by diperiodatocuprate (III) coordination ion solution, Fuel Process. Technol. 106 (2013) 468-473.
[24] P.C. Santos-Munguía, F. Nava-Alonso, V.M. Rodríguez-Chávez, O. Alonso-González, Hidden gold in fire assay of gold telluride ores, Miner. Eng. 141 (2019) 105844.
[25] P. Cyganowski, K. Garbera, A. Leśniewicz, J. Wolska, P. Pohl, D. Jermakowicz-Bartkowiak, The recovery of gold from the aqua regia leachate of electronic parts

using a core–shell type anion exchange resin, J. Saudi Chem. Soc. 21 (2017) 741-750.

[26] R.K. Biswas, P. Khan, S. Mukherjee, A.K. Mukhopadhyay, J. Ghosh, K. Muraleedharan, Study of short range structure of amorphous Silica from PDF using Ag radiation in laboratory XRD system, RAMAN and NEXAFS, J. Non-Cryst. Solids 488 (2018) 1-9.

[27] T.P. Jose, S.M. Tuwar, Oxidation of threonine by the analytical reagent diperiodatocuprate(III) – An autocatalysed reaction, J. Mol. Struct. 827 (2007) 137-144.

[28] B. Chowdhury, M.H. Mondal, M.K. Barman, B. Saha, A study on the synthesis of alkaline copper(III)-periodate (DPC) complex with an overview of its redox behavior in aqueous micellar media, Res. Chem. Intermed. 45 (2019) 789-800.

[29] J. Wang, R. Wang, Y. Pan, F. Liu, Z. Xu, Thermodynamic analysis of gold leaching by copper-glycine-thiosulfate solutions using Eh-pH and species distribution diagrams, Miner. Eng. 179 (2022) 107438.

[30] X. Yuan, D. Tang, T. Zou, C. Xu, Y. Qiu, Combined leaching of Carlin-type gold deposit in Guizhou by potassium chlorate and bleaching powder, Mater. Res. Express 9 (2022) 126506.

[31] L. Pan, X. Zhang, S. He, G. Zhang, W. Xu, Gold leaching from waste mobile phone PCBs in a solution mixture of sodium persulfate and potassium iodide, J. Environ. Chem. Eng. 10 (2022) 107712.

[32] B. Altansukh, K. Haga, N. Ariunbolor, S. Kawamura, A. Shibayama, Leaching and adsorption of gold from waste printed circuit boards using iodine-iodide solution and activated carbon, Eng. J. 20 (2016) 29-40.

[33] G. Senanayake, The role of ligands and oxidants in thiosulfate leaching of gold, Gold Bull. 38 (2005) 170-179.

[34] L. Hou, A.L. Valdivieso, Y. Chen, P. Chen, N.Z. Zainiddinovich, C. Wu, S. Song, F. Jia, A highly efficient clean hydrometallurgy process for gold leaching in a Fenton oxidation assisted thiourea system, Sustainable Mater. Technol. 40 (2024) e00975.

[35] O. Sitando, G. Senanayake, X. Dai, A.N. Nikoloski, P. Breuer, A review of factors affecting gold leaching in non-ammoniacal thiosulfate solutions including degradation and in-situ generation of thiosulfate, Hydrometallurgy 178 (2018) 151-175.

[36] C.J. Liang, J.Y. Li, Recovery of gold in iodine-iodide system – a review, Sep. Sci. Technol. 54 (2019) 1055-1066.

[37] Q. Jin, M. Kirk, pH as a Primary Control in Environmental Microbiology: 1. Thermodynamic Perspective, Front. Environ. Sci. 6 (2018) 21.

[38] H. Wang, C. Sun, S. Li, P. Fu, Y. Song, L. Li, W. Xie, Study on gold concentrate leaching by iodine-iodide, Int. J. Min. Met. Mater. 20 (2013) 323-328.

[39] M. Lampinen, S. Seisko, O. Forsström, A. Laari, J. Aromaa, M. Lundström, T. Koiranen, Mechanism and kinetics of gold leaching by cupric chloride,

Hydrometallurgy 169 (2017) 103-111.
[40] T. Chen, Y. Sun, H. Dong, J. Chen, Y. Yu, Z. Ao, X. Guan, Understanding the Importance of Periodate Species in the pH-Dependent Degradation of Organic Contaminants in the H_2O_2/Periodate Process, Environ. Sci. Technol. 56 (2022) 10372-10380.
[41] K. Sharanabasamma, M.A. Angadi, M.S. Salunke, S.M. Tuwar, Kinetics of Oxidation of L-Valine by a Copper(III) Periodate Complex in Alkaline Medium, J. Solution Chem. 41 (2012) 187-199.
[42] K. Nassau, J.W. Shiever, B.E. Prescott, Transition metal iodates. I. Preparation and characterization of the 3d iodates, J. Solid State Chem. 7 (1973) 186-204.
[43] S.V. Kireev, S.L. Shnyrev, Study of molecular iodine, iodate ions, iodide ions, and triiodide ions solutions absorption in the UV and visible light spectral bands, Laser Phys. 25 (2015) 075602.
[44] D. Li, L. Shi, J. Chen, J. Gao, Chlorine Dioxide–Iodine–Acetylacetone Oscillation Reaction Investigated by UV–Vis and Online FTIR Spectrophotometric Methods, J.Solution Chem. 45 (2016) 81-94.
[45] M. Baghalha, The leaching kinetics of an oxide gold ore with iodide/iodine solutions, Hydrometallurgy 113-114 (2012) 42-50.
[46] A.G. Zelinsky, O.N. Novgorodtseva, EQCM study of the dissolution of gold in thiosulfate solutions, Hydrometallurgy 138 (2013) 79-83.
[47] P.H. Qi, J.B. Hiskey, Electrochemical behavior of gold in iodide solutions, Hydrometallurgy 32 (1993) 161-179.
[48] L. Hou, A.L. Valdivieso, P. Chen, G. Zhang, Q. Zhang, Y. Chen, S. Song, F. Jia, An electrochemical study of the dissolution behavior of gold in a novel glycine-thiosulfate system, Miner. Eng. 202 (2023) 108273.
[49] Y. Nie, L. Yang, Q. Wang, C. Shi, F. Zi, H. Yu, Connection between gold dissolution in thiosulfate leaching and Cu(II) complexes during the cathodic process, Electrochim. Acta 328 (2019) 135079.
[50] B. Xu, Y. Nie, X. Feng, Q. Wang, Dissolution patterns of gold on various structural surfaces in thiosulfate solutions: The effect of interface adsorption on thiosulfate oxidation and gold atom dissociation, Electrochim. Acta 497 (2024) 144602.
[51] J. Wu, B. Xu, X. Liu, Z. Dong, T. Jiang, Development of a novel cobalt-glycine catalyzed thiosulfate system by DFT calculation for eco-friendly and efficient gold extraction, Sep. Sci. Technol. 354 (2025) 128959.
[52] F. Feng, M. Wang, J. Zhang, H. Ding, L. Yu, W. Guo, L. Guo, Q. Liang, Q. Zhang, C. Lu, X. Li, Hydrogen bonding-based deep eutectic solvents for choline chloride/sulfamide and its application in the recycling of precious metals, J. Environ. Chem. Eng. 12 (2024) 113611.
[53] Y. Lin, X. Hu, F. Zi, Thiocyanate facilitating thiosulfate extraction of gold via inhibiting formation of passive layer, Sustainable Mater. Technol. 40 (2024) e00878.

Chapter VIII General conclusions, integrative discussion, and perspectives

8.1 General conclusions

This thesis focused on the development of advanced chemical oxidation systems for gold hydrometallurgy, with particular emphasis on refractory gold ore pretreatment and cyanide-free gold leaching. The central idea of this work is that oxidation plays two different but closely connected roles in gold extraction. First, oxidation can be used as a pretreatment strategy to decompose sulfide minerals and expose encapsulated precious metals. Second, oxidation can be used as a redox-control strategy to drive the dissolution of metallic gold in cyanide-free leaching systems.

Radical-based oxidation was first used to overcome mineralogical refractoriness and then to accelerate gold dissolution. In the stepwise persulfate pretreatment system, persulfate was activated by heating and subsequently by Fe ions released from pyrite dissolution, generating reactive oxidizing species that decomposed the pyrite's refractory matrix. This process reduced particle size and formed pores and channels in pyrite, improving the exposure of encapsulated Au and Ag. This led to significantly increased leaching efficiencies for Au and Ag in the subsequent leaching. In the Fenton-thiourea system, radicals also promoted rapid gold leaching. However, excessive oxidation caused serious thiourea decomposition. By introducing NTA to regulate the Fe-based redox environment, thiourea consumption was greatly reduced while high gold extraction was maintained. These results show that radical oxidation is effective, but its intensity must be controlled to avoid unnecessary lixiviant degradation.

Copper-based oxidation systems were then developed to provide more tunable redox control for cyanide-free leaching. In the copper(II)-glycine-thiosulfate system, pH-dependent Cu-glycine speciation strongly affected gold dissolution, with the $Cu(C_2H_4NO_2)_3^-$-dominated alkaline system showing lower passivation behavior and faster gold dissolution kinetics. In the copper(II)-DTPA-thiosulfate system, DTPA stabilized Cu(II) and suppressed thiosulfate decomposition, while ammonia improved the redox activity of the Cu-DTPA complex, enabling high gold leaching with low thiosulfate consumption. Finally, the Cu(III)/KI system extended this strategy to high-valent copper chemistry. Depending on pH, Cu(III) either directly oxidized gold or catalyzed the formation of active I_2/I_3^- species, achieving efficient gold leaching from acidic to alkaline media.

Overall, this thesis establishes a controlled-oxidation framework for gold hydrometallurgy: radical oxidation is suitable for mineral liberation and rapid leaching, while copper complex oxidation provides adjustable redox activity, improved lixiviant stability, and efficient cyanide-free gold dissolution.

8.2 Integrative discussion

Although the experimental chapters investigate different leaching systems, they are connected by the same scientific principle: gold extraction requires controlled oxidation processes. During pyrite oxidation and gold dissolution, electrons are released from the solid phase. Therefore, an oxidant must accept these electrons to allow the reaction to continue. In this thesis, radicals and copper complexes were designed as oxidants (i.e., electron acceptors). Their functions were investigated in different chemical systems, including oxidation pretreatment of refractory sulfide ore by persulfate, Fenton-thiourea leaching, copper(II)-glycine-thiosulfate leaching, copper(II)-DTPA-thiosulfate leaching, and copper(III)-iodide leaching (Figure 8.1).

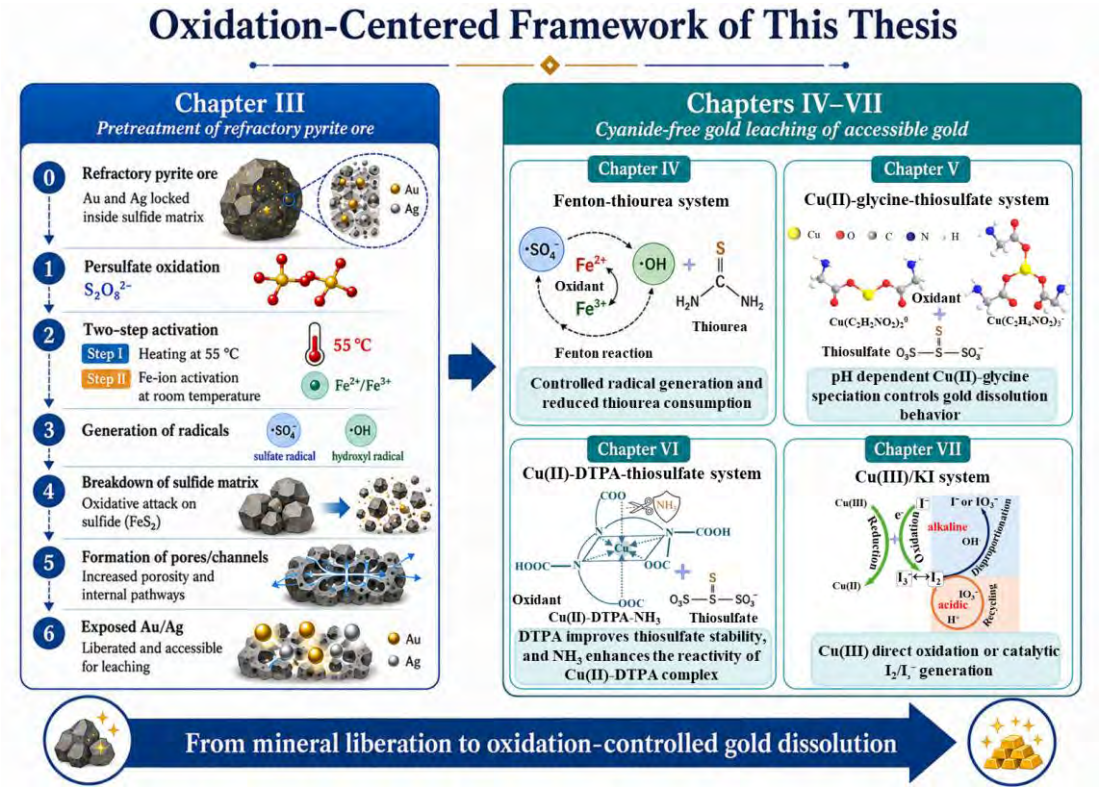

Figure 8.1 Oxidation-centered framework of this thesis

The first important connection among the chapters is the role of gold accessibility. Chapter III directly addresses the mineralogical refractoriness problem. In this chapter,

oxidation is used to open pyrite's refractory matrix and expose encapsulated Au and Ag. Without this pretreatment, the gold and silver are physically blocked from the lixiviant, so even an effective leaching system cannot work well. Therefore, Chapter III establishes the first block of the thesis: oxidation as a liberation strategy for refractory sulfide ores. In contrast, Chapters IV-VII mainly study the leaching chemistry of already accessible gold. The samples investigated in these chapters include roasted concentrates, multi-stage pretreated concentrates (prepared by roasting and subsequent sulfuric acid leaching for copper removal), gold electrodes, and e-waste. These chapters do not directly solve the initial encapsulation problem of raw refractory ore. Instead, they answer a different question: once gold is accessible, how can a cyanide-free leaching system dissolve it efficiently and stably? Therefore, Chapters IV-VII form the second block of the thesis: oxidation as a redox-control strategy for cyanide-free gold dissolution.

The second important connection is the evolution from radical oxidation to coordination-controlled oxidation. In Chapters III and IV, radical chemistry is the main oxidation pathway. Persulfate and H_2O_2 contain unstable O-O bonds, which can be activated by heating, Fe ions, or the Fenton reaction to produce strong reactive oxygen species. These radicals can oxidize pyrite or gold rapidly. However, Chapter IV also shows that uncontrolled radical oxidation may damage the lixiviant, especially thiourea. This result leads to an important general principle: oxidants must be strong enough to oxidize gold, but not so strong that they cause severe side reactions. Chapters V and VI further develop this idea using coordination chemistry. In thiosulfate leaching, Cu(II) is needed as an oxidant, but free or poorly controlled Cu(II) can also accelerate thiosulfate decomposition. Therefore, ligand coordination becomes a key strategy to regulate Cu(II). Glycine controls the pH-dependent Cu(II) speciation and affects passivation and electron transfer during gold dissolution. DTPA strongly stabilizes Cu(II), while NH_3 improves the redox reactivity of the Cu-DTPA complex. These results show that the performance of a Cu-based oxidant is not determined only by copper concentration, but also by its coordination environment, ligand type, pH, and even redox reactivity. Chapter VII extends this coordination-based oxidation concept to high-valent copper chemistry. In the iodide leaching system, the oxidant Cu(III) can play different roles depending on the solution chemistry: it can be a direct oxidant, a redox mediator, or a catalyst for generating another active oxidizing species. This finding further supports the central conclusion that oxidant function must be understood within the whole solution environment, rather than as an isolated reagent.

Taken together, the chapters show that successful cyanide-free gold extraction depends on four linked factors: gold accessibility, oxidizing strength, ligand stability, and pH-controlled speciation. Gold accessibility determines whether the lixiviant can reach the metal surface. Oxidizing strength determines whether Au(0) can be converted to Au(I) or Au(III). Ligand stability determines whether the dissolved gold can remain in solution without excessive reagent loss. pH controls radical generation, oxidant speciation, and the stability of lixiviants. Therefore, the main scientific contribution of this thesis is not only the development of several leaching systems, but also the establishment of an oxidation-centered framework for understanding gold pretreatment and cyanide-free leaching.

8.3 Perspectives and future work

Although the results of this thesis are promising, further work is still needed to move these systems from laboratory study toward industrial application.

First, the integration of pretreatment and leaching should be further studied. Chapter III demonstrates that persulfate oxidation can effectively expose Au and Ag from refractory pyrite, while Chapters IV-VII provide different cyanide-free leaching routes for accessible gold. In the future, these two blocks should be connected into complete flowsheets. For example, radical oxidation pretreatment could be followed by optimized thiosulfate, thiourea, or iodide leaching, depending on ore mineralogy, reagent cost, and environmental requirements.

Second, the recycling and regeneration of leaching solutions should be investigated. Industrial applications require stable reagent circulation, low oxidant consumption, and low wastewater generation. Therefore, future research should focus on how to regenerate oxidants, maintain suitable redox potential, reuse lixiviants, and control the accumulation of decomposition products in recycled solutions.

Third, efficient gold recovery from cyanide-free leachates remains a key challenge. Conventional activated carbon works very well in cyanide systems, but it is often less effective for recovering gold from thiosulfate or other cyanide-free solutions. Therefore, new gold recovery materials and methods, such as ion-exchange resins, functional adsorbents, electrochemical recovery, or selective precipitation, should be developed and coupled with the leaching systems studied in this thesis.

Fourth, the scalability and environmental performance of these oxidation systems should be evaluated. Future studies should include tests with larger pulp densities,

continuous or semi-continuous operation, different real ore types, impurity effects, reagent cost analysis, and environmental assessment. These studies are necessary to identify which system is most suitable for practical gold production.

In summary, this thesis confirms that advanced chemical oxidation is a powerful strategy for gold hydrometallurgy. By controlling radical generation, metal complexation, pH, and redox potential, it is possible to improve refractory ore pretreatment and develop efficient cyanide-free leaching systems. Future work should focus on process integration, solution recycling, gold recovery from leachate, and scale-up evaluation, which are essential steps for moving these systems from laboratory research toward industrial application.

Appendix I

Articles published during the Ph.D. studies

1. **Lei Hou**, Alejandro López Valdivieso, Yu. Chen, Peng Chen, Nasriddinov Zamoniddin Zainiddinovich, Chunhui Wu, Shaoxian Song, Feifei Jia. A highly efficient clean hydrometallurgy process for gold leaching in a Fenton oxidation-assisted thiourea system. ***Sustainable Materials and Technologies***, 40 (2024), e00957.
2. **Lei Hou**, Alejandro López Valdivieso, Aurora Robledo-Cabrera, Nasriddinov Zamoniddin Zainiddinovich, Chunhui Wu, Shaoxian Song, Feifei Jia. Stepwise oxidation of refractory pyrite using persulfate for efficient leaching of gold and silver by an eco-friendly copper (II)-glycine-thiosulfate system[J]. ***Powder Technology***, 448 (2024): 120323.
3. **Lei Hou**, Alejandro López Valdivieso, Peng Chen, Nasriddinov Zamoniddin Zainiddinovich, Chunhui Wu, Shaoxian Song, Feifei Jia. Pentetic acid/ammonia cooperatively stabilizes Cu(II) as an efficient oxidant for green thiosulfate leaching of gold[J]. ***Minerals Engineering***, 218 (2024): 109043.
4. **Lei Hou**, Alejandro López Valdivieso, Peng. Chen, Guowei Zhang, Qi Zhang, Yu Chen, Shaoxian Song, Feifei Jia. An electrochemical study of the dissolution behavior of gold in a novel glycine-thiosulfate system. ***Minerals Engineering***, 202 (2023), 108273.
5. **Lei Hou**, Baolin. Xing, Hui Guo, Huihui Zeng, Song Cheng, Mingliang Meng, Xiaoxiao Qu, Alejandro López Valdivieso, Chuanxiang Zhang, Yijun Cao. Effect of mineralogical characteristics evolution of vermiculite upon thermal and chemical expansions on its adsorption behavior for aqueous Pb (II) removal. ***Powder Technology***, 430 (2023), 119040.
6. **Lei Hou**, Aurora Robledo Cabrera, Hui Guo, Zhenshuai Wang, Huihui Zeng, Jiushuai Deng, Baolin Xing. Dissolution mechanism of gold in a high-valent Cu(III)-assisted iodide system: Towards eco-friendly and fast gold oxidative leaching from ore and e-waste. ***Minerals Engineering***, 245 (2026), 110344.
7. Guowei. Zhang, **Lei Hou**, Alejandro López Valdivieso, Peng Chen, Qi Zhang, Yu Chen, Nasriddinov Zamoniddin Zainiddinovich, Chunhui Wu, Alejandro López Valdivieso, Feifei Jia. Efficient and stable leaching of gold in a novel ethydiaminedhephen acetic-thiosulfate system. ***Minerals Engineering***, 209 (2024), 108639. (Corresponding author)